Understanding the Roles Played by Receptor Tyrosine Kinase(s) and Non-Coding RNA(s) in Neurodegeneration

By

Kaushik Chanda

LIFE05201504005

Saha Institute of Nuclear Physics, Kolkata

A thesis submitted to the
Board of Studies in Life Sciences

In partial fulfilment of requirements
for the Degree of

DOCTOR OF PHILOSOPHY

of

HOMI BHABHA NATIONAL INSTITUTE

February, 2021

Homi Bhabha National Institute

Recommendations of the Viva Voce Committee

As members of the Viva Voce Committee, we certify that we have read the dissertation prepared by **Kaushik Chanda (LIFE05201504005)** entitled **"UNDERSTANDING THE ROLES PLAYED BY RECEPTOR TYROSINE KINASES AND NON-CODING RNAs IN NEURODEGENERATION"** and recommend that it may be accepted as fulfilling the thesis requirement for the award of Degree of Doctor of Philosophy.

Chairman - **Prof. Udayaditya Sen**

Udayaditya Sen **22.4.2021**

Guide / Convener - **Prof. Debashis Mukhopadhyay**

Debashis Mukhopadhyay 22.4.21

Examiner - **Dr. Shantanu Sengupta, CSIR-IGIB, New Delhi**

Shantanu Sengupta 22.04.2021

Member 1- **Prof. Oishee Chakrabarti**

Oishee Chakrabarti 22/4/2021

Member 2- **Prof. Partha Saha**

Partha Saha 22/4/2021

Member 3- **Prof. Chandrima Das**

Chandrima Das 22.4.2021

Final approval and acceptance of this thesis is contingent upon the candidate's submission of the final copies of the thesis to HBNI.

I hereby certify that I have read this thesis prepared under my direction and recommend that it may be accepted as fulfilling the thesis requirement.

Date: 22.4.2021

Place: Kolkata

Debashis Mukhopadhyay

Signature

Guide

STATEMENT BY AUTHOR

This dissertation has been submitted in partial fulfilment of requirements for an advanced degree at Homi Bhabha National Institute (HBNI) and is deposited in the Library to be made available to borrowers under rules of the HBNI.

Brief quotations from this dissertation are allowable without special permission, provided that accurate acknowledgement of source is made. Requests for permission for extended quotation from or reproduction of this manuscript in whole or in part may be granted by the Competent Authority of HBNI when in his or her judgment the proposed use of the material is in the interests of scholarship. In all other instances, however, permission must be obtained from the author.

KAUSHIK CHANDA

Name & Signature of the student

DECLARATION

I, hereby declare that the investigation presented in the thesis has been carried out by me. The work is original and has not been submitted earlier as a whole or in part for a degree / diploma at this or any other Institution / University.

KAUSHIK CHANDA

Name & Signature of the student

List of Publications arising from the thesis

Journal

1. "Altered Levels of Long NcRNAs Meg3 and Neat1 in Cell and Animal Models Of Huntington's Disease.", Chanda, K., Das, S., Chakraborty, J., Bucha, S., Maitra, A., Chatterjee, R., Mukhopadhyay, D., & Bhattacharyya, N. P., *RNA biology*, **2018**, *15*(10), 1348–1363.
2. "LncRNA Xist, X-chromosome Instability and Alzheimer's Disease." Chanda, K., & Mukhopadhyay, D., *Current Alzheimer research*, **2020**, *17*(6), 499–507.
3. "Amyloid Precursor Protein Intra-Cellular Domain (AICD), Aβ and their Confounding Synergistic Effects Differentially Regulate the Degradome of Cellular Models of Alzheimer's Disease."
   Chanda, K., Laha, S., Chatterjee, R., & Mukhopadhyay, D.
   Gene Reports, Volume 23, **2021**, *101082*, *ISSN 2452-0144*, https://doi.org/10.1016/j.genrep.2021.101082.
4. "Long non-coding RNA MALAT1 Protects Against $A\beta_{1-42}$ Induced Toxicity by Regulating the Expression of Receptor Tyrosine Kinase EPHA2 via Quenching miR-200a/26a/26b in Alzheimer's Disease.'', Kaushik Chanda, Nihar Ranjan Jana and Debashis Mukhopadhyay, (Communicated, under review.)
5. "Amelioration of $A\beta_{1-42}$ Induced Cytoskeletal Instability by Receptor Tyrosine Kinase ROR1 and its Regulation by miR-146a-NEAT1 Nexus in Alzheimer's Disease.'', Kaushik Chanda, Nihar Ranjan Jana and Debashis Mukhopadhyay, (Communicated, under review.)

Chapters in books and lectures notes

1. NOT APPLICABLE.

Conferences

1. SINP international cancer meeting 2018. Cancer biology-still a challenge in 21st century & SINP School on epigenetics during **26th – 28th September, 2018** at SINP, Kolkata, India. (poster presentation)
   POSTER TITLE: THE FINE BALANCE BETWEEN ALZHEIMER'S AND CANCER: WHEN BOTH TOO MUCH AND TOO LITTLE ARE BAD.

2. School and symposium on advances in biomedical mass spectrometry and workshop on metabolomics (SSABMS, 2019) during **11-17th November, 2019** at SINP, Kolkata, India. (poster presentation)
   POSTER TITLE: ALTERED LEVELS OF LONG NON-CODING RNAs IN CELL AND ANIMAL MODELS OF ALZHEIMER'S DISEASE.

3. Advances in Alzheimer's and Parkinson's therapies:2nd AAT- AD/PD™ FOCUS MEETING during **1-5 April, 2020** at Vienna, Austria. (Virtual conference).
(poster presentation)
POSTER TITLE:
a. Abstract 104-
A MIRNA 146A- NEAT1- ROR1 AXIS REGULATES THE CYTOSKELETAL ARCHITECTURE IN ALZHEIMER'S DISEASE.
b. Abstract 112-
SETS OF MIRNA-LNCRNA-TF REGULATORS CONTROL SEVERAL RTKS IMPLICATED IN ALZHEIMER'S DISEASE.

4. AAIC Neuroscience Next. Alzheimer's Association International Conference®
Virtual Event during November 9-10, 2020.
Abstracts published in "*Alzheimer's and Dementia: THE JOURNAL OF THE ALZHEIMER'S ASSOCIATION",* **December 2020,** Volume 16, Issue 12, 117-123, 175-180.

Others

1. Zeiss Imaging Workshop on **26/10/2017 & 27/10/2017** at IICB, Kolkata, True Campus.

2. Xth Bangalore Microscopy Course, National Centre for Biological Sciences (NCBS), Bangalore, India during **16-23 September, 2018**. (poster presentation).
POSTER TITLE: UNDERSTANDING THE ROLES PLAYED BY RECEPTOR TYROSINE KINASES AND NON-CODING RNAs IN ALZHEIMER'S DISEASE.

KAUSHIK CHANDA

Kaushik Chanda.

Name & Signature of the student

DEDICATIONS

One Ring to rule them all, One Ring to find them,

One Ring to bring them all and in the darkness bind them

I have always been a Tolkien buff. However, this Elvish saying has always mesmerised me the most. Its not the ring per se, but what it represents. A ring is a circle which represents life as a cycle. It has no beginning and end. I have always believed that memories are similar. They represent a continuum. And all of us are essentially a summation of memories. One of the strongest motivations as to why I chose to pursue my Ph.D. in neurodegeneration was to find out the what and the how (in whatever little measure) of memory loss, which is a hallmark of diseases like Alzheimer's. And in that endeavour, I have tried to delineate the causal mechanisms in AD which form an interconnected loop (hence the ring reference). But as the saying goes, "I am standing on the shoulders of giants". So, the primary dedication of this work goes to those researchers and scientists who are slowly, but surely, inching their way towards finding a cure for this devastating disease with the hope that my findings compound this effort.

The next part of dedications goes to my family for their unending support. My wife and best friend Antarika (an accomplished dancer herself), who supports me unequivocally in all my endeavours and whose boundless energy is a constant source of inspiration. My parents in law for their constant encouragement; Kakima, Chotkakaku and Ahona (an excellent writer who is inching towards a Ph.D. herself); Bappamama, Mami, Niljit (a brilliant student and good human being) and Amma. I miss Dadu and Didun, whose blessings will always be with me. I wish you could see me graduate. I am what I am because of my Baba and Maa. Baba is my hero and Maa is my confidante. They saw me through the hard times and never gave up on me. Their unconditional love and unwavering support are the biggest strength in my life. Live long and prosper.

A last part of the dedication to all those scholars who are tirelessly pursuing a PhD. Science is hard, and abundant with failures. Often, you would feel like giving up. Please don't. At the end of the day, when you have contributed to expanding the cumulative human knowledge, even by a bit, you will live forever in your work.

KAUSHIK CHANDA

ACKNOWLEDGEMENTS

I am about to submit my thesis, which represents my thoughts, ideas, and actions over the past five years at Biophysics and Structural Genomics (B&SG) Division at SINP. This place for me is a laboratory, a recreation zone, a world of endless possibilities and a fortress of solitude- combined in one. And this was possible because of my PhD supervisor Prof. Debashis Mukhopadhyay. I was late in joining his lab, but from the moment we met, he placed his trust in me, as I did in him. That trust culminated in a wonderful journey of half a decade, where, instead of being a mentor and protégé, we were more like friends (read Samwise *Gamgee and Frodo Baggins). He allowed me to pursue experiments, no matter how stupid they were, and learn from my mistakes. His positive approach and subtle sense of sarcasm are something which I plan to imbibe someday. In essence, for me Debashis sir is a friend > philosopher > guide.*

I express my gratitude to my collaborators Prof. Arindam Maitra from NIBMG, Prof. Nitai P. Bhattacharya (superannuated), Prof. Nihar Ranjan Jana from IIT Kharagpur, without whose help, this work would not be possible.

I formally thank SINP and its director, Prof. Gautam Bhattacharya. I would like to acknowledge Homi Bhabha National Institute (HBNI) and DAE, Govt. of India for funding my fellowship and IBOP project (DAE) for funding my work during my Ph.D. tenure. I am also thankful to Prof. Subrata Banerjee, Prof. Partha Saha (Head, Life Sciences and Dean, HBNI), Dr. Oishee Chakrabarti, Dr. Kaushik Sengupta, Dr. Chandrima Das, Dr.Sangram Bagh, Dr. Soumen Manna, Dr.Subhabrata Majumder, Dr.Udayaditya Sen, Dr. Sankar De and all the other faculties who helped me in various stages of my Post M.Sc coursework and Ph.D. tenure.

I sincerely thank Dr. Piyali Majumder, Dr. Srijit Das, Dr. Arunabha Chakrabarti and Dr. Shounak Baksi, for helping me in various stages over the last few years. Sincere thanks to my lab colleagues Suparna Saha, Priyanka Sengupta, Russa Das, Somenath Sen and Pallavi Chatterjee for all their help (although I think I did my part in helping them too). Thank you to my other lab mates Tulika, Sayak, Kathakali, Rajdeep, Deepro, Rajkamal, Chandreyee, Rachayita, for all the fun we had.

I would like to sincerely thank Dr. Debdatto Mookherjee. We are friends for nearly a decade now, but he is family. From helping with experiments, overcoming personal troubles, he has been there all along. The good times that we shared together are priceless memories.

KAUSHIK CHANDA

Contents

Page No.

Summary I

Chapter 1: Exordium

1.1. Neurodegenerative diseases with a focus on Alzheimer's disease 1

1.2. Introduction to Receptor Tyrosine Kinase(s) and their roles in the brain 2

1.3. Linking Alzheimer's disease, the Amyloid Precursor Protein (APP) and RTK 5

1.4. Central role of APP, AICD and Aβ in Alzheimer's disease 12

1.5. Comprehending the complexity of APP biology independently of Aβ to dissect AD pathology 16

1.6. Search of new molecular players governing AD

1.6.1. MicroRNAs in Alzheimer's disease 18

1.6.2. LncRNAs in Neurodegeneration 21

1.7. Objective of the thesis 25

Chapter 2: Materials and Techniques

2.1. Ethics declaration 34

2.2. Cell culture and transfection 34

2.3. Cell Models of AD 35

2.4. $A\beta_{1-42}$ treated Cell Model 35

2.5. APP/PS1 mice 35

2.6. Cell Models of HD 36

2.7. Mouse HD Model R6/2 36

2.8. Small RNA sequencing (for the AD study) 37

2.9. Small RNA sequencing (for the HD study) 39

2.10. Bioinformatics Analysis 40

2.11. RT2 lncRNA PCR Array 43
2.12. Patient Samples, constructs, reagents and siRNAs 45
2.13. RNA isolation from cultured cells and paraffinized tissue 45
2.14. Quantitative real-time PCR 47
2.15. Gene-specific primers 47
2.16. RNA Immunoprecipitation (RIP) Assay 53
2.17. Sequential Immunocytochemistry (ICC) and RNA Fluorescence *in situ* Hybridisation (FISH) Assay 54
2.18. Isolation of cell extract and Western blot analysis 55
2.19. Antibodies 56
2.20. Immunocytochemistry 68
2.21. Aggregate counting 68
2.22. F/G Actin Assay 59
2.23. Trypan Blue Exclusion Assay 59
2.24. MTT Assay 60
2.25. Live and Dead Cell Assay 60
2.26. Databases 61
2.27. Enrichment analysis for biological processes defined by Gene Ontology (GO), pathways by KEGG, miRNA target interaction, miRNA - lncRNA interaction and lncRNA – RBP interactions 61
2.28. Statistical analysis 63

Chapter 3: Effect of AICD and Aβ$_{1-42}$ on Cellular Degradome in AD

3.1. Several miRNAs are differentially expressed in cell models of AD 64
3.2. Functional clustering, Gene Set Enrichment Analysis and pathway enrichment analysis reveals concurrent behaviour of several deregulated miRNAs 67
3.3. Quantitative real time PCR validates the top miRNA hits from the sequencing results in cell models of AD 70
3.4. Multi-dimensional scaling and Principal Component Analysis of deregulated miRNAs show distinctive clusters for different sample sets 72
3.5. Six lncRNAs are consistently deregulated in cell models of AD 75

3.6. Fourteen selected lncRNAs having AD association have miRNA, RNA Binding Protein (RBP) and Transcription Factor (TF) Interacting partners 79
3.7. Differentially regulated miRNAs have several RTK Targets 81
3.8. Discussion 84

Chapter 4: MALAT1 Regulatory Networks in AD

4.1. Several lncRNAs are deregulated in a mouse model of AD 90
4.2. Validation of short-listed lncRNAs and their human homologs in respective animal model, cell model and brain tissue of AD 93
4.3. MALAT1 sponges miR 26a, b, 200a as revealed and validated by qRT-PCR, RNA FISH and RIP 95
4.4. MALAT1 interacting miRNAs are strongly up regulated in $A\beta_{1-42}$ treated cell model and AD brain targeting EPHA2, involved in core neurological pathways 99
4.5. Deregulated EPHA2 in AD confers protection against $A\beta_{1-42}$ cytotoxicity through its downstream effectors CREB, p38 and Synaptophysin 102
4.6. Discussion 106

Chapter 5: Cytoskeletal functions of ROR1 in AD

5.1. ROR1 and key cytoskeletal proteins are deregulated in $A\beta_{1-42}$ treated cell model compromising the cytoskeletal architecture 113
5.2. ROR1 over expression abrogates $A\beta_{1-42}$ induced degradation of cytoskeletal components 115
5.3. Over expressed ROR1 promotes neurite elongation in presence of $A\beta_{142}$ 116
5.4. hsa-miR-146a-5p and 34a-5p are up regulated by $A\beta_{1-42}$ and target ROR1 and Vimentin 118
5.5. LncRNA NEAT1 exerts a protective effect by sponging miR146a and miR-34 120
5.6. Discussion 124

Chapter 6: XIST and X- Chromosome Instability in AD

6.1. Introduction 128

6.2. XIST: A lnc transcript indispensable for X inactivation process 131

6.3. Regulatory roles of XIST has now been identified in NDDs 134

6.3.1. XIST is identified as a possible gene involved in the early stages of AD using microarray and neural network algorithm 134

6.3.2. XIST is identified as a major effector of apoptosis in Aβ treated rat hippocampal neurons 135

6.3.3. XIST levels were found to be up regulated in mouse tissues and mouse cell models of HD 136

6.3.4. XIST levels were experimentally found to be consistently and significantly up regulated in human and mouse cell models of AD 136

6.4. Discussion and therapeutic association 139

Chapter 7: lncRNA Transcriptome in HD

7.1 Introduction 148

7.2. Altered levels of non-coding RNAs in the mouse model of HD 150

7.3. Validation of the results in animal and cell models of HD using real-time PCR 152

7.4. Validation of the differential gene expressions in cell models 154

7.5. Meg3 and Neat1 enhance aggregation of mutant N-terminal HTT in cell models of HD and stabilize Tp53 155

7.6. Interactions of MEG3, NEAT1, and XIST with protein-coding genes and microRNAs 159

7.7. Enrichment of biological processes and pathways with MEG3, NEAT1, and XIST interacting proteins 159

7.8. Huntington's disease pathway (KEGG: 05016 and PANTHER: P00029): probable involvement of MEG3, NEAT1, and XIST in HD pathogenesis 161

7.9. Interacting partners of MEG3, NEAT1, and XIST associated Huntington's disease pathways (KEGG: 05016 and PANTHER: P00029) are also co-expressed 162

7.10. Transcription regulation of NEAT1, MEG3, and XIST 165
7.11. Discussion 166

Chapter 8: Précis and Inference

Précis 175
Inference 181

List of Figures

Page No.

Figure 1.1: Different classes of RTK 3

Figure 1.2: Activation of RTK signal transduction 3

Figure 1.3: Schematic illustration of APP 7

Figure 1.4: APP processing pathways 9

Figure 1.5: Schematic overview showing APP trafficking pathways and cleavage 10

Figure 1.6: The Amyloid Hypothesis 14

Figure 2.1: QC of total RNA samples on 1% Agarose gel 38

Figure 2.2: Small RNA libraries from total RNA through size selection 38

Figure 2.3: RT2 lncRNA PCR Array protocol schematic 44

Figure 3.1: Heat map of statistically significant differentially regulated miRNAs in Aβ vs Control (1a.) and Aβ vs AD (1b.) samples by small RNA sequencing 64

Figure 3.2: Venn diagram showing the overlaps of de regulated miRNAs between the groups Aβ vs Control, AD vs Control and Aβ vs AD 65

Figure 3.3: KEGG (3a.) and GO (3b.) analysis of de regulated miRNAs in the Aβ vs. Control group. KEGG (3c.) and GO (3d.) analysis of the miRNAs in the AD vs. Control group 69

Figure 3.4: Molecular signalling pathway enrichment analysis of top 10 miRNAs from Aβ vs Control, AD vs Control and Aβ vs AD groups 71

Figure 3.5: qPCR-based validation of top 4 up regulated and top 5 down regulated miRNAs from the Aβ vs Control group 73

Figure 3.6: Principal Component Analysis of the deregulated miRNAs from Aβ vs Control, AD vs Control and Aβ vs AD groups 75

Figure 3.7: Heat map of statistically significant differentially regulated lncRNAs in AD vs Control (7a.) by small RNA sequencing 77

Figure 4.1: Heat map of statistically significant differentially regulated lncRNAs in Wild Type vs. AD Transgenic mice samples by RT2 lncRNA PCR Array Mouse Cell Development & Differentiation kit 90

Figure 4.2: Altered levels of selected lncRNAs in AD mice model, $A\beta_{1-42}$ treated cell model and AD brain 94

Figure 4.3: Endogenous interaction and regulation of 3 miRNAs by MALAT1 in SHSY5Y cells 96

Figure 4.4: Altered levels of 3 miRNAs in $A\beta_{1-42}$ treated cell model and AD brain 100

Figure 4.5: Altered levels of EPHA2 and its downstream proteins in $A\beta_{1-42}$ treated cell model and in cells over expressing EPHA2 + $A\beta_{1-42}$ 104

Figure 4.6: Effect of EPHA2 over expression on cell viability in $A\beta_{1-42}$ treated cell model 105

Figure 4.7: Co-localization Analysis – Immunocytochemistry (ICC) assay. AGO2 with FUS in SHSY5Y cells 109

Figure 5.1: Deregulation of ROR1, key signalling proteins and actin cytoskeleton in $A\beta_{1-42}$ treated cell model 113

Figure 5.2: Consequences of ROR1 over expression on cytoskeletal components in $A\beta_{1-42}$ treated cells 115

Figure 5.3: Effect of ROR1 over expression on neurite elongation and actin dynamics in $A\beta_{1-42}$ treated cells 117

Figure 5.4: Dysregulation of hsa-mir-146a-5p, hsa-mir-34a-5p in $A\beta_{1-42}$ treated cell model and mice AD model 121

Figure 5.5: Endogenous interaction and regulation of miR146a and miR-34a by NEAT1 in SHSY5Y cells 123

Figure 6.1: Transcript level changes of XIST lncRNA in human and mouse AD cell models 137

Figure 6.2: XIST IN NDDs: A cartoon representing the working model of XIC and its aberration in NDDs 142

Figure 7.1: Heatmap of statistically significant differentially regulated ncRNAs Xist, Meg3, Peg3os, Vaultrc5, Snora21, Gm12238, Snord53, Snord85, Snhg12, Snord42a, Gm22650, Gm38671 and Neat1 in early stage and late-stage Huntington's mouse cortex compared to the control cortex from small RNA sequencing (n=2) 150

Figure 7.2: Altered levels of non-coding RNAs in HD animal model and in cells expressing N-terminal mutant Huntingtin 153

Figure 7.3: Reduction in the numbers of HTT-83Q-DsRed aggregates in Neuro2A and SHSY5Y cells 157

Figure 7.4: Endogenous p53 protein levels alter after treatment with siRNA against Meg3 or Neat1 in HD cell model 158

Figure 7.5: Comparison of Biological processes in noncoding RNA interacting proteins (dark black) and in human Genome (light black) 160

Figure 8.1: Schematic summary of the molecular paradigm in AD cell model 175

Figure 8.2: Schematic representation of molecular events on exposure to $A\beta_{1-42}$ in neuronal cells 177

Figure 8.3: Cartoon representation of $A\beta_{1-42}$ effect on cytoskeleton 179

Figure 8.4: Intracellular aggregates of mutant Huntingtin 180

List of Tables

Page No.

Table 1.1: Summary of potential phosphorylation sites within the AICD sequence and their corresponding kinases) if known 12

Table 1.2: MicroRNAs alterations in AD and possible effects on disease 19

Table 1.3: lncRNAs implicated in Neurodegeneration 22

Table 2.1: Quantification of RNA samples using Nanodrop 39

Table 2.2: Quantification of RNA samples using Nanodrop 46

Table 3.1: Summary of differentially regulated miRNAs, with the up regulated ones shown in bold font 66

Table 3.2: Summary of differentially regulated lncRNAs 78

Table 3.3: Summary of miRNA and RBP interactors of selected lncRNAs 80

Table 3.4: Summary of miRNA and RTK targets from Aβ vs. Control and AD vs. Control groups 81

Table 3.5: Summary of miRNA pathways and functions implicated in AD from the unique miRNAs of Aβ vs. Control and AD vs. Control groups 83

Table 4.1: Summary of the expression level changes of lncRNAs in 12-month-old APP/PS1 mouse brain cortex compared to age matched wild type mouse brain cortex (Human lncRNAs are in capitals; AD associated ones are highlighted in bold) 91

Table 6.1: PCR primers used to validate the expression of XIST 137

Table 6.2: XIST expression in patients and disease models of NDDs 138

Table 7.1: Summary of the levels of non-coding RNAs in different models of HD 151

Table 7.2: Summary of protein and miRNA interactions of non-coding RNAs Meg3, Neat1, and Xist 159

Table 7.3: Expression of genes in HD associated with Huntington's disease pathway 162

Table 7.4: Summary of co-expressed genes of MEG3, NEAT1, and XIST 163

Table 7.5: MEG3, NEAT1 and XIST interacting protein enriched with HD pathway 164

Table 7.6: Transcription factors that bind within 5 Kb upstream sequences of NEAT1, MEG3, and XIST 166

Chapter 8: Précis and Inference

Précis

The principal intention of this thesis was the discovery, causality and effect of specific RTKs and non–coding RNAs which are relevant in AD. Hence, considering that RTKs reside on the cell surface (top) and ncRNAs predominantly in the nucleus (bottom), we employed both top-down and bottom-up approaches to address the problem. We initiated the discourse by first analysing the deregulated ncRNAs using a high throughput NGS pipeline (small RNA sequencing data) in a cell model of AD **(Chapter 3)**. For this, ncRNAs under cues of Aβ and AICD were looked at separately. The reason for this was due to the fact that the effect of Aβ on the cellular degradome is studied, but those of AICD are scarce. This revealed the exclusive effect of AICD on the cellular ncRNA landscape **(Figure 8.1)**.

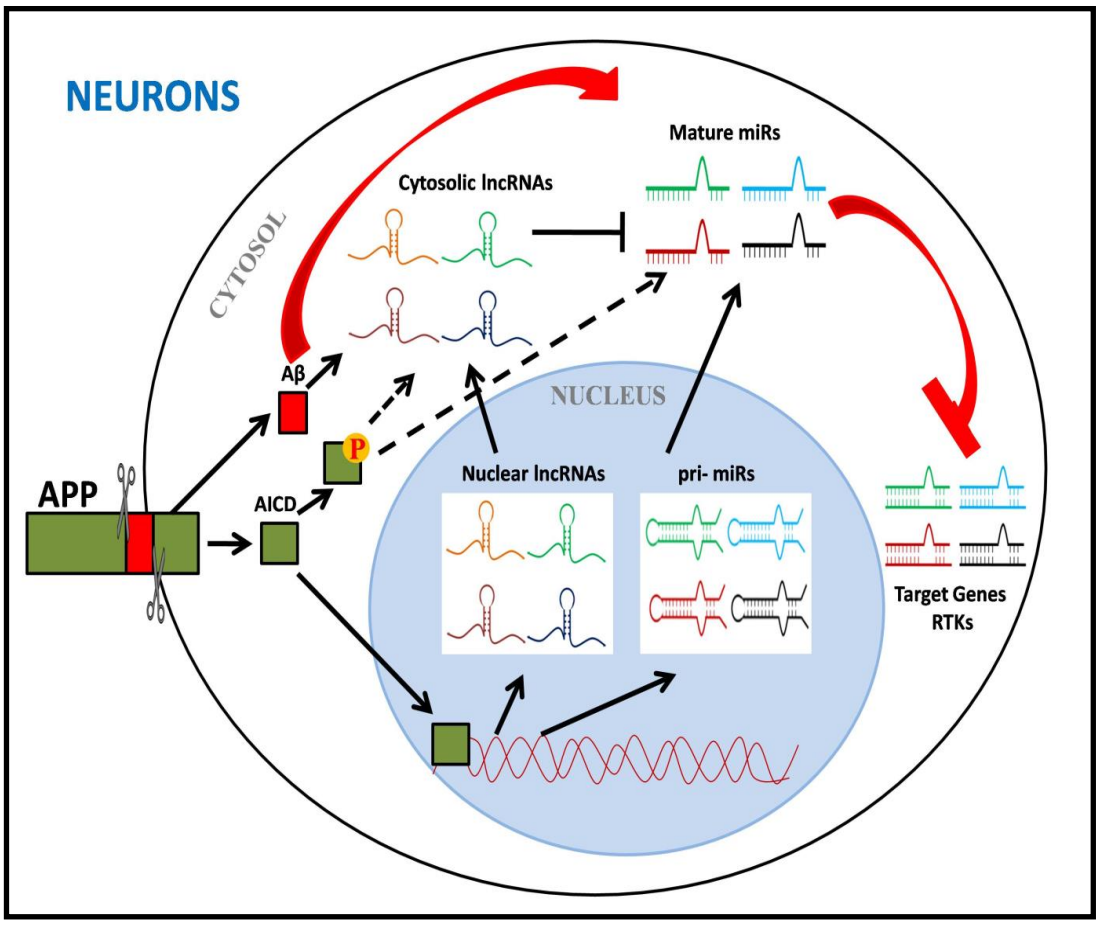

Figure 8.1: Schematic summary of the molecular paradigm in AD cell model. Sequential cleavage of APP leads to the generation of AICD and Aβ fragments which

differentially regulate the miRNA and lncRNA population in cells. The non-phosphorylated AICD enters the nucleus to regulate both miRNAs and lncRNAs generation, whereas the phosphorylated part (predominantly cytosolic) acts on the mature miRNAs. Together, with the effect of Aβ, they regulate the target RTKs.

This group had the largest number of unique miRNAs, implying that AICD might have a stronger effect on the miRNA population, compared to Aβ alone or AICD + Aβ combined. Several miRNAs were found to be common between the comparison groups which could be explained by the fact that both Aβ and AICD are in abundance in *post mortem* AD brains, and their synergistic effects could be a degeneration enhancing cue. From this analysis, a single miRNA- hsa-miR-4697-3p, which was common for all the 3 groups, could be used as a novel AD signature. Analysis of 4 top up regulated (221-3p, 222-3p, 155-5p and 4697-3p) and 5 top down regulated (3648, 1251-5p, 3607-5p, 3117-3p and 335-3p) miRNAs from the Aβ group using additional variants – AICD only and AICD + Aβ were performed, which yielded confounding results; Aβ and AICD had antagonistic effects on the miRNAs. It was also found that a large population of lncRNAs were deregulated, both from the Aβ and the AICD + Aβ sets which included RMST, NEAT1, MEG3, GAS5, H19, MALAT1, EVF2, TUG1 and several novel ones. Finally, a consolidated analysis of miRNAs targeting RTKs implicated in AD was performed which that the deregulated RTKs (specially the Eph and erbB members) were targets of significantly deregulated miRNAs in the AD vs Control group. An interesting find was the fact that specific miRNAs targeted a sub-class of RTKs (Eph, ErbB and IGF1R) which clustered together.

In continuum with the above stated total degradome study, the next agenda **(Chapter 4)** was to look at the differential levels of lncRNAs in AD mice brain which revealed 41 deregulated lncRNAs, of which 7 had AD associations. Validation studies showed that 4 out of the 7 lncRNAs had similar patterns of deregulation - RMST and NEAT1

were up regulated, while MEG3 and MALAT1 were down regulated. MALAT1 was chosen for further investigation as it showed the most consistent and strongest downregulation. Next, we investigated its miRNA interacting components by employing bioinformatics analysis, knock down assays and RNA Immunoprecipitation, which showed that MALAT1 interacted with miR-200a-3p, 26a-5p and 26b-5p. FUS protein, the RBP interactor of MALAT1 was used as a bait to pull MALAT1 down. The 3 miRNAs were found to be up regulated in AD and affected neuronal cell physiology indirectly through one of their common targets, EPHA2 which was proved by transiently over expressing mature miRNA mimics leading to repression of EPHA2 **(Figure 8.2)**.

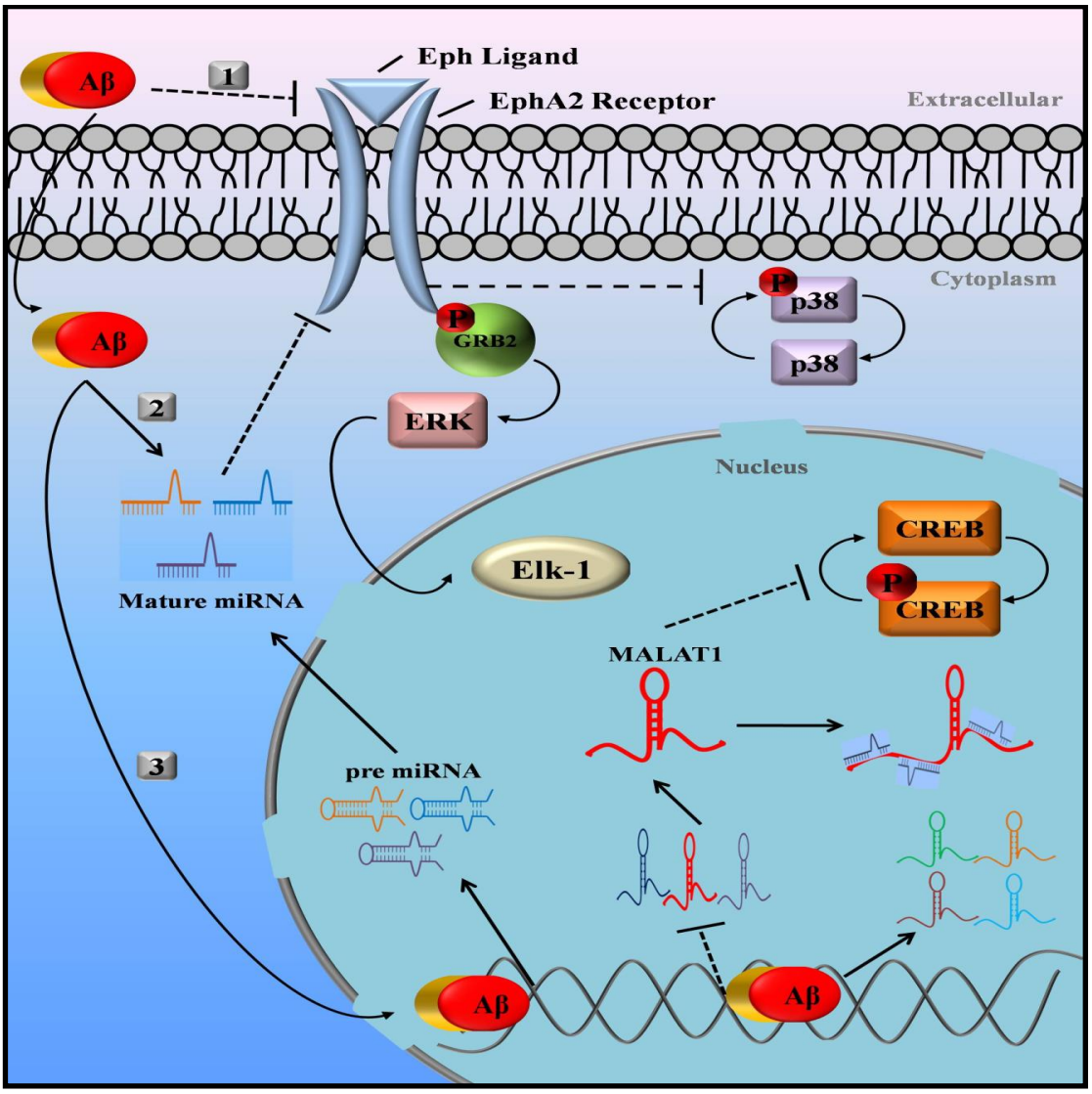

Figure 8.2: Schematic representation of molecular events on exposure to $A\beta_{1-42}$ in neuronal cells. Extracellular treatment of $A\beta_{1-42}$ has multiple effects on cells- 1. Extracellular $A\beta_{1-42}$ seems to inhibit the basal levels of RTK EPHA2 and its downstream effectors, notably CREB and p38. 2. Cytosolic $A\beta_{1-42}$ affects the mature miRNA pool, which targets and inhibits EPHA2. 3. Nuclear translocated $A\beta_{1-42}$ differentially activates miRNA and a subset of lncRNA, but represses another subset of lncRNAs. Out of the repressed lncRNAs, MALAT1 sponges the miRNAs and also inhibits the dephosphorylation of TF CREB.

For the next part of the study, a top-down approach was employed by focussing on the microtubule associated RTK ROR1 **(Chapter 5)** with the motivation that AD involves extensive cytoskeleton disruption due to $A\beta_{1-42}$. ROR1 over expression led to neuritogenesis, while intuitively, it was found that ROR1 levels decrease in the AD model. A transient over expression of ROR1 in presence of $A\beta_{1-42}$ abrogated cytoskeletal degradation of structural proteins, promoted neuritogenesis and altered the F: G actin ratio. Furthermore, miR-146a and miR-34a, up regulated in AD were found to co-repress ROR1 and Vimentin. Adding to this complexity, these miRNAs were revealed to be regulated by the lncRNA NEAT1, itself up regulated in AD. This exercise revealed the complex effect of $A\beta_{1-42}$ on cells (**Figure 8.3**). $A\beta_{1-42}$ not just deregulated the expression of RTK ROR1 and cytoskeleton proteins but also perturbed miR-146a and miR-34a levels, thereby repressing ROR1. Moreover, $A\beta_{1-42}$ differentially regulated nuclear NEAT1, which in turn sponged the miRNAs.

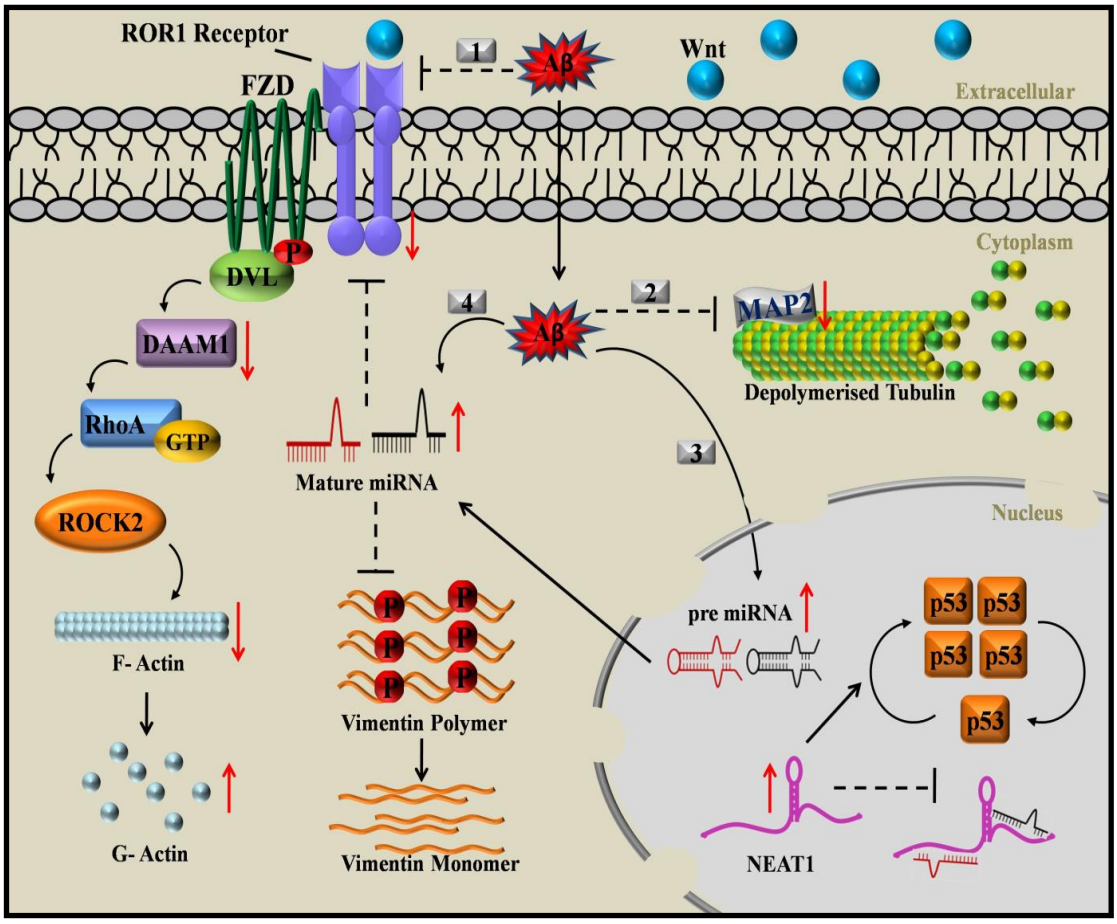

Figure 8.3: Cartoon representation of $A\beta_{1-42}$ effect on cytoskeleton. $A\beta_{1-42}$ has multifaceted effects - 1. Extracellular $A\beta_{1-42}$ inhibits the levels of microtubule associated RTK ROR1, both at the transcript and protein levels thereby affecting the planar cell polarity pathway leading to the alteration of F: G actin dynamics. 2. Cytosolic $A\beta_{1-42}$ affects microtubule dynamics by deregulation of MAP2. 3. Nuclear translocated $A\beta_{1-42}$ up regulates the precursor miRNAs and NEAT1.Up regulated NEAT1 in the nucleus exerts a protective role by sponging miRNAs and stabilising p53. 4. The compounded effect of cytosolic and nuclear $A\beta_{1-42}$ affects the mature miRNA pool, which targets and co-represses ROR1 and Vimentin.

Extending the idea that ncRNAs play a pivotal role in AD, the succeeding endeavour was to look at the aberrations in XIST expression and in some cases, a disruption of the X-Chromosome Inactivation as a whole in AD **(Chapter 6)**. Hence, the available

knowledge on the possible XIST involvement and deregulation from the perspective of molecular mechanisms governing NDDs was collated (in the form of a review article) with a primary focus on Alzheimer's disease. Preliminary investigation using mice and human AD cell model showed a strong deregulation of XIST expression. Possibilities of XIST mediated therapeutic intervention and linkages between XIC and preferential predisposition of females to AD have also been discussed.

Since the broad scope of this thesis encompassed Neurodegenerative Diseases (and just not AD), it was deemed prudent to investigate the involvement of other non-coding RNAs, especially long non-coding RNAs (lncRNA), in another NDD- Huntington's disease **(Chapter 7)**. Using small RNA sequencing and PCR arrays it was observed that the levels of 12 non-coding RNAs in HD mouse brain were perturbed, eight of which had human homologs. Of these, Meg3, Neat1, and Xist showed a consistent and significant increase in HD cell and animal models. Transient knock-down of Meg3 and Neat1 in cell models of HD led to a significant decrease of aggregates formed by mutant huntingtin **(Figure 8.4)** and downregulation of the endogenous Tp53 expression.

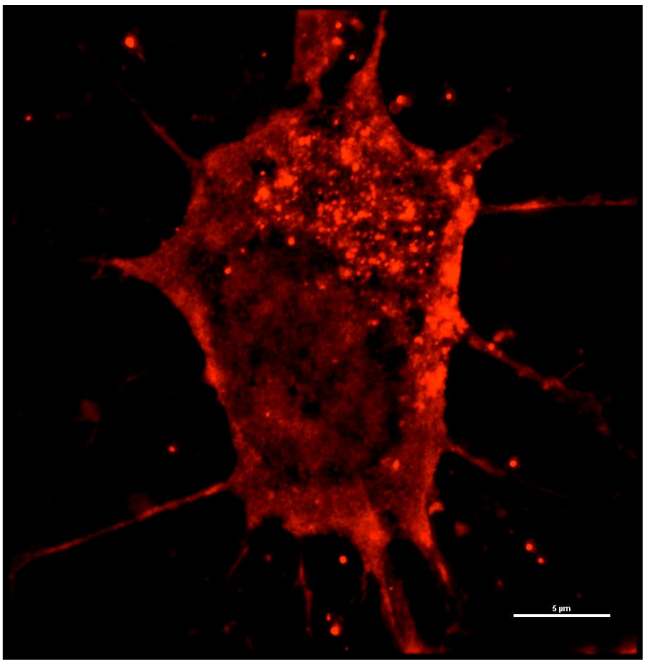

Figure 8.4: Intracellular aggregates of mutant Huntingtin.

Super resolution image of Neuro2a cells transfected with Htt- 83Q DsRed construct showing distinct cytosolic aggregates of huntingtin protein.

Scale bar = 5µm.

Inference at a glance:

- 6 miRNAs from NGS analysis (542-3p, 185-5p, 502-3p, 143-5p, 6824-3p and 501-3p) directly linked Aβ and Synaptic function.
- 4 novel miRNAs were unearthed from the validation sets (4697-3p, 3648, 3607-5p and 3117-3p) which target common RTKs (Eph, ErbB and IGF1R).
- 4 lncRNAs DLX6-AS1/EVF2, MALAT1, TUG1 and SNHG8 showing the most consistent pattern of deregulation, promises to be novel targets for AD research and possible intervention.
- MALAT1 was deregulated in cell and animal models of AD.
- MALAT1 interacted with and sponged miR-200a-3p, 26a-5p and 26b-5p. These 3 were up regulated in AD.
- These miRNAs repressed RTK EPHA2, which is down regulated in AD.
- Over expression of EPHA2 in presence of Aβ abrogated cellular cytotoxicity through the pro-survival CREB pathway.
- $A\beta_{1\text{-}42}$ deregulated the expression of RTK ROR1 and relevant cytoskeleton associated components.
- Over expression of ROR1 in presence of Aβ preserved cytoskeletal integrity and promoted neurite formation.
- Cytosolic $A\beta_{1\text{-}42}$ affected the mature miRNAs- miR-146a and miR-34a, which in turn repressed ROR1
- Nuclear $A\beta_{1\text{-}42}$ differentially regulated NEAT1, which in turn sponged the miRNAs.
- XIST was identified as a probable candidate involved in the early stages of AD using microarray data.
- XIST affected apoptosis in Aβ treated rat hippocampal neurons.
- XIST expression was up regulated in mouse tissues and mouse cell models of HD.
- XIST levels were experimentally found to be significantly up regulated in human and mouse cell models of AD (preliminary data).
- Several lncRNAs were deregulated in cell and mice models of HD from sequencing data.
- MEG3, NEAT1 and XIST showed the most uniform and strong deregulation in validation sets.
- Transient knockdown of MEG3 and NEAT1 decreased mutant Huntingtin aggregates in cell and stabilised Tp53 levels.

Summary

Proteomic alterations and small regulatory RNAs have been implicated in the pathogenesis of Alzheimer's disease (AD). The disrupted miRNA landscape (degradome) has been studied in AD mainly from the Aβ perspective. That Amyloid Precursor Protein C- terminal Domain (AICD) is involved in perturbing the cellular transcriptome has been reported, but its role in the degradome is still unexplored. The involvement of other long non-coding RNAs (lncRNA) is now under active scrutiny. In this discourse, using small RNA sequencing from an AD cell model, perturbations in the levels of 47 miRNAs were unearthed between the control and Aβ groups, and 26 between the control and AICD + Aβ (AD) groups. Using a novel bioinformatics pipeline, total of 263 differentially expressed lncRNAs were obtained in Aβ versus control group, and 41 deregulated lncRNAs in the AD versus control group. Effect of Aβ and AICD, individually and in combination, were validated with top regulated miRNA hits. Several of these miRNAs were found to target key Receptor Tyrosine Kinase (RTK) - many of which are implicated in AD. Additionally, using mice qPCR assays changes in the expression levels of 41 lncRNAs in AD mice were recorded, of which 7 have AD associations. Among these, MEG3 and MALAT1 showed consistent and significant decrease in AD models and human AD brain tissues, but MALAT1 showed a more pronounced decrease. Using a combination of bioinformatics and biochemical techniques, it was established that MALAT1 regulated miRNAs -200a, -26a and -26b, which are naturally elevated in AD. These, in turn, targeted the RTK EPHA2 and its downstream effectors. Intuitively, EPHA2 over expression protected against $A\beta_{1-42}$ cytotoxicity. Transiently knocking down MALAT1 validated these unique regulatory facets.

Cytoskeletal degradation and microtubule disruption are hallmarks of Alzheimer's disease (AD). Hence, the deregulation of ROR1, a microtubule associated Receptor

Tyrosine Kinase (RTK), was investigated, which revealed that it was significantly decreased in an $A\beta_{1-42}$ treated cell model of AD. A rescue experiment comprising of overexpressed ROR1 and $A\beta_{1-42}$ led to the recovery of key proteins like cleaved MAP2, SMA and Vimentin. Even in presence of $A\beta_{1-42}$, ROR1 preserved the actin cytoskeleton integrity, altered the dynamics of F: G actin and led to an increase in neurite numbers and length. Two miRNAs hsa-miR-146a and 34a were predicted to target ROR1. miR-146a and miR-34a were strongly upregulated in the cell model and their overexpression decreased ROR1 levels. Bioinformatics also predicted the interaction of miR-146a and miR-34a with lncRNA NEAT1, whose levels increased in mice AD brain tissues and human AD models concordantly. RIP followed by RT-PCR showed interaction between the miR-146a, miR-34a and NEAT1. Conversely, knocking down NEAT1 increased their levels.

As an extension of the lncRNA investigation, using NGS and low throughput PCR validation, the levels of 12 non-coding RNAs were found to be deregulated in HD mouse brain. Of these, Meg3, Neat1, and Xist showed a consistent and significant increase in HD cell and animal models. Transient knock-down of Meg3 and Neat1 in cell models of HD led to a significant decrease of aggregates formed by mutant huntingtin and downregulation of the endogenous Tp53 expression. Understanding the lncRNA topography, especially Meg3 and Neat1 functions in the context of HD pathogenesis is likely to open up new strategies to control the disease. Moreover, the available knowledge on the possible Xist involvement and deregulation, from the perspective of molecular mechanisms governing NDDs (with a primary focus on Alzheimer's disease), was collated in the form of a review. Possibilities of XIST mediated therapeutic intervention, linkages between XIC and preferential predisposition of females to AD have also been discussed.

Chapter 1: Exordium

1.1. Neurodegenerative diseases with a focus on Alzheimer's Disease

Neurodegenerative diseases (NDD) are the major contributors of age-related causes of mental disability on a global scale. Most NDDs, like Alzheimer's Disease (AD), are complex in nature – implying that they are multi-parametric both in terms of heterogeneous clinical outcomes and underlying molecular paradigms. They represent the most common form of neuropathology and are the causal agents for late age disabilities. In recent times, better food habits, targeted drugs and precise healthcare have significantly elevated the average life expectancy and hence, NDDs constitute the biggest threat. Alzheimer's disease (AD), Huntington's Disease (HD), Parkinson's Disease (PD), Amyotrophic lateral sclerosis (ALS) etc belong to this group and involve major motor and cognitive impairments, collectively affecting nearly half a billion individuals throughout the world, often leading to morbidity. The complex NDDs have multifactorial molecular mechanisms leading to gradual, irreversible loss of specific neuronal sub-populations [1], followed by gross neuronal impairments. The complexity of these NDDs makes therapeutic strategies against them a difficult, if not impossible task

Alzheimer's disease (AD), an irreversible neurodegenerative disorder, usually is an affliction in the elderly (Late Onset), although less than 10 percent of cases show early manifestation (Early Onset) [2, 3]. The disease is characterised by memory impairments (anterograde amnesia), cognitive defects like speech and language deficits, and a spectrum of behavioural problems [2, 3]. The two schools of thought as to the causality of AD includes the Amyloid Beta (Aβ) hypothesis leading to Amyloid plaques in brains of AD patients and the Neurofibrillary Tangle (NFT) hypothesis due to hyperphosphorylated Tau protein leading to neuronal structural damage [4] although researchers suggest that these two pathways could work in tandem to bring

about the AD pathophysiology. In recent years, core cellular processes like transcriptional dysregulation [5,6], axonal transport defects [7-9], Autophagy [10-12], Apoptosis [13-15], ER stress [16-18], disruption of mitochondrial dynamics [19] and LTP impairment [20, 21] have been implicated in AD.

1.2. Introduction to Receptor Tyrosine Kinase(s) and their roles in the brain

Receptor Tyrosine Kinases are high affinity, cell surface receptors for many polypeptide growth factors, cytokines, and hormones. RTK mediated signals play pivotal and diverse roles in the regulation of various physiological functions, ranging from cell proliferation, cell adhesion, cell migration, differentiation, survival, and apoptosis [22]. The human genome encodes 58 RTKs that are categorized into 20 subfamilies. These include nerve growth factor receptors (NGFR), tropomyosin-receptor-kinases (Trk) family receptors, epidermal growth factor receptors (EGFRs), fibroblast growth factor receptors (FGFR), glial cell-derived neurotrophic factor receptor (GFR), and the insulin and insulin-like growth factor receptor (IR and IGFR) **(Figure 1.1)** [23]. The identification of several new members of RTK provides unique insights into their broader specificity and largely overlapping signal transductions, coupled with their multiple roles in the nervous systems.

RTKs are characterised by four main domains: the extracellular ligand binding domain; the intracellular/cytoplasmic highly conserved catalytic protein tyrosine kinase domain which regulates intracellular signal transduction; the transmembrane domain that connects both intra and extracellular domains, the regulatory domain which contains kinase inserts, and sites for autophosphorylation. With the exception of IR and insulin like receptors (ILR), the activation of all RTK takes place *via* the lateral dimerization of their two cytoplasmic catalytic domains as a starting point and the subsequent intermolecular autophosphorylation upon binding to extracellular

ligands. The auto-phosphorylation of particular dimers of RTK in turn activates the signalling cascades to phosphorylate their corresponding cytoplasmic substrates **(Figure 1.2)** that regulate their physiological functions through various signalling pathways including the Ras/MAP and PI3 kinase pathways. Some proteins that interact with activated RTK function as adaptor proteins and lack intrinsic enzymatic activity of their own.

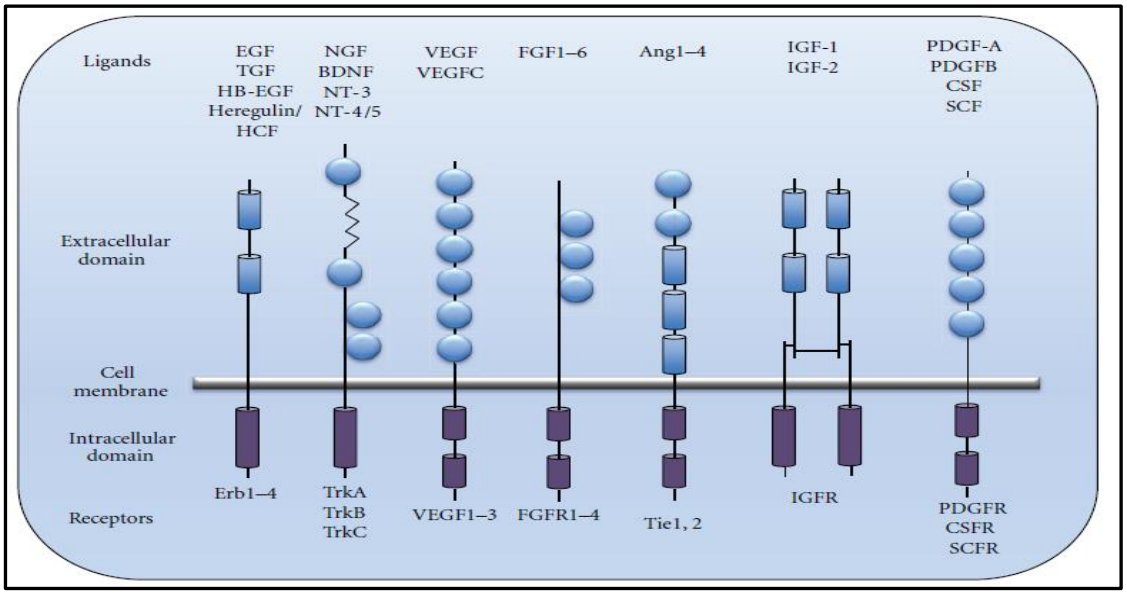

Figure 1.1: Different classes of RTK.

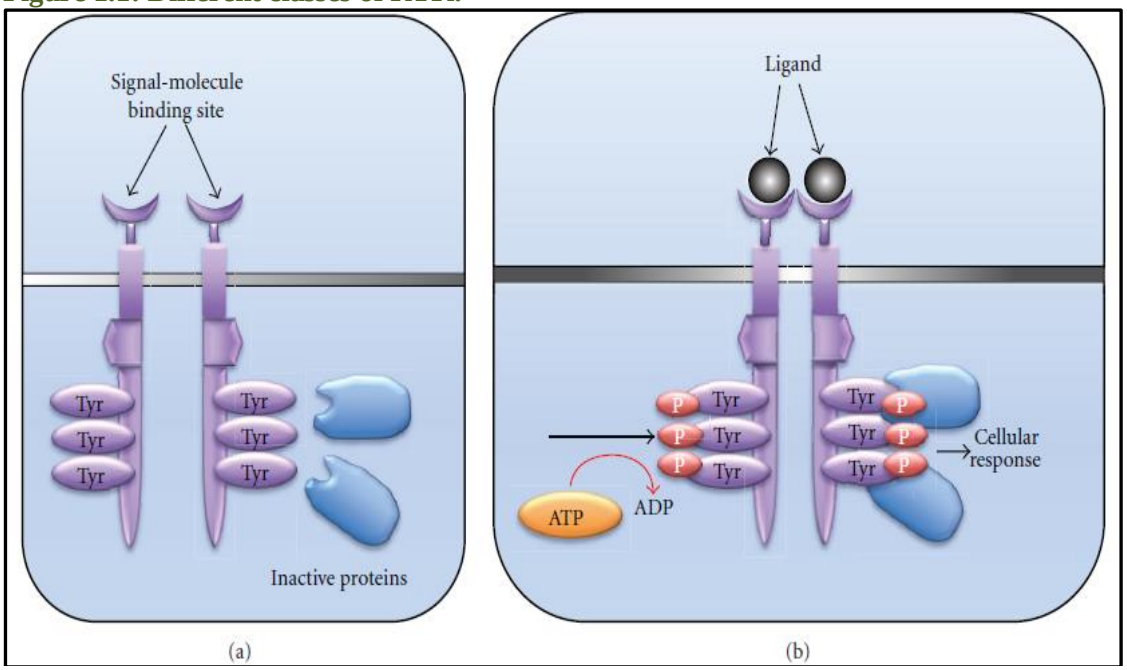

Figure 1.2: Activation of RTK signal transduction. (a) Inactive RTK are monomeric but after ligand binding dimerization of the extracellular domain occurs (b) and since cytoplasmic domains are juxtaposed, phosphorylation of tyrosine residues (ovals with

Tyr labels) is facilitated. Phosphorylation allows inactive proteins to interact with the tyrosine residues and elicit appropriate cellular responses. Adapted from Hubbard, 2004.

EGFR-mediated signalling pathways have been implicated in various neuromodulatory effects on several types of CNS neurons. These include hippocampal neurons, retinal ganglion cells (RGC) after CNS injury, and in the development of neurological disorders such as Alzheimer's disease [24].The expression of NGF, BDNF, NT- 3, and NT-4 has been detected in both neuronal somata and their axons in a wide variety of neurons including those in the cerebrum, cerebellum, and hippocampus [25]. However, they have different capacities in promoting relevant physiological functions. For example, BDNF, NT-4/5, and the TrkB-mediated signalling pathway shows the strongest axon outgrowth responses compared to NT-3 and NGF. How neurotrophins regulate these diverse biological effects in development and throughout life in the CNS is under intense investigation. More recently EphA4 receptor, also a subfamily of RTK has been implicated in CNS injury. The inhibition of EphA4 promotes axon regeneration and functional recovery by blocking astrocyte gliosis in spinal cord injury models and this receptor type may be subjected to considerable attention in future studies for the treatment of spinal cord injuries [26]. GDNF is a family member of the transforming growth factor-beta (TGF-β) super family and preferentially binds glycosylphosphatidylinositol (GPI)-anchored protein receptor (GFR), which is dynamically located on the plasma membrane. Initially GDNF was thought to play a survival-promoting role in CNS neurons, since it enhanced the survival of injured dopaminergic neurons, motor neurons, and RGC. It has been suggested that GDNF activates Muller cells to secrete growth factors and thereby promotes the survival of axotomized RGC [27]. CNTF, a potent survival factor for neurons and oligodendrocytes, elicits its signals after binding its receptor,

CNTFR, promoting neurotransmitter synthesis, neuronal survival, and neurite outgrowth in certain neuronal populations. Previous studies reported that CNTF stimulates neurite outgrowth from spinal cord neurons and the neurite growth promoting effects of CNTF, however, does not appear to be a consequence of its survival-promoting effect [28].

The effects of IGF-1 have also been studied in various neuronal populations. In one study, IGF-I gene delivery enhanced adult corticospinal neuron survival but failed to promote their axon regeneration after injury [29].

RTKs have been shown to govern critical aspects of neuronal development and physiology like axonal growth cone guidance, synaptic signal transduction, cell to cell communication, among others [30-32]. In the last decade, RTK-like orphan receptor (Ror) proteins have come into prominence governing crucial physiological and developmental aspects like motility, polarity determination, Wnt signalling modulation, skeletal and cardiac system development [33,34]. The Ror family comprises of ROR1, ROR2 and Ryk. Of these, ROR1 and ROR2 are specifically implicated in the process of neurite extension and neurogenesis - two events critical to establish neuronal network [35-37]. Transient knock down led to shorter neuritic processes whereas, their over expression led to formation of highly branched processes. MAP1B and MAP2, two critical microtubule associated proteins, were found to change significantly upon Ror intervention [38].

1.3. Linking Alzheimer's disease, the Amyloid Precursor Protein (APP) and RTK

APP is a type 1 transmembrane glycoprotein with a molecular weight of 110-135 kDa [39].It belongs to a protein family that includes APPL in Drosophila melanogaster [40], appa and appb in zebrafish[41] and APL-1 in *Caenorhabditis elegans* [42]. In

mammals there are, in addition to APP, APP-like proteins 1 and 2 (APLP1 and APLP2) [43].APP is expressed ubiquitously, albeit high in neurons, where it is found in the soma, axons and dendrites [44]. It shares large overlapping expression patterns with APLP2 during embryonic development and adulthood and is up regulated during neuronal maturation and differentiation [45]. Due to alternative splicing of the APP gene, which contains 19 exons, several isoforms ranging from 365 to 770 amino acids have been described in the literature. The most abundant isoforms are APP 695, APP751 and APP770, with APP695 being preferentially expressed in neurons [45]. As depicted in **Figure 1.3**, APP can be divided into three parts; a large extracellular N-terminus, a hydrophobic transmembrane domain and a short intracellular C-terminus [46]. Within the N-terminus there are two conserved regions, E1 and E2, which are shared among all APP family proteins and play an important role in their cis- and trans- dimerization. E1 can be divided into a heparin-binding/ growth factor-like domain (HBD1) and a metal (copper or zinc) binding domain (Cu/Zn BD). E2 contains a second heparin binding domain (HBD2) and a RERMS motif that shows tropic functions [45]. Between E1 and E2 there is an acidic region followed by a Kunitz protease inhibitor (KPI) domain, which is absent in the APP695 isoform. KPI is thought to enhance APP dimerization and alter APP trafficking and processing [47], which is consistent with the elevated levels of APP isoforms with a KPI domain found in AD patients [48].

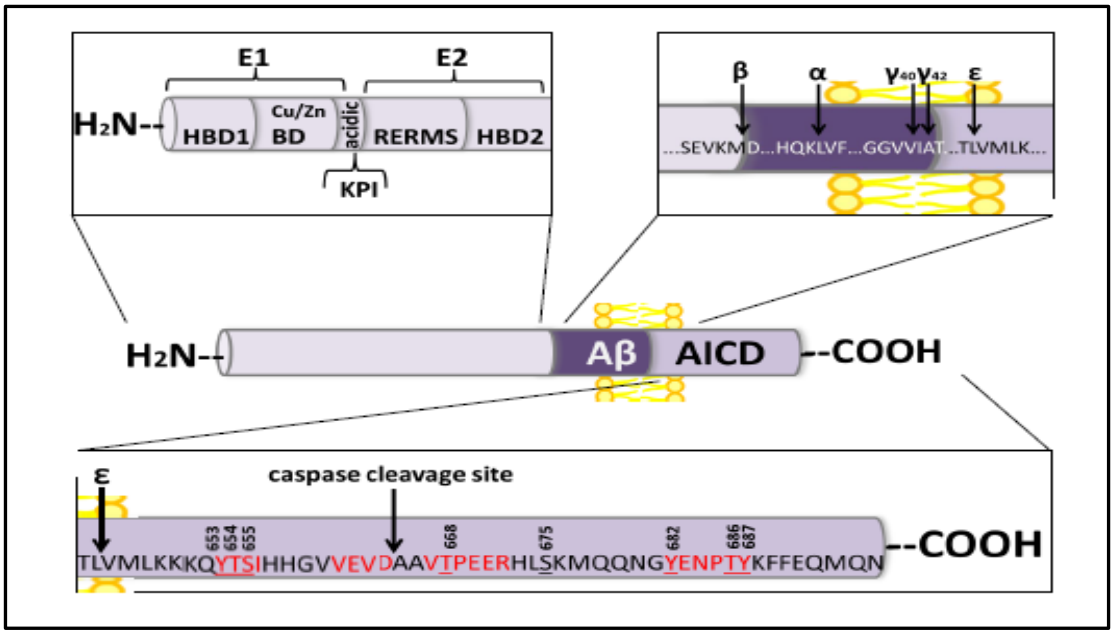

Figure 1.3: Schematic illustration of APP; N-terminal domains (upper left), the Aβ sequence (upper right) and the AICD sequence (lower). Cleavage sites are marked with arrows and C-terminal phosphorylation sites are numbered and underlined (APP695 numbering). Conserved sequences are marked in red.

Interestingly, the Aβ sequence is unique to APP (no other APP family member contains this region), whereas the C-terminus of APP is highly conserved among all APP family members [49]. When analysing the physiological functions of APP, it has to be considered that APP exists in different splicing variants. All of them undergo complex proteolytic processing, thereby generating numerous biologically active polypeptides. Furthermore, APP belongs to a gene family with partially overlapping and compensating functions, which was clearly shown by APP and APLP single, double or triple knock-out mice [50]. Several studies support APP playing an important role as an adhesion molecule. Contributing to cell-matrix adhesion, APP is able to bind different extracellular matrix components, and colocalizes with integrins on the surface of axons [45]. By the formation of homo and heterodimers, also with other APP family members, APP promotes cell-cell adhesion [45]. Regarding the secondary structure and cleavage pattern of APP, similarities to the cell surface

receptor Notch have been proposed. Indeed, APP was found to interact with several cell surface proteins like F-spondin, Reelin, Nogo-66 receptor, Notch2 and Netrin thereby influencing multiple cellular processes in the peripheral nervous system and CNS [51].

A beneficial role of full-length APP as well as its soluble form sAPPα was proposed in neurite outgrowth, synaptogenesis and the formation of synaptic boutons at neuromuscular junctions [52]. Nevertheless, synaptotoxic properties were also associated with APP through its different cleavage products [53]. Together, there is a large body of evidence for APP and its fragments being fundamental for neuronal development and maturation, many forms of cell adhesion, synaptogenesis, and neural plasticity. The underlying mechanisms and exact physiological functions of APP, however, remain undefined and need further investigation.

The two known proteolytic processing pathways of APP (**Figure 1.4**), have been named after their functional outcome, whether they lead to Aβ formation (amyloidogenic APP processing) or not (non-amyloidogenic APP processing). This way of protein processing, also termed regulated intramembrane proteolysis (RIP), basically consists of two events, a first cleavage in the extracellular domain (α- or β-cleavage) and a second in the transmembrane region of APP (γ-cleavage). In the amyloidogenic pathway the first cleavage is performed by β-secretase. The major neuronal β-secretase is β-site APP-cleaving enzyme 1 (BACE-1), a transmembraneaspartyl protease [54]. β-Cleavage generates an extracellular soluble sAPPβ fragment, which is then further processed to stimulate axonal pruning and neuronal cell death, and a membrane-tethered C-terminal fragment- β (CTF- β) or C99.In the non-amyloidogenic pathway in contrast, the initial cleavage is performed by α-secretase within the Aβ sequence. The α-secretase activity is executed by several

zinc metalloproteinases from the ADAM (a disintegrin and metalloproteinase) family, namely ADAM9, ADAM10 and ADAM17, among which ADAM10 is the main α-secretase [55]. α -Cleavage likewise sheds a soluble N-terminal fragment, sAPP α, which is reported to stimulate neurogenesis and neurite outgrowth, and a membrane-anchored CTF- α or C83.

While the soluble sAPP α and β are released into the extracellular space, CTF's are further processed by a second protease called γ-secretase, a high-molecular intramembrane protease complex that consists of four essential subunits, nicastrin, anterior pharynx defective 1, presenilin enhancer 2 and the catalytically active PS1 and PS2 Recently, another interesting component of γ- secretase has been identified, TMP21, which was shown to modulate γ -secretase activity, but does not influence ε -secretase activity [56].

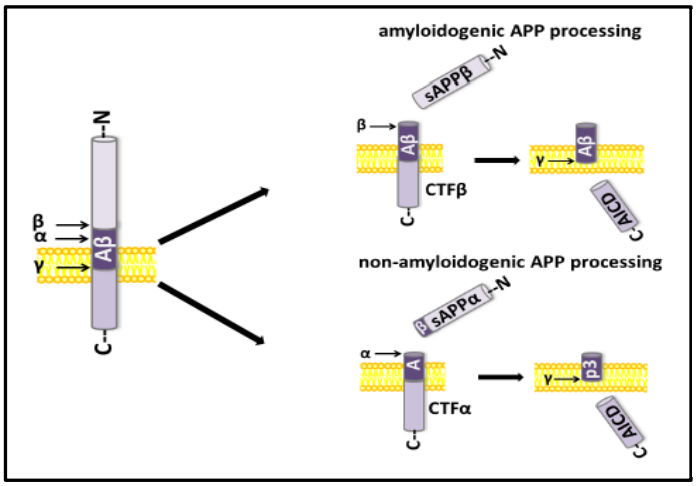

Figure 1.4: APP processing pathways; amyloidogenic (upper right) and non-amyloidogenic (lower right). Secretases are indicated with greek letters, α= α -secretase, β= β –secretase and γ= γ -secretase.

The γ-secretase complex cleaves APP intramembranously at multiple cleavage sites within the APP transmembrane domain [57,58]. The first cleavage of γ –secretase occurs at the so-called ε-site [59] and generates a C-terminal fragment termed APP intracellular domain (AICD) (**Figure 1.4**). The following more N-terminal cleavages of γ-secretase generate small peptides with a size around 4kDa (Aβ 37 to 43) in the amyloidogenic pathway or around 3kDa (p3 fragments) in the non-amyloidogenic

pathway. Keeping in mind all the events of APP processing, it is not surprising that approaches aiming to intervene in AD pathology target APP processing. In this context, γ -secretase modulators are promising therapeutic candidates, because they successfully inhibit Aβ42 production without altering Aβ40 levels [59]. A simplified overview of the APP trafficking pathways is shown in **Figure 1.5**. After its synthesis, APP moves along the common secretory pathway: endoplasmic reticulum (ER), Golgi apparatus, plasma membrane. In neurons, APP is transported from the cell body to the axon via the fast-anterograde microtubule-based pathway and localizes to the synapse (27). During the transport, that requires the binding of APP to the kinesin machinery, APP is proteolytically processed and modified [51]. In non-neuronal cells, cleavage by α-secretase takes place at the plasma membrane, β-cleavage is predominantly observed during endocytosis/APP recycling in endosomes and γ-secretase-mediated cleavage is believed to occur at both plasma membrane and intracellular compartments including ER, Golgi and endosomes [60]. Therefore, the majority of Aβ is produced in endocytic vesicles and the Golgi and some of Aβ is released via exosomes [46].

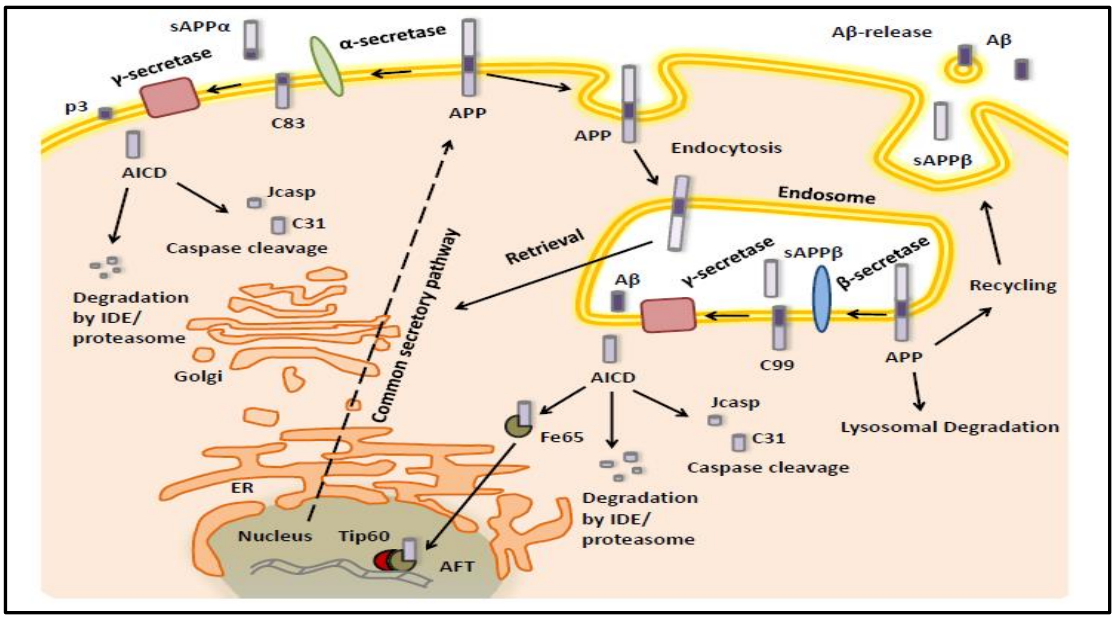

Figure 1.5: Schematic overview showing APP trafficking pathways and cleavage.

Protein phosphorylation, a common PTM, has been extensively studied in a broad range of different contexts. It has been found to be crucial in the regulation of many biological processes such as cell signalling pathways or protein-protein interactions. Deregulated phosphorylation has been implicated in many diseases including AD [61]. Phosphorylation refers to the covalent attachment of a phosphate group from an energy-rich substrate, often Adenosine-5'-triphosphate (ATP), to specific amino acid residues by a kinase. The three standard amino acids that can be phosphorylated are tyrosine, serine and threonine with serine being the most frequently phosphorylated (about 87% compared to threonine 11% and tyrosine 2%) [62]. In the sequence of APP, there are several potential phosphorylation sites. Among the eight potential phosphorylation sites within the intracellular C-terminal AICD sequence, seven (Y653, S665, T668, S675, Y682, T686 and Y687) have been found to be phosphorylated in AD patients in a neuron-specific manner [63]. Additionally, T654 as well as other phosphorylation sites have been found to be phosphorylated in several model organisms such as the rat or mouse [64]. An overview of the kinases involved in APP C-terminal phosphorylation is given in **Table 1.1**. Since most of these sites are located within conserved regions that are known to be important for APP and AICD interaction with adaptor proteins, it has been proposed, that phosphorylation may modulate their binding affinity, thereby influencing multiple downstream processes. Further functional outcomes of phosphorylation may include the regulation of subcellular trafficking, proteolytic processing and the activation or inactivation of physiological or pathological pathways.

RESIDUE	PHOSPHORYLATED BY
T653	Unknown.
T654	PKC, Cdc2, CaMKII, GSK3, JNK.
S665	PKC, Cdc2, CaMKII, APP kinase I, GSK3, JNK.
T668	PKC, Cdc2, Cdk5, CaMKII, , GSK3, JNK, DYRK1A.
S675	Unknown.
Y682	cAbl, Src, TrkA.
T686	Unknown.
Y687	Unknown.

Table 1.1: Summary of potential phosphorylation sites within the AICD sequence and their corresponding kinases) if known. PKC= protein kinase C, Cdc2= Cdc2 protein kinase (homologue of Cdk5), CaMKII=calcium/calmodulin-dependent protein kinase II, Cdk5= cyclin-dependent protein kinase 5, GSK3= glycogen synthase kinase-3, JNK= c-jun amino-terminal kinase, DYRK1A= Dual-specificity tyrosine-phosphorylation regulated kinase 1A, c-Abl= Abelson tyrosine kinase, Src= Src tyrosine kinase, TrkA= Tyrosine kinase A.

1.4. Central role of APP, AICD and Aβ in Alzheimer's disease

Studies of familial EOAD uncovered genetic links between the APP gene and AD [64]. APP is processed into smaller peptide fragments, one of which is Aβ, via cleavage by α-, β- and γ-secretases. Importantly, EOAD-linked point mutations were identified not only in APP itself but also in presenilin-1 (PSEN1) and presenilin-2 (PSEN2) [65] the key catalytic subunits of γ-secretase, known to cleave APP (Figure 5). No known AD-causing mutations are present in the gene encoding the β-secretase gene, beta-site APP cleaving enzyme 1(BACE1). The genetic mutations are reasoned

to cause AD through aberrant processing of APP, leading to either increased levels of Aβ or an increased production of the 42 and 43 amino acid forms of Aβ (Aβ42/Aβ43) over the 40 amino acid form of Aβ (Aβ40). It is argued this triggers aggregation of Aβ. The discovery that transgenic mice expressing familial human APP and PSEN mutations recapitulate many, but not all, of the features of the human disease [65] further established the link between aberrant Aβ production and the AD phenotype. This latter discovery, perhaps more than any other, tied the field to the amyloid hypothesis for the next decades. The conclusions of the aforementioned studies were grounded in an unquestioned assumption that Aβ, rather than altered expression of APP or its products, causes AD pathology. The assumption arose because Aβ was the key component of plaques and because Aβ caused neurotoxicity in healthy cells. Further, hyperphosphorylation of tau, thought to be downstream of Aβ, was seen as a critical mediator of the neurotoxic effects of Aβ [66] placing Aβ at the top of the pathological chain of AD events. A cycle thus began to develop early whereby studies were designed and then interpreted on the basis of the hypothesis that Aβ caused AD pathology, rather than being critically evaluated in the context of a range of possible interpretations. Further, given the impact discoveries of mutations in APP, PSEN1 and PSEN2 have had in driving the amyloid theory, it is notable that, while these mutations account for the majority of EOAD cases, EOAD only comprises less than 5% of all AD cases [67]. In fact, the majority of AD cases are sporadic, idiopathic LOAD. It seems in retrospect presumptive to have extrapolated a role for Aβ in all AD based on the genetic evidence suggesting a role for altered APP processing in EOAD. In general, the risk genes identified for LOAD are subtle, with no direct genetic association to the APP gene or its processing enzymes. The most well-known genetic link to LOAD is the apolipoprotein genotype ε4 (APOE4) [68]. Recently

another strong risk gene for LOAD was identified, a variant of the triggering receptor expressed on myeloid cells 2 gene (TREM2), implicating excessive innate immunity in Alzheimer's pathogenesis [69]. Although these two mutations have been the strongest to date, many more have been associated with LOAD.

Based on these observations, the Amyloid Cascade hypothesis was formulated which states that amyloid-beta (Aβ), in a variety of forms, triggers a cascade harming synapses and ultimately neurons, producing the pathological presentations of Aβ plaques, tau tangles, synapse loss and neurodegeneration, leading to dementia. Aβ accumulation is thought to initiate AD pathology by destroying synapses, causing formation of NFTs, and subsequently inducing neuron loss (**Figure 1.6**). Although some changes to the hypothesis have occurred since the original publications, notably a shift toward defining soluble Aβ oligomers as the toxic agent, rather than plaques, the theory and the way data is interpreted have remained largely the same, i.e. Aβ accumulation as oligomers or plaques triggers AD. A large, growing literature espouses the amyloid hypothesis.

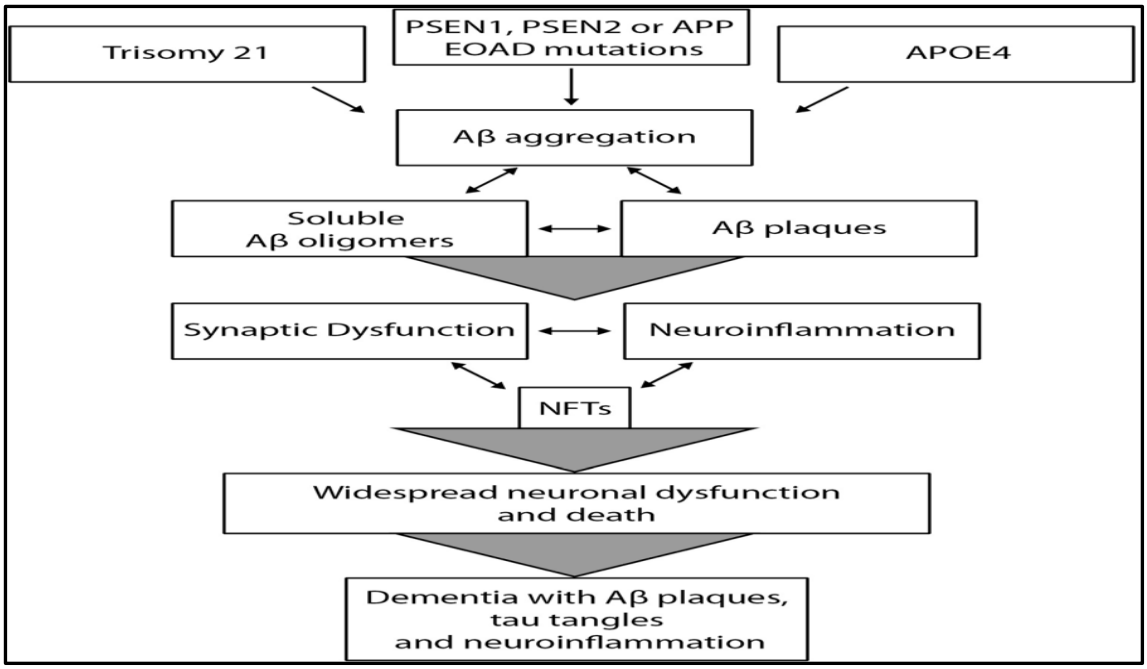

Figure 1.6: The Amyloid Hypothesis.

The Food and Drug Administration (FDA) has over the years approved five drugs for AD; Donepzil, Galantamine, Memantine, Rivastigimine and Tacrine. It is notable that each of these are unrelated to the amyloid hypothesis and were not tested in transgenic AD mice before being used in the clinic. Meanwhile, many anti-amyloid treatments that were tested in mice have completed, or are undergoing, extensive clinical trials in humans. They are divided into those directly targeting Aβ by active and passive immunization, those targeting inhibition or modulation of the γ-secretase APP cleaving enzyme presenilin, and those targeting the APP β-secretase cleavage enzyme BACE1. So far, anti-Aβ treatments have broadly failed to meet their primary clinical endpoints and some major phase 3 trials were halted early. None of the tested treatments have produced a discernible functional recovery, or altered the course of disease. In fact, alarmingly some, specifically inhibitors of γ-secretase, lead to an increased decline in cognition. With each successive failure the validity and foundations of the amyloid hypothesis, on which these drugs have been based, is called increasingly into question. A 'presenilin hypothesis' of AD has been articulated [70]. It was suggested that presenilin mutations fit best within a hypothesis that AD is a disease driven by synapse loss. Though the AD literature has largely focused on the role of PSEN1 in APP cleavage, presenilin mutations affect a range of proteins and therefore processes, particularly those involved in synaptic function. Given that presenilin appears important for cleaving proteins that are crucial at synapses, presenilin mutations would lead to synaptic dysfunction. It would also follow that drugs targeting presenilin in humans are destined to have profound detrimental effects on the brain with long term use. This indeed was the result of recent clinical trials of presenilin antagonists, also termed γ-secretase inhibitors.

1.5. Comprehending the complexity of APP biology independently of Aβ to dissect AD pathology

APP synthesis, trafficking and cleavage are complex and highly regulated processes. It is important to recognise that familial AD-APP and presenilin mutations may not only impact Aβ production, but also the production of the other peptides produced from APP including sAPPα, sAPPβ, p3 and AICD, as well as the relative levels of full-length APP. Interestingly, over expression of AICD can cause an AD-like phenotype, whilst increased cleavage of sAPPβ is associated with familial Danish Dementia with similar aetiology to AD [71]. Furthermore, lowered levels of neurotrophic sAPPα are seen in AD, and mutations which inhibit the α-secretase enzyme ADAM10, which liberates sAPPα from its precursor, are found in the promoter region and coding sequence of some individuals with AD [72]. Depletion of sAPPα by inhibition of ADAM10 trafficking can bring about sporadic AD phenotypes [73], corroborating an independent role for APP cleavage products other than Aβ in bringing about disease phenotypes. Whilst the functions of p3 and sAPPβ are little explored (which in itself is a remarkable reflection of the intense focus on Aβ at the expense of other cleavage products of APP), a wealth of evidence exists for physiological functions of sAPPα, Aβ, AICD and full-length APP [74]. These studies raise questions as to whether familial AD driven by presenilin and APP mutations is primarily a result of aberrant Aβ expression, or if it is in fact a result of altered APP cleavage, and the resultant effects of altered APP cleavage on sAPPα, sAPPβ, Aβ, AICD, p3 and full-length APP. This brief discussion does not even approach the possible physiological functions of C83, C99, the different functions of the multiple isoforms of APP including APP695, APP751 and APP770, or the highly homologous

proteins to APP, APLP1 and APLP2, which are also physiologically expressed in the human brain and may serve redundant functions with APP proteins.

Of all the proteins that are being targeted by the ncRNAs, the importance of membrane proteins (or their fragments) like Amyloid Precursor Protein C- terminal Domain (AICD) and Receptor Tyrosine Kinase (RTK) are gaining ground in AD research, over the last decade. The Interactomes of AICD, both in phosphorylated and unphosphorylated conditions are well known [75, 76], and their roles in transcriptional transactivation have been well studied [77, 78]. Besides that, AICD targets key regulatory proteins affecting cellular physiology like GSK-3β, p53 and EGFR [79, 80, and 81]. Direct effect of AICD on GSK-3β and p53 manifests in cells via the apoptotic pathway, involving other key proteins like caspases and bax [82, 83]. A body of evidence suggests that the AICD/FE65 complex is integral for neuron development and plasticity [84, 85, 86]. It was previously shown that the proteins that are being deregulated by AICD are mostly involved in signalling and cytoskeleton stability [87] besides some key cellular receptors like PTCH1 and TRPC5 [88]. The interaction of AICD with the cellular adaptor protein Grb2 and its functional consequences has also been exhaustively characterised [89, 90]. Overall, the role of AICD in cellular health is well established, despite antagonistic data about its protective/toxic role.

1.6. Search of new molecular players governing AD.

As evident from the above discussion, the inadequacy of the amyloid cascade hypothesis and the idea that more than just proteins or their processing thereof governs AD shifted the paradigm of AD research to newer avenues, notably, the small regulatory RNAs. For the present thesis work, I focussed on two such regulatory ncRNAs – micro RNA (miRNA) and long non-coding RNA (lncRNA).

1.6.1. MicroRNAs in Alzheimer's disease

One important class of gene expression regulators is miRNAs [91]. These short (~21–23 nucleotides) conserved non-protein-coding RNAs are transcribed from the genome [92]. In mammals, one thousand miRNAs have been identified (www.mirbase.org). Approximately one-third of miRNA genes are located within protein-coding messenger RNAs (mRNAs), while the remaining genes are intergenic [93]. Successive processing of the miRNA precursor molecule generates a single-stranded miRNA that is able to interact with complementary mRNA sequences in the 3′UTR of genes [94]. The binding of the miRNA to its target mRNA results in either translational repression or degradation of the target [94]. In 2007, Walter J. Lukiw used small-scale profiling studies to provide the first clues into miRNA changes in AD. Since then, several groups, including the Lukiw laboratory, have performed large-scale genome-wide studies demonstrating that miRNA expression patterns are altered not only in the AD brain but also in blood and cerebrospinal fluid (CSF) [95]. Nevertheless, it remains difficult to predict whether these changes are a cause or a consequence of the neurodegenerative process and dementia. As discussed in detail elsewhere [96], further validation is required; however, these observations open the door to novel diagnostic and possibly therapeutic tools for AD. The most recent profiling data show that a subset of miRNAs seems to be specifically altered in the AD brain. These "AD-specific" miRNAs include miR-29, miR-15, miR-107, miR-181, miR-146, miR-9, miR-101 and miR-106, all of which have been independently validated in two or more studies. Interestingly, several of these candidates might play a direct role in modulating the expression and/or processing of AD-related genes, such as APP, BACE1 and MAPT (which encodes for Tau). An overview of each miRNA and their putative role(s) in AD pathophysiology (**Table 1.2**).

MicroRNA	Expression alterations in AD	Target genes	Related pathways to AD	Possible consequence on AD development
miR-29	Down regulated	BIM, BMF, HRK, Puma	Apoptosis	Increased # of apoptotic markers
		BACE1	APP processing	Increased Aβ production
miR-15	Down regulated	Bcl-2	Apoptosis	Increased # of apoptotic markers
		ERK1	Tau posttranslational modification	Increased Tau pathology
miR-107	Down regulated	BACE1	APP processing	Increased Aβ production
		Cofilin	Actin processing	Increased # of rod like structures
		CDK6	Cell cycle arrest	Increased cell cycle re-entry
		Dicer	MicroRNA processing	Altered microRNA processing
miR-181	Down regulated	ATM	Defense against DNA damage	Increased DNA damage
miR-146	Up/down regulated	RANTES, IRAK1	Inflammation	Altered inflammation response
miR-9	Up/down regulated	Neurofilament H	Axonal conduction	Altered axonal conductance
		SIRT1	Tau posttranslational modification	Increased Tau pathology
miR-101	Down regulated	APP	APP expression regulation	Increased APP expression/increased Aβ production
		COX2	Inflammation	Altered inflammation response
		MAGI2	Tau posttranslational modification	Increased Tau pathology
miR-106	Down regulated	Rb1, p21	Cell cycle regulation	Altered cell cycle regulation
		APP	APP expression regulation	Increased APP expression/increased Aβ production
		p73	Tau posttranslational modification/apoptosis	Increased Tau pathology/increased # of apoptotic markers
		p62	Autophagy	Altered Aβ clearance

Table 1.2: MicroRNAs alterations in AD and possible effects on disease.

miRNAs are of particular interest for the understanding of complex disorders, such as AD,

because they can potentially regulate several pathways involved in disease progression. Current literature as well as bioinformatics predictions suggests that miRNAs could function either upstream, concomitantly, or downstream of Aβ and Tau pathologies to coordinate the cascade of events leading to the severe

neurodegeneration observed in AD patients. Other studies also implicate miRNAs, for instance miR-34, directly in memory consolidation [97]. In addition, the role of mutations in miRNA genes themselves have not yet explored, which are increasingly associated with human disease. Interestingly, a number of polymorphisms have been identified in or near the miR-29a/b-1 cluster, and individuals carrying both risk genotypes rs535860 (in BACE1 3′UTR) and rs34772568 (near miR-29 genes) exhibited a decreased risk for AD [98].

Additionally, in the recent past, several miRNAs have been identified to be key modulators of cellular cytoskeleton circuitry. miR-142 affects the critical proteins required for the cytoskeleton dynamics in mature megakaryocytes [99] targeting several actin cytoskeleton-associated proteins, like Cofilin-2 (Cfl2), Glucocorticoid receptor DNA binding factor 1 (Grlf1), Biorientation of chromosomes in cell division 1 (Bod1), Integrin alpha V (ItgaV) among others. miR-34-5p is found to regulate the expression of cytoskeleton genes during early insect development and segmentation [100]. Increased miR-155 levels in human endothelial cells affects the morphology and filamentous (F)-actin organization and the molecule targets EC cytoskeleton components RhoA and myosin light chain kinase (MYLK) [101]. Several other miRNAs also target key proteins in AD, like miR-106a, miR-106b, miR-520c, miR-101 and miR-153 directly target Amyloid Precursor Protein and control Aβ levels; miR-29a/b/c, miR-107, miR-195 and miR- 124 targets BACE1, thereby regulating the intramembrane cleavage of APP; miR-132 targets Tau; miR-34a targets TREM2 and miR-146a targets a critical component of actin modulator, ROCK1 [102]. It is interesting to note that miR-146a, implicated in AD, also affects the actin dynamics by targeting RhoA [103]. Similarly, miR-34a which regulates RhoA/Rac1 levels [104] has a strong correlation to AD.

1.6.2. LncRNAs in Neurodegeneration

Long non-coding RNAs (long ncRNAs, lncRNA) are non-protein coding transcripts longer than 200 nucleotides. This somewhat arbitrary limit distinguishes long ncRNAs from small regulatory RNAs such as microRNAs (miRNAs), short interfering RNAs (siRNAs), Piwi-interacting RNAs (piRNAs), small nucleolar RNAs (snoRNAs), and other short RNAs. lncRNAs are RNA molecules that may function as either primary or spliced transcripts and not belong to the known classes of small RNAs in one category, and structural RNAs in the other [105]. This definition implies the lncRNAs can have either coding or noncoding characteristic, however, the definition immensely enlarges the number of lncRNAs, some RNAs which may not know so far are falsely classified as lncRNAs. The latest definition proposed by HUGO Gene Nomenclature Committee (HGNC) describes lncRNAs as spliced, capped, and polyadenylated RNAs [106].

lncRNAs have broad spectrum of functions involved in almost every aspect of the biological process, from chromatin structure to the protein level. Although the full functions of lncRNAs are not yet clearly defined, the paradigms of how lncRNAs function have been well summarized by Wilusz et al. (2009) [107]. Their possible roles in cell physiology are described as: (I) signals for integrating temporal, spatial, developmental and stimulus-specific cellular information; (II) decoys with the ability to sequester a range of RNA and protein molecules, thereby inhibiting their functions; (III) guides for genomic site-specific and more widespread recruitment of transcriptional and epigenetic regulatory factors; (IV) scaffolds for macromolecular assemblies with varied functions. The specific functions of a single lncRNA may belong to any or combined roles which are determined by many elements, such as the tissue specific, and the physiological status of cells [105].

A summary of several lncRNA along with their disease associations, dysregulation and known biological functions are summarized in the table below **(Table 1.3).**

lncRNAS	DESCRIPTION	DISEASE ASSOCIATED	DOWN OR UP	BIOLOGICAL FUNCTION
Sox2OT	As a biomarker of neurodegeneration	AD and PD	Up	Regulate co-transcribed Sox2 gene expression to down neurogenesis
1810014B01Rik	Sever as the biomarker of neurodegeneration	AD and PD	Up	The function of 1810014B01Rik is not known yet
BC200	Homologous with rodent BC1 lncRNA, the earliest specific example showed lncRNAs conservation	AD and PD	Soma: Up Dendritic: Down	Modulate local proteins in postsynaptic dendritic microdomains to maintenance of long-term synaptic plasticity
BACE1-AS	Transcribe from the Antisense protein-coding BACE 1gene	AD	Up	Increase BACE1 mRNA stability resulting additional Aβ42 generation through a post-transcriptional feed-forward mechanism
NAT-Rad18	Transcribed from the antisense of protein coding gene Rad18	AD	Up	Down the expression of DNA repair protein Rad18 resulting the neuron more sensitive to apoptosis
17A	Embedded in the human G-protein-coupled receptor 51 gene	AD	Up	Impair GABAB signaling pathway by decreasing GABAB R2 transcription
GDNFOS	Transcribed from the opposite strand of GDNF gene only in primate genomes, with different isoforms.	AD	Deregulated/differences in tissue expression patterns	Modulate the expression of endogenous GDNF inhuman brain

Table 1.3: lncRNAs implicated in Neurodegeneration.

Of late lncRNAs have emerged as the regulator of key cellular processes like cellular homeostasis [108], transcription [109, 110] among others, possibly by interacting with proteins and RNA [111]. Three key lncRNAs have been extensively studied and characterised in AD, namely - BACE1-AS, BC200 and 17A. BACE1-AS is antisense to the BACE1 gene and is highly expressed in the AD brain on exposure to $A\beta_{1-42}$. BC200 is exclusive to neuronal synapses and down regulated in the prefrontal cortex normally but significantly increased in the AD brain. The lncRNA 17A gets its activation cue from the inflammatory reaction in the brain of AD patients and in turn increases Aβ secretion and the $A\beta_{42}/A\beta_{40}$ ratio, ameliorating the disease. [112-114]. In the last few years, the lncRNA MALAT1 (metastasis-associated lung adenocarcinoma transcript 1) has come to the forefront of ncRNA research due to its implication in a wide variety of physiological and pathological functions. MALAT1 is abundant and evolutionarily conserved in mammals. Originally investigated from a cancer perspective, MALAT1 is up regulated in a plethora of cancer subtypes [115]. It has also been found to promote dendrite maturation and synaptogenesis in cultured hippocampal neurons [116]. Very recently, MALAT1 was implicated in retinal neurodegeneration acting via the CREB pathway [117] and the authors reported lower MALAT1 levels in the CSF of AD patients. The contrasting outcomes in AD (degenerative) and Cancer (proliferative) [118, 119], and the involvement of MALAT1 in both, demands further investigation.

Besides Aβ oligomers, RTK signalling and miRNA mediated regulations, an emerging subset of long non-coding RNAs (lncRNAs) have been implicated in governing the cytoskeleton. lncRNA Down-regulated in hepatocellular carcinoma (*Dreh)* regulates vimentin, changing the cytoskeleton structure and cell morphology in cancer cells [120, 121]. LINC00152 alters the F-actin dynamics by perturbing the

levels of GOLPH3 [122, 123]. GAS5 suppresses glioma proliferation, migration and invasion by sponging miR-222. MiR-222 in turn is implicated in cofilin dephosphorylation [124, 125]. UCA1 regulates hsa-miR-145–ZEB1/2– FSCN1 pathway in bladder cancer [126]. Apart from directly exerting effects on the cytoskeleton, several lncRNAs act indirectly via the small GTPases Rho, Rac1 and Cdc42. LncRNA LERFS (lowly expressed in rheumatoid fibroblast-like synoviocytes) quenches RhoA, Rac1, and Cdc42 in fibroblast-like synoviocytes [127]. PCGEM1 (prostate cancer gene expression marker 1) and TBILA (TGFβ-induced lncRNA) activates RhoA [128, 129]. LncRNA TUNAR (neural differentiation-associated RNA) sponges miR-200a which suppresses the expression of Rac1 [130]. The lncRNA H19 and SNHG15 (small nucleolar RNA host gene 15) upregulate Cdc42 expression by acting as buffers for associated miRNAs [131, 132]. In recent times Nuclear Enriched Abundant Transcript 1 (NEAT1) has come to the forefront of research. Originally discovered as a virus inducible RNA [133], NEAT1 is specifically located in the nuclear substructures called paraspeckles, and is essential for their formation and maintenance [134, 135]. Of late, NEAT1 has been implicated in several types of cancers, including, but not limited to ovarian, prostrate, non-small lung, breast and hepatocellular carcinoma [136- 140]. Apart from diverse carcinogenesis, NEAT1 has also been studied in several neurodegenerative scenarios namely Fronto-temporal dementia, Amyotrophic lateral sclerosis, Huntington's disease and Parkinson's disease [141- 144]. Although the exact mechanism of action is unknown, research suggests that interaction of NEAT1 with associated miRNAs could be one paradigm which governs disease pathology. Such regulatory networks have been reported involving NEAT1 in Alzheimer's disease as well [145, 146], but the knowledge is rudimentary.

At this backdrop it can be proposed that several miRNAs and lncRNAs are significantly and uniformly deregulated in cell models of AD, where both Aβ and AICD have their effects. One could posit that such deregulation could potentially affect their interacting components in tandem, ending at the level of RTKs.

1.7. Objective of the thesis

The specific aims of the present study are to

(i) Look at the differentially regulated miRNAs and lncRNAs in AD models using NGS;

(ii) Identify and validate the top miRNAs that are affected upon differential exposures to AICD or Aβ or AICD + Aβ both;

(iii) Identify the RTK targets of the aforesaid ncRNAs **(Chapter 3)**;

(iv) To access the expression levels of lncRNA MALAT1 using AD mice, cell models and brain tissues from an AD patient;

(v) To identify and validate miRNA interacting partners of MALAT1 and their status in AD;

(vi) To identify and validate the protein targets of MALAT1 interacting miRNAs, specifically focussing on RTKs;

(vii) To delineate the regulatory roles of those RTKs in AD **(Chapter 4)**;

(viii) Access the levels of ROR1 in an AD cell model,

(ix) Identify and validate miRNA repressors of ROR1 and their status in AD,

(x) Identify and validate the lncRNAs associated with ROR1 miRNAs, and

(xi) To functionally link the lncRNA-miRNA-RTK regulatory network in AD **(Chapter 5)**.

Since the preliminary focus of this thesis is Alzheimer's Disease, the analysis of non-coding transcriptome in Huntington's Disease **(Chapter 7)** and delineating the XIST, X Chromosome Inactivation and AD connection **(Chapter 6)** have been included as standalone chapters.

1.8. References

[1]. Pringsheim, T., Fiest, K., & Jette, N. (2014). The international incidence and prevalence of neurologic conditions: How common are they? Neurology, 83(18), 1661–1664.doi:10.1212/wnl.0000000000000929.

[2]. Mendez MF. Early-onset Alzheimer's disease: non amnestic subtypes and type 2AD. Arch Med Res. 2012 Nov;43(8):677-85. doi: 10.1016/j.arcmed.2012.11.009. Epub 2012 Nov 21. Review. PubMed PMID: 23178565; PubMed Central PMCID: PMC3532551.

[3]. Ballard C, Gauthier S, Corbett A, Brayne C, Aarsland D, Jones E. Alzheimer's disease. Lancet. 2011 Mar 19;377(9770):1019-31. doi: 10.1016/S0140-6736(10)61349-9. Epub 2011 Mar 1. Review. PubMed PMID: 21371747.

[4]. Small SA, Duff K. Linking Abeta and tau in late-onset Alzheimer's disease: a dual pathway hypothesis. Neuron. 2008 Nov 26;60(4):534-42. doi: 10.1016/j.neuron.2008.11.007. Review. PubMed PMID: 19038212; PubMed Central PMCID: PMC2692134.

[5]. Meng G, Mei H. Transcriptional Dysregulation Study Reveals a Core Network Involving the Progression of Alzheimer's Disease. Front Aging Neurosci. 2019 May 7; 11:101. doi: 10.3389/fnagi.2019.00101. eCollection 2019. PubMed PMID: 31133844; PubMed Central PMCID: PMC6513962.

[6]. Citron BA, Dennis JS, Zeitlin RS, Echeverria V. Transcription factor Sp1 dysregulation in Alzheimer's disease. J Neurosci Res. 2008 Aug 15;86(11):2499-504. doi: 10.1002/jnr.21695. PubMed PMID: 18449948.

[7]. Wang ZX, Tan L, Yu JT. Axonal transport defects in Alzheimer's disease. Mol Neurobiol. 2015;51(3):1309-21. doi: 10.1007/s12035-014-8810-x. Epub 2014 Jul 23. Review. PubMed PMID: 25052480.

[8]. Mórotz GM, Glennon EB, Gomez-Suaga P, Lau DHW, Robinson ED, Sedlák É, Vagnoni A, Noble W, Miller CCJ. LMTK2 binds to kinesin light chains to mediate anterograde axonal transport of cdk5/p35 and LMTK2 levels are reduced in Alzheimer's disease brains. Acta Neuropathol Commun. 2019 May 8;7(1):73. doi: 10.1186/s40478-019-0715-5. PubMed PMID: 31068217; PubMed Central PMCID: PMC6505310.

[9]. Gadhave K, Bolshette N, Ahire A, Pardeshi R, Thakur K, Trandafir C, Istrate A, Ahmed S, Lahkar M, Muresanu DF, Balea M. The ubiquitin proteasomal system: a potential target for the management of Alzheimer's disease. J Cell Mol Med. 2016 Jul;20(7):1392-407. doi: 10.1111/jcmm.12817. Epub 2016 Mar 29. Review. PubMed PMID: 27028664; PubMed Central PMCID: PMC4929298.

[10]. Uddin MS, Stachowiak A, Mamun AA, Tzvetkov NT, Takeda S, Atanasov AG, Bergantin LB, Abdel-Daim MM, Stankiewicz AM. Autophagy and Alzheimer's Disease: From Molecular Mechanisms to Therapeutic Implications. Front Aging Neurosci. 2018 Jan 30; 10:04. doi: 10.3389/fnagi.2018.00004. eCollection 2018. Review. PubMed PMID: 29441009; PubMed Central PMCID: PMC5797541.

[11]. Zeng Q, Siu W, Li L, Jin Y, Liang S, Cao M, Ma M, Wu Z. Autophagy in Alzheimer's disease and promising modulatory effects of herbal medicine. Exp Gerontol. 2019 May; 119:100-110. doi: 10.1016/j.exger.2019.01.027. Epub 2019 Jan 30. Review. PubMed PMID: 30710681.

[12]. Liu J, Li L. Targeting Autophagy for the Treatment of Alzheimer's Disease: Challenges and Opportunities. Front Mol Neurosci. 2019 Aug 22; 12:203. doi: 10.3389/fnmol.2019.00203. eCollection 2019. PubMed PMID: 31507373; PubMed Central PMCID: PMC6713911.

[13]. Obulesu M, Lakshmi MJ. Apoptosis in Alzheimer's disease: an understanding of the physiology, pathology and therapeutic avenues. Neurochem Res. 2014 Dec;39(12):2301-12. doi: 10.1007/s11064-014-1454-4. Epub 2014 Oct 17. Review. PubMed PMID: 25322820.

[14]. Behl C. Apoptosis and Alzheimer's disease. J Neural Transm (Vienna). 2000;107(11):1325-44. Review. PubMed PMID: 11145007.

[15]. P Calissano, C Matrone & G Amadoro (2009) Apoptosis and in vitro Alzheimer's disease neuronal models, Communicative & Integrative Biology, 2:2, 163-169, DOI: 10.4161/cib.7704

[16]. Gerakis Y, Hetz C. Emerging roles of ER stress in the etiology and pathogenesis of Alzheimer's disease. FEBS J. 2018 Mar;285(6):995-1011. doi: 10.1111/febs.14332. Epub 2017 Dec 15. Review. PubMed PMID: 29148236.

[17]. Li JQ, Yu JT, Jiang T, Tan L. Endoplasmic reticulum dysfunction in Alzheimer's disease. Mol Neurobiol. 2015 Feb;51(1):383-95. doi: 10.1007/s12035-014-8695-8. Epub 2014 Apr 9. Review. PubMed PMID: 24715417.

[18]. Santos LE, Ferreira ST. Crosstalk between endoplasmic reticulum stress and brain inflammation in Alzheimer's disease. Neuropharmacology. 2018 Jul 1;136(Pt B):350-360. doi: 10.1016/j.neuropharm.2017.11.016. Epub 2017 Nov 10. Review. PubMed PMID: 29129774.
[19]. Flannery PJ, Trushina E. Mitochondrial dynamics and transport in Alzheimer's disease. Mol Cell Neurosci. 2019 Jul;98:109-120. doi: 10.1016/j.mcn.2019.06.009. Epub 2019 Jun 16. Review. PubMed PMID: 31216425; PubMed Central PMCID: PMC6614006.
[20]. Lesuis SL, Lucassen PJ, Krugers HJ. Early life stress amplifies fear responses and hippocampal synaptic potentiation in the APPswe/PS1dE9 Alzheimer mouse model. Neuroscience. 2019 Jul 11. pii: S0306-4522(19)30484-1. doi: 10.1016/j.neuroscience.2019.07.012. [Epub ahead of print] PubMed PMID: 31302265.
[21]. Ondrejcak T, Hu NW, Qi Y, Klyubin I, Corbett GT, Fraser G, Perkinton MS, Walsh DM, Billinton A, Rowan MJ. Soluble tau aggregates inhibit synaptic long-term depression and amyloid β-facilitated LTD in vivo. Neurobiol Dis. 2019 Jul;127:582-590. doi: 10.1016/j.nbd.2019.03.022. Epub 2019 Mar 22. PubMed PMID: 30910746.
[22. E. M. Beyer and G. Macbeath, "Crosstalk between receptor tyrosine kinase and tumor necrosis factor-alpha signaling networks regulates apoptosis but not proliferation," *Molecular & Cellular Proteomics*, vol. 11, no. 6, 2012.
[23. D. R. Robinson, Y.M.Wu, and S. F. Lin, "The protein tyrosine kinase family of the human genome," *Oncogene*, vol. 19, no.49, pp. 5548–5557, 2000.
[24]. M. Erschbamer, K. Pernold, and L. Olson, "Inhibiting epidermal growth factor receptor improves structural, locomotor, sensory, and bladder recovery from experimental spinal cord injury," *Journal of Neuroscience*, vol. 27, no. 24, pp. 6428– 6435, 2007.
[25]. H. T. Zhang, L. Y. Li, X. L. Zou et al., "Immunohistochemical distribution of NGF, BDNF, NT-3, and NT-4 in adult rhesus monkey brains," *Journal of Histochemistry and Cytochemistry*, vol. 55, no. 1, pp. 1–19, 2007.
[26]. Y. Goldshmit, M. D. Spanevello, S. Tajouri et al., "EphA4 blockers promote axonal regeneration and functional recovery following spinal cord injury in mice," *The PLoS ONE*, vol. 6, no. 9, p. e24636, 2011.
[27]. M.Watanabe, Y. Tokita, M. Kato, and Y. Fukuda, "Intravitreal injections of neurotrophic factors and forskolin enhance survival and axonal regeneration of axotomized*β* ganglion cells in cat retina," *Neuroscience*, vol. 116, no. 3, pp. 733–742,2003.
[28]. N. M. Oyesiku and D. J. Wigston, "Ciliary neurotrophic factor stimulates neurite outgrowth from spinal cord neurons," *Journal of Comparative Neurology*, vol. 364, no. 1, pp. 68–77, 1996.
[29]. E. R. Hollis II, P. Lu, A. Blesch, and M. H. Tuszynski, "IGFI gene delivery promotes corticospinal neuronal survival but not regeneration after adult CNS injury," *Experimental Neurology*, vol. 215, no. 1, pp. 53–59, 2009.
[30]. Schlessinger J. Cell signaling by receptor tyrosine kinases. Cell. 2000 Oct 13;103(2):211-25. Review. PubMed PMID: 11057895.
[31]. Skaper SD, Moore SE, Walsh FS. Cell signalling cascades regulating neuronal growth-promoting and inhibitory cues. Prog Neurobiol. 2001 Dec;65(6):593-608. Review. PubMed PMID: 11728645.
[32]. Huang EJ, Reichardt LF. Trk receptors: roles in neuronal signal transduction. Annu Rev Biochem. 2003; 72:609-42. Epub 2003 Mar 27. Review. PubMed PMID: 12676795.
[33]. Green JL, Kuntz SG, Sternberg PW. Ror receptor tyrosine kinases: orphans no more. Trends Cell Biol. 2008 Nov;18(11):536-44. doi: 10.1016/j.tcb.2008.08.006. Epub 2008 Oct 9. Review. PubMed PMID: 18848778; PubMed Central PMCID: PMC4672995.
[34]. Yoda A, Oishi I, Minami Y. Expression and function of the Ror-family receptor tyrosine kinases during development: lessons from genetic analyses of nematodes, mice, and humans. J Recept Signal Transduct Res. 2003 Feb;23(1):1-15. Review. PubMed PMID: 12680586.
[35]. Paganoni S, Ferreira A. Expression and subcellular localization of Ror tyrosine kinase receptors are developmentally regulated in cultured hippocampal neurons. J Neurosci Res. 2003 Aug 15;73(4):429-40. PubMed PMID: 12898527.
[36].Oishi I, Takeuchi S, Hashimoto R, Nagabukuro A, Ueda T, Liu ZJ, Hatta T, Akira S, Matsuda Y, Yamamura H, Otani H, Minami Y. Spatio-temporally regulated expression of receptor tyrosine kinases, mRor1, mRor2, during mouse development: implications in development and function of the nervous system. Genes Cells. 1999 Jan;4(1):41-56. PubMed PMID: 10231392.
[37]. Al-Shawi R, Ashton SV, Underwood C, Simons JP. Expression of the Ror1 and Ror2 receptor tyrosine kinase genes during mouse development. Dev Genes Evol. 2001 Apr;211(4):161-71. PubMed PMID: 11455430.

[38]. Paganoni S, Ferreira A. Neurite extension in central neurons: a novel role for the receptor tyrosine kinases Ror1 and Ror2. J Cell Sci. 2005 Jan 15;118(Pt 2):433-46. PubMed PMID: 15654020; PubMed Central PMCID: PMC1351101.

[39]. Kang, J., Lemaire, H. G., Unterbeck, A., Salbaum, J. M., Masters, C. L., Grzeschik, K. H., Multhaup, G., Beyreuther, K., & Muller-Hill, B. 1987. The precursor of Alzheimer's disease amyloid A4 protein resembles a cell-surface receptor. Nature, 325(6106), 733-6.

[40]. Rosen, D. R., Martin-Morris, L., Luo, L. Q., & White, K. 1989. A Drosophila gene encoding a protein resembling the human beta-amyloid protein precursor. Proceedings of the national academy of sciences of the united states of america, 86(7), 2478{82.

[41]. Musa, A., Lehrach, H., & Russo, V. A. 2001. Distinct expression patterns of two zebrafish homologues of the human APP gene during embryonic development. Development genes and evolution, 211(11),56-{7.

[42]. Daigle, I., & Li, C. 1993. apl-1, a Caenorhabditis elegans gene encoding a protein related to the human beta-amyloid protein precursor. Proceedings of the national academy of sciences of the united states of america, 90(24), 12045-9.

[43]. Wasco, W., Gurubhagavatula, S., Paradis, M. D., Romano, D. M., Sisodia, S. S., Hyman,B. T., Neve, R. L., &Tanzi, R. E. 1993. Isolation and characterization of APLP2 encoding a homologue of the Alzheimer's associated amyloid beta protein precursor. Nature genetics, 5(1), 95-100.

[44]. Muller, U. C., & Zheng, H. 2012. Physiological Functions of APP Family Proteins. Cold spring harbor perspectives in medicine, 2(2), a006288.

[45]. Selkoe, D. J., & Wolfe, M. S. 2007. Presenilin: running with scissors in the membrane. Cell, 131(2),215-21.

[46]. Ben Khalifa, N., Tyteca, D., Marinangeli, C., Depuydt, M., Collet, J. F., Courtoy, P. J.,Renauld, J. C., Constantinescu, S., Octave, J. N., & Kienlen-Campard, P. 2012. Structural features of the KPI domain control APP dimerization, tra_cking, and processing. FASEB journal: official publication of the federation of american societies for experimental biology, 26(2), 855-67.

[47]. Menendez-Gonzalez, M., Perez-Pinera, P., Martinez-Rivera, M., Calatayud, M. T., & Blazquez Menes, B. 2005. APP processing and the APP-KPI domain involvement in the amyloid cascade. Neuro-degenerative diseases, 2(6), 277-83.

[48]. Thinakaran, G., & Koo, E. H. 2008. Amyloid precursor protein tracking, processing, and function. The journal of biological chemistry, 283(44), 29615-9.

[49]. Zhang, H., Ma, Q., Zhang, Y. W., &Xu, H. 2012. Proteolytic processing of Alzheimer's beta-amyloid precursor protein. Journal of neurochemistry, 120 Suppl 1, 9-21.

[50]. Zheng, H., & Koo, E. H. 2006. The amyloid precursor protein: beyond amyloid. Molecular neurodegeneration, 1, 5.

[51]. Wang, J., & Chen, J. 2010. SIRT1 regulates autoacetylation and histone acetyltransferase activity ofTIP60. The journal of biological chemistry, 285(15), 11458{64.

[52]. Turner, P. R., O'Connor, K., Tate, W. P., & Abraham, W. C. 2003. Roles of amyloid precursor protein and its fragments in regulating neural activity, plasticity and memory. Progress in neurobiology, 70(1), 1-32.

[53]. Vassar, R., Bennett, B. D., Babu-Khan, S., Kahn, S., Mendiaz, E. A., Denis, P., Teplow,D. B., Ross, S., Amarante, P., Loeloff, R., Luo, Y., Fisher, S., Fuller, J., Edenson, S.,Lile, J., Jarosinski, M. A., Biere, A. L., Curran, E., Burgess, T., Louis, J. C., Collins,F., Treanor, J., Rogers, G., & Citron, M. 1999. Beta-secretase cleavage of Alzheimer's amyloid precursor protein by the transmembrane aspartic protease BACE. Science, 286(5440), 735-41.

[54]. Kuhn, P. H., Wang, H., Dislich, B., Colombo, A., Zeitschel, U., Ellwart, J. W., Kremmer,E., Rossner, S., & Lichtenthaler, S. F. 2010. ADAM10 is the physiologically relevant, constitutivealpha-secretase of the amyloid precursor protein in primary neurons. The EMBO journal, 29(17),302-32.

[55]. Chen, F., Hasegawa, H., Schmitt-Ulms, G., Kawarai, T., Bohm, C., Katayama, T., Gu,Y., Sanjo, N., Glista, M., Rogaeva, E., Wakutani, Y., Pardossi-Piquard, R., Ruan, X.,Tandon, A., Checler, F., Marambaud, P., Hansen, K., Westaway, D., St George-Hyslop,P., & Fraser, P. 2006. TMP21 is a presenilin complex component that modulates gamma-secretase but not epsilon-secretase activity. Nature, 440(7088), 1208-12.

[56]. Yu, C., Kim, S. H., Ikeuchi, T., Xu, H., Gasparini, L., Wang, R., &Sisodia, S. S. 2001.Characterization of a presenilin-mediated amyloid precursor protein carboxyl-terminal fragment gamma. Evidence for distinct mechanisms involved in gamma -secretase processing of

the APP and Notch1transmembrane domains. The journal of biological chemistry, 276(47), 43756-60.
[57]. Sastre, M., Steiner, H., Fuchs, K., Capell, A., Multhaup, G., Condron, M. M., Teplow,D. B., &Haass, C. 2001.Presenilin-dependent gamma-secretase processing of beta-amyloid precursor protein at a site corresponding to the S3 cleavage of Notch.EMBO reports, 2(9), 835-41.
[58]. De Strooper, B., &Annaert, W. 2010.Novel research horizons for presenilins and gamma-secretasesin cell biology and disease. Annual review of cell and developmental biology, 26, 235-60.
[59]. Sisodia, S. S. 1992. Beta-amyloid precursor protein cleavage by a membrane-bound protease. Proceedings of the national academy of sciences of the united states of america, 89(13), 6075-9.
[60]. Gotz, J. 2001. Tau and transgenic animal models. Brain research. brain research reviews, 35(3), 266-86.
[61]. Olsen, J. V., Blagoev, B., Gnad, F., Macek, B., Kumar, C., Mortensen, P., & Mann, M. 2006. Global, in vivo, and site-specific phosphorylation dynamics in signaling networks. Cell, 127(3), 635-48.
[62]. Oishi, M., Nairn, A. C., Czernik, A. J., Lim, G. S., Isohara, T., Gandy, S. E., Greengard, P., & Suzuki, T. 1997. The cytoplasmic domain of Alzheimer's amyloid precursor protein is phosphorylated at Thr654, Ser655, and Thr668 in adult rat brain and cultured cells. Molecular medicine, 3(2), 111-23.
[63]. Levy E, Carman M, Fernandez-Madrid I, Power MD, Lieberburg I, van Duinen SG, Bots GT, Luyendijk W, Frangione B (1990) Mutation of the Alzheimer's disease amyloid gene in hereditary cerebral hemorrhage, Dutch type. Science 248:1124–1126.
[64]. Levy-Lahad E, Wasco W, Poorkaj P, Romano DM, Oshima J, Pettingell WH, Yu CE, Jondro PD, Schmidt SD, Wang K, Crowley AC, Fu YH, Guenette SY, Galas D, Nemens E, Wijsman EM, Bird TD, Schellenberg GD, Tanzi RE (1995) Candidate gene for the chromosome 1 familial Alzheimer's disease locus. Science 269:973–977.
[65]. Games D, Adams D, Alessandrini R, Barbour R, Borthelette P, Blackwell C, Carr T, Clemens J, Donaldson T, Gillespie F, Guido T, Hagopian S, Johnson-Wood K, Khan K, Lee M, Leibowitz P, Lieberburg I, Little S, Masliah E, Mcconlogue L, Montoya-Zavala M, Mucke L, Paganini L, Penniman E, Power M, Schenk D, Seubert P, Snyder B, Soriano F, Tan H et al (1995) Alzheimer-type neuropathology in transgenic mice overexpressing V717F beta-amyloid precursor protein. Nature 373:523–527.
[66]. Ittner LM, Gotz J (2011) Amyloid-beta and tau–a toxic pas de deux in Alzheimer's disease. Nat Rev Neurosci 12:65–72.
[67]. Thies W, Bleiler L (2011) 2011 Alzheimer's disease facts and figures. Alzheimer's and Dementia 7:208–244.
[68]. Corder EH, Saunders AM, Strittmatter WJ, Schmechel DE, Gaskell PC, Small GW, Roses AD, Haines JL, Pericak-Vance MA (1993) Gene dose of apolipoprotein E type 4 allele and the risk of Alzheimer's disease in late onset families. Science 261:921–923.
[69]. Jonsson T, Atwal JK, Steinberg S, Snaedal J, Jonsson PV, Bjornsson S, Stefansson H, Sulem P, Gudbjartsson D, Maloney J, Hoyte K, Gustafson A, Liu Y, Lu Y, Bhangale T, Graham RR, Huttenlocher J, Bjornsdottir G, Andreassen OA, Jonsson EG, Palotie A, Behrens TW, Magnusson OT, Kong A, Thorsteinsdottir U,Watts RJ, Stefansson K (2012) A mutation in APP protects against Alzheimer/'s disease and age-related cognitive decline. Nature 488:96–99.
[70]. Shen J, Kelleher RJ 3rd (2007) The presenilin hypothesis of Alzheimer's disease: evidence for a loss-of-function pathogenic mechanism. ProcNatlAcadSci U S A 104:403–409.
[71]. Tamayev R, Matsuda S, Giliberto L, Arancio O, D'Adamio L (2011) APP heterozygosity averts memory deficit in knockin mice expressing the Danish dementia BRI2 mutant. EMBO J 30:2501–2509.
[72]. Kuhn PH, Wang H, Dislich B, Colombo A, Zeitschel U, Ellwart JW, Kremmer E, Rossner S, Lichtenthaler SF (2010) ADAM10 is the physiologically relevant, constitutive alpha-secretase of the amyloid precursor protein in primary neurons. EMBO J 29:3020–3032.
[73]. Epis R, Marcello E, Gardoni F, Vastagh C, Malinverno M, Balducci C, Colombo A, Borroni B, Vara H, Dell'Agli M, Cattabeni F, Giustetto M, Borsello T, Forloni G, Padovani A, Di Luca M (2010) Blocking ADAM10 synaptic trafficking generates a model of sporadic Alzheimer's disease. Brain 133:3323–3335.
[74]. Turner PR, O'Connor K, Tate WP, Abraham WC (2003) Roles of amyloid precursor protein and its fragments in regulating neural activity, plasticity and memory. Prog Neurobiol 70:1–32.

[75]. Bressler, S.L., Gray, M.D., Sopher, B.L., Hu, Q., Hearn, M.G., Pham, D.G., Dinulos, M.B., Fukuchi, K., Sisodia, S.S., Miller, M.A., Disteche, C.M., Martin, G.M., 1996. cDNA cloning and chromosome mapping of the human Fe65 gene: interaction of the conserved cytoplasmic domains of the human beta-amyloid precursor protein and its homologues with the mouse Fe65 protein. Hum. Mol. Genet. 5, 1589– 1598.

[76]. Cao, X., Sudhof, T.C., 2001. A transcriptionally active complex of APP with Fe65 and histone acetyltransferase Tip60. Science 293, 115–120.

[77]. Scheinfeld, M.H., Roncarati, R., Vito, P., Lopez, P.A., Abdallah, M., D'Adamio, L., 2002. Jun NH2-terminal kinase (JNK) interacting protein 1 (JIP1) binds the cytoplasmic domain of the Alzheimer's beta-amyloid precursor protein (APP). J. Biol. Chem. 277, 3767–3775.

[78]. Borg, J.P., Ooi, J., Levy, E., Margolis, B., 1996. The phosphor tyrosine interaction domains of X11 and FE65 bind to distinct sites on the YENPTY motif of amyloid precursor protein. Mol. Cell. Biol. 16, 6229–6241.

[79].. Chang, K.A., Kim, H.S., Ha, T.Y., Ha, J.W., Shin, K.Y., Jeong, Y.H., Lee, J.P., Park, C.H., Kim, S., Baik, T.K., Suh, Y.H., 2006. Phosphorylation of amyloid precursor protein (APP) at Thr668 regulates the nuclear translocation of the APP intracellular domain and induces neurodegeneration. Mol. Cell. Biol. 26, 4327–4338.

[80]. Alves, d.C., Sunyach, C., Pardossi-Piquard, R., Sevalle, J., Vincent, B., Boyer, N., Kawarai, T., Girardot, N., George-Hyslop, P., Checler, F., 2006. Presenilin-dependent gamma-secretase-mediated control of p53-associated cell death in Alzheimer's disease. J. Neurosci. 26, 6377–6385.

[81]. Zhang, Y.W., Wang, R., Liu, Q., Zhang, H., Liao, F.F., Xu, H., 2007. Presenilin/{gamma}-secretase-dependent processing of beta-amyloid precursor protein regulates EGF receptor expression. Proc. Natl. Acad. Sci. U.S.A. 104, 10613–10618.

[82]. Muller, T., Concannon, C.G., Ward, M.W., Walsh, C.M., Tirniceriu, A.L., Tribl, F., Kogel, D., Prehn, J.H., Egensperger, R., 2007. Modulation of gene expression and cytoskeletal dynamics by the amyloid precursor protein intracellular domain (AICD). Mol. Biol. Cell 18, 201–210.

[83]. Checler, F., Sunyach, C., Pardossi-Piquard, R., Sevalle, J., Vincent, B., Kawarai, T., Girardot, N., St George-Hyslop, P., da Costa, C.A., 2007. The gamma/epsilon secretase- derived APP intracellular domain fragments regulate p53. Curr. Alzheimer Res. 4, 423–426.

[84]. Ermekova, K.S., Zambrano, N., Linn, H., Minopoli, G., Gertler, F., Russo, T., Sudol, M., 1997. TheWWdomain of neural protein FE65 interacts with proline-rich motifs in Mena, the mammalian homolog of Drosophila enabled. J. Biol. Chem. 272, 32869–32877.

[85]. Sabo, S.L., Ikin, A.F., Buxbaum, J.D., Greengard, P., 2003. The amyloid precursor protein and its regulatory protein, FE65, in growth cones and synapses in vitro and in vivo. J. Neurosci. 23, 5407–5415.

[86]. Muller, T., Concannon, C.G., Ward, M.W., Walsh, C.M., Tirniceriu, A.L., Tribl, F., Kogel, D., Prehn, J.H., Egensperger, R., 2007. Modulation of gene expression and cytoskeletal dynamics by the amyloid precursor protein intracellular domain (AICD). Mol. Biol. Cell 18, 201–210.

[87]. Chakrabarti A, Roy K, Mukhopadhyay D. Differential expression of neuroblastoma cellular proteome due to AICD overexpression. J Alzheimers Dis. 2014;38(4):845-55.

[88] Raychaudhuri M, Mukhopadhyay D. AICD Overexpression in Neuro 2A Cells Regulates Expression of PTCH1 and TRPC5. Int J Alzheimers Dis. 2010 Aug 15; 2011.

[89] Raychaudhuri M, Mukhopadhyay D. Grb2-mediated alteration in the trafficking of AbetaPP: insights from Grb2-AICD interaction. J Alzheimers Dis. 2010; 20(1):275-92.

[90] Das S, Raychaudhuri M, Sen U, Mukhopadhyay D. Functional implications of the conformational switch in AICD peptide upon binding to Grb2-SH2 domain. J Mol Biol. 2011 Nov 25; 414(2):217-30.32. E. M. Beyer and G. Macbeath, "Crosstalk between receptor tyrosine kinase and tumor necrosis factor-alpha signalling networks regulates apoptosis but not proliferation," *Molecular & Cellular Proteomics*, vol. 11, no. 6, 2012.

[91]. Ambros, V., 2004. The functions of animal microRNAs. Nature 431, 350–355.

[92] Lagos-Quintana, M., et al., 2001. Identification of novel genes coding for small expressed RNAs. Science 294, 853–858.

[93 Peters, L., Meister, G., 2007. Argonaute proteins: mediators of RNA silencing. Mol. Cell 26, 611–623.

[94]. Eulalio, A., et al., 2009. Deadenylation is a widespread effect of miRNA regulation. RNA 15, 21–32.

[95]. Cogswell, J.P., et al., 2008. Identification of miRNA changes in Alzheimer's disease brain and CSF yields putative biomarkers and insights into disease pathways. J. Alzheimers Dis. 14, 27–41.

[96]. Hébert, S.S., De Strooper, B., 2009. Alterations of the microRNA network cause neurodegenerative disease. Trends Neurosci. 32, 199–206.
[97]. Zovoilis, A., et al., 2011. MicroRNA-34c is a novel target to treat dementias. EMBO J. 30, 4299–4308.
[98]. Bettens, K., et al., 2009. APP and BACE1 miRNA genetic variability has no major role in risk for Alzheimer disease. Hum. Mutat. 30, 1207–1213.
[99].Chapnik E, Rivkin N, Mildner A, Beck G, Pasvolsky R, Metzl-Raz E, Birger Y, Amir G, Tirosh I, Porat Z, Israel LL, Lellouche E, Michaeli S, Lellouche JP, Izraeli S, Jung S, Hornstein E. miR-142 orchestrates a network of actin cytoskeleton regulators during megakaryopoiesis. Elife. 2014 May 23;3: e01964. doi: 10.7554/eLife.01964. PubMed PMID: 24859754; PubMed Central PMCID: PMC4067751.
[100]. Freitas FC, Pires CV, Claudianos C, Cristino AS, Simões ZL. MicroRNA-34 directly targets pair-rule genes and cytoskeleton component in the honey bee. Sci Rep. 2017 Jan 18; 7:40884. doi: 10.1038/srep40884. PubMed PMID: 28098233; PubMed Central PMCID: PMC5241629.
[101]. Weber M, Kim S, Patterson N, Rooney K, Searles CD. MiRNA-155 targets myosin light chain kinase and modulates actin cytoskeleton organization in endothelial cells. Am J Physiol Heart Circ Physiol. 2014 Apr 15;306(8):H1192-203. doi: 10.1152/ajpheart.00521.2013. Epub 2014 Jan 31. PubMed PMID: 24486510; PubMed Central PMCID: PMC3989748.
[102]. Wang M, Qin L, Tang B. MicroRNAs in Alzheimer's Disease. Front Genet. 2019 Mar 1; 10:153. doi: 10.3389/fgene.2019.00153. eCollection 2019. Review. PubMed PMID: 30881384; PubMed Central PMCID: PMC6405631.
[103]. Liu Q, Wang W, Yang X, Zhao D, Li F, Wang H. MicroRNA-146a inhibits cell migration and invasion by targeting RhoA in breast cancer. Oncol Rep. 2016 Jul;36(1):189-96. doi: 10.3892/or.2016.4788. Epub 2016 May 6. PubMed PMID: 27175941; PubMed Central PMCID: PMC4899025.
[104]. Kim D, Song J, Kim S, Park HM, Chun CH, Sonn J, Jin EJ. MicroRNA-34a modulates cytoskeletal dynamics through regulating RhoA/Rac1 cross-talk in chondroblasts. J Biol Chem. 2012 Apr 6;287(15):12501-9. doi: 10.1074/jbc.M111.264382. Epub 2012 Feb 20. PubMed PMID: 22351754; PubMed Central PMCID: PMC3320999.
[105]. Mercer, T.R., Dinger, M.E., Mattick, J.S., 2009. Long non-coding RNAs: insights into functions. Nature Reviews Genetics 10, 155–159.
[106]. Wright, M.W., Bruford, E.A., 2011. Naming 'junk': human non-protein coding RNA (ncRNA) gene nomenclature. Human Genomics 5, 90–98.
[107]. Wilusz, J.E., Sunwoo, H., Spector, D.L., 2009. Long noncoding RNAs: functional surprises from the RNA world. Genes and Development 23, 1494–1504.
[108]. Sin O, Ellen AA. Regulation of protein homeostasis in neurodegenerative diseases: the role of coding and ncgenes. Cell Mol Life Sci. 2015; 72:4027–4047.
[109]. Kopp F, Mendell JT. Functional classification and experimental dissection of long noncoding RNAs. Cell. 2018 Jan 25;172(3):393– 407.
[110]. Böhmdorfer G, Wierzbicki AT. Control of chromatin structure by long noncoding RNA. Trends Cell Biol. 2015; 25:623–632.
[111]. Szcześniak MW, Makałowska I. lncRNA-RNA interactions across the human transcriptome. PLoS One. 2016 Mar 1;11: e0150353.
[112]. Zhang Z. Long non-coding RNAs in Alzheimer's disease. Curr Top Med Chem. 2016;16(5):511-9. Review. PubMed PMID: 26268333.
[113]. Luo Q, Chen Y. Long noncoding RNAs and Alzheimer's disease. Clin Interv Aging. 2016 Jun 29; 11:867-72. doi: 10.2147/CIA.S107037. eCollection 2016. Review. PubMed PMID: 27418812; PubMed Central PMCID: PMC4933566.
[114]. Wei CW, Luo T, Zou SS, Wu AS. The Role of Long Noncoding RNAs in Central Nervous System and Neurodegenerative Diseases. Front Behav Neurosci. 2018 Sep 28; 12:175. doi: 10.3389/fnbeh.2018.00175. eCollection 2018. Review. PubMed PMID: 30323747; PubMed Central PMCID: PMC6172704.
[115]. Zhang X, Hamblin MH, Yin KJ. The long noncoding RNA Malat1: Its physiological and pathophysiological functions. RNA Biol. 2017 Dec 2;14(12):1705-1714. doi: 10.1080/15476286.2017.1358347. Epub 2017 Oct 6. Review. PubMed PMID: 28837398; PubMed Central PMCID: PMC5731810.
[116]. Wang A, Wang J, Liu Y, Zhou Y. Mechanisms of Long Non-Coding RNAs in the Assembly and Plasticity of Neural Circuitry. Front Neural Circuits. 2017 Oct 23; 11:76. doi:

10.3389/fncir.2017.00076. eCollection 2017. Review. PubMed PMID: 29109677; PubMed Central PMCID: PMC5660110.
[117]. Yao J, Wang XQ, Li YJ, Shan K, Yang H, Wang YN, Yao MD, Liu C, Li XM, Shen Y, Liu JY, Cheng H, Yuan J, Zhang YY, Jiang Q, Yan B. Long non-coding RNA MALAT1 regulates retinal neurodegeneration through CREB signaling. EMBO Mol Med. 2016 Sep 1;8(9):1113. doi: 10.15252/emmm.201606749. PubMed PMID: 27587362; PubMed Central PMCID: PMC5009814.
[118]. Nixon DW. The Inverse Relationship Between Cancer and Alzheimer's Disease: A Possible Mechanism. Curr Alzheimer Res. 2017; 14(8):883-893. doi: 10.2174/1567205014666170216152905. Review. PubMed PMID: 28215174.
[119]. Majd S, Power J, Majd Z. Alzheimer's Disease and Cancer: When Two Monsters Cannot Be Together. Front Neurosci. 2019 Mar 1; 13:155. doi: 10.3389/fnins.2019.00155. eCollection 2019. PubMed PMID: 30881282; PubMed Central PMCID: PMC6407038.
[120]. Lv D, Wang Y, Zhang Y, Cui P, Xu Y. Downregulated long non-coding RNA DREH promotes cell proliferation in hepatitis B virus-associated hepatocellular carcinoma. Oncol Lett. 2017 Aug;14(2):2025-2032. doi: 10.3892/ol.2017.6436. Epub 2017 Jun 21. PubMed PMID: 28789433; PubMed Central PMCID: PMC5530050.
[121]. Lopez CG, Saldanha O, Huber K, Köster S. Lateral association and elongation of vimentin intermediate filament proteins: A time-resolved light-scattering study. Proc Natl Acad Sci U S A. 2016 Oct 4;113(40):11152-11157. Epub 2016 Sep 21. PubMed PMID: 27655889; PubMed Central PMCID: PMC5056051.
[122]. Petrie RJ, Doyle AD, Yamada KM. Random versus directionally persistent cell migration. Nat Rev Mol Cell Biol. 2009 Aug;10(8):538-49. doi: 10.1038/nrm2729. Epub 2009 Jul 15. Review. PubMed PMID: 19603038; PubMed Central PMCID: PMC2752299.
[123]. Mattila PK, Lappalainen P. Filopodia: molecular architecture and cellular functions. Nat Rev Mol Cell Biol. 2008 Jun;9(6):446-54. doi: 10.1038/nrm2406. Epub 2008 May 9. Review. PubMed PMID: 18464790.
[124]. Zhao X, Wang P, Liu J, Zheng J, Liu Y, Chen J, Xue Y. Gas5 Exerts Tumor-suppressive Functions in Human Glioma Cells by Targeting miR-222. Mol Ther. 2015 Dec;23(12):1899-911. doi: 10.1038/mt.2015.170. Epub 2015 Sep 15. PubMed PMID: 26370254; PubMed Central PMCID: PMC4700110.
[125]. Lappalainen P, Drubin DG. Cofilin promotes rapid actin filament turnover in vivo. Nature. 1997 Jul 3;388(6637):78-82. Erratum in: Nature 1997 Sep 11;389(6647):211. PubMed PMID: 9214506.
[126]. Fotouhi Ghiam A, Taeb S, Huang X, Huang V, Ray J, Scarcello S, Hoey C, Jahangiri S, Fokas E, Loblaw A, Bristow RG, Vesprini D, Boutros P, Liu SK. Long non-coding RNA urothelial carcinoma associated 1 (UCA1) mediates radiation response in prostate cancer. Oncotarget. 2017 Jan 17;8(3):4668-4689. doi: 10.18632/oncotarget.13576. PubMed PMID: 27902466; PubMed Central PMCID: PMC5354863.
[127]. Zou Y, Xu S, Xiao Y, Qiu Q, Shi M, Wang J, Liang L, Zhan Z, Yang X, Olsen N, Zheng SG, Xu H. Long noncoding RNA LERFS negatively regulates rheumatoid synovial aggression and proliferation. J Clin Invest. 2018 Oct 1;128(10):4510-4524. doi: 10.1172/JCI97965. Epub 2018 Sep 10. PubMed PMID: 30198906; PubMed Central PMCID: PMC6159954.
[128]. Chen S, Wang LL, Sun KX, Liu Y, Guan X, Zong ZH, Zhao Y. LncRNA PCGEM1 Induces Ovarian Carcinoma Tumorigenesis and Progression Through RhoA Pathway. Cell Physiol Biochem. 2018;47(4):1578-1588. doi: 10.1159/000490931. Epub 2018 Jun 27. PubMed PMID: 29949791.
[129]. Lu Z, Li Y, Che Y, Huang J, Sun S, Mao S, Lei Y, Li N, Sun N, He J. The TGFβ-induced lncRNA TBILA promotes non-small cell lung cancer progression in vitro and in vivo via cis-regulating HGAL and activating S100A7/JAB1 signaling. Cancer Lett. 2018 Sep 28; 432:156-168. doi: 10.1016/j.canlet.2018.06.013. Epub 2018 Jun 15. PubMed PMID: 29908210.
[130]. Dai J, Ma J, Yu B, Zhu Z, Hu Y. Long Noncoding RNA TUNAR Represses Growth, Migration, and Invasion of Human Glioma Cells Through Regulating miR-200a and Rac1. Oncol Res. 2018 Dec 27;27(1):107-115. doi: 10.3727/096504018X15205622257163. Epub 2018 Mar 14. PubMed PMID: 29540255.
[131]. Hou Y, Fan RG, Qin CL, Jia J, Wu XD, Zha WZ. LncRNA-H19 activates CDC42/PAK1 pathway to promote cell proliferation, migration and invasion by targeting miR-15b in hepatocellular carcinoma. Genomics. 2018 Dec 10. pii: S0888-7543(18)30497-X. doi: 10.1016/j.ygeno.2018.12.009. [Epub ahead of print] PubMed PMID: 30543848.

[132]. Ma Y, Xue Y, Liu X, Qu C, Cai H, Wang P, Li Z, Li Z, Liu Y. SNHG15 affects the growth of glioma microvascular endothelial cells by negatively regulating miR-153. Oncol Rep. 2017 Nov;38(5):3265-3277. doi: 10.3892/or.2017.5985. Epub 2017 Sep 21. PubMed PMID: 29048682.
[133]. Saha S, Rangarajan PN. Common host genes are activated in mouse brain by Japanese encephalitis and rabies viruses. *J Gen Virol*. 2003;84(Pt 7):1729-1735.
[134]. Clemson CM, Hutchinson JN, Sara SA, et al. An architectural role for a nuclear noncoding RNA: NEAT1 RNA is essential for the structure of paraspeckles. *Mol Cell*. 2009;33(6):717-726.
[135]. Sunwoo H, Dinger ME, Wilusz JE, Amaral PP, Mattick JS, Spector DL. MEN epsilon/beta nuclear-retained non-coding RNAs are up-regulated upon muscle differentiation and are essential components of paraspeckles. *Genome Res*. 2009;19(3):347-359.
[136]. Chen Z.J., Zhang Z., Xie B.B., Zhang H.Y. Clinical significance of up-regulated lncRNA NEAT1 in prognosis of ovarian cancer. Eur. Rev. Med. Pharmacol. Sci. 2016; 20:3373–3377.
[137]. Xiong W., Huang C., Deng H., Jian C., Zen C., Ye K., Zhong Z., Zhao X., Zhu L. Oncogenic non-coding RNA NEAT1 promotes the prostate cancer cell growth through the SRC3/IGF1R/AKT pathway. Int. J. Biochem. Cell Biol. 2018; 94:125–132.
[138]. Jen J., Tang Y.A., Lu Y.H., Lin C.C., Lai W.W., Wang Y.C. Oct4 transcriptionally regulates the expression of long non-coding RNAs NEAT1 and MALAT1 to promote lung cancer progression. Mol. Cancer. 2017; 16:104.
[139]. Lo P.K., Zhang Y., Wolfson B., Gernapudi R., Yao Y., Duru N., Zhou Q. Dysregulation of the BRCA1/long non-coding RNA NEAT1 signaling axis contributes to breast tumorigenesis. Oncotarget. 2016; 7:65067–65089.
[140]. Zhang X.N., Zhou J., Lu X.J. The long noncoding RNA NEAT1 contributes to hepatocellular carcinoma development by sponging miR-485 and enhancing the expression of the STAT3. J. Cell. Physiol. 2018;233: 6733–6741.
[141]. Tollervey, J. R., Curk, T., Rogelj, B., Briese, M., Cereda, M., Kayikci, M., König, J., Hortobágyi, T., Nishimura, A. L., Zupunski, V., Patani, R., Chandran, S., Rot, G., Zupan, B., Shaw, C. E., & Ule, J. (2011). Characterizing the RNA targets and position-dependent splicing regulation by TDP-43. *Nature neuroscience*, *14*(4), 452–458.
[142]. Nishimoto, Y., Nakagawa, S., Hirose, T., Okano, H. J., Takao, M., Shibata, S., Suyama, S., Kuwako, K., Imai, T., Murayama, S., Suzuki, N., & Okano, H. (2013). The long non-coding RNA nuclear-enriched abundant transcript 1_2 induces paraspeckle formation in the motor neuron during the early phase of amyotrophic lateral sclerosis. *Molecular brain*, *6*, 31.
[143]. Chanda, K., Das, S., Chakraborty, J., Bucha, S., Maitra, A., Chatterjee, R., Mukhopadhyay, D., & Bhattacharyya, N. P. (2018). Altered Levels of Long NcRNAs Meg3 and Neat1 in Cell and Animal Models of Huntington's Disease. *RNA biology*, *15*(10), 1348–1363.
[144]. Yan W, Chen ZY, Chen JQ, Chen HM. LncRNA NEAT1 promotes autophagy in MPTP-induced Parkinson's disease through stabilizing PINK1 protein. *Biochem Biophys Res Commun*. 2018;496(4):1019-1024.
[145]. Puthiyedth N, Riveros C, Berretta R, Moscato P. Identification of Differentially Expressed Genes through Integrated Study of Alzheimer's Disease Affected Brain Regions. *PLoS One*. 2016;11(4): e0152342.
[146]. Spreafico M, Grillo B, Rusconi F, Battaglioli E, Venturin M. Multiple Layers of *CDK5R1* Regulation in Alzheimer's Disease Implicate Long Non-Coding RNAs. *Int J Mol Sci*. 2018;19(7):2022.

Chapter 2: Materials and Techniques

2.1. Ethics declaration

Animal experiments were performed by adhering to the guidelines for the use and care of animals and approved by the Institutional Animal and Ethics Committee of the National Brain Research Centre (NBRC/IAEC/2012/71).

2.2. Cell culture and transfection

Immortalized striatal ST*Hdh*^{Q7}/*Hdh*^{Q7} cells and ST*Hdh*^{Q111}/*Hdh*^{Q111}cells were kindly provided by Prof. Marcy E. MacDonald of Massachusetts General Hospital, USA and cultured routinely in DMEM (Gibco) supplemented with 10% (v/v) heat-inactivated FBS (Gibco), antibiotics penicillin/streptomycin PS 1% (v/v) and 400 µg/ml G418 (Invitrogen, USA) at 33^{0}C in humidified condition and 5% CO_2. Mouse neuroblastoma cell lines, Neuro2A and Human neuroblastoma cell lines SHSY5Y were procured from NCCS, Pune, India and were cultured routinely in DMEM (Gibco) and DMEM-F12 (Gibco), respectively, supplemented with 10% (v/v) heat-inactivated FBS (Gibco), antibiotics penicillin/streptomycin PS 1% (v/v) and 400 µg/ml G418 (Invitrogen, USA) at 37^{0}C in humidified condition and 5% CO_2. All transfections were carried on 70-80% confluent cells using Lipofectamine 2000 (Invitrogen) as per manufacturer's protocol. Unless otherwise mentioned, for single transfection experiment 1 µg (30mm plate), 2.5µg (60mm plate) or 5µg (100 mm plate) of plasmid DNA constructs as well as 5µl, 10µl or 15µl of Lipofectamine 2000 respectively were used. Transfection efficiency was normalized by co-transfecting cells with pEGFP-C1 (Clontech) or pDsRed-Monomer-C1 (Clontech) and counting and determining the percentage of GFP or DsRed positive cells under the microscope.

2.3. Cell Models of AD

Transfection of cells with different constructs, like pGFP C1 and AICD-GFP was performed using Lipofectamine 2000 Transfection Reagent (Invitrogen). After 48 h, transiently transfected cells were checked for transfection efficiency by monitoring GFP or expression under the fluorescence microscope and were then used for experiments. $A\beta_{1-42}$ protein fragment (Sigma, A980) was added to the medium at a concentration of 0.5 µM 3 h after transfection, and samples were collected 48 h after addition. The sets were human SHSY5Y cells treated with either Aβ only or transfected with AICD only or treated with Aβ and transfected with AICD (AICD + Aβ). The 3 groups had appropriate controls as either treated with DMSO only or transfected with empty GFP only or treated with DMSO and transfected with empty GFP (GFP+DMSO) respectively.

2.4. $A\beta_{1-42}$ treated Cell Model

Lyophilised $A\beta_{1-42}$ protein fragment (Sigma, A980) was weighed and reconstituted in DMSO to make a stock of 2 µM. From this stock, the requisite amount of $A\beta_{1-42}$ was added to the petri-dishes (0.5 µl for 35mm, 1 µl for 60mm and 2 µl for 90mm plates) to make the working concentration of 1 µM. Only DMSO in the same concentration and amount was used as a control.

2.5. APP/PS1 mice

APP/PS1 or B6C3-Tg (/APPswe, PSEN1dE9/) 85Dbo/J mice were obtained from the Jackson Laboratory and maintained in the institute's animal house facility. These transgenic mouse lines for AD express human APPswe mutations (K670N and M671L) and exon-9-deleted human presenilin 1(PSEN1dE9) under the control of the mouse prion gene promoter. Animals were provided water and food *ad libitum.* AD

mice, along with controls at their age of 12 months, were anaesthetized with xylazine (10 mg/kg body weight) and ketamine (100 mg/kg body weight) and perfused transcardially with PBS followed by 4% paraformaldehyde (w/v) in PBS. Brains were collected and further placed in 4% paraformaldehyde for 24 h and then treated with 10, 20 and 30% sucrose (in PBS) followed by sectioning in a cryomicrotome (20 μm thickness). Sections (both control and AD) were placed on the same slides.

2.6. Cell Models of HD

Immortalized striatal ST*Hdh*^{Q7}/*Hdh*^{Q7}cells were originally established from wild-type Hdh knock-in mice which express full-length wild-type *HTT* with 7 Glu (Q) residues. ST*Hdh*^{Q7}/*Hdh*^{Q7}cells, expressing full-length wild *HTT* gene from the chromosomal region in homozygous condition are primarily used as controls for HD. ST*Hdh*^{Q111}/*Hdh*^{Q111} cells, expressing endogenous full-length mutant *HTT* gene with 111Glu (Q) residues also from the chromosomal region in homozygous condition, exhibit many characteristics of HD are used as cell model of HD. These cells are extensively used as a cell model of HD for identifying molecular alterations in the disease pathogenesis. Prof. Marcy E. MacDonald of Massachusetts General Hospital, USA kindly donated us these cell lines.

ST*Hdh*^{Q7}/*Hdh*^{Q7}cells transiently transfected with exon1 of mutant *HTT* gene when expressed translated into N-terminal HTT with 83Q were used another cell model of HD as described by many authors including us. For control, ST*Hdh*^{Q7}/*Hdh*^{Q7}cells transiently transfected with exon1 of wild-type *HTT* gene tagged with green fluorescent protein (GFP) when translated expressed N-terminal HTT with 16Q.

2.7. Mouse HD Model R6/2

Dr. Nihar Ranjan Jana, National Brain Research Centre, Manesar, Haryana, Pin- 122 050, India kindly provided us with paraffinized cortical tissue from R6/2 mice and

control mice of same age. R6/2 is one of the first mouse models of HD express ~130 CAG repeats from human HD promoter. Even though there are differences in time of appearance of first symptoms in motor activities among the colonies grown in standard living conditions, R6/2 mice typically are severely impaired by 8-12 weeks of age. I have used R6/2 mice at age 6 weeks and 8 weeks representing early and late stage of HD.

2.8. Small RNA sequencing (for the AD study)

Small RNA sequencing was performed on NextSeq500 platform to generate 1x75bp reads for an average of 15 million raw reads per sample. The quality and quantity of the RNA samples were checked on 1% denaturing RNA agarose and nanodrop, respectively. The small RNA sequencing libraries were prepared from the QC passed total RNA using Illumina TruSeq Small RNA Library Preparation Kit as per the manufacturer's instruction. The protocol includes adapter ligation, reverse transcription, PCR amplification, and pooled gel purification to generate a library product. The RNA 3' adapter is specifically modified to target microRNAs and other small RNAs that have a 3' hydroxyl group resulting from enzymatic cleavage by Dicer or other RNA processing enzymes. The adapters are ligated to each end of the RNA molecule and a reverse transcription reaction is used to create single stranded cDNA. The cDNA is then PCR amplified using a common primer and a primer containing one of the index sequences. The amplified PCR product with index sequences were size selected and purified on 6% TBE gel. The gel size selected and purified libraries were analysed on 4200 Tape Station system (Agilent Technologies) using high sensitivity D1000 Screen tape as per manufacturer's instructions. After obtaining the Qubit concentration for the libraries and mean peak size from Agilent Tape Station profile, the SE Illumina libraries were loaded onto NextSeq 500 for

cluster generation and sequencing. Agarose gel profiles, Sample Ids, nanodrop readings and gel profiles of cDNA construct are given in **Fig 2.1, Fig 2.2 and Table 2.1.**

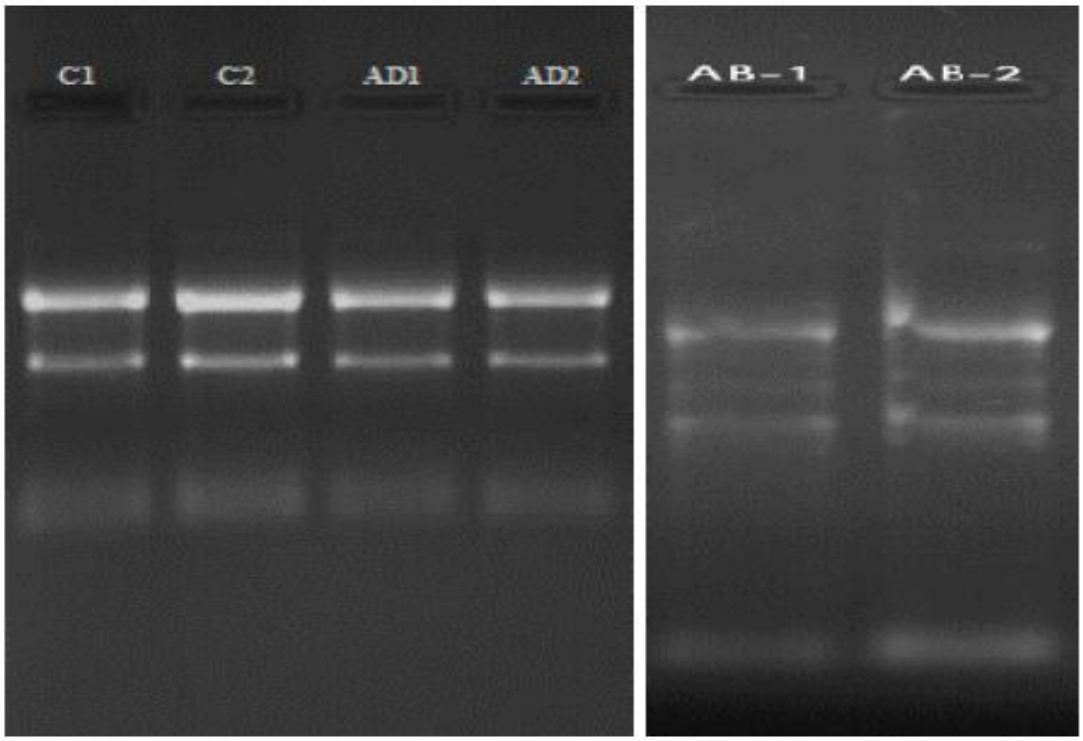

Fig 2.1: QC of total RNA samples on 1% Agarose Gel.

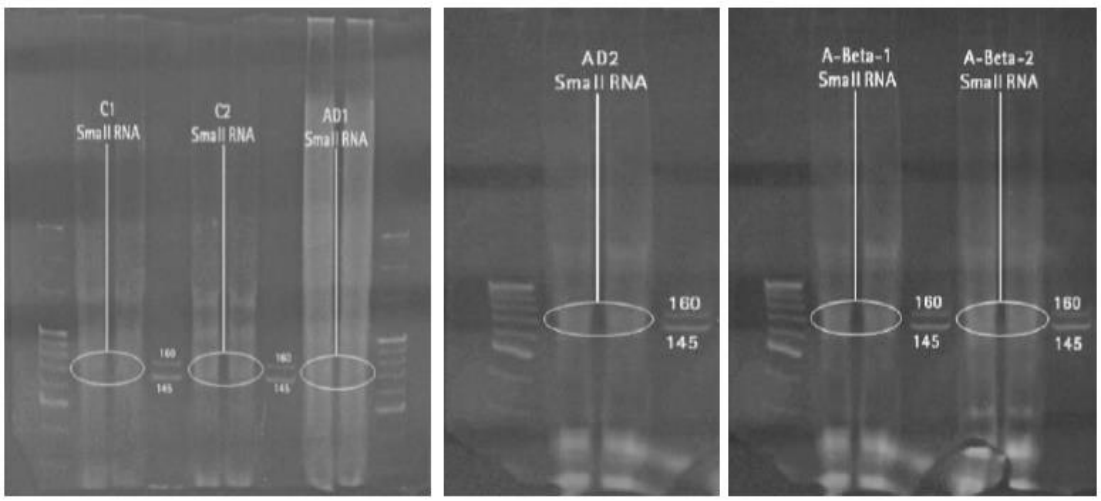

Figure 2.2: Small RNA libraries from total RNA through size selection.

SR NO.	SAMPLE ID	NANODROP READINGS (ng/µl)	NANODROP READINGS (260/280)	NANODROP READINGS (260/230)	REMARKS
1	C1	354.9	1.88	1.93	QC PASS
2	C2	934.8	2.01	2.03	QC PASS
3	AD1	542.1	1.92	1.92	QC PASS
4	AD2	405.0	1.95	1.94	QC PASS
5	Aβ1	915.4	1.90	2.21	QC PASS
6	Aβ2	1971.5	1.98	2.29	QC PASS

Table 2.1: Quantification of RNA samples using Nanodrop.

2.9. Small RNA sequencing (for the HD study)

Small RNA-seq library was prepared using IlluminaTruSeq Small RNA library preparation kit following manufacturer's protocol. Cluster generation and 50bp single end read sequencing were performed in IlluminaHiSeq platform. After quality checking and post-processing of Fastq files, sequences were mapped to the mouse genome (mm10) using Novoaligner (http://www.novocraft.com/). Only uniquely aligned reads are considered for further analysis. Read counts for non-coding RNAs excluding miRNAs are generated using htseq-count module of the HT-seq. It was observed that levels of 92 known miRNAs altered significantly altogether; expression of 2 miRNAs was increased both 6-week and 8-week old mice, levels 42 miRNAs were decreased in both the mice. Besides, levels of 29 miRNAs decreased exclusively in 8-week old mice and that of 19 other miRNAs decreased only in 6-week old mice. The differential expression analysis of non-coding RNAs other than microRNA was performed using DESeq package in R statistical computing tool. The deregulated noncoding RNAs were identified comparing control cortex sample versus the cortex of 6 weeks old and 8 weeks old R6/2 mice mouse.

2.10. Bioinformatic Analysis

Small-RNA-Seq analysis was done on 6 samples, grouped into 2 samples each of Control (C1 and C2), Aβ (Aβ1 and Aβ2) and AICD + Aβ (AD1 and AD2), obtained from the small RNA fraction of total RNA from SHSY5Y cell model. Around 20-40 million reads of length 75 nucleotides were generated. The qualities of the reads generated were checked by running the tools FastQC. The adapter sequences used were determined from the 'overrepresented sequence' category of the FastQC report. The adapter sequences were trimmed off from the reads using CutAdapt (v1.16). In addition, any bases whose quality scores were less than 30 were clipped from the 3' ends of the reads. To prevent very short reads from mapping to too many genomic regions leading to erroneous results during alignment, only reads which had a minimum length of 16 nucleotides after adapter and quality-trimming were retained and the remaining discarded.

The reads were next mapped to the reference human genome (UCSC, GrCh37 version) using Novoalign (V3.09.01). Prior to alignment, the reference genome was indexed using the novoindex package. The alignments were obtained in SAM format (Sequence Alignment Map). They were converted to binary format (BAM) using Samtools. The unaligned reads as well as reads with low mapping quality were filtered out.

The raw counts for all the annotated miRNAs (annotation file for miRNAs was obtained from miRBase in gff3 format) were obtained by using HTSeq-count (v0.11.1), by counting the number of reads mapped against each mature miRNA as present in the annotation file.

After obtaining the raw counts, differential expression analysis between the respective groups (Aβ vs Control, AD vs Control and AD vs Aβ) was done using a Bioconductor package, edgeR. EdgeR uses TMM (Trimmed mean of M-values) to normalize for library composition by computing a set of scale factors with which the effective library sizes are calculated. It thereby estimates dispersion and fits generalized linear models based on negative binomial distribution. The correction for false discovery rates (FDR) was done by Benjamini-Hochberg method. The miRNAs with FDR less than 0.05 and which are deregulated at least 2-folds were considered to be differentially expressed. In addition, I considered those miRNAs which had average expression levels, i.e., log (counts per million) >=2 for further studies.

An MDS (Multi-dimensional scaling) plot was generated in edgeR, to assess the level of similarity or dissimilarity among the samples in the groups under study. The function PlotMDS was used which computes the distances corresponding to the root mean square of the maximum of the absolute logarithm of fold changes between each pair of samples. Upon studying the plot, I saw that the samples in the Aβ group were well separated from the remaining two groups. However, on further inspection, I noticed that distance between the Control and AD groups was not sufficiently large so as to separate them in two distinct, well-separated clusters.

Based on these criteria I obtained a total of 47 miRNAs which were deregulated between the control and Aβ groups, with 14 of them up regulated in Aβ samples and 33 miRNAs down regulated in Aβ samples with respect to the control samples.

The differential expression analysis between the groups AD and Control yielded no candidates with adjusted p-value (FDR) <= 0.05. So, in this case I selected the miRNAs with raw p-values <= 0.05 to be differentially expressed.

The heatmaps representing the deregulated miRNAs between the respective groups were plotted using gplots package in R. Hierarchical clustering was done using Ward's Minimum Variance Method (Ward.D2), and Pearson's distant measure was used to compute the distances between the rows and columns.

I next checked for long non-coding RNAs (lncRNAs) which were deregulated between our respective groups of study. The same pipeline was used as in the case of miRNAs, except that the annotation file for lncRNAs (obtained from Gencode hg19 version) was used to obtain the raw counts for the lncRNAs. The differential analysis was performed again with edgeR, using the same filtering criteria as used in the case of miRNAs (FDR <= 0.05, |log(fold change)} >= 1, log(counts per million) >= 2)

As in the previous case, I did not find any lncRNAs which had adjusted p-values (FDR) <= 0.05, when compared between the control and AD groups. So, as in case of miRNAs, I selected the lncRNAs with raw p-values <= 0.05 to be the ones significantly deregulated between these two groups. By this measure, I obtained 19 up regulated and 22 down regulated lncRNAs in the group AD as compared to the samples in the Control group.

Next I looked to identify the RTKs (Receptor Tyrosine Kinases) which could be putative targets for the miRNAs, found differentially expressed between the respective groups. I used the database miRCarta to identify potential RTK targets for the miRNAs. I considered the target RTKs among the genes which had been experimentally validated.

In addition, I used miRanda to predict for prospective RTK targets. miRanda is a tool which is used to identify potential miRNA targets in genome sequences. miRanda was run, with strict 5'-seed pairing between the miRNA and the 3-utr of the RTKs and the

score threshold was set to 160. The lists of RTKs for the differentially expressed miRNAs between the respective groups were thus obtained.

2.11. RT2 lncRNA PCR Array

Total RNA from wild type mouse brain cortex and APP/PS1 mouse brain cortex was extracted as mentioned above. The control groups (Wild Type 1 and Wild Type 2) were total RNA from wild type mouse brain cortex. AD Transgenic 1 and AD Transgenic 2 were total RNA from APP/PS1 mouse brain cortex (biological replicates). The RT2 First Strand Kit was used for cDNA synthesis (200 ng RNA/20 µl RT reaction) and the RT2 lncRNA qPCR Array Mouse Cell Development & Differentiation kit **(**CATALOG No. - LAMM-003Z PRODUCT No. – 330721) was used for lncRNA detection with the RT2 SYBR® Green qPCR Mastermix **(Fig 2.3.)**. This lncRNA array contains 84 separate probes against mice lncRNAs implicated in various developmental and differentiation pathways like adult neural stem cells, cell-fate programming, embryonic stem cell pluripotency among others. In addition to these, there are 18 lncRNA probes which are directly implicated in neurogenesis-which is severely impaired in AD. Real-time PCR was performed on an Applied Biosystems® StepOnePlus™.

Real-Time PCR System. The QIAGEN® PCR array analysis tool was used for gene expression analysis. Raw Ct values from 4 plates i.e., two control mice and two transgenic mice (biological replicates) were used for lncRNA data analysis. Out of 84 mouse lncRNA, it was found that raw Ct values of several were undetermined from across the 4 plates (probably due to assay error or limit of detection). So only those lncRNAs that had Ct values in all 4 plates were used for analysis.

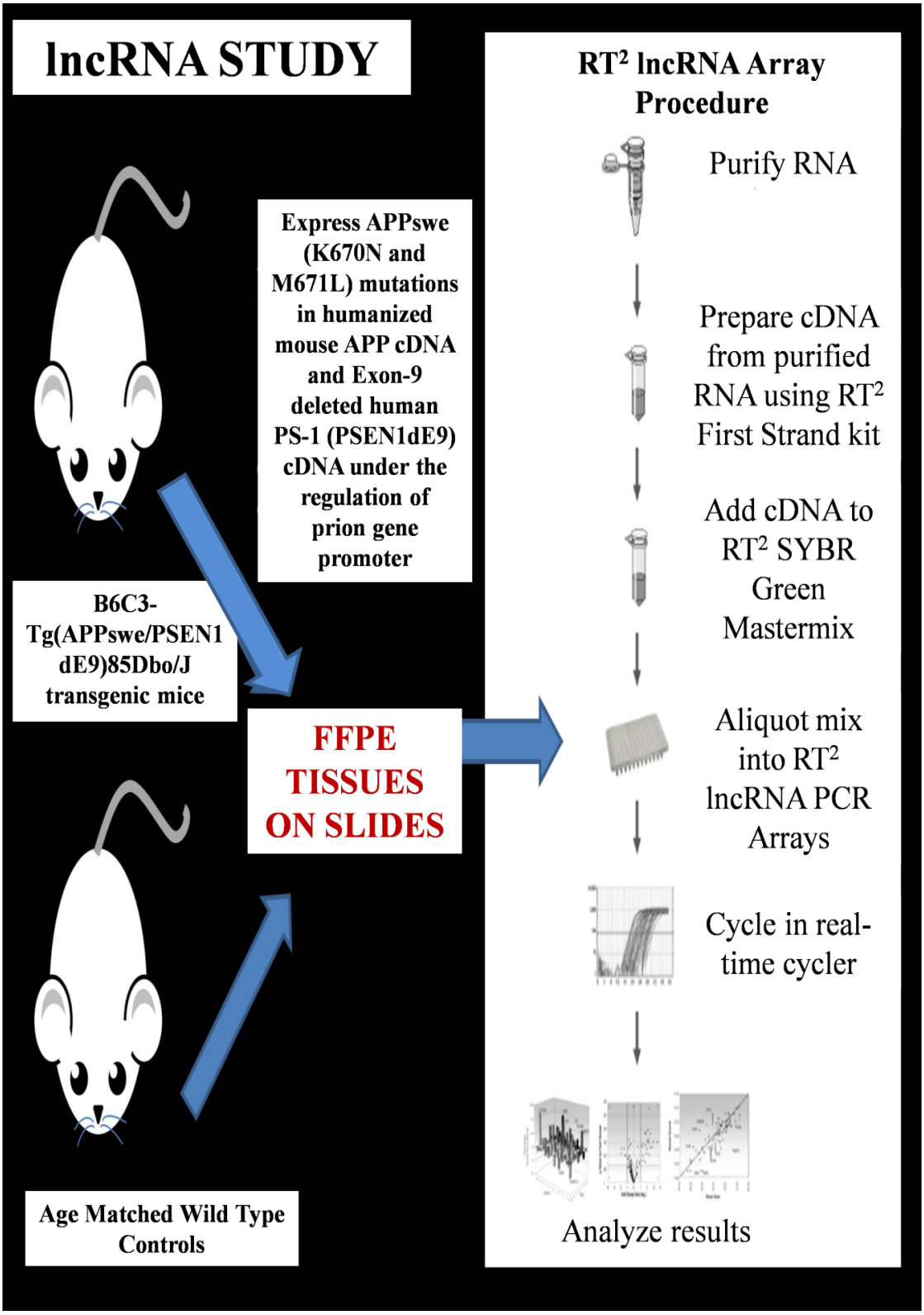

Figure 2.3: RT2 lncRNA PCR Array protocol schematic.

2.12. Patient Samples, constructs, reagents and siRNAs

Patient Samples: R1236035Alz-50 - Total RNA – Alzheimer's disease: Brain 50ug. (Lot #A507294) (Male 87 years old, Clinical Diagnosis – Alzheimer's disease, 1 donor); R1234035-50 - Total RNA–Human Adult Normal Tissue: Brain 50ug. (Lot #C210018) (Male 29 years old, Clinical Diagnosis – Normal, 1 donor); **Constructs:** Human ROR1 ORF mammalian expression plasmid, C-GFPSpark tag (HG13968-ACG)**;** Human EphA2/Eph Receptor A2, C-GFP Spark tag (Cat: HG13926-ACG)/ Human EphA2/Eph Receptor A2 Gene cDNA ORF Clone, Human, untagged (Cat: HG13926-UT**); miRNA mimics:** HMI0350-5NMOL (hsa-miR-200a-3p),HMI0415-5NMOL(hsa-miR-26a-5p), HMI0419-5NMOL (hsa-miR-26b-5p), HMC0002-5NMOL (negative control- Sequence from *Arabidopsis thaliana* with no homology to human gene sequences); **Reagents:** Cytochalasin D - (ab143484), Jasplakinolide - (ab141409), DRAQ5™ (ab108410); **siRNA:** FlexiTube GeneSolution GS378938 for MALAT1- 4 siRNAs : SI04347056 (FlexiTube siRNA),SI04342233 (FlexiTube siRNA),SI03670548 (FlexiTube siRNA), SI03670541 (FlexiTube siRNA); 4 siRNAs for Entrez gene 283131 for NEAT1: SI05189765 (FlexiTube siRNA), SI05189758, SI05189751, SI03682126 , Product no: 1027416, Cat no:GS283131, Negative control siRNA (1022076).

2.13. RNA isolation from cultured cells and paraffinized tissue

Total RNA was prepared from cultured cells using TriZol Reagent (Invitrogen, USA) according to manufacturer's protocol. I isolated RNA from paraffin-embedded tissue samples of AD mice; along with controls. In brief, isolation method for RNA from paraffin-embedded tissues consists of the following steps: De-paraffinization: For RNA extraction from tissue sections obtained from AD mice or controls, two sections each of 20 µm thickness were taken per 1.5 ml Eppendorf tube. The sections were

deparaffinized by two rinses in xylene for 5 min each at room temperature followed by two centrifugations at room temperature for 10 min each at 10,000 g. Rehydration: After paraffin solubilization, a rehydration step was introduced where the supernatants from the previous step were carefully removed and the pellets were successively washed with 1 ml of absolute ethanol and 1 ml of 95% ethanol in DEPC water. After each step, the tissue was collected by centrifugation at 10,000 g for 10 min. Protein digestion: After the final wash, alcohol was aspirated and the tissue pellets were air dried in a thermoblock at 37°C and re-suspended in 500 µl of digestion buffer (10 mMNaCl, 500 mMTris, pH 7.6, 20 mM EDTA and 1% SDS). To obtain purified RNA, tissue proteins were removed by adding 500 µg/ml of the proteolytic enzyme proteinase K. The sections were then incubated at 45°C for 16 hours (overnight). Prior to RNA purification, proteinase K was inactivated at 100°C for 7 min in order to nullify its effects on PCR. RNA extraction: Total RNA was then extracted from these tissue sections by using the Trizol reagent and following the manufacturer's protocol. The concentration of total RNA was measured using Biophotometer (Eppendorf, Germany). Details about tissues and their nanodrop concentrations given in the **Table 2.2.**

SR NO.	SAMPLE ID	NANODROP READINGS (ng/µl)	NANODROP READINGS (260/280)	NANODROP READINGS (260/230)	REMARKS
1	WILD TYPE 1	858.4	1.8	1.991.99	QC PASS
2	WILD TYPE 2	769.35	1.88	1.98	QC PASS
3	WILD TYPE 3	824	1.9	2.01	QC PASS
4	AD TRANSGENIC 1	687.3	1.85	2.03	QC PASS
5	AD TRANSGENIC 2	242	1.82	1.94	QC PASS
6	AD TRANSGENIC 3	469.6	2.1	1.89	QC PASS

Table 2.2: Quantification of RNA samples using Nanodrop.

2.14. Quantitative real-time PCR

Two microgram total RNA was subjected to DNase treatment (Sigma) followed by cDNA preparation using oligo dT primer or random hexamer primer, dNTPs and MuLv-Reverse transcriptase (Fermentas). Quantitative Real-time PCR (qRT-PCR) was carried out using Sybr green 2X Universal PCR Master Mix (Applied Biosystems) in StepOne Real-time PCR system (Applied Biosystems) using the Absolute Quantitation method. For each gene, non-template control was used at the same condition to ascertain the baseline and threshold value for the analysis. The absolute quantification given by the software was in terms of C_t values. The relative quantification (fold change) of a target gene in a sample compared to the parental cell is expressed in terms of $2^{-\Delta\Delta Ct}$ values after normalization with respect to internal control.

2.15. Gene-specific primers

Primers related to Chapter 3	
Primer name	**Sequence (5'-3')**
hsa-miR-221-3p STEM_LOOP	CTCAACTGGTGTCGT GGAGTCGGCAAT TCAGTTGAGGAAACCCA
hsa-miR-221-3p REAL_TIME_FORWARD	ACACTCCAGCTGGGAGCTACATTG TCTGCT
hsa-miR-222-3p STEM_LOOP	CTCAACTGGTGTCGTGGAGTCGGC AATTCAGTTGAGACCCAGTA
hsa-miR-222-3p REAL_TIME_FORWARD	ACACTC CAG CTG GGAGCTACATCT GGCTAC
hsa-miR-155-5p STEM_LOOP	CTCAACTGGTGTCGTGGAGTCGGC AATTCAGTTGAGAACCCCTA
hsa-miR-155-5p REAL_TIME_FORWARD	ACACTCCAGCTGGGTTAATGCTAA TCGTGA

hsa-miR-4697-3p STEM_LOOP	CTCAACTGGTGTCGTGGAGTCGGC AATTCAGTTGAGACCAAGGG
hsa-miR-4697-3p REAL_TIME_FORWARD	ACACTCCAGCTGGGTGTCAGTGAC TCCTGC
hsa-miR-3648 STEM_LOOP	CTCAACTGGTGTCGTGGAGTCGGC AATTCAGTTGAGCCC TCG GC
hsa-miR-3648 REAL_TIME_FORWARD	ACA CTC CAG CTGGGAGCCGCGGGG ATCGCC
hsa-miR-1251-5p STEM_LOOP	CTCAACTGGTGTCGTGGAGTCGGC AATTCAGTTGAGAGCGCCTT
hsa-miR-1251-5p REAL_TIME_FORWARD	ACACTCCAGCTGGGACTCTAGCTG CCAAAG
hsa-miR-3607-5p STEM_LOOP	CTCAACTGGTGTCGTGGAGTCGGC AATTCAGTTGAGACTGATTT
hsa-miR-3607-5p REAL_TIME_FORWARD	ACACTCCAGCTGGGGCATGTGATG AAGCAA
hsa-miR-3117-3p STEM_LOOP	CTCAACTGGTGTCGTGGAGTCGGC AATTCAGTTGAGCTGGCACT
hsa-miR-3117-3p REAL_TIME_FORWARD	ACACTCCAGCTGGGATAGGACTCA TATAGT
hsa-miR-335-3p STEM_LOOP	CTCAACTGGTGTCGTGGAGTCGGC AATTCAGTTGAGGGTCAGGA
hsa-miR-335-3p REAL_TIME_FORWARD	ACACTCCAGCTGGGTTTTTCATTAT TG CTC
UNIVERSAL REVERSE PRIMER	GTG CAG GGT CCG AGG T
Human_U6 snRNA_FORWARD	CTC GCT TCG GCA GCA CAT TC
Human_U6 snRNA_REVERSE	AAC GCT TCA CGA ATT TGC GT
Primers related to Chapter 4	
Primer name	**Sequence (5'-3')**
200a-3p_STEM_LOOP	CTC AAC TGG TGT CGT GGA GTC GGC AAT TCA GTT GAG ACA TCG

	TT
200a-3p_RT_FWD	ACA CTC CAG CTG GGT AAC ACT GTC TGG TAA
26a-5p_STEM_LOOP	CTC AAC TGG TGT CGT GGA GTC GGC AAT TCA GTT GAG TGC CTA TC
26a-5p _RT_FWD	ACA CTC CAG CTG GGT TCA AGT AAT CCA GGA
26b-5p _STEM_LOOP	CTC AAC TGG TGT CGT GGA GTC GGC AAT TCA GTT GAG ACC TAT CC
26b-5p _RT_FWD	ACA CTC CAG CTG GGT TCA AGT AAT TCA GGA
Universal Reverse Primer	CCA GTG CAG GGT CCG AGG TA
Mouse_H19_FORWARD	AGATGGACGACAGGTGGGTA
Mouse_H19_REVERSE	GAGACTCAAAGCACCCGTGA
Mouse_GAS5_FORWARD	AGAGGGAAAGTTTTGTGGGC
Mouse_GAS5_ REVERSE	GTGACGTCAAGACGCAAAGC
Mouse_RMST_FORWARD	GGCACTGCCAAGTAGTCTGA
Mouse_RMST_ REVERSE	TCCCTGGCCGAACAGTATTT
Mouse_TUG1_ FORWARD	CACCCTTCAGGCACCCTATG
Mouse_TUG1_ REVERSE	TGAAGCCCCCATTTGAGTCC
Mouse_MEG3_FORWARD	GACCCACCTACTGACTGATGAACTG
Mouse_MEG3_ REVERSE	GTGAAGACACAACAGCCTTTCTCC
Mouse_NEAT1_FORWARD	GCTCTGGGACCTTCGTGACTCT
Mouse_NEAT1_ REVERSE	CTGCCTTGGCTTGGAAATGTAA
Mouse_MALAT1_FORWARD	GGCCAGCTGCAAACATTCAA

Mouse_MALAT1_ REVERSE	TGCAGTGTGCCAATGTTTCG
Mouse_U6 snRNA_FORWARD	CGCTTCGGCAGCACATATAC
Mouse_U6 snRNA_REVERSE	AAAATATGGAACGCTTCACGA
Human_H19_FORWARD	CCCACCAGCCTAAGGTGTTC
Human _H19_REVERSE	CGGTGGACGTGACAAGCAG
Human _GAS5_FORWARD	GATTTCACTTCCGGGACGGT
Human _GAS5_ REVERSE	GGCGGGGTGAAGGAAAGTAG
Human _RMST_FORWARD	GCCCCACAAAAGGGAGTCTA
Human _RMST_ REVERSE	GCTTTTCGGTCCCCCTCATT
Human _TUG1_ FORWARD	ATGGCACCCAGTGTAAAGCA
Human _TUG1_ REVERSE	CCGCTTGCTAAAAGTCCACG
Human _MEG3_FORWARD	ATCATCCGTCCACCTCCTTGTCTT
Human _MEG3_ REVERSE	GTATGAGCATAGCAAAGGTCAGGG
Human _NEAT1_FORWARD	CTTCCTCCCTTTAACTTATCCAATCAC
Human _NEAT1_ REVERSE	CTCTTCCTCCACCATTACCAACAATAC
Human _MALAT1_FORWARD	AGTACAGCACAGTGCAGCTT
Human _MALAT1_ REVERSE	CCCACCAATCCCAACCGTAA
Human_EPHA2_FORWARD	GCAACATCCTCGTCAACAGC
Human_EPHA2_REVERSE	TGGCTTTCATCACCTCGTGG
Human_GAPDH_FORWARD	GTCTCCTCTGACTTCAACAGCG
Human_GAPDH_REVERSE	ACCACCCTGTTGCTGTAGCCAA
Human_U6 snRNA_FORWARD	CTCGCTTCGGCAGCACATTC
Human_U6 snRNA_REVERSE	AACGCTTCACGAATTTGCGT

Primers related to Chapter 5	
Primer name	**Sequence (5'-3')**
146a-5p_STEM_LOOP	CTC AAC TGG TGT CGT GGA GTC GGC AAT TCA GTT GAG AAC CCA TG
146a-5p _RT_FWD	ACA CTC CAG CTG GGT GAG AAC TGA ATT CCA
34a-5p_STEM_LOOP	CTC AAC TGG TGT CGT GGA GTC GGC AAT TCA GTT GAG ACA ACC AG
34a-5p _RT_FWD	ACA CTC CAG CTG GGT GGC AGT GTC TTA GCT
Mouse_NEAT1_FORWARD	GTGAAGACACAACAGCCTTTCTCC
Mouse_NEAT1_ REVERSE	GCTCTGGGACCTTCGTGACTCT
Mouse_U6 snRNA_FORWARD	TGCAGTGTGCCAATGTTTCG
Mouse_U6 snRNA_REVERSE	CGCTTCGGCAGCACATATAC
Human _NEAT1_FORWARD	GTATGAGCATAGCAAAGGTCAGGG
Human _NEAT1_ REVERSE	CTTCCTCCCTTTAACTTATCCAATC AC
Human_ROR1_FORWARD	TAATCGGAGAGCAACTTCA
Human_ROR1_REVERSE	TGTAGTAATCAGCGGAGTAA
Human_GAPDH_FORWARD	TGGCTTTCATCACCTCGTGG
Human_GAPDH_REVERSE	GTCTCCTCTGACTTCAACAGCG
Human_U6 snRNA_FORWARD	ACCACCCTGTTGCTGTAGCCAA
Human_U6 snRNA_REVERSE	CTCGCTTCGGCAGCACATTC
Primers related to Chapter 6	
Primer name	**Sequence (5'-3')**
Mouse Xist_RT_F	TTGTGGCTTGCTAATAAT

Mouse Xist_RT_R	AAACCCCATCCTTTATG
Human XIST RT_F	TGACCTTGTTAAGCAAGCG
Human XIST RT_R	ATGGACCACTGTTTGATAGAC
Mouse GAPDH_RT_F	AGCCTCGTCCCGTAGACAAAA
Mouse GAPDH_RT_R	TGGCAACAATCTCCACTTTGC
Human GAPDH_RT_F	TCCCTGCACCACCAACTGTTAG
Human GAPDH_RT_F	GGCATGGCATGTGGTCATGAG
Primers related to Chapter 7	
Primer name	**Sequence (5'-3')**
Xist_RT_F	TTGTGGCTTGCTAATAAT
Xist_RT_R	AAACCCCATCCTTTATG
Meg3_RT_F	GACCCACCTACTGACTGATGAACTG
Meg3_RT_R	GTGAAGACACAACAGCCTTTCTCC
Neat1_RT_F	GCTCTGGGACCTTCGTGACTCT
Neat1_RT_R	CTGCCTTGGCTTGGAAATGTAA
Snhg12_RT_F	GATTGTGAGGAGGGAGACCA
Snhg12_RT_R	GCTGGCCTTAATCTGACTGC
Vaultrc5_RT_F	AGCGGTTACTTCGACAGTGG
Vaultrc5_RT_R	TCTCGAACCAAACACTCACG
Gm22650_RT_F	AATCCAGCTGGTTCAAGGCT
Gm22650_RT_R	TGTATAATCCATTTTGATGGTTTAGGG
Snhg3_RT_F	TCTCTCTAGGCGTCGCTCTC
Snhg3_RT_R	AATATGGTCTGGGGGAAACC
Brip1os_RT_F	ATAACTGGGCAGGGACTGTG

Brip1os_RT_R	TCTATGGCAGCCCTCAGACT
Snora21_RT_F	AGCCTTTTGCTAGTGACCCA
Snora21_RT_R	TCTTGTCACAACACCGATTGA
Snord53_RT_F	GATATCCTCATGGTTTCGCGT
Snord53_RT_R	ATGCTCAGACAGCCAAGAGAAA
Snord85_RT_F	TGCAGGGATGATACATACTT
Snord85_RT_R	GCTCAGAACAAAGCTCTCAT

2.16. RNA Immunoprecipitation (RIP) Assay

RNA Immunoprecipitation was performed on fixed cells (4% formaldehyde) following the Abcam RIP protocol (https://www.abcam.com/protocols/RIP) following the manufacturer's instruction with modifications. SHSY5Y cells were harvested by trypsinization and resuspended in PBS, freshly prepared nuclear isolation buffer (1.28 M sucrose, 40 mM Tris-HCl, pH 7.5, 20 mM $MgCl_2$, 4% Triton X- 100) and water, and kept on ice for 20 min with frequent mixing. Nuclei were pelleted by centrifugation at 2,500 G for 15 min. Then the nuclear pellet was resuspended in freshly prepared RIP buffer (150 mM KCl, 25 mM Tris pH 7.4, 5 mM EDTA, 0.5 mM DTT, 0.5% NP40, 100 U/ml RNAase inhibitor, Protease inhibitors). The nuclei fraction was sonicated with the following parameters – 30% amplitude – 10 seconds – 1-minute gap, and the process was repeated 4 times. Following this, the solution was nutated at 20rpm for 90 minutes at 4^oC**.** After nutation, the lysate was centrifuged at 12,000 RCF for 20 minutes at 4^oC. The pellet was discarded and the supernatant was used for protein estimation using Bradford reagent. 5 mg of total protein in RIP buffer was used for each sample to which 3µg of antibody (FUS or IgG) was added and incubated at 4^oC with gentle rotation overnight. After that, to each tube 40 µl protein

A/G beads were added and incubated for 2 hr at 4°C with gentle rotation. Then, beads were pelleted by centrifugation at 2,500 rpm for 30 s, the supernatant was removed, and the beads resuspended in 500 µl RIP buffer. Beads were washed for a total of three RIP washes, followed by one wash in PBS. The co precipitated RNAs were isolated by resuspending beads in TRIzol RNA extraction reagent (1 ml) according to manufacturer's instructions. RNA was eluted with 15 µl nuclease-free water. The total RNA was used to make cDNA with Random Hexamer or miRNA specific stem loop primers. The following steps were same as the Quantitative Real-time PCR (qRT-PCR) protocol stated above.

2.17. Sequential Immunocytochemistry (ICC) and RNA Fluorescence *in situ* Hybridisation (FISH) Assay

Sequential Immunocytochemistry (ICC) and RNA Fluorescence In Situ Hybridisation (FISH) Assay was performed following Stellaris® RNA FISH protocol according to the manufacturer's instruction, with modifications. Briefly, SHSY5Y cells were seeded on 18 mm coverglass in a 35mm cell culture plate. The growth medium was aspirated, and washed with 1 mL of 1X PBS. 1 mL of fixation buffer (3.7% (vol./vol.) formaldehyde in 1X PBS) was added and incubated at room temperature for 10 minutes. Then cells were washed twice with 1 mL of 1X PBS. To permeabilize, cells were immersed in 1 mL of 0.1% Triton X-100 in 1X PBS for 5 minutes at room temperature followed by washing with 1 mL of 1X PBS. Then, the cells on cover glass were inverted on 100 µl of appropriately diluted (1:100) primary antibody (anti-FUS antibody) in 1X PBS and incubated at 4^{o}C overnight. Following this, cells were inverted again in culture plate and washed with 1 mL of 1X PBS for 10 minutes, and repeated 2 more times. Then, 1 mL of appropriately diluted secondary antibody (1:300) in 1X PBS was added to the plate and incubated at room temperature for 2

hours in the dark. Again, they were washed with 1 mL of 1X PBS for 10 minutes, and repeated 2 more times. Then, 1 mL of fixation buffer was added and incubated at room temperature for 10 minutes followed by two washes 1 mL of 1X PBS. The 1X PBS was aspirated off the cover glass containing adherent cells within the 35 mm plate. 1 mL of Wash Buffer A was added, and incubated at room temperature for 2-5 minutes. Within a humidified chamber, 100 µL of the Hybridization Buffer containing probe (Human NEAT1 with Quasar® 570 dye) onto the Parafilm was dispensed and the cover glass was gently transferred, cells side down, onto the 100 µL drop of Hybridization Buffer containing probe. The humidified chamber was covered with the tissue culture lid, and sealed with Parafilm. Cells were incubated in the dark at 37 °C for 16 hours. Then the cover glass was gently transferred, cells side up, to a fresh 35 mm plate containing 1 mL of Wash Buffer A and incubated in the dark at 37 °C for 30 minutes. The Wash Buffer A was aspirated, and then 1 mL of DAPI nuclear stain (Wash Buffer A consisting of 5 ng/mL DAPI) was added to counter stain the nuclei followed by incubation in the dark at 37 °C for 30 minutes. The DAPI staining buffer was aspirated, and then 1 mL of Wash Buffer B was added with incubation at room temperature for 2-5 minutes. Finally, a small drop (approximately 15 µL) of Vectashield Mounting Medium was added onto a microscope slide, and the cover glass was mounted onto the slide, cells side down. Excess anti-fade from the perimeter of the cover glass was gently wicked away. The cover glass perimeter was sealed with clear nail polish, and allowed to dry.

2.18. Isolation of cell extract and Western blot analysis

Phosphate buffer saline (PBS) washed pellet from cell lines were lysed on on ice in lysis buffer (1M Tris-HCl, pH 7.5, 1N NaCl, 0.5 M EDTA, 1M NaF, 1M Na_3VO_4, 10% SDS, 20mM PMSF, 10% Triton X-100, 50% glycerol) for 30 min in presence of

complete protease inhibitor (Roche Diagnostics) and centrifuged at 13,000 g for 15 min. Protein concentration was determined by Bradford protein estimation assay.

The cell lysate was separated on SDS gel according to molecular weight then it was transferred to PVDF membrane (Millipore Corporation) which was blocked by 5% skimmed milk in TBST (50 mMTris-HCl, 150 mM NaCl, pH 7.5 containing 0.05% Tween 20). After that membrane was probed with primary antibody, followed by the incubation with HRP conjugated secondary antibody. The immunoreactive bands in the membrane were then developed with ECL kit (Super Signal West Pico Substrate; Pierce or Abcam). Quantification of western blots was carried out using Quantity One software of Bio-Rad. At least three separate experiments were analyzed and band intensities were normalized to loading control. Significant levels (*p*-values) were determined using the unpaired *t*-test.

2.19. Antibodies

Antibody name (cat no.)	**Dilution Used**
Rabbit monoclonal anti-EPHA2 (ab133501)	1:500
Mouse monoclonal anti-CREB (ab178322)	1:3000 (for Western Blot), 1:100 (for ICC)
Rabbit monoclonal anti-CREB (phospho S133) (ab32096)	1:1000
Mouse monoclonal anti-CREB (ab178322)	1:1000
Rabbit monoclonal anti-p38 (ab32142)	1:2000
Rabbit polyclonal anti-p38 (phospho Y182)	1:1000
Rabbit monoclonal anti-Synaptophysin (ab32127)	1:1000
Rabbit monoclonal anti-GAPDH (ab181602)	1:3000
Rabbit monoclonal anti-TLS/FUS (ab243880)	1:100 (for ICC) , 3µg total (for RIP)

Mouse monoclonal anti- Argonaute-2 (ab57113)	1:100 (for ICC)
Goat anti- mouse IgG (Alexa Fluor 488) (ab150113)	1:200 (for ICC)
Goat anti- mouse IgG (Alexa Fluor 568) (ab175473)	1:200 (for ICC)
Goat anti- mouse IgG (Alexa Fluor 647) (ab150115)	1:200 (for ICC)
Goat anti- rabbit IgG (Alexa Fluor 488) (ab150077)	1:200 (for ICC)
Goat anti- rabbit IgG (Alexa Fluor 568) (ab175471)	1:200 (for ICC)
Goat anti- rabbit IgG (Alexa Fluor 488) (ab150079)	1:200 (for ICC)
Mouse monoclonal anti-ROR1 (ab91187)	1:500
Rabbit polyclonal anti- α-tubulin (ab24246)	1:3000
Mouse monoclonal anti-SMA (ab7817)	1:2000
Rabbit monoclonal anti-Vimentin (ab92547)	1:2000
Mouse monoclonal anti-MAP2 (ab11267)	1:1000
Rabbit monoclonal anti-Vinculin (ab219649)	1:2000
Rabbit monoclonal anti-GAPDH (ab181602)	1:3000
Mouse monoclonal Anti-*Actin (Pan) antibody* [C4] (ab14128)	1:2000
Rabbit monoclonal anti-p53 (ab32389)	1:2000
Mouse monoclonal anti- β Actin (ab170325)	1:6000
Goat Anti-Rabbit IgG (HRP) (ab7090)	1:3000
Goat Anti-Mouse IgG (HRP) (ab97040)	1:3000

2.20. Immunocytochemistry

Immunocytochemistry was performed on fixed cells following the abcam ICC protocol (https://www.abcam.com/protocols/immunocytochemistry-immunofluorescence-protocol)

following the manufacturer's instruction with slight modifications. Briefly, cells were fixed using 4% paraformaldehyde in PBS pH 7.4 for 12 min at room temperature. Cells were washed three times with ice-cold PBS. Cells were then permeabilized with 0.1–0.25% Triton X-100 for 10 min at room temperature followed by PBS washes for three times for 5 min. Cells were then blocked with 1% BSA, 22.52 mg/mL glycine in PBST (PBS+ 0.1% Tween 20) for 30 min to block unspecific binding of the antibodies. Then, the cells were incubated with diluted primary antibody in 1% BSA in PBST in a humidified chamber for overnight at 4°C. The solution was decanted and the cells washed three times in PBS, 5 min each wash. Cells were then incubated with the secondary antibody in 1% BSA for 1 h at room temperature in the dark. The secondary antibody solution was decanted and cells washed three times with PBS for 5 min each in the dark. Finally, the cells were incubated with 0.1–1 μg/mL DAPI (DNA stain) for 5 min. The DAPI solution was discarded and cells were rinsed twice with PBS. Cover slips were mounted on fresh, cleaned and dried slides with a drop of mounting medium and sealed with nail polish to prevent drying and movement under microscope.

2.21. Aggregate counting

Aggregates of mutant HTT tagged with DsRed were determined using methods described earlier [**35**]. In brief mouse Neuro2A or human SHSY5Y cells were cultured on coverslips in 35 mm culture dish (Nunc, USA) and transfected with HTT-83Q-DsRed or cotransfected with HTT-83Q-DsRed and siRNAs against Neat1 and

Meg3. Twenty-four hours of post-transfection, coverslips were washed with PBS and then mounted on slides for aggregate counting using a confocal microscope (Zeiss LSM 710, Germany). An average of 50 cells was counted for each slide and the experiment was performed three times.

2.22. F/G Actin Assay

After appropriate treatments, cells were scrapped from the petri dishes and washed twice in PBS. Cells were then centrifuged at 800 RCF for 3 min at 4°C. The cell pellets were then resuspended in 200 µl PBS with 0.1% Triton-X-100 (with protease inhibitors). After incubation for 15 min with slight agitation, cells were again centrifuged at 15,000 RCF at 4°C for 5 min. The soluble supernatant (which contained G-actin) was separated and the Triton-X-100 insoluble pellet (predominantly F-actin) was resuspended in 200 µl RIPA buffer. The soluble and insoluble fractions were mixed with 5X Loading dye, heated at 98°C for 10 min, equal volumes of the two fractions were loaded and separated on a 12% SDS gel using standard electrophoresis protocol. Actin levels were assayed using the pan actin antibody (Clone C4).

2.23. Trypan Blue Exclusion Assay

For the Trypan Blue Exclusion Assay, SHSY-5Ycells were seeded in 6 well clear bottom plates (Thermo). After the appropriate treatments, media was discarded from cell cultures and washed twice with PBS. Cells were trypsinised and resuspended in 1 ml fresh media (without FBS). 50 µL of cells and 50 µL of 0.4% Trypan blue solution were mixed properly and incubated for 2 minutes at room temperature. Then 10 µL of the cell suspension with dye was pipetted on the haemocytometer and covered with a coverslip. The haemocytometer was placed under a light microscope and round cells (blue – dead; white – live) were counted from the 4 large corner squares and the

central square. Viable and non-viable cell percentages were calculated after the different treatments and for each set, experiments were repeated thrice. Cell viability was plotted as % viability compared to controls.

2.24. MTT Assay

For the MTT cell viability assay, cells were seeded in 96 well clear bottom plates (Thermo). After the appropriate treatments, media was discarded from cell cultures and washed twice with PBS. After that 50 µL of FBS free media and 50 µL of MTT (5mg/ml) solution was added into each well and the plate was incubated at 37°C for 3 hours. Then, 150 µL of DMSO (MTT solvent) was added into each well. The plate was wrapped in foil and shaken on an orbital shaker (15 min). Occasionally, the liquid was pipetted to fully dissolve the MTT formazan (violet colour). Finally, a Micro plate Reader was used to read the absorbance at OD=590 nm. Each sample had 10 replicates.

2.25. Live and Dead Cell Assay

Live and Dead Cell Assay was performed on live cells following the abcam Live and Dead Cell Assay protocol (https://www.abcam.com/live-and-dead-cell-assay-ab115347.html) following the manufacturer's instruction. Briefly, cells were cultured on 35 mm dishes (Thermo). Following appropriate treatments, cells were washed twice in PBS and trypsinised for 5 min with resuspension in fresh PBS. 5X dye (from 1000X stock) in PBS was added directly to the cells and incubated in the dark for 10 min at room temperature. 10µL of the stained cell suspension was put onto a freshly cleaned and dried slide (Himedia), covered with a 18mm x 18mm glass coverslip (Himedia) and imaged with a Carl Zeiss 710 confocal microscope immediately. Live cells were stained green and dead cells were stained red [LIVE: Excitation (max): 495nm, Emission (max): 515nm DEAD: Excitation (max): 528nm, Emission (max):

617nm.]. 1 µL of Hydrogen Peroxide (for 10 minutes) per 35mm dish was used as a negative control. Experiments were repeated thrice and each time at least 50 cells per field were counted for each sample.

2.26. Databases

To identify the interacting partners of Meg3, Neat1 and Xist, I used the database NPInter (http://www.bioinfo.org/NPInter/, version 3.0) based on experimental data from high throughput assays like crosslinking and immunoprecipitation followed by deep sequencing (CLIP-seq), chromatin isolation by RNA purification followed by high-throughput sequencing (ChIRP-seq) and also manually curetted from scientific literature. This online resource provides information for interactions of long non-coding RNA with protein-coding genes and microRNA in the mouse as well as human genes**.** To find out the co-expressed genes with these three long non-coding RNAs, I used Gene Friends database (http://genefriends.org/microArray/). This database 'GeneFriends:Microarray" also catalogs data derived from gene expression studies using microarray. This online resource provides information on co-expressed protein-coding genes, non-coding genes including microRNAs, anti-sense RNA, and pseudogenes for a given query. To find out the transcription regulation of Meg3, Neat1, and Xist, I used the database at http://deepbase.sysu.edu.cn/chipbase/. This database catalogs transcription factor binding sites from ChIP-seq data obtained experimentally.

2.27. Enrichment analysis for biological processes defined by Gene Ontology (GO), pathways by KEGG, miRNA target interaction, miRNA - lncRNA interaction and lncRNA – RBP interactions

To find out the function (s) of miRNAs and possible involvement in AD pathogenesis, I carried out a gene set enrichment analysis of the protein interacting partners of these

miRNAs. Enrichment of biological processes associated with GO terms and pathways defined by Kyoto Encyclopaedia of Genes and Genomes (KEGG) was analysed with the help of DIANA tools (http://diana.imis.athena-innovation.gr/DianaTools/index.php). The miRPath tool was used for functional assessment of miRNAs in specific pathways (http://www.microrna.gr/miRPathv2). Pathways were generated with the modified settings – P- value threshold – 0.005, Micro T threshold – 0.8 and the default FDR correction. Top regulatory pathways involving miRNAs were analysed using miRPathDB v2.0 (mpd.bioinf.uni-sb.de/) using present parameters. Protein interacting partners of miRNAs were investigated and visualised in a network with the help of the database MIENTURNET (MicroRNA ENrichment TURned NETwork) (http://userver.bio.uniroma1.it/apps/mienturnet/) with the settings minimum number of target interactions -2, adjusted p-value (FDR) -0.5. The functional network of the most strongly enriched protein component common to all 3 groups (Aβ vs control, AD vs control and Aβ vs AD) was further analysed with the help of KEGG pathway map (https://www.genome.jp/kegg-bin/show_pathway?ko04068+K09385) and the components were coded according to the specific AD associated pathways. Additionally, protein interacting partners of lncRNAs were investigated with the help of the database – LIVE (LncRNA Interaction Validated Encyclopaedia) (https://live.bioinfotech.org/home/) which integrates experimentally validated interactions involved with lncRNAs. Only the protein and transcription factor (TFs) tabs were considered for this analysis. MiRNA target interaction, miRNA- lncRNA interaction and lncRNA- RNA Binding Protein (RBP) interactions were analysed with the help of ENCORI (The Encyclopaedia of RNA Interactomes) database with default pre-set parameters

(http://starbase.sysu.edu.cn/). The hyper geometric p-value was computed after correction for multiple testing.

2.28. Statistical analysis

Statistical significance was determined by student's unpaired *t*-test using online Graph Pad Software QuickCalcs (http://www.graphpad.com/quickcalcs/index.cfm).

Chapter 3: Effect of AICD and $A\beta_{1\text{-}42}$ on Cellular Degradome in AD

3.1. Several miRNAs are differentially expressed in cell models of AD

Small-RNA-Seq data was compared between 6 samples, grouped as Control (C1 and C2), Aβ (Aβ1 and Aβ2) and AICD + Aβ (AD1 and AD2) to identify differential miRNAs levels **(Fig 3.1a. and 3.1b.).**

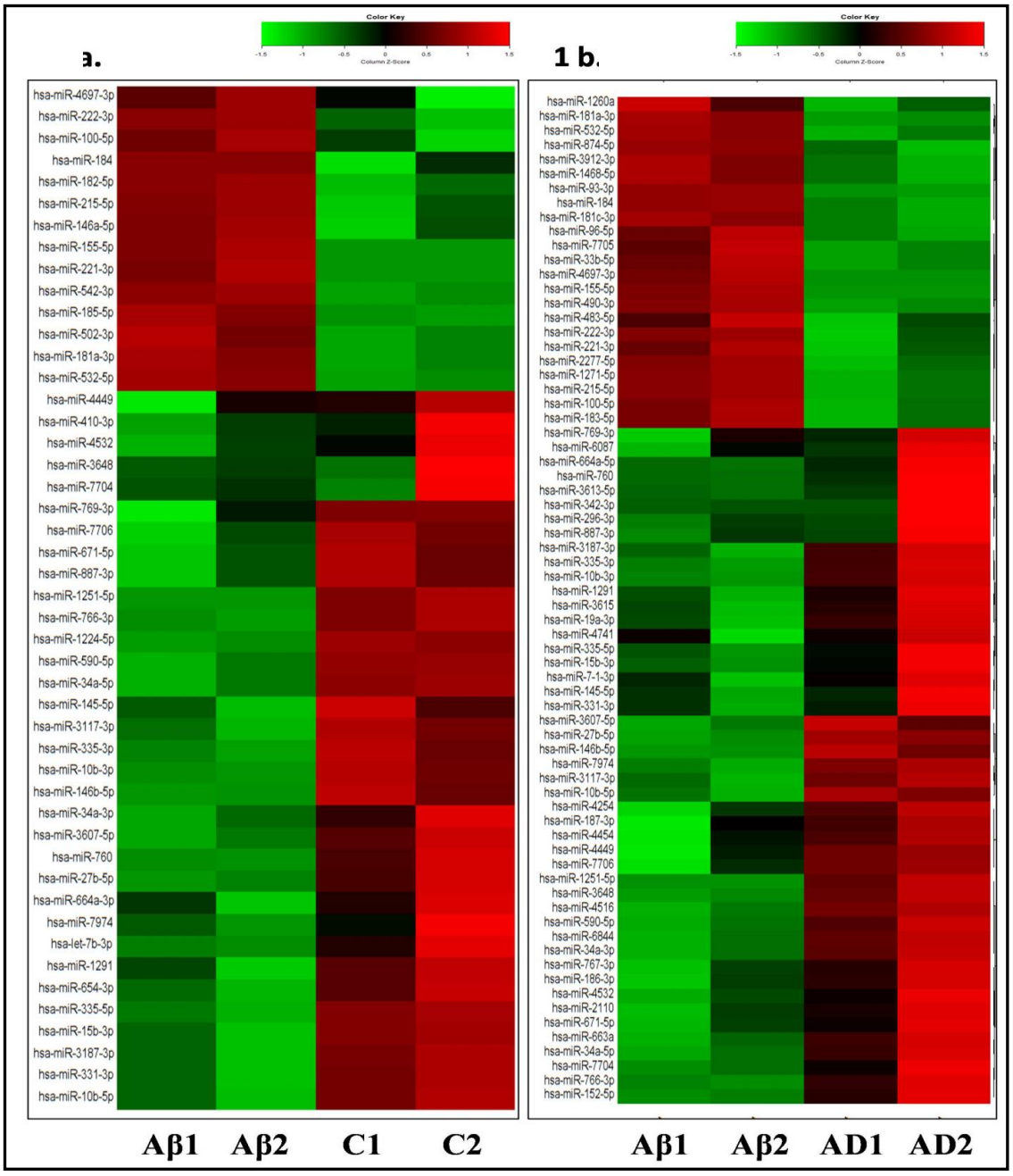

Figure 3.1: Heat map of statistically significant differentially regulated miRNAs in Aβ vs Control (1a.) and Aβ vs AD (1b.) samples by small RNA sequencing. Each sample has two biological replicates. Color codes indicate normalized fold changes- Red = up regulation; Green = down regulation.

After stringent quality controls, 47 (14 up regulated, 33 down regulated) miRNAs were found to be altered in the Aβ vs. Control group, 25 (19 up regulated, 6 down regulated) miRNAs in the AD vs. Control group and 70 (23 up regulated, 47 down regulated) miRNAs in the Aβ vs. AD group. Next it was found out how many and which miRNAs were common between the groups **(Fig 3.2a and Table 3.1)**.

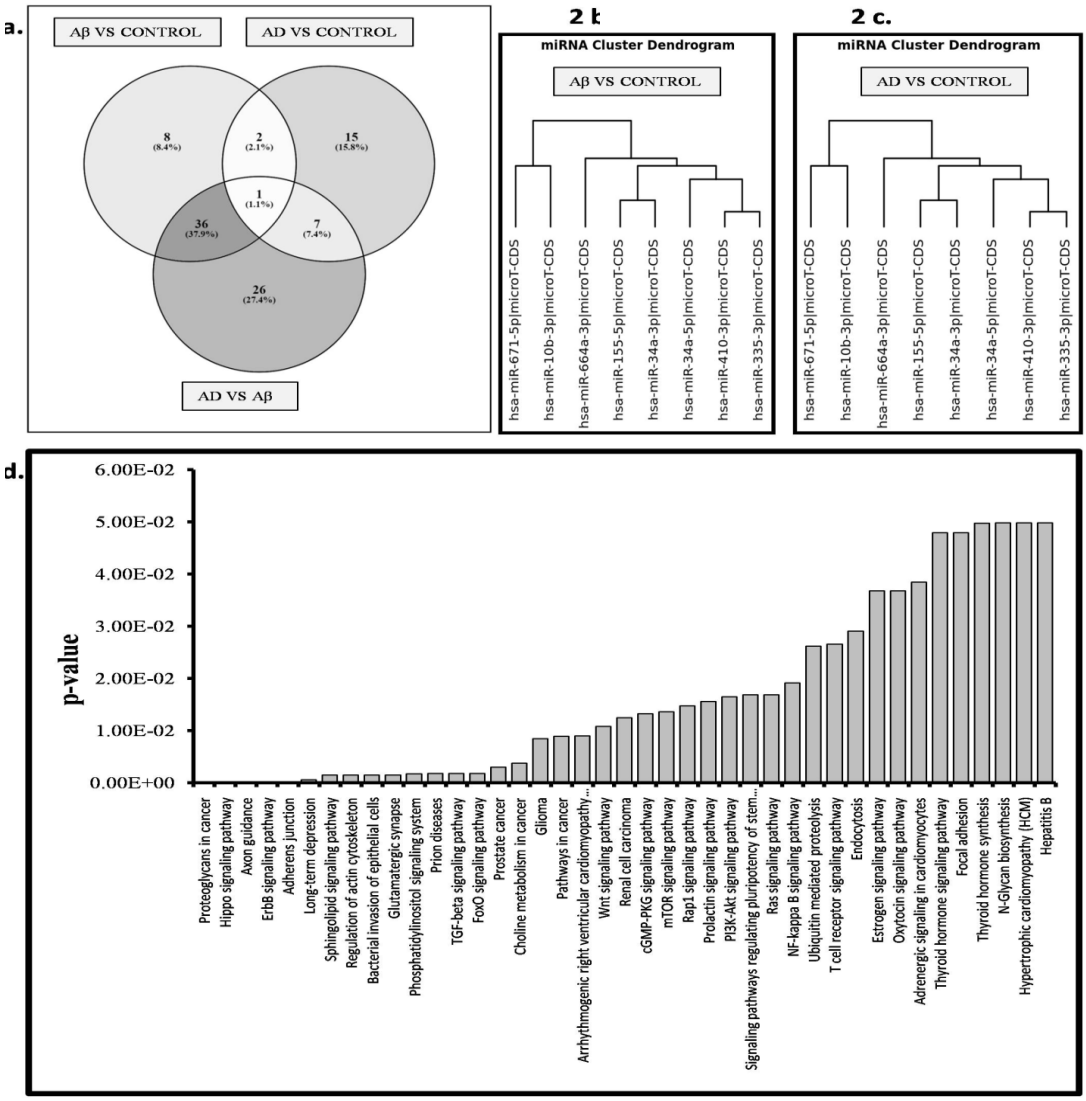

Figure 3.2: Venn diagram showing the overlaps of de regulated miRNAs between the groups Aβ vs Control, AD vs Control and Aβ vs AD (2a.) Hierarchical clustering of the significantly enriched miRNAs from Aβ vs Control (2b.) and AD vs Control groups (2c.). GSEA analysis of enriched processes involving de regulated miRNAs in the Aβ vs. Control group (2d.).

Of all the altered miRNAs, 8 were unique for the Aβ vs. Control group, 15 were unique for the AD vs. Control group and were unique for the Aβ vs. AD group.

Table 3.1. Summary of differentially regulated miRNAs, with the up regulated ones shown in bold font.

UNIQUE miRNAs			OVERLAPPING miRNAs		
Aβ vs. Control	**AD vs. Control**	**Aβ vs. AD**	**Aβ vs. Control AND AD vs.Control**	**AD vs. Control AND Aβ vs. AD**	**Aβ vs. Control AND Aβ vs. AD**
542-3p, 185-5p, **Let-7b-3p**, **654-3p, 410-3p,** 502-3p, **664a-3p**	**627-3p, 126-5p, 6742-3p,** 573**, 339-3p, 143-5p,** 502-5p**, 641, 101-5p, 450b-5p,** 3679-5p**, 6824-3p, 501-3p, 2681-3p, 548e-3p**	**186-3p,** 181c-3p, **19a-3p, 664a-5p**, **342-3p, 3615, 152-5p, 6087, 767-3p, 7-1-3p, 296-3p,** 33b-5p, **3613-5p, 663a,** 7705, 96-5p, 874-5p**, 4254**, 3912-3p, 1468-5p, **187-3p**, 483-5p, **4741**, **6844,** 2277-5p, **2110**	146a-5p, 1224-5p	4454, 93-3p, 1260a, 183-5p, 1271-5p, 4516, 490-3p.	221-3p, 222-3p, 155-5p, 532-5p, 146b-5p, 3117-3p, 3648, 335-3p, 331-3p, 1251-5p, 671-5p, 100-5p, 27b-5p, 215-5p, 4532, 145-5p, 184, 181a-3p, 769-3p, 15b-3p, 7706, 3607-5p, 10b-5p, 766-3p, 10b-3p, 34a-5p, 7704, 335-5p, 887-3p, 1291, 34a-3p, 7974, 760, 4449, 3187-3p, 590-5p.

Numbers of miRNAs common between the 3 groups were also limited - 2 miRNAs between Aβ vs. Control and AD vs. Control groups and 7 miRNAs between AD vs. Control and Aβ vs. AD groups. It was interesting to note that the Aβ vs. Control and

Aβ vs. AD groups had the largest number (36) of miRNAs in common. There was only one miRNA which was common to all the three comparative groups - hsa-miR-4697-3p.

3.2. Functional clustering, Gene Set Enrichment Analysis and pathway enrichment analysis reveal concurrent behaviour of several deregulated miRNAs

The miRPath module of DIANA TOOLS was used for functional clustering, GSEA analysis and Pathway enrichment of the significantly altered miRNAs obtained from the sequence data using the Aβ vs. Control and AD vs. Control groups. The hierarchical clustering of the miRNAs from the 2 groups is given in **Fig 3.2b and 3.2c.** GSEA analysis revealed a total of 41 processes, significantly enriched in the Aβ vs. Control group **(Fig 3.2d).** It was interesting to note that out of these, the strongly enriched processes included the core neurological ones - Axon guidance (p value - 3.26E-06), Long-term depression (p value - 0.000607481), Regulation of actin cytoskeleton (p value - 0.001500418) and Glutamatergic synapse (p value - 0.001513803) to name a few. Next, KEGG analysis of the miRNAs in the Aβ vs. Control group showed overrepresentation of pathways like Hippo signalling, Gabaergic synapse, steroid hormone biosynthesis, ErbB signalling, PI3-Akt signalling, Pluripotency of Stem cells, TGF-β signalling, and Prion diseases **(Fig 3.3a.).** GO enrichment analysis of the same group showed refinement of a total of 13 processes - biosynthetic process, organelle, ion binding, molecular function, cellular nitrogen compound, metabolic process, nucleic acid binding transcription factor activity, cellular protein modification process, plasma membrane adhesion molecules and cell death to name a few **(Fig 3.3b.)**. There was a specific cluster of 5 miRNAs - 664a-3p, 335-3p, 410-3p, 155, 5p and 34a-5p which enriched in almost all the processes. The same KEGG and GO analysis was performed with the significantly

altered miRNAs from the AD vs. Control group. The enriched KEGG pathways were overlapping with those of the Aβ vs. Control group namely, Pluripotency of Stem cells, TGF-β signalling, Thyroid hormone synthesis, and Prion diseases and exclusive ones like Cholinergic synapse, Axon Guidance, Prolactin signalling, lysine degradation Ras signalling to name a few. **(Fig 3.3c.)**. 21 GO processes were enriched with the miRNAs from the AD vs. Control group **(Fig 3.3d.)**, with the top enriched ones being similar to the previous group.

Here also, a tight cluster of 4 miRNAs - 627-3p, 548e-3p, 183 and 641 were involved in almost all the processes while some processes - ion binding, organelle, cellular nitrogen compound, biosynthetic process, nucleic acid binding transcription factor activity and cellular protein modification process involved almost all the miRNAs. Top significant pathways for altered miRNAs unique for the Aβ vs. Control group were analysed from miRPathDB v2.0, which revealed that 654-3p, 410-3p, 664a-3p and 654-3p were most enriched in DNA- binding transcription factor activity, RNA polymerase II-specific and 542-3p, 185-5p, 542-3p, 185-5p and 502-3p were most enriched in synaptic function. A similar analysis of AD vs. Control group showed that 627-3p, 126-5p, 6742-3p were most enriched in DNA- binding transcription factor activity, RNA polymerase II-specific, 339-3p was most enriched in Neurogenesis, 143-5p, 6824-3p, 501-3p were most enriched in synaptic function, 101-5p and 548e-3p were most enriched in Gene expression (Transcription), 450b-5p was most enriched in Regulation of RNA biosynthetic process, 2681-3p was most enriched in Cation binding. An additional investigation of the protein interacting components of

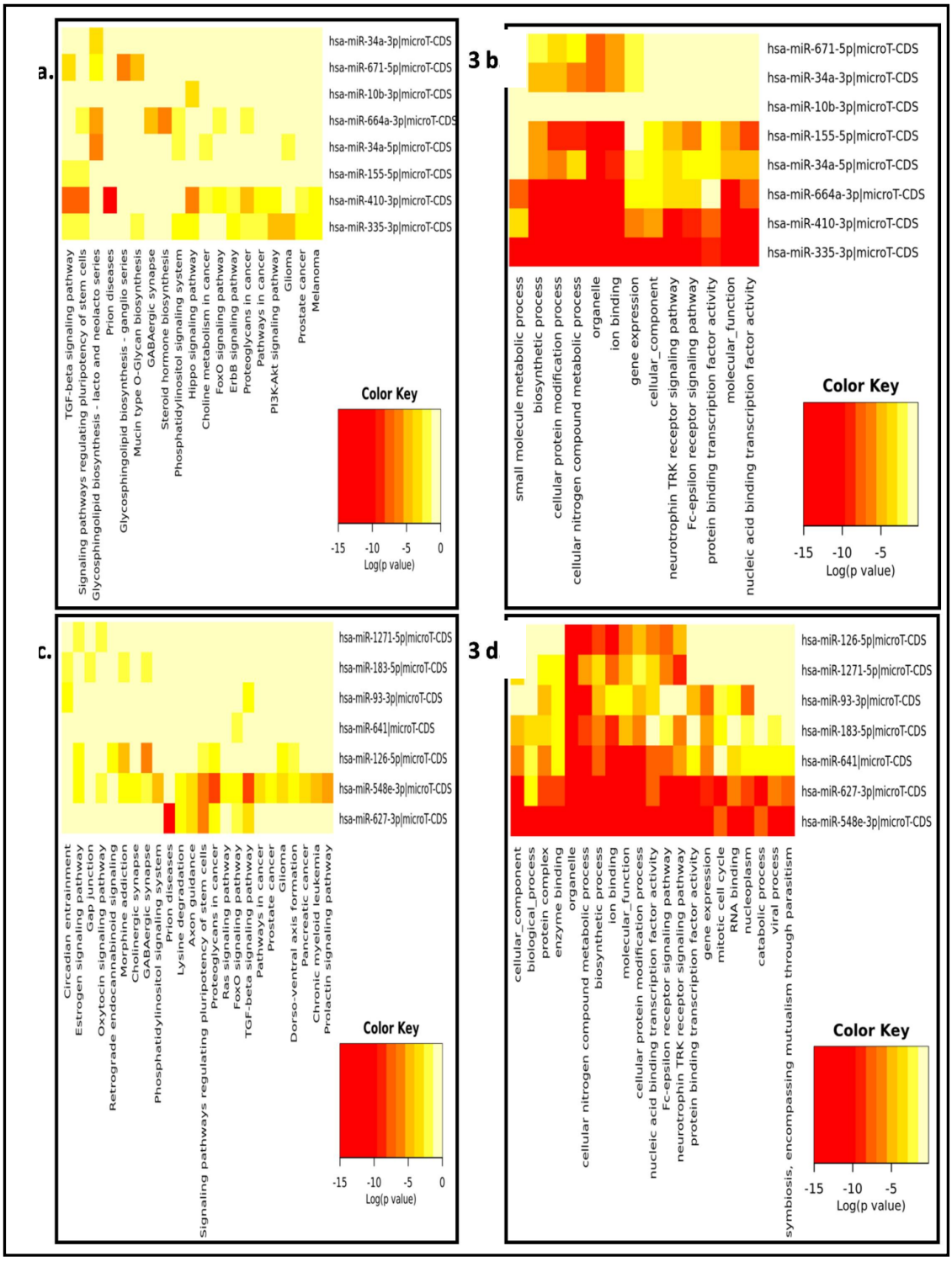

Figure 3.3: KEGG (3a.) and GO (3b.) analysis of de regulated miRNAs in the Aβ vs. Control group. KEGG (3c.) and GO (3d.) analysis of the miRNAs in the AD vs. Control group.

the top 10 deregulated miRNAs from the 3 groups were performed with the help of the database MIENTURNET using target data from miRTarBase. Among the several

protein components, all three groups showed enrichment of the FOXO protein (FOXO3 and FOXO1). Using this cue, the FOXO signalling pathway from KEGG was looked into **(Fig 3.4.)**, which revealed that the miRNA interacting protein partners are core components of diverse biological pathways including TGF-β signalling, Insulin signalling, IL (inflammation), mitochondrial, Jak-STAT, MAPK (Aβ and Tau), Synapse- all of which are involved in AD.

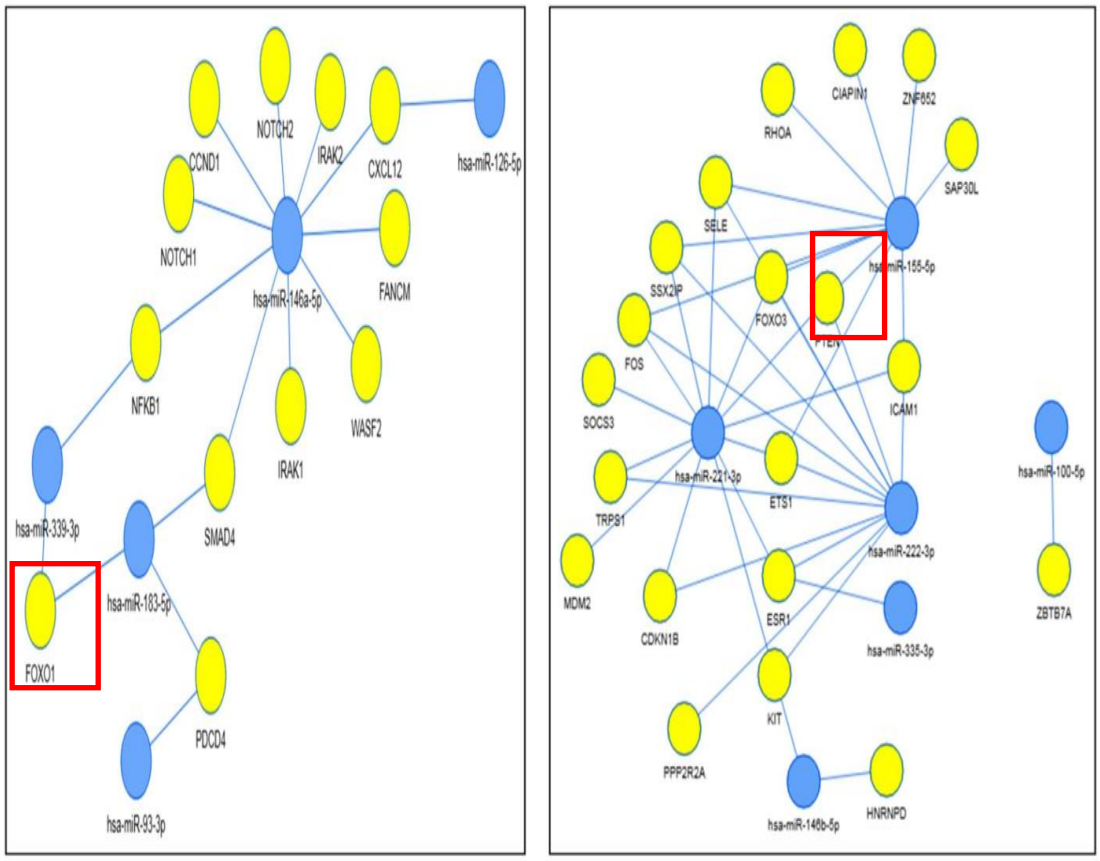

Network of protein interacting components of the top 10 deregulated miRNAs from the Aβ vs Control and AD vs Control groups. The common protein component is marked in red.

3.3. Quantitative real time PCR validates the top miRNA hits from the sequencing results in cell models of AD

In order to validate the changes in the miRNA levels from the sequencing data, I chose to look at the levels of 4 top up regulated (221-3p, 222-3p, 155-5p and 4697-3p) and 5 top down regulated (3648, 1251-5p, 3607-5p, 3117-3p and 335-3p)

miRNAs from the Aβ vs. Control group using real time PCR. **Fig 3.5a.** showed that only Aβ elicited a strong up regulation in all the 4 miRNAs with the highest change in 155-5p, followed by 4697-3p and almost same levels of increase in 221-3p and 222-3p, compared to controls. It was intriguing to see that only AICD affected these miRNAs reversibly from that of Aβ by decreasing their levels with

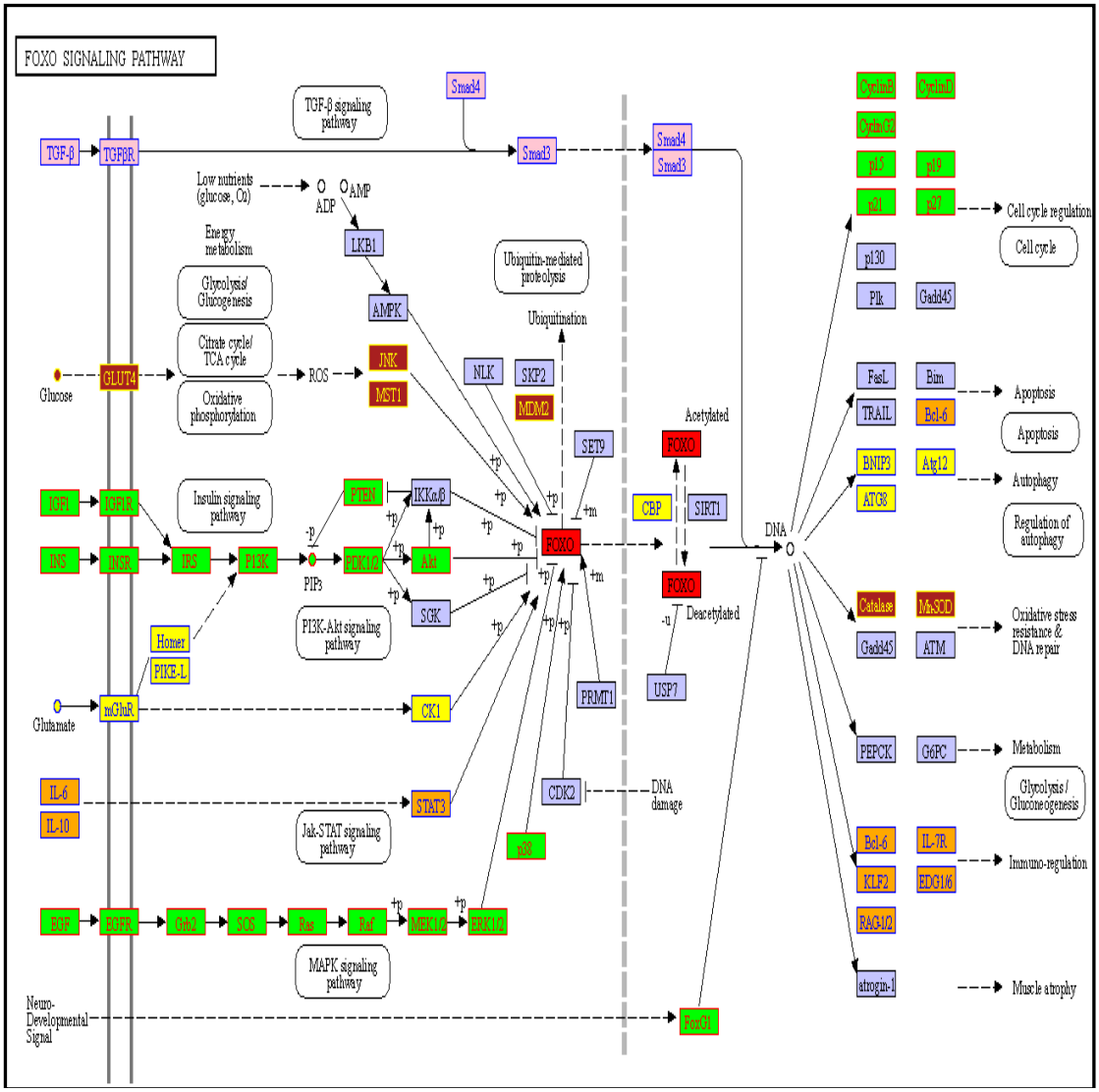

Figure 3.4: Molecular signalling pathway enrichment analysis of top 10 miRNAs from Aβ vs Control, AD vs Control and Aβ vs AD groups. Based on in silico analysis by using MIENTURNET database, FOXO signalling pathway was identified as the commonality. Subsequent KEGG FOXO network is shown with AD associated protein components colour coded by pathways. Pink – Aβ effectors; Brown – Mitochondrial related components; Green – AD (Aβ + Tau) associated proteins; Yellow – Glutamatergic and LTP components; Orange- Inflammatory response effectors; Red- FOXO proteins; Blue – All non- related proteins. Pathways containing the components are correspondingly coloured in boxes.

155-5p and 221-3p showing more down regulation than 222-3p and 4697-3p, compared to controls. In the AICD + Aβ group however, all the 4 miRNAs had an increasing trend more like the Aβ group, with 221-3p and 222-3p showing the stronger up regulation, followed by 4697-3p and lastly 155-5p, compared with controls. It was also observed that the upward trend of increase in these 4 miRNA species in the AICD + Aβ group was not as much as that due to Aβ alone.

Conversely, from **Fig 3.5b.** I saw that only Aβ led to a strong down regulation in all the 5 miRNAs tested- 3648, 1251-5p, 3607-5p, 3117-3p and 335-3p, compared to controls; while only AICD in this case elicited a reverse up regulation of 335-3p and 3117-3p; and 3648, 1251-5p, 3607-5p showed a down regulation which was however not pronounced as that due to only Aβ. The more confounding observation was that AICD + Aβ together increased the levels of 4 of these 5 miRNAs, with 3607-5p and 3648 showing the strongest up regulation, followed by 1251-5p and 335-3p, while 3117-3p showed a slight down regulation, compared to controls. Combining the above results, it was found that the low throughput real time PCR data was in concordance with the sequencing results, but the only AICD group was behaving counter intuitively.

3.4. Multi-dimensional scaling and Principal Component Analysis of deregulated miRNAs show distinctive clusters for different sample sets

An MDS (Multi-dimensional scaling) plot was generated in edge R, to assess the level of similarity or dissimilarity among the samples in the groups under study. The function Plot MDS was used which computes the distances corresponding to the root mean square of the maximum of the absolute logarithm of fold changes between each pair of samples. Upon studying the plot, I could see that the samples in the Aβ group are well separated from the Control and AICD + Aβ groups. However, on further

inspection, I noticed that distance between the Control and AD groups was not sufficiently large so as to separate them in two distinct, well-separated clusters. A Principal Component Analysis of the deregulated miRNAs from the 3 groups showed a similar trend like the MDS plot, with a 53% variance of Principal Component 1 and a 16% variance of Principal Component 2. The Aβ samples clustered tightly and separated distinctly from the Control and AICD + Aβ groups **(Fig 3.6a)**. It was also interesting to note that the individual samples of both the Control and AICD + Aβ groups were not closely spaced, which might hint at the differential expression of the transfected AICD causing a cell-to-cell variation, as opposed to Aβ treatment, which affected the cells homogeneously.

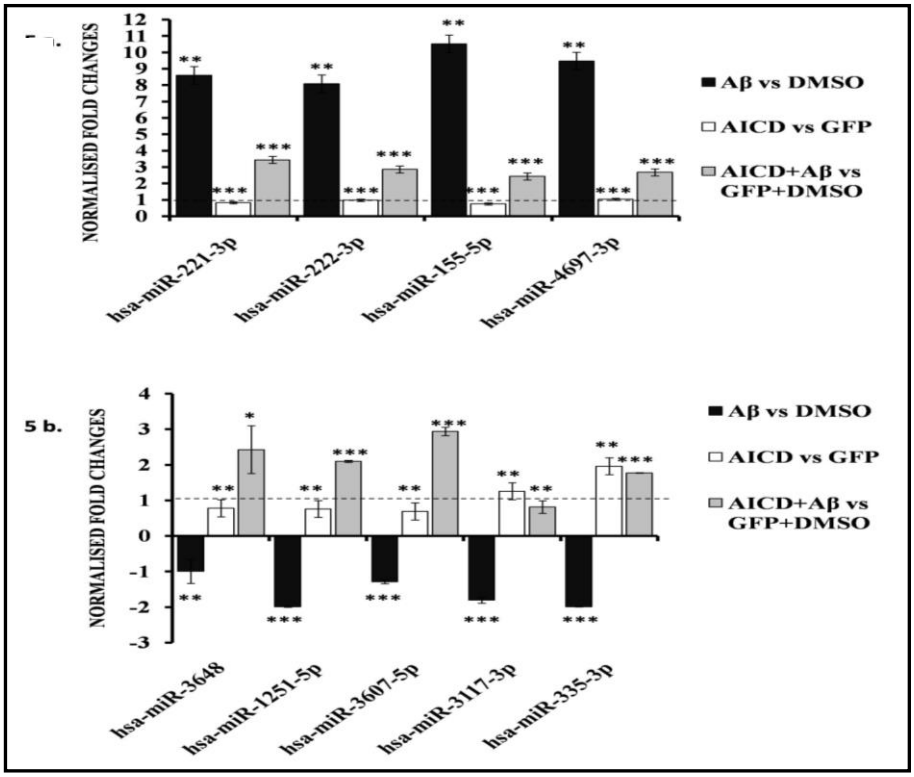

Figure 3.5: qPCR-based validation of top 4 up regulated and top 5 down regulated miRNAs from the Aβ vs Control group (5a.). Bar graphs representative of three (n = 3) independent experiments measuring levels of hsa-miR-221-3p, hsa-miR-222-3p, hsa-miR-155-5p and hsa-miR-4697-3p under conditions of Aβ vs DMSO, AICD vs GFP and AICD + Aβ vs GFP + DMSO (5b.). Bar graphs representative of three (n = 3) independent experiments measuring levels of hsa-miR-3648, hsa-miR-1251-5p,

hsa-miR-3607-5p, hsa-miR-3117-3p and hsa-miR-335-3p under same conditions as above. Levels were accessed by qRT-PCR in total RNA from SHSY-5Y cells treated with Aβ alone, transiently expressing AICD or treated with Aβ and transiently expressing AICD, using mature miRNA specific primers. Levels of U6snRNA were taken as endogenous control. The levels of individual miRNAs were normalized by the corresponding U6snRNA levels. For comparison between the groups, the fold changes of DMSO, GFP or GFP + DMSO were taken as 1. Error bars indicate ± SD. Significance values were calculated between the following pairs: Aβ with DMSO, AICD with GFP and AICD + Aβ with GFP + DMSO. The statistical significance level is indicated (NS, not significant; *, $p < 0.05$; **, $p < 0.01$; ***, $p < 0.001$).

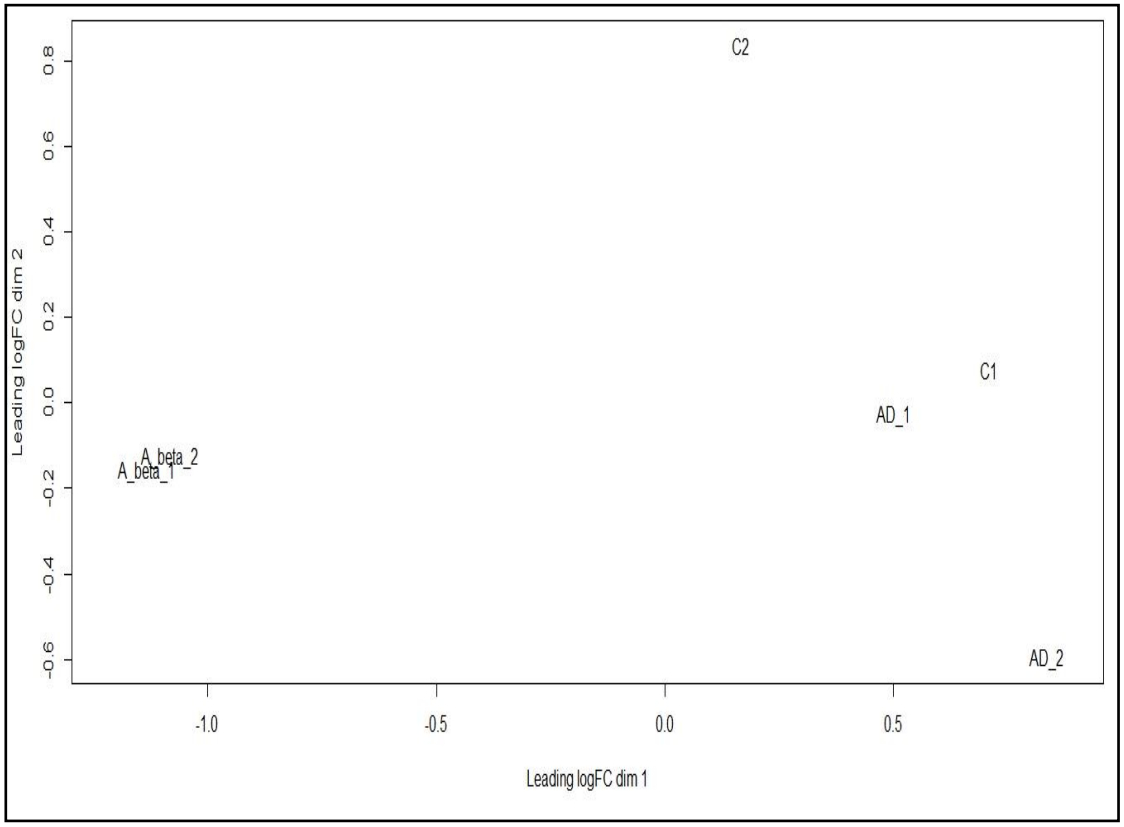

MDS (Multi-dimensional scaling) plot, to assess the level of similarity or dissimilarity among the de regulated miRNAs in the Aβ, AICD + Aβ and Control (GFP + DMSO) groups.

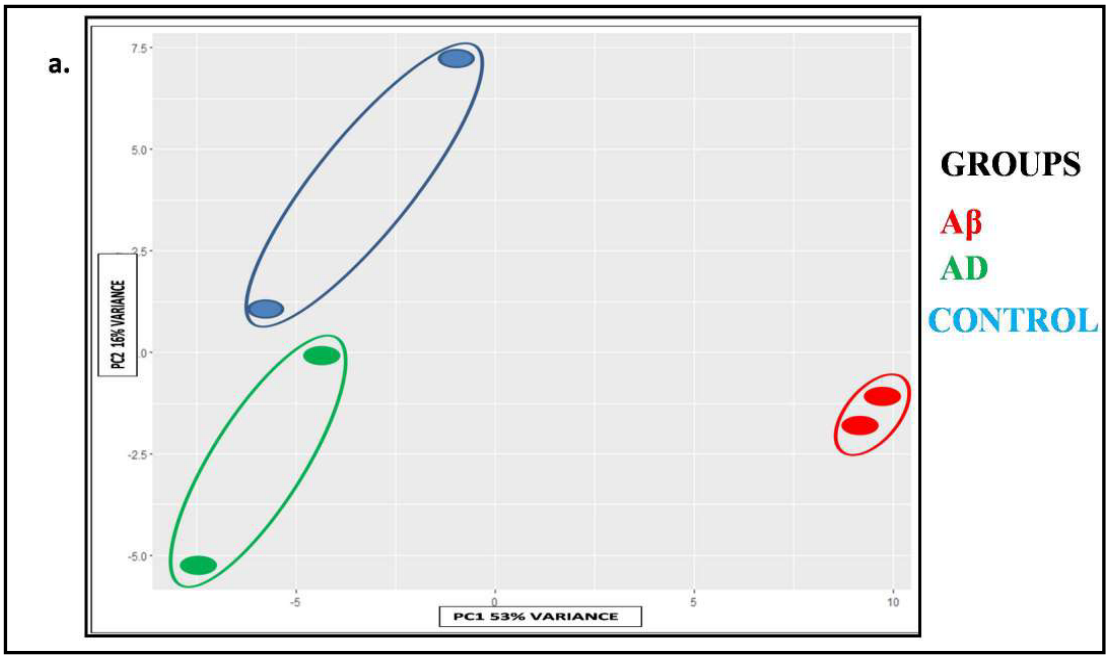

Figure 3.6: Principal Component Analysis of the deregulated miRNAs from Aβ vs Control, AD vs Control and Aβ vs AD groups (6a). Heat map of statistically significant differentially regulated top 25 up regulated and top 25 down regulated lncRNAs in Aβ vs Control (6b.) by small RNA sequencing. Each sample has two biological replicates. Color codes indicate normalized fold changes- Red = up regulation; Green = down regulation.

3.5. Six lncRNAs are consistently deregulated in cell models of AD

Besides the annotated miRNAs, rest of the aligned sequences for other ncRNAs were aligned against the annotated non-coding regions in the human genome with sufficient depth. In case of the Aβ vs. Control group, I obtained a total of 263 differentially expressed lncRNAs, with 224 of them up regulated and 39 down regulated respectively in Aβ treated cells**)**. From this large dataset, A Heatmap was plotted taking only the top 25 up regulated and down regulated lncRNAs, using Heatmap.2 function in R **(Fig 3. 6b. And Table 3.2.)**.

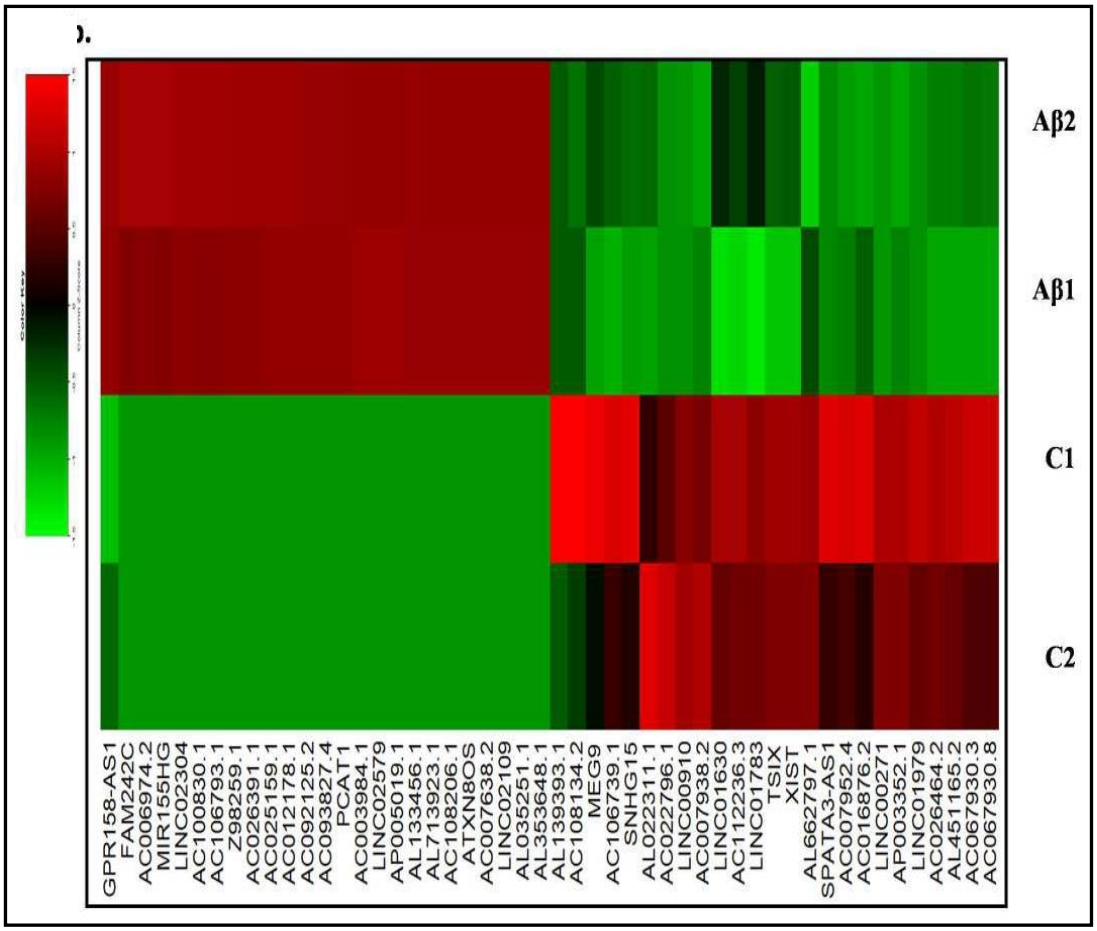

Likewise, the AD vs. Control yielded a total of 41 deregulated lncRNAs (**Fig 3.7a. and Table 3.2**). Moreover, I also looked at the levels of 14 selected lncRNAs in a consolidated Heatmap taking all the samples into consideration, which had known associations with AD, directly or through interactors and mediators **(Fig 3.7b.)**. In this refined set, RMST, FENDRR and AIRN were found to have a higher abundance in only one Aβ sample, while being less abundant in all the other five. MEG3 increased uniformly in the Aβ treated cells, but decreased in both the Controls and AICD+ Aβ samples. NEAT1 similarly showed an increasing trend in the Aβ samples, but behaved aberrantly in others. MEG8 and H19 did not show any consistent trend. HOTAIRM1 was increased in only one AICD+ Aβ sample, while being reduced in all other 5.

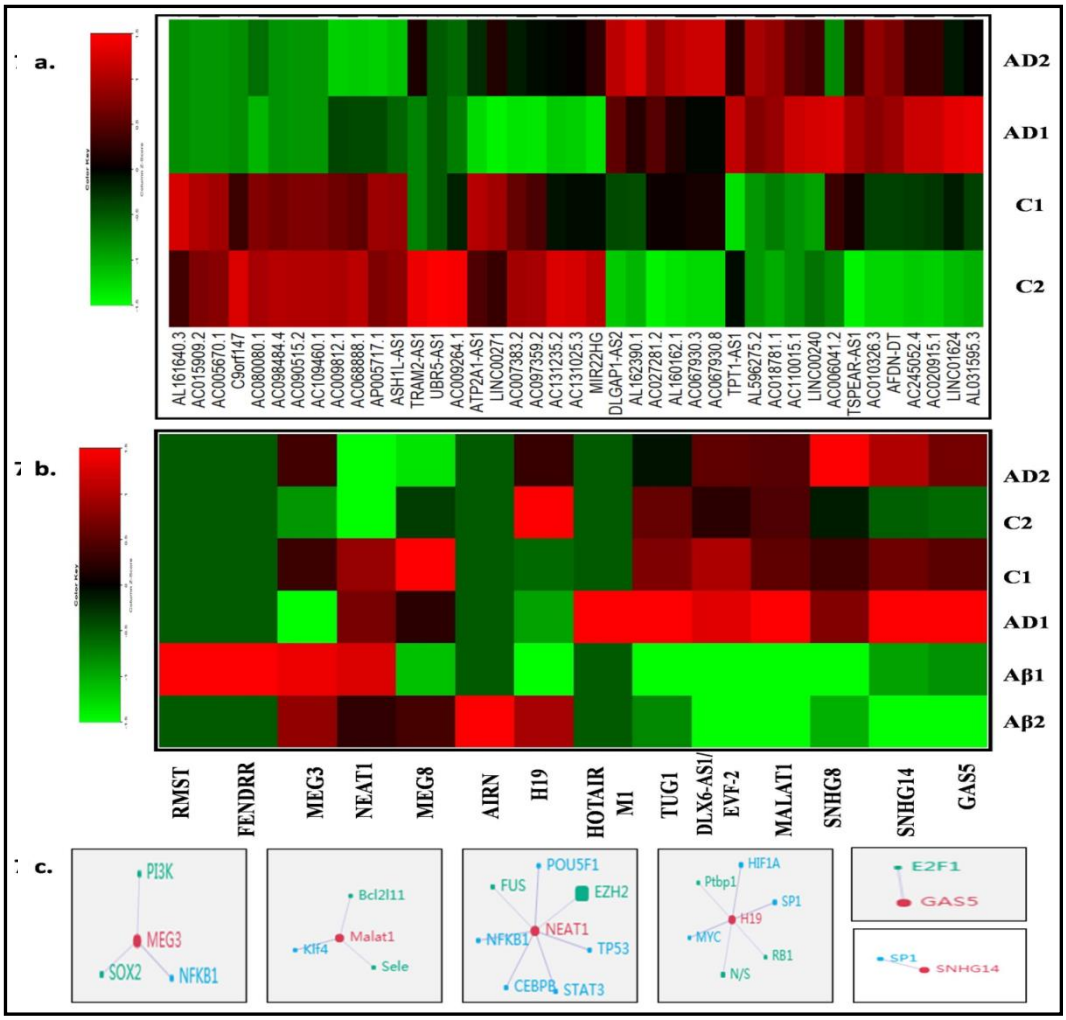

Figure 3.7: Heat map of statistically significant differentially regulated lncRNAs in AD vs Control (7a.) by small RNA sequencing. Each sample has two biological replicates. Color codes indicate normalized fold changes- Red = up regulation; Green = down regulation. Heat map of selected lncRNAs in Aβ vs Control group (7b.). Protein interacting partners of selected lncRNAs (7c.). lncRNAs are marked in red, Transcription factors in blue and proteins in green.

Table 3.2. Summary of differentially regulated lncRNAs.

Aβ vs. Control		AD vs. Control	
TOP 25 UPREGULATED	**TOP 25 DOWNREGULATED**	**UPREGULATED**	**DOWNREGULATED**
AC003984.1, AC006974.2, AC007638.2, AC012178.1, AC025159.1, AC026391.1, AC092125.2, AC093827.4, AC100830.1, AC106793.1, AC108206.1, AL035251.1, AL133456.1, AL353648.1, AL713923.1, AP005019.1, ATXN8OS, FAM242C, GPR158-AS1, LINC02109, LINC02304, LINC02579, MIR155HG, PCAT1, Z98259.1	AC007938.2, AC007952.4, AC016876.2, AC022796.1, AC026464.2, AC067930.3, AC067930.8, AC106739.1, AC108134.2, AC112236.3, AL022311.1, AL139393.1, AL451165.2, AL662797.1, AP003352.1, LINC00271, LINC00910, LINC01630, LINC01979, ATXN8OS, MEG9, SNHG15, SPATA3-AS1, TSIX, XIST	AL031595.3, DLGAP1-AS2, AC018781.1, AL596275.2, LINC00240, AC245052.4, AC110015.1, AC010326.3, AC006041.2, TSPEAR-AS1, AL160162.1, TPT1-AS1, AC027281.2, AL162390.1, AC067930.3, AC067930.8, AC020915.1, AFDN-DT, LINC01624	AC098484.4, AC005670.1, AC090515.2, AC109460.1, AC015909.2, TRAM2-AS1, AL161640.3, UBR5-AS1, AC068888.1, AC131025.3, C9orf147, AC131235.2, ATP2A1-AS1, AC009264.1, AP005717.1, AC009812.1, AC097359.2, AC007383.2, AC080080.1, MIR22HG, LINC00271, ASH1L-AS1

DLX6-AS1/EVF2, MALAT1, TUG1 and SNHG8 showed a similar trend of uniform decrease exclusively in the Aβ samples, while an increase in both of the Controls and AICD+ Aβ groups. SNHG14 and GAS5 showed a uniform decrease in the Aβ sets, a uniform increase in the AICD+ Aβ sets, but behaved aberrantly in the Controls (increase in one and decrease in the other). Taking all these data into consideration, out of the selected 14, 6 lncRNAs – MEG3, NEAT1, DLX6-AS1/EVF2, MALAT1, TUG1 and SNHG8 showed a consistent pattern of deregulation in the Aβ and AICD+ Aβ sets compared to the Controls.

3.6. Fourteen selected lncRNAs having AD association have miRNA, RNA Binding Protein (RBP) and Transcription Factor (TF) Interacting partners

Using the LIVE database, I found significant protein – lncRNA interaction with only 6 candidates, MEG3, NEAT1, MALAT1, GAS5, H19 and SNHG14 **(Fig 3.7c.)**. The Protein and Transcription factor (TF) tabs were used from the database, which revealed that MEG3 interacted with the proteins PI3K and SOX2, and the TF NFKβ1; MALAT1 interacted with proteins Bcl2l11 and Sele, and the TF Klf4; NEAT1 interacted with the proteins FUS and EZH2 and the TFs POU5F1, NFKβ1, TP53, CEBPB and STAT3; H19 interacted with the proteins Ptbp1and RB1 and the TFs HIF1A, SP1 and MYC and GAS5 interacted with the protein E2F1. No significant protein or transcription factor interactors were found for the other 8 lncRNAs. NFKβ1 emerged as the co- regulator of lncRNAs MEG3 and NEAT1, while SP1 was the common TF governing H19 and SNHG14. To better understand the functional roles of these selected lncRNAs, I looked at their miRNA and RNA Binding Protein (RBP) partners from ENCORI (The Encyclopaedia of RNA Interactomes) database. The total numbers of miRNA and RBP interacting partners of each of the lncRNAs, their involvement in AD and the possible mechanisms are summarised in **Table 3.3.**

Table 3.3. Summary of miRNA and RBP interactors of selected lncRNAs.

lncRNA	Number of different genes		Implicated in AD	Function
	RBP	miRNA		
RMST	25	2	YES	Neurogenesis
FENDRR	38	53	UNKNOWN	
MEG3	47	11	YES	PI3K/Akt pathway.
NEAT1	117	56	YES	Binds to and stabilises p53.
H19	60	100	YES	Neuroinflammation and Insulin signalling
TUG1	111	12	YES	Inhibits neuronal apoptosis by suppressing ROCK1.
SNHG8	106	23	UNKNOWN	
GAS5	122	14	YES	Interacts with p53, BRCA1. Regulate cell cycle and cell death
MALAT1	118	40	YES	Synaptogenesis.
SNHG14	70	39	UNKNOWN	
MEG8	11	-	UNKNOWN	
HOTAIRM1	60	-	UNKNOWN	
DLX6-AS1/EVF2	-	-	YES	Adult neurogenesis.
AIRN	4	-	UNKNOWN	

3.7. Differentially regulated miRNAs have several RTK Targets

Next, I looked to identify the RTKs which could be putative targets for the miRNAs, found differentially expressed between the respective groups. I used the database miRCarta to identify potential RTK targets for the miRNAs. I considered the target RTKs among the genes which had been experimentally validated. The lists of RTKs for the differentially expressed miRNAs between the respective groups were thus obtained. I obtained a shortlist of 22 miRNA hits which targeted at least one RTK in the Aβ vs Control group and 10 hits in the AD vs Control Group **(Table 3.4)**. It was found that out of all the miRNAs, miR-34a-5p and miR-335-5p were most diverse in terms of their RTK targets as the prior had 9 targets and the latter had 11 targets respectively.

Table 3.4. Summary of miRNA and RTK targets from Aβ vs. Control and AD vs. Control groups.

Aβ vs. Control		**AD vs. Control**	
miRNA	**VALIDATED TARGETS**	**miRNA**	**VALIDATED TARGETS**
221-3p	ERBB4, KIT.	93-3p	EPHB4
222-3p	KIT.	146a-5p	ERBB4
155-5p	AXL, CSF1R.	627-3p	EPHB1
146b-5p	PDGFRA, KIT.	183-5p	IGF1R
146a-5p	ERBB4.	143-5p	EPHA4
331-3p	ERBB2, ERBB3, EPHA7.	502-5p	IGF1R
1251-5p	RYK.	450b-5p	EPHB1
100-5p	FGFR3, IGF1R.	1271-5p	IGF1R

215-5p	IGF1R, RET.	3679-5p	EPHA2
145-5p	ERBB4, IGF1R, VEGFA.	6824-3p	IGF1R, EPHB3
182-5p	IGF1R.		
10b-5p	AXL, EPHA4.		
766-3p	VEGFC.		
10b-3p	IGF1R, EPHA7.		
34a-5p	IGF1R, AXL, MST1, PDGFRA, PDGFRB, KIT, CSF1R, EPHA2, EPHA5.		
542-3p	EPHB4.		
335-5p	IGF1R, MERTK, KIT, FLT3, ROR2, NTRK2, VEGFA, EPHA1, EPHA4, EPHB4, DDR1.		
185-5p	IGF1R, NTRK3, VEGFA, EPHB2.		
34a-3p	IGF1R		
410-3p	NTRK3, VEGFA.		
3187-3p	TYRO3, EPHA2, RYK.		

Apart from the RTK targets, I found that several of the deregulated miRNAs had very strong AD connections involving processes of Aβ generation, proteasomal degradation, lysosomal pathway, autophagy, neuronal cell viability and apoptosis. A summary of such functions is compiled in **Table 3.5**, highlighting the role of these miRNAs as AD signatures as shown from our study and reinforced by existing literature.

Table 3.5. Summary of miRNA pathways and functions implicated in AD from the unique miRNAs of Aβ vs. Control and AD vs. Control groups.

miRNA	Cellular Role	Function
542-3p	Proteasomal degradation	Targets MID1 ubiquitin ligase and suppresses mTOR signalling
185-5p	Lysosomal pathway	Targets Granulin and regulates protein homeostasis
Let-7b-3p	Autophagy	Negatively regulates autophagy by targeting Caspase 3 and regulates cellular response to reactive oxygen species.
410-3p	Neuronal cell viability and apoptosis	Exerts neuroprotection by regulating PTEN/AKT/mTOR signalling
502-3p	Neuronal apoptosis	Suppresses SET protein and affects Jcasp-induced cell death
664a-3p	Proteostasis control, immune-inflammatory control, and neurotrophic support.	Downregulates MOB1A and inactivates Hippo signalling
126-5p	Cellular homeostasis and apoptosis	Targets TOM1 and affects the IL-1β ad TNF-α signalling
339-3p	Aβ generation and turnover	Unknown
143-5p	Differentiation, proliferation and apoptosis	Targets and represses KLF4 and affects transcription
502-5p	Inflammation	Targets IL-1β
101-5p	Aβ generation	Negative regulator of Amyloid Precursor Protein
501-3p	Cell differentiation and apoptosis	Targets TGFBR3 and affects the TGF- β signalling
548e-3p	Oxidative stress	Unknown

3.8. Discussion

In the present study, I analysed the levels of significantly deregulated miRNAs using small RNA sequencing data in a cell model of AD. I specifically looked at the differential regulation of subsets of miRNAs under cues of Aβ and AICD expressions separately, normalised to their respective controls. The motivation behind looking at the regulation separately was due to the fact that there is a large body of literature investigating the effect of Aβ on the cellular degradome [1], but studies on the effect of AICD is scarce. The unique hits that I obtained and the comparison of Aβ vs. AD revealed the exclusive effect of AICD on the cellular miRNA landscape. It is interesting to note that this group has the largest number of unique miRNAs, hinting at the fact that AICD might have a stronger effect on the miRNA population, compared to Aβ alone or AICD + Aβ combined. Our analysis also revealed a large body of miRNAs which were common between the comparison groups which could be explained by the fact that both Aβ and AICD are in abundance in *post mortem* AD samples, and their synergistic effects could be a degeneration enhancing cue. The most interesting find is the potential discovery of a single miRNA- hsa-miR-4697-3p, common for all the 3 groups and has not been reported before, which could be used as a novel AD signature. Validation of 4 top up regulated (221-3p, 222-3p, 155-5p and 4697-3p) and 5 top down regulated (3648, 1251-5p, 3607-5p, 3117-3p and 335-3p) miRNAs from the Aβ set was performed taking additional variants – AICD only and AICD + Aβ. These experiments yielded confounding results; treatment with Aβ only and AICD only were having antagonistic effects on the miRNA milieu. This was unexpected because in the amyloid pathway AICD is stabilised implicating that it plays some role in AD pathophysiology [2]. This role of AICD till date is disputed, but our data establishes that AICD reverses the toxic effect of Aβ to a large extent- and this putative protective role of AICD (by differentially affecting the degradome)

is in concordance with the studies which implicate AICD in neuronal development and plasticity [3-5]. Of the up regulated set, hsa-miR-221-3p, hsa-miR-222-3p and hsa-miR- 155-5p are implicated in AD [6-8]. Similarly, hsa-miR-1251-5p and hsa-miR-335-3p from the down regulated set are also implicated in AD [9, 10]. Taking all these data into consideration, it would be prudent to confer that 4 miRNAs from the validation sets (4697-3p, 3648, 3607-5p and 3117-3p), not reported earlier, should serve as novel targets for AD research. GSEA analysis with stringent cut off parameters showed that the deregulated miRNAs in the Aβ group affected the neuronal signalling and cytoskeletal processes like axon guidance, long-term depression, regulation of actin cytoskeleton and glutamatergic synapse. A similar picture arose from KEGG analysis which involved morphine addiction, TGF-β signalling and thyroid hormone synthesis. GO analysis on the other hand revealed that this subset of miRNAs controlled not just the neuronal processes, but housekeeping ones as well - nucleic acid binding transcription factor activity, enzyme regulator activity, cellular protein modification process, and cell death, among others. The interesting find from our analysis was that the top regulated pathway for several miRNAs altered in both groups (542-3p, 185-5p, 502-3p, 143-5p, 6824-3p and 501-3p) was Synaptic function, which implies their deregulation might be a driving cause for the synaptic aberrations predominant in AD. In gist, the importance of these miRNAs in AD pathology is irrefutable.

Using an in-house bioinformatics pipeline, I also unearthed a fairly large population of deregulated lncRNAs, both from the Aβ and the AICD + Aβ sets. On critical inspection, I found that the top 50 hits from both the sets contained a majority of hitherto unreported lncRNAs in AD, which has to be experimentally investigated thoroughly in future studies. Expectedly, familiar ones were also observed, and these

were studied separately as a smaller subgroup. Of these, lncRNA RMST, among other things, is implicated in regulating neurogenesis [11], a process in direct contrast to what occurs in AD. NEAT1, one of the best studied lncRNAs in recent past is implicated in several Neurodegeneration scenarios, like HD and ALS [12, 13]. MEG3 has been directly implicated in AD by working via the PI3K/Akt pathway [14]. GAS5, although not causally linked to AD, can interact with p53 and BRCA1 to regulate cell cycle and cell death [15]. H19 is implicated in inflammatory response in neurons and to govern Insulin signalling, MALAT1 and EVF2 governs key aspects of synaptogenesis and adult neurogenesis, respectively [16] and TUG1 counters neuronal apoptosis via the Rho/ROCK1 pathway [17]. Leaving aside these few, there remains a plethora of other significantly deregulated lncRNAs from our analysis, which remains to be investigated.

The implication of novel miRNAs and lncRNAs in human AD models mimicking neurodegeneration is quite evident from our work. Recent related studies implicating non-coding RNAs in AD involving Aβ, aberrant mitochondrial signalling and synaptic disruption further highlights the need to look at AD pathology from a systems perspective [18-20] A large body of miRNAs targeting key mitochondrial proteins are altered in AD [reviewed in 21], while several others are specifically Aβ responsive [22]. Recently, in line with our analysis, several sets of miRNAs were reported to be linked to Tau hyperphosphorylation, Inflammation and synaptic irregularities in AD [23] In the last few years it is found that several classes of RTKs are deregulated in terms of their activity in AD cell model and post-mortem AD tissues [24]. The most significant among them are ALK and RYK, both of which showed marked downregulation in AD The up regulated ones are members of the erbB family, FGFR1, members of the Eph family and DDR2. The down regulated

ones include Axl, M-CSFR and members of the VEGFR family. It is interesting to note that these deregulated RTKs (specially the Eph and erbB members) were found to be targets of significantly deregulated miRNAs in the AD vs Control group (**Table 3.4**). The most interesting find however, was the fact that specific sets of deregulated miRNAs in the AD group targeted a sub-class of RTKs (Eph, ErbB and IGF1R) which clustered tightly together in the AD cell model [25]. This probably implies that this sub-group of miRNAs along with their cognate RTK targets could well be established as a novel signature for AD.

Apart from Aβ, which is a well-known trigger for disruption of the cellular degradome in AD, for the first time, I have established the role of AICD in differentially regulating a large body of hitherto unreported miRNAs independently and in conjunction with Aβ. Through a 'domino' effect, these miRNAs in turn interact and are regulated by lncRNAs and then they target several RTKs downstream.

Summary:

- 6 miRNAs from both groups (542-3p, 185-5p, 502-3p, 143-5p, 6824-3p and 501-3p) directly linked Aβ and Synaptic function.
- 4 novel miRNAs were unearthed from the validation sets (4697-3p, 3648, 3607-5p and 3117-3p) which target common RTKs (Eph, ErbB and IGF1R).
- 4 lncRNAs DLX6-AS1/EVF2, MALAT1, TUG1 and SNHG8 showing the most consistent pattern of deregulation, promises to be novel targets for AD research and possible intervention.

3.9. References

[1]. Amakiri N, Kubosumi A, Tran J, Reddy PH. Amyloid Beta and MicroRNAs in Alzheimer's Disease. Front Neurosci. 2019 May 3;13:430.
[2]. Roy K, Raychaudhuri M, Chakrabarti O, Mukhopadhyay D. Growth factor receptor-bound protein 2 promotes autophagic removal of amyloid-β protein precursor intracellular domain overload in neuronal cells. J Alzheimers Dis. 2014;38(4):881-95.
[3]. Cao, X., Sudhof, T.C., 2001. A transcriptionally active complex of APP with Fe65 and histone acetyltransferase Tip60. Science 293, 115–120.
[4]. Scheinfeld, M.H., Roncarati, R., Vito, P., Lopez, P.A., Abdallah, M., D'Adamio, L., 2002. Jun NH2-terminal kinase (JNK) interacting protein 1 (JIP1) binds the cytoplasmic domain of the Alzheimer's beta-amyloid precursor protein (APP). J. Biol. Chem. 277, 3767–3775.
[5]. Borg, J.P., Ooi, J., Levy, E., Margolis, B., 1996. The phosphotyrosine interaction domains of X11 and FE65 bind to distinct sites on the YENPTY motif of amyloid precursor protein. Mol. Cell. Biol. 16, 6229–6241.
[6]. Manzine PR, Pelucchi S, Horst MA, Vale FAC, Pavarini SCI, Audano M, Mitro N, Di Luca M, Marcello E, Cominetti MR. microRNA 221 Targets ADAM10 mRNA and is Downregulated in Alzheimer's Disease. J Alzheimers Dis. 2018;61(1):113-123.
[7]. Dangla-Valls A, Molinuevo JL, Altirriba J, Sánchez-Valle R, Alcolea D, Fortea J, Rami L, Balasa M, Muñoz-García C, Ezquerra M, Fernández-Santiago R, Lleó A, Lladó A, Antonell A. CSF microRNA Profiling in Alzheimer's Disease: a Screening and Validation Study. Mol Neurobiol. 2017 Nov;54(9):6647-6654.
[8]. Song J, Lee JE. miR-155 is involved in Alzheimer's disease by regulating T lymphocyte function. Front Aging Neurosci. 2015 Apr 30;7:61.
[9]. Lau P, Bossers K, Janky R, Salta E, Frigerio CS, Barbash S, Rothman R, Sierksma AS, Thathiah A, Greenberg D, Papadopoulou AS, Achsel T, Ayoubi T, Soreq H, Verhaagen J, Swaab DF, Aerts S, De Strooper B. Alteration of the microRNAs network during the progression of Alzheimer's disease. EMBO Mol Med. 2013 Oct;5(10):1613-34.
[10]. Raihan O, Brishti A, Molla MR, Li W, Zhang Q, Xu P, Khan MI, Zhang J, Liu Q. The Age-dependent Elevation of miR-335-3p Leads to Reduced Cholesterol and Impaired Memory in Brain. Neuroscience. 2018 Oct 15;390:160-173.
[11]. Ng SY, Bogu GK, Soh BS, Stanton LW. The long noncoding RNA RMST interacts with SOX2 to regulate neurogenesis. Mol Cell. 2013 Aug 8;51(3):349-59.
[12]. Chanda K, Das S, Chakraborty J, Bucha S, Maitra A, Chatterjee R, Mukhopadhyay D, Bhattacharyya NP. Altered Levels of Long NcRNAs Meg3 and Neat1 in Cell And Animal Models Of Huntington's Disease. RNA Biol. 2018;15(10):1348-1363.
[13]. An H, Skelt L, Notaro A, Highley JR, Fox AH, La Bella V, Buchman VL, Shelkovnikova TA. ALS-linked FUS mutations confer loss and gain of function in the nucleus by promoting excessive formation of dysfunctional paraspeckles. Acta Neuropathol Commun. 2019 Jan 14;7(1):7.
[14]. Wang, M., Qin, L., & Tang, B. (2019). MicroRNAs in Alzheimer's Disease. *Frontiers in genetics*, *10*, 153. https://doi.org/10.3389/fgene.2019.00153.
[15]. Yi J, Chen B, Yao X, Lei Y, Ou F, Huang F. Upregulation of the lncRNA MEG3 improves cognitive impairment, alleviates neuronal damage, and inhibits activation of astrocytes in hippocampus tissues in Alzheimer's disease through inactivating the PI3K/Akt signaling pathway. J Cell Biochem. 2019 Oct;120(10):18053-18065.
[16]. Kim, Y. K., & Song, J. (2018). The Role of Long Noncoding RNAs in Diabetic Alzheimer's Disease. *Journal of clinical medicine*, *7*(11), 461. https://doi.org/10.3390/jcm7110461.
[17]. Li, X., Wang, S. W., Li, X. L., Yu, F. Y., & Cong, H. M. (2020). Knockdown of long non-coding RNA TUG1 depresses apoptosis of hippocampal neurons in Alzheimer's disease by elevating microRNA-15a and repressing ROCK1 expression. *Inflammation research : official journal of the European Histamine Research Society ... [et al.]*, *69*(9), 897–910. https://doi.org/10.1007/s00011-020-01364-8.
[18]. Reddy, P. H., & Beal, M. F. (2008). Amyloid beta, mitochondrial dysfunction and synaptic damage: implications for cognitive decline in aging and Alzheimer's disease. *Trends in molecular medicine*, *14*(2), 45–53.
[19]. Vijayan, M. & Reddy, P. H. (2020). Non-Coding RNAs Based Molecular Links in Type 2 Diabetes, Ischemic Stroke, and Vascular Dementia. *Journal of Alzheimer's disease: JAD*, *75*(2), 353–383.

[20]. Kumar, S., & Reddy, P. H. (2016). Are circulating microRNAs peripheral biomarkers for Alzheimer's disease?. *Biochimica et biophysica acta, 1862*(9), 1617–1627. 126,143,502,101.
[21]. John A, Kubosumi A, Reddy PH. Mitochondrial MicroRNAs in Aging and Neurodegenerative Diseases. *Cells*. 2020;9(6):1345.
[22]. Amakiri N, Kubosumi A, Tran J, Reddy PH. Amyloid Beta and MicroRNAs in Alzheimer's Disease. *Front Neurosci*. 2019;13:430.
[23]. Kou X, Chen D, Chen N. The Regulation of microRNAs in Alzheimer's Disease. *Front Neurol*. 2020;11:288. Published 2020 Apr 17. doi:10.3389/fneur.2020.00288.
[24]. Mazar J, Rosado A, Shelley J, Marchica J, Westmoreland TJ. The long non-coding RNA GAS5 differentially regulates cell cycle arrest and apoptosis through activation of BRCA1 and p53 in human neuroblastoma. Oncotarget. 2017 Jan 24;8(4):6589-6607.
[25]. Majumder, P., Roy, K., Bagh, S., and Mukhopadhyay, D. (2019) Receptor tyrosine kinases (RTKs) consociate in regulatory clusters in Alzheimer's disease and type 2 diabetes. *Mol. Cell. Biochem.*

Chapter 4: MALAT1 Regulatory Networks in AD

4.1. Several lncRNAs are deregulated in a mouse model of AD

This study was initiated by looking at the expression levels of lncRNAs with a PCR Array Mouse kit using total RNA from 12-month-old APP/PS1 mouse brain cortex with that of age matched normal mice**.** Out of the 84 lncRNAs, 41 were found to be significantly altered (p value <0.05; n=2) **(Figure 4.1)**.

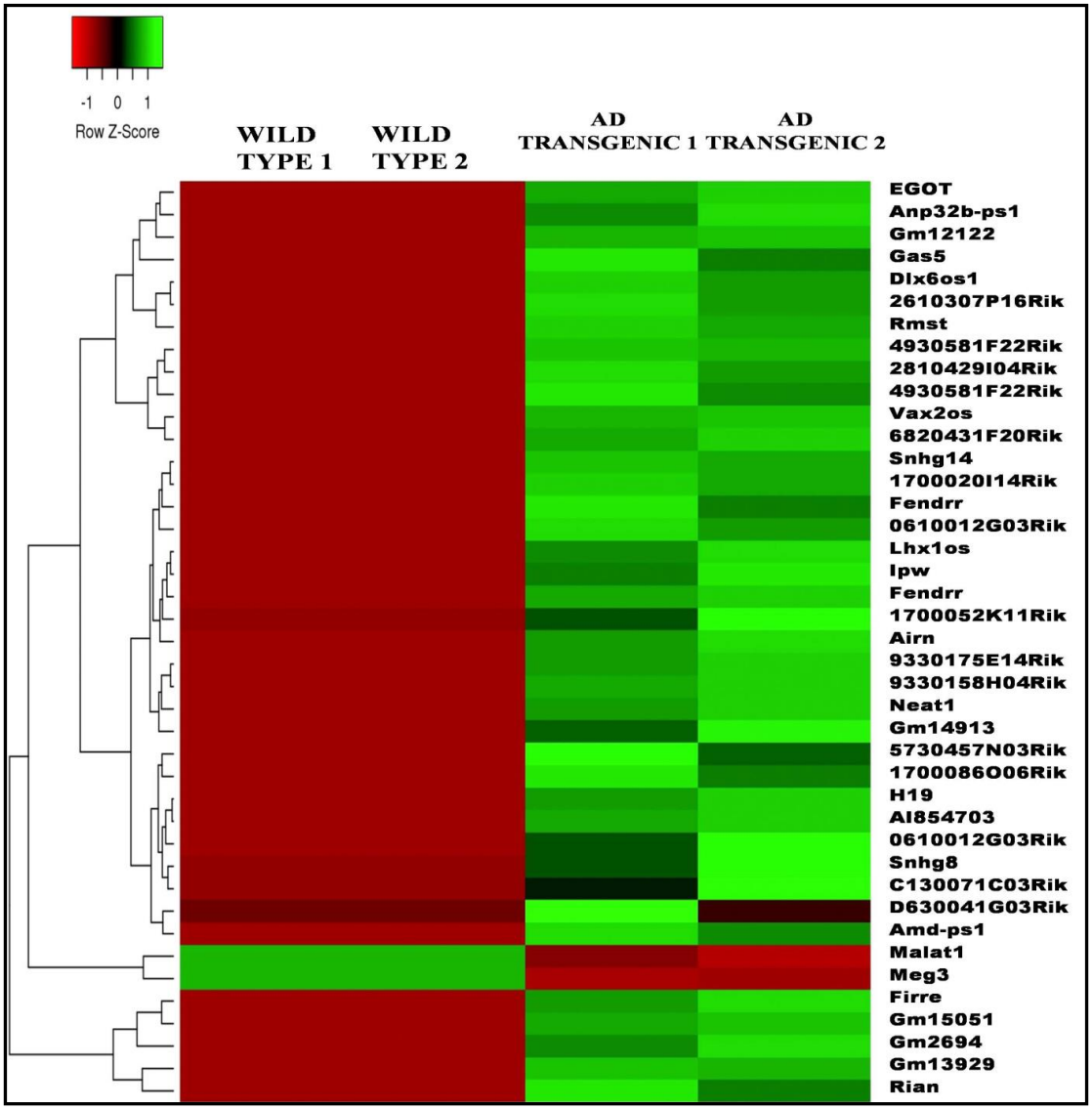

Figure 4.1: Heat map of statistically significant differentially regulated lncRNAs in Wild Type vs. AD Transgenic mice samples by RT2 lncRNA PCR Array Mouse Cell Development & Differentiation kit. Each sample has two biological replicates. For the purpose of simplicity, fold change values of Wild Type samples have been normalised to 1. Colour codes indicate normalized fold changes- Red = down regulation; Green = up regulation, p – value <0.05.

Out of these 41, only two lncRNAs, Meg3 and Malat1 were down regulated, while rest 39 had strong up regulation. To identify the human counterparts of these mice lncRNA, the NCBI database (https://www.ncbi.nlm.nih.gov/gene/) was further explored which revealed that 17 out of 41 mouse genes had human homologs (**Table 1**), of which 7 human lncRNAs i.e., TUG1, H19, GAS5, RMST, MEG3, NEAT1 AND MALAT1 had reported AD

Table 4.1. Summary of the expression level changes of lncRNAs in 12-month-old APP/PS1 mouse brain cortex compared to age matched wild type mouse brain cortex (Human lncRNAs are in capitals; AD associated ones are highlighted in bold).

Non coding RNA	Human Homolog	Mouse Chromosome	Human Chromosome	Levels in AD mouse brain cortex
H19	**H19**	**7**	**11**	**UP**
Gm2694	-	8	-	UP
2810429I04Rik	-	13	-	UP
EGOT	EGO	6	3	UP
Gas5	**GAS5**	**1**	**1**	**UP**
Rmst	**RMST**	**10**	**12**	**UP**
Snhg8	SNHG8	3	4	UP
Gm12122	-	11	-	UP
Fendrr	FENDRR	8	16	UP
Gm13929	-	2	-	UP
C130071C03Rik	-	13	-	UP
Vax2os	-	6	-	UP
4930581F22Rik	-	9	-	UP
9330158H04Rik	-	6	-	UP

5730457N03Rik	-	6	-	UP
4930594C11Rik	-	1	-	UP
Lhx1os	-	11	-	UP
Rian	MEG8	12	14	UP
9330175E14Rik	-	8	-	UP
Dlx6os1	EVF2	6	7	UP
1700052K11Rik	-	11	-	UP
AI854703	-	7	-	UP
610012G03Rik	-	16	-	UP
Gm15051	HOTAIRM1	6	7	UP
Neat1	**NEAT1**	**19**	**11**	**UP**
Kcnq1ot1	KCNQ1OT1	7	11	UP
2610307P16Rik	-	13	-	UP
1700086O06Rik	-	18	-	UP
6820431F20Rik	-	8	-	UP
Airn	AIRN	17	6	UP
Ipw	IPW	7	15	UP
1700020I14Rik	-	2	-	UP
Snhg14	SNHG14	7	-	UP
D630041G03Rik	-	7	-	UP
Tug1	**TUG1**	**11**	**22**	**UP**
Anp32b-ps1	-	4	-	UP
Meg3	**MEG3**	**12**	**14**	**DOWN**
Malat1	**MALAT1**	**19**	**11**	**DOWN**

associations by either regulating neurogenesis and synaptic function, Aβ accumulation, insulin signalling, immune response, glucose homeostasis, or by regulating key miRNAs implicated in AD. Interestingly, chromosomal groupings between mice and human showed that 4 deregulated lncRNAs (H19, NEAT1, KCNQ10TI and MALAT1) were specific for chromosome 11 11 in humans, although such a grouping was absent in mice. Rest of the lncRNAs had a heterogeneous distribution throughout the chromosomal landscape **(Table 4.1)**.

4.2. Validation of short-listed lncRNAs and their human homologs in respective animal model, cell model and brain tissue of AD

qRT-PCR and gene-specific primers were used to validate the data obtained PCR Array and bioinformatics analysis of shortlisted lncRNAs**.** Transcript level changes were validated in 12-month-old APP/PS1 mouse brain cortex or a cell model (human neuroblastoma cell line SHSY5Y treated with $A\beta_{1-42}$) and brain tissue RNA of an AD patient, respectively.

As shown in **Figure 4.2a.** out of 7 lncRNAs analysed in the RT^2 Mouse PCR Array, all of them were in concordance with the subsequent validation in AD transgenic mice and wild type controls, albeit with varied levels of regulation, with Gas5, H19, Tug1, Rmst and Neat1 showing up- and Meg3 and Malat1 showing downregulation. Subsequent validation in the $A\beta_{1-42}$ treated cell model showed an inverse trend for only GAS5, while the other 6 lncRNAs behaved similarly as in the Mouse PCR Array (**Figure 4. 2 b.)**.

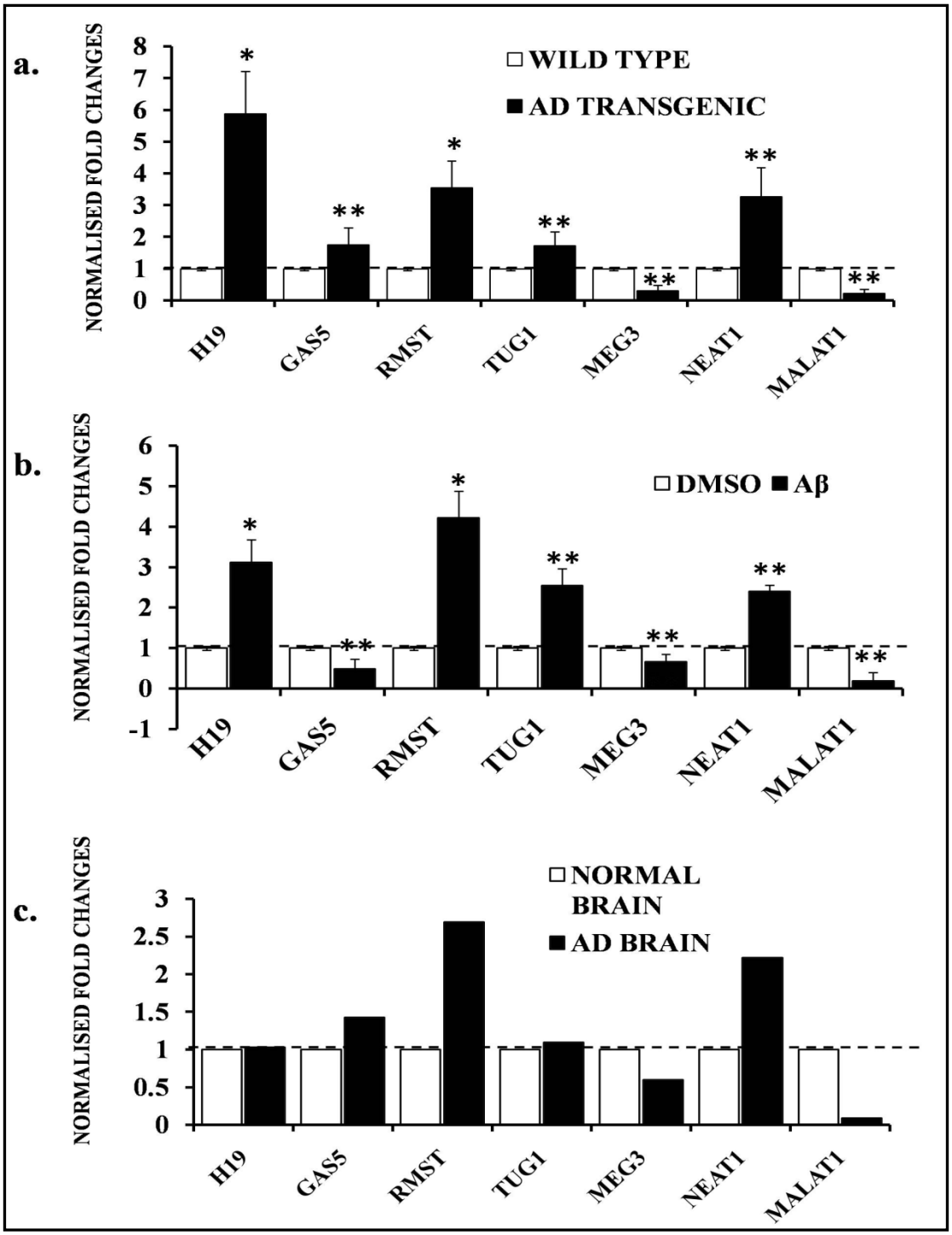

Figure 4.2: Altered levels of selected lncRNAs in AD mice model, $A\beta_{1-42}$ treated cell model and AD brain (a). Bar diagrams indicative of three (n = 3) independent biological replicates quantifying levels of H19, Gas5, Rmst, Tug1, Meg3, Neat1 and Malat1 by qRT-PCR in 12 months old AD mice and age-matched wild-type mice. (b). Bar diagrams indicative of three (n = 3) independent biological replicates quantifying levels of H19, GAS5, RMST, TUG1, MEG3, NEAT1 and MALAT1 by qRT-PCR in SHSY5Y cells treated with 0.5 µM $A\beta_{1-42}$ or

treated with only DMSO. **(**c) Bar graphs representative of two experiments (n = 2; technical replicate) measuring levels of H19, GAS5, RMST, TUG1, MEG3, NEAT1 and MALAT1 by qRT-PCR in total RNA isolated from the brain of 1 AD patient compared to total RNA from the brain of a non –AD control. For all qRT based studies, levels of U6snRNA were taken as endogenous control, unless stated otherwise. Individual lncRNA values were normalized by the corresponding U6snRNA levels. Fold changes were computed taking the relative levels of lncRNA in corresponding controls to be 1. Error bars indicate ± SD. Significance level between different experimental pairs is indicated (NS, not significant; *, $p < 0.05$; **, $p < 0.01$; ***, $p < 0.001$).

In the human AD brain set (n=1), H19 and TUG1 were not significantly altered, whereas other 4 lncRNAs behaved similarly (**Figure 4.2 c.)**. Taking all the sets into consideration, out of the 7 lncRNAs, RMST and NEAT1 showed up regulation, while MEG3 and MALAT1 showed downregulation. MALAT1 however showed most consistent and pronounced downregulation in all the 3 validation models.

4.3. MALAT1 sponges miR 26a, b, 200a as revealed and validated by qRT-PCR, RNA FISH and RIP

The significant downregulation in MALAT1 expression led us to find its miRNA interacting partners using the database ENCORI **(**http://starbase.sysu.edu.cn/index.php). The miRNA-lncRNA tool was used which catalogs data from Ago-CLIP seq experiments and predictive data from miRanda program, with the search parameters- CLIP data, (≥3) and Degradome data, (≥2). MALAT1 was predicted to interact with hsa-miR-200a-3p, hsa-miR-26a-5p and hsa-miR-26b-5p. Real time PCR with primers designed against the human mature miRNA sequences showed that the hsa-miR 26 family (26a-5p and 26b-5p) was more abundant in SHSY5Y cells compared to hsa-miR-200a-3p, with hsa-miR-26a-5p being the most abundant (compared to U6snRNA).Since lncRNAs are known to act

like sponges for miRNAs, it was tested whether MALAT1 had the same effect on these by employing 3 assays to study such putative interactions. First, MALAT1 was transiently silenced with a pool of 4 redundant siRNAs in SHSY5Y cells and

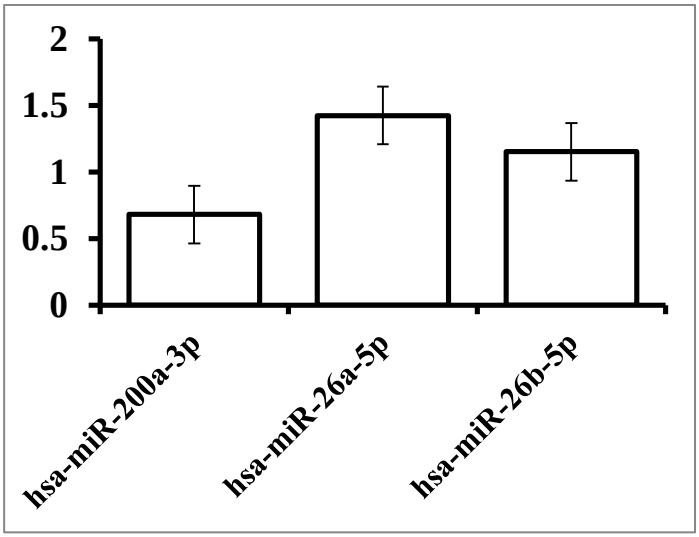

Endogenous expression levels of hsa-miR- 200a-3p, hsa-miR- 26a-5p and hsa-miR- 26b-5p: Bar diagrams indicative of three (n = 3) independent biological replicates quantifying relative endogenous expression levels of hsa-miR- 200a-3p, hsa-miR- 26a-5p and hsa-miR- 26b-5p in SHSY5Y cells by qRT-PCR. U6sNRNA was used as endogenous control.

the expression levels were checked. Analysis of MALAT1 levels after siRNA treatment showed nearly 70% repressions of its endogenous transcripts

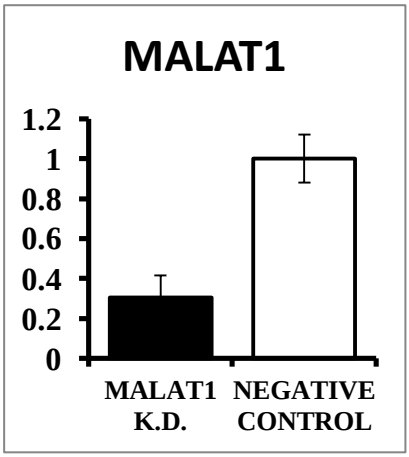

Decrease in expression of MALAT1 after treatment with siRNA: Bar diagrams indicative of three (n = 3) independent biological replicates quantifying levels of MALAT1 by qRT-PCR in SHSY5Y cells transfected with MALAT1 siRNA or corresponding negative control siRNA. U6SNRNAwas used as endogenous control. Fold change was calculated by considering the normalised levels of MALAT1 in negative control siRNA treated cells to be 1. Error bars indicate ± SD. significance level between experimental pairs is SHOWN (NS, not significant; *,p<0.05; **,p<0.01; ***,p<0.001).

Figure 4.3 a. showed a transient increase of all the 3 on MALAT1 knockdown and was most pronounced for miR- 26a. Thus, knocking down MALAT1 reversed the quenching of these 3

miRNAs. Further, miRNA mimics of the 3 miRNAs were over expressed in cells and subsequently MALAT1 transcript levels were assayed by qRT-PCR in order to determine whether the lncRNA-miRNA repression was bidirectional. **Figure 4.3 b.**

showed that over expression of the miRNAs had no significant effects on MALAT1 levels, thereby demonstrating that MALAT1 repressed them by sponging and not vice-versa. Second,

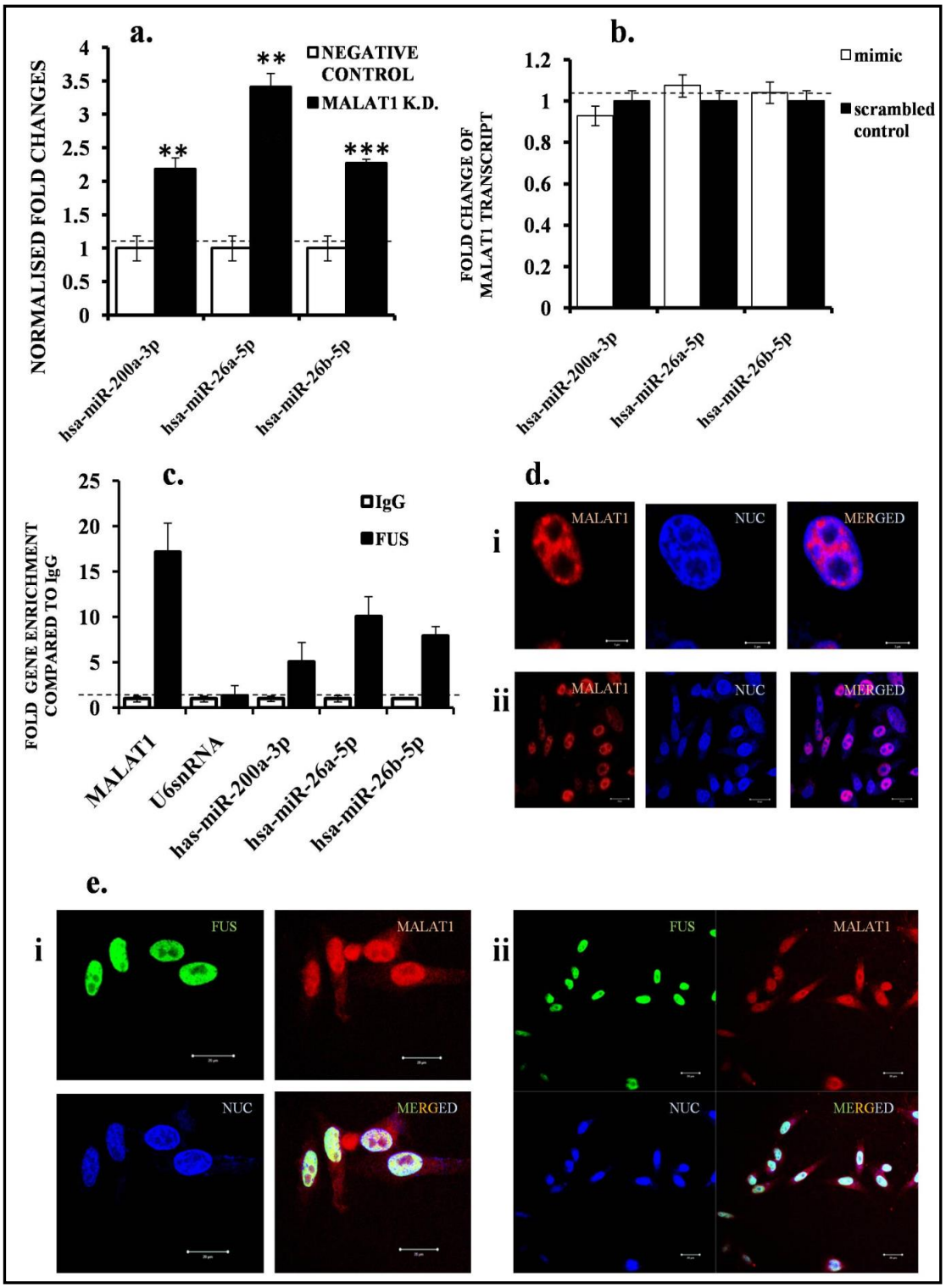

Figure 4.3: Endogenous interaction and regulation of 3 miRNAs by MALAT1 in SHSY5Y cells. (a). Bar diagrams indicative of three (n = 3) independent biological replicates quantifying levels of hsa-miR-200a-3p, hsa-miR-26a-5p and hsa-miR-26b-5p by qRT-PCR in SHSY5Y cells treated with MALAT1 specific siRNAs or scrambled control. (b). Bar diagrams indicative of three (n = 3) independent biological replicates quantifying levels of MALAT1 by qRT-PCR in SHSY5Y cells treated with hsa-miR-200a-3p, hsa-miR-26a-5p and hsa-miR-26b-5p mimics or corresponding scrambled controls. (c). Bar diagrams indicative of three (n = 3) independent biological replicates quantifying the enrichment of MALAT1, U6snRNA, hsa-miR-200a-3p, hsa-miR-26a-5p and hsa-miR-26b-5p by qRT-PCR in SHSY5Y cells after pull down with FUS antibody or control IgG antibody in RIP Assays. (d). RNA-FISH assay of MALAT1 in SHSY5Y cells showing its enrichment in the areas of the nucleus distinct from the nuclear stain DRAQ5®; panel (i) High magnification (4x) image of a single nucleus. Scale bars, 5µm; panel (ii) Low magnification (1x) image of a cell population. Scale bars, 20µm. (e). Co localization Analysis - Sequential Immunocytochemistry (ICC) and RNA Fluorescence In Situ Hybridisation (FISH) assay of MALAT1 combined with FUS in SHSY5Y cells; panel (i) High magnification (3x) image of cell nuclei. Scale bars, 20µm; panel (ii) Low magnification (1x) image of a cell population. Scale bars, 20µm. For each FISH or combined ICC-FISH experiment, images of at least 30 cells (or cell fields) were captured and the experiments were repeated thrice (n = 3).

MALAT1 was also predicted to interact with a RBP - FUS (with 236 target sites), from ENCORI. Indeed, co localization assays with MALAT1 specific RNA-FISH probes followed by ICC with FUS antibody showed a strong correlation between the two (Pearson's co relation coefficient- 0.83; Mander's overlap coefficient- 0.92) (**Figure 4.3e. panels i and ii**). RNA- FISH of MALAT1 confirmed its specific nuclear localisation which was heterogeneously distributed within the nucleus (**Figure 4.3d. panels i and ii).** Third, to ascertain a direct interaction of MALAT1 and the 3 miRNAs, a RNA Immunoprecipitation assay was performed. Having confirmed

the co localisation and possible interaction of MALAT1 and FUS, the FUS antibody was used to pull down MALAT1 and its interacting miRNAs from SHSY5Y cell lysates. **Figure 4.3 c.** showed the pronounced enrichment of MALAT1 (by qRT-PCR) by FUS compared to control IgG pull down. The same RNA after immunoprecipitation was used to probe for the enrichment of the MALAT1 interacting miRNAs. **Figure 4.3 c.** also showed that miRNA 26a, 26b and 200a were enriched along with MALAT1 in the FUS precipitate, thereby confirming their direct interaction. MiR-26a was the most enriched, followed by miR- 26b and then miR-200a.

4.4. MALAT1 interacting miRNAs are strongly up regulated in $A\beta_{1-42}$ treated cell model and AD brain targeting EPHA2, involved in core neurological pathways

After confirming the interaction and regulation of the 3 miRNAs- 26a, 26b and 200a with MALAT1, the expression levels of these in an $A\beta_{1-42}$ treated cell model and AD brain was investigated. First the basal level expressions of these three in SHSY5Y cells were checked. Using primers designed against the mature miRNA sequences, it was found that the miR-26 family was relatively more abundant than miR-200a, with miR- 26a being the most abundant, followed by miR-26b and then miR-200a. After assaying the basal level expression, it was investigated if these were altered in the $A\beta_{1-42}$ treated cell model. **Fig 4.4 a.** showed that all three were strongly and significantly up regulated, with hsa-miR-26a-5p showing the strongest increase, followed by hsa-miR-26b-5p and then hsa-miR-200a-3p. Validation using AD brain tissues revealed almost the same pattern of up regulation, although the fold change of increase was much larger for each. **(Fig 4.4 b.).**

After looking into the deregulation of the 3 miRNAs in AD, the possible downstream protein targets of these 3 were examined. Bioinformatics prediction using the

miRNA- target tool of ENCORI with the following parameters: stringency of CLIP data -3; predicting program – 5 and miRNA-mRNA with Pan- Cancer analysis -2. Based on these selection criteria, the common protein targets of all 3 miRNAs were found to be a RTK EPHA2 (Ephrin Type –A Receptor 2). The interaction and possible repression of these 3 miRNAs with EPHA2 was investigated by over expressing mature miRNA mimics in SHSY5Y cells and measuring the levels of EPHA2 mRNA by qRT-PCR. **Fig 4.4 c.** showed that although miR-200a was predicted to target EPHA2, there was no significant downregulation of the same on over expressing the mimic. However, the results were completely different for the

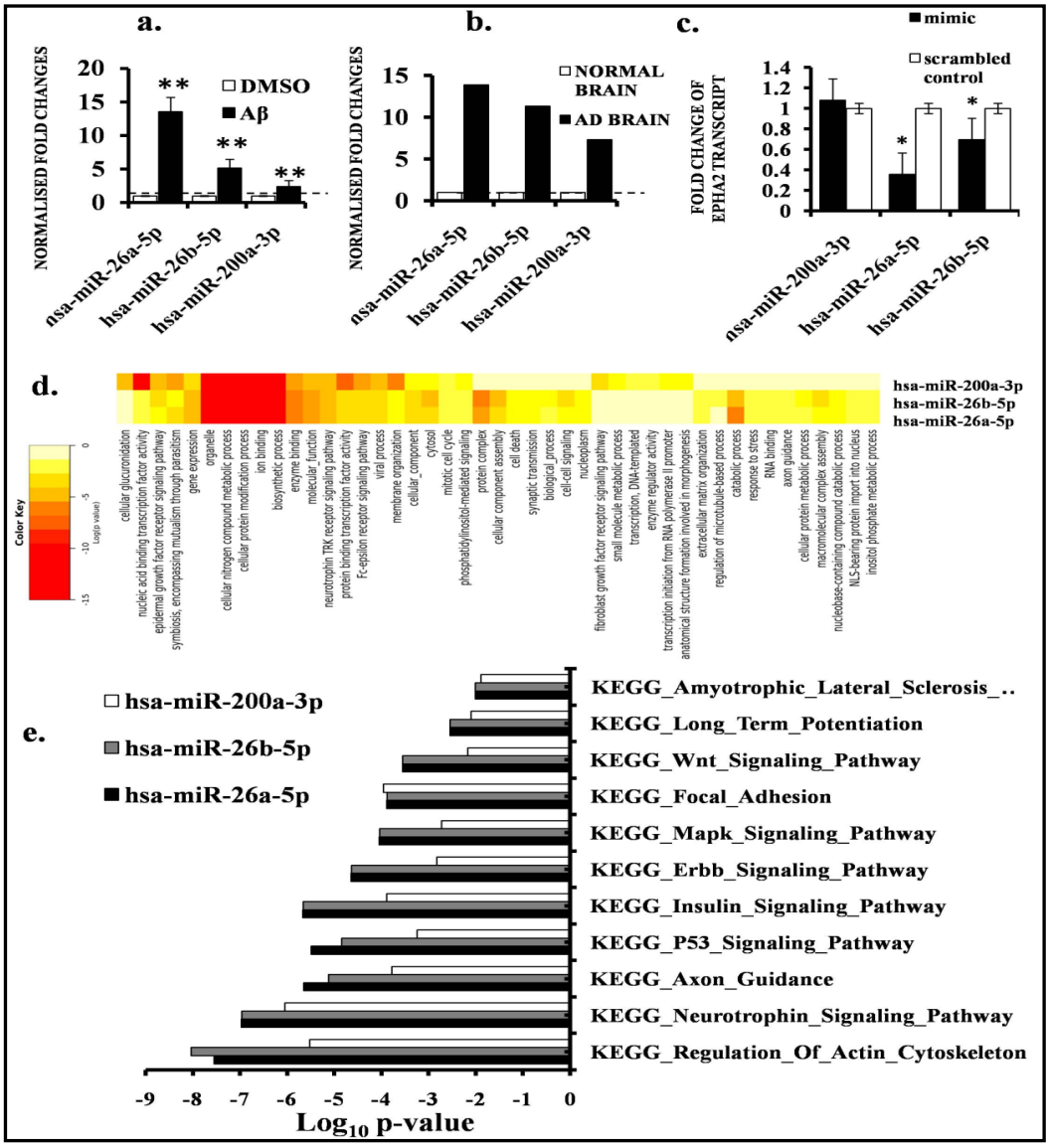

Figure 4.4: Altered levels of 3 miRNAs in $A\beta_{1-42}$ treated cell model and AD brain.

(a). Bar diagrams indicative of three (n = 3) independent biological replicates quantifying levels of hsa-miR-200a-3p, hsa-miR-26a-5p and hsa-miR-26b-5p by qRT-PCR in SHSY5Y cells treated with 0.5 μM $A\beta_{1-42}$ or treated with only DMSO. (b) Bar graphs representative of two experiments (n = 2; technical replicate) measuring levels of hsa-miR-200a-3p, hsa-miR-26a-5p and hsa-miR-26b-5p in total RNA isolated from the brain of 1 AD patient compared to total RNA from the brain of a non –AD control. (c). Bar diagrams indicative of three (n = 3) independent biological replicates quantifying levels of EPHA2 by qRT-PCR in SHSY5Y cells treated with hsa-miR-200a-3p, hsa-miR-26a-5p and hsa-miR-26b-5p mimics or corresponding scrambled controls. (d). GO analysis of the 3 de regulated miRNAs; colour codes indicate Log (p value) and ranges from -15 to 0. (e). KEGG analysis of the 3 de regulated miRNAs; bar graphs indicate Log (p value) and ranges from -9 to 0.

other two miRNAs of the miR-26 family. MiR-26a mimic decreased the level of EPHA2 to 0.3 (scrambled control taken as 1), while the repression by miR-26b mimic was close to 0.7 (scrambled control taken as 1) and both the repressions were significant. Arguably the miRNA targets of EPHA2 could also be a part of the neurobiological processes, further supported by GO and KEGG pathway analysis. The miRPath module of DIANA TOOLS was used for GO and KEGG pathway enrichment involving the 3 MALAT1 interacting miRNAs which targeted EPHA2. **Fig 4.4 d.** showed the GO analysis of the 3 miRNAs involving the same in 44 biological pathways. Out of these all three were most strongly enriched in 5 – namely, organelle, ion binding, biosynthetic process, cellular protein modification process and cellular nitrogen compound metabolic process. Interestingly, miR-26a and -26b were not only more abundant in SHSY5Y cells but also were strongly up regulated in AD and were relatively more enriched in neurological processes like cell-cell signalling, synaptic transmission and axon guidance. This same observation was reinforced with

KEGG analysis (**Fig 4.4 e.)** which showed the enrichment of mostly neurological processes like Amyotrophic Lateral Sclerosis, Long term potentiation, Axon Guidance and Neurotrophin signalling pathway, among others.

4.5. Deregulated EPHA2 in AD confers protection against $A\beta_{1-42}$ cytotoxicity through its downstream effectors CREB, p38 and Synaptophysin

On establishing that the 3 MALAT1 interacting miRNAs repressed EPHA2, it was examined if EPHA2 itself was deregulated in our $A\beta_{1-42}$ treated cell model. **Fig 4.5 a.** showed that indeed EPHA2 mRNA was down regulated (fold change – 0.6; DMSO control taken as 1). The down regulation was also evident in the protein level of EPHA2 (fold change – 0.4 DMSO control taken as 1) (**Fig 4.5 b. and Fig 4.5 c.).** Moreover, EPHA2 clones were transfected in SHSY5Y cells and 24 hours post transfection, 0.5 μM of $A\beta_{1-42}$ was added to the cells for 3 hours. After this, cells were lysed and the protein was used for western blot. **Fig 4.5 d. and Fig 4.5 e.** showed that the $A\beta_{1-42}$ exposure was strong enough to elicit a significant downregulation of CREB phosphorylation (control vs. Aβ), but a prior over expression of EPHA2 not only overcame the down regulation due to Aβ, but also increased phospho-CREB above the basal levels (control vs. EPHA2+ Aβ). Intuitively, the phospho-CREB levels were highest with only EPHA2 over expression (control vs. EPHA2). Conversely, the same EPHA2 over expression was able to restore the Aβ stress induced increase of phospho-p38 (**Fig 4.5f. and Fig 4.5g).** However, it was interesting to note that EPHA2 over expression (control vs. EPHA2) by itself had no significant difference with it's over expression in presence of Aβ (control vs. EPHA2+ Aβ) on phospho-p38 levels. The protein levels of Synaptophysin were looked at to see whether the over expression of EPHA2 affected the synaptic process. **Fig 4.5h. and Fig 4.5i.** showed that EPHA2 was sufficient to reverse the decrease of Synaptophysin due to Aβ

treatment, but it could not restore Synaptophysin level to the basal one. Finally, in order to see if our regulatory network was indeed connected, MALAT1 was knocked down and the levels of EPHA2 transcript analysed. As expected, the transient decrease of MALAT1 elicited a marked decrease of the EPHA2 transcript (**Fig 4.5 j).** Since CREB and p38 were both involved in neuronal survival, our next logical line of investigation was to see whether EPHA2 affected the gross cell viability. For this, three cell viability assays with increasing specificities were employed. First, Trypan Blue Dye exclusion assay was performed to access how the SHSY5Y cell populations were behaving on exposure to only Aβ or exposure to Aβ with prior over expression of EPHA2. Concordant to the results in Fig 5, Aβ decreased the gross cell viability as expected, but EPHA2 was able to overcome such deficit (**Fig 4.6 a.**). Second, the same pattern of recovery was replicated with the MTT assay (**Fig 4.6 b.**), but the % viability due to prior EPHA2 over expression was more pronounced. Third, a Live and Dead Cell Assay was performed to not only measure the viable population, but also to visualize the same.

Fig 4.6 c. and Fig 4.6 d. – panel ii showed that more than 50% cells were killed due to only Aβ treatment (compared to DMSO control **Fig 4.6 d. – panel i**) but EPAH2 over expression restored the viability to almost basal levels (**Fig 4.6 c. and Fig 4.6 d. – panel iii**). A strong negative control was taken to see the efficiency of the assay. **Fig 4.6 c. and Fig 4.6d. – panel iv** showed that treatment of 1 µL of Hydrogen Peroxide (for 10 minutes) per 35mm dish was sufficient to kill nearly 90% of the cell population. Thus, it was evident that EPHA2 was acting as a pro-survival cue by operating through the CREB/p38 signalling pathway and affecting the gross viability of neuronal cell populations by itself or in the presence of Aβ.

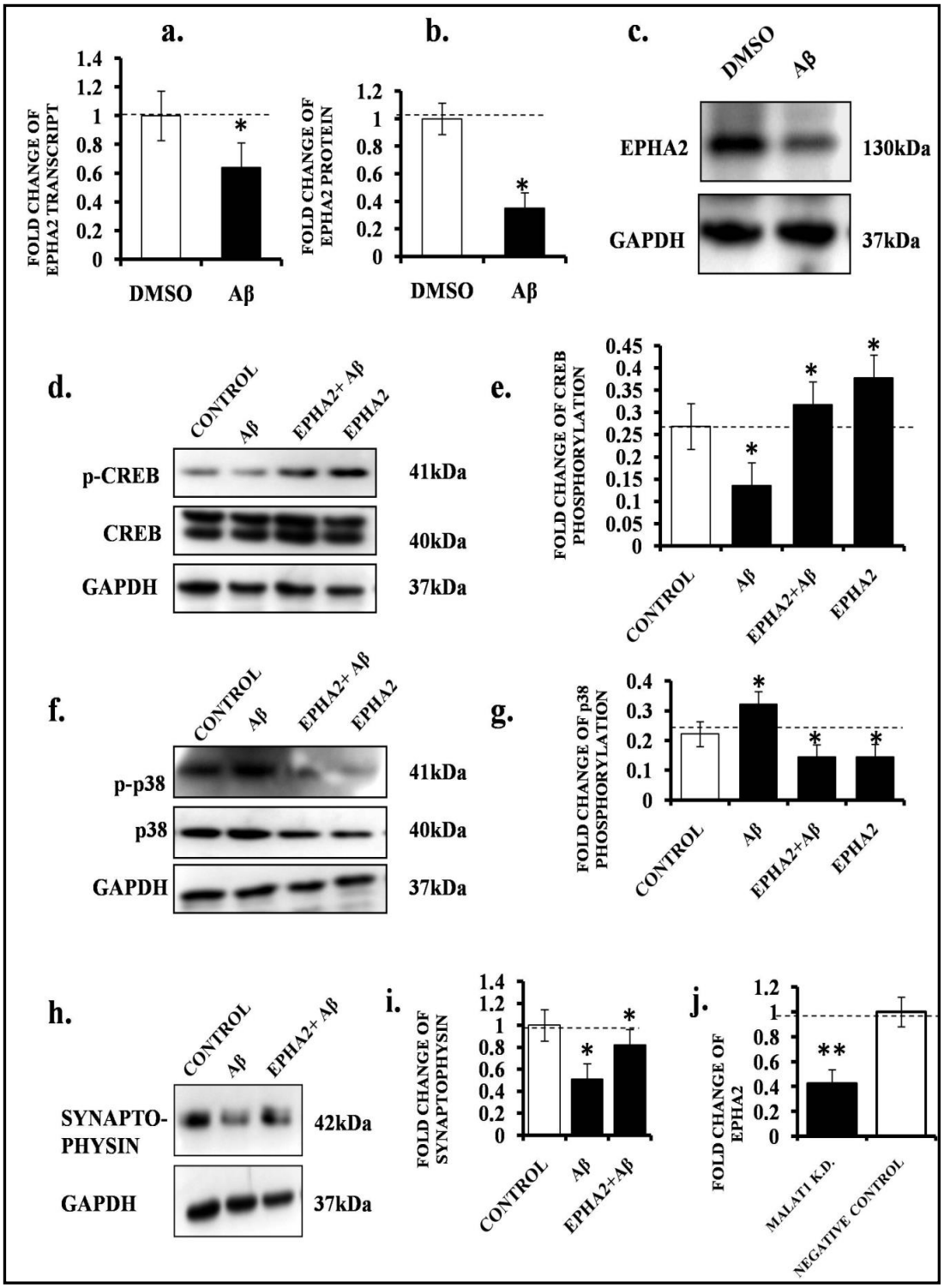

Figure 4.5: Altered levels of EPHA2 and its downstream proteins in $A\beta_{1-42}$ treated cell model and in cells over expressing EPHA2 + $A\beta_{1-42}$. (a). Bar diagrams indicative of three (n = 3) independent biological replicates quantifying levels of EPAH2 by qRT-PCR in SHSY5Y cells treated with 0.5 µM $A\beta_{1-42}$ or treated with only DMSO. (b). Histogram representing the mean value of optical density of the EPHA2 bands, normalized against GAPDH. (c). Western blot

(n=3) showing the EPAH2 and GAPDH levels in $A\beta_{1-42}$ treated AD cell model**.** (d). Western blot (n=3) showing the phospho CREB, CREB and GAPDH levels in Control cells, $A\beta_{1-42}$ treated cells (Aβ), $A\beta_{1-42}$ treated cells with EPHA2 over expressed (EPAH2+ Aβ) and only EPHA2 over expressed cells (EPHA2) (e). Histogram representing the mean percentage phosphorylation of CREB, normalized against GAPDH. (f). Western blot (n=3) showing the phospho p38, p38 and GAPDH levels in Control cells, $A\beta_{1-42}$ treated cells (Aβ), $A\beta_{1-42}$ treated cells with EPHA2 over expressed (EPAH2+ Aβ) and only EPHA2 over expressed cells (EPHA2). (g). Histogram representing the percentage phosphorylation of p38, normalized against GAPDH (h). Western blot (n=3) showing the Synaptophysin and GAPDH levels in Control cells, $A\beta_{1-42}$ treated cells (Aβ) and $A\beta_{1-42}$ treated cells with EPHA2 over expressed (EPAH2+ Aβ). (i). Histogram representing the mean value of optical density of the Synaptophysin bands, normalized against GAPDH. (j). Bar diagrams indicative of three (n = 3) independent biological replicates quantifying levels of EPAH2 by qRT-PCR in SHSY5Y cells treated with MALAT1 siRNA or negative control siRNA.

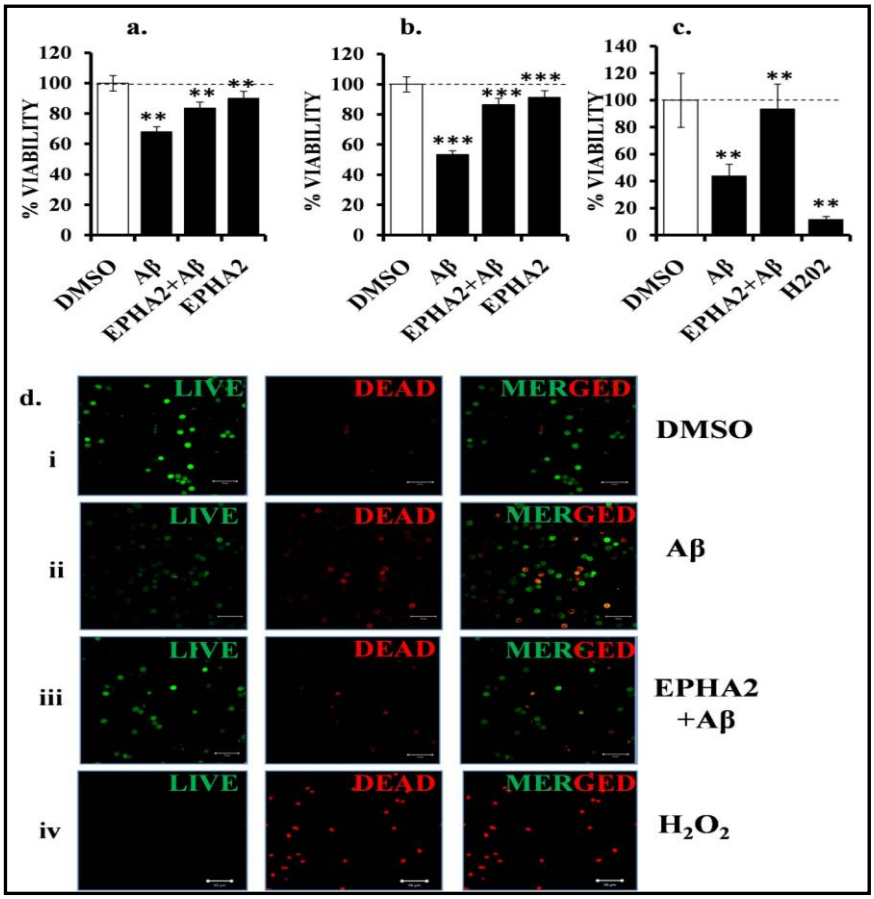

Figure 4.6: Effect of EPHA2 over expression on cell viability in $A\beta_{1-42}$ treated cell model. (a). Bar graphs representative of four (n = 4) independent experiments of Cell viability in SHSY5Y cells, detected by Trypan Blue Exclusion Assay in Control cells, $A\beta_{1-42}$ treated cells (Aβ), $A\beta_{1-42}$ treated cells with EPHA2 over expressed (EPAH2+ Aβ), and only EPHA2 over expressed cells (EPHA2). (b). Bar graphs representative of 10 (n = 10) independent experiments of Cell viability in SHSY5Y cells, detected by MTT Assay in Control cells, $A\beta_{1-42}$ treated cells (Aβ), $A\beta_{1-42}$ treated cells with EPHA2 over expressed (EPAH2+ Aβ) and only EPHA2 over expressed cells (EPHA2). (c). Bar diagrams indicative of three (n = 3) independent biological replicates quantifying levels of Cell viability in SHSY5Y cells, detected by Live and Dead Cell Assay in Control cells, $A\beta_{1-42}$ treated cells (Aβ), $A\beta_{1-42}$ treated cells with EPHA2 over expressed (EPAH2+ Aβ) and H_2O_2 treated cells (H_2O_2). (d). Confocal microscope images representative of three (n = 3) independent experiments of Cell viability in SHSY5Y cells, detected by Live and Dead Cell Assay in Control cells (panel i), $A\beta_{1-42}$ treated cells (Aβ) (panel ii), $A\beta_{1-42}$ treated cells with EPHA2 over expressed (EPAH2+ Aβ) (panel iii) and H_2O_2 treated cells (H_2O_2) (panel iv). Green represents live and red represents dead cells. For each set, at least 30 images were captured. Scale bars, 20μm.

4.6. Discussion

In this current investigation, the differential levels of lncRNAs in AD mice brain were examined using a RT^2 lncRNA PCR Array. Out of the 41 significantly deregulated lncRNAs, 7 had AD associations [1-3]. Combining data from the 3 independent experiments, it was found that 4 out of the 7 lncRNAs showed similar patterns of deregulation - RMST and NEAT1 were up regulated, while MEG3 and MALAT1 were down regulated. Furthermore, I focussed my attention especially on MALAT1 because; i) Data from this and several prior studies show that MALAT1 enrichment in predominantly the prerogative of neurons and neural tissues [4], ii) MALAT1 is implicated in synaptogenesis [5] and iii) MALAT1 levels are altered in Parkinson's

Disease and Retinal Neurodegeneration, in addition to AD [6, 7]. Indeed, MALAT1 showed the most consistent and strongest downregulation in all our validation models under consideration. Next, in order to decipher the relevance of MALAT1 deregulation, its miRNA interacting components were investigated. Combining bioinformatics analysis, knock down assays and RNA Immunoprecipitation, it was shown that MALAT1 interacted with miR-200a-3p, 26a-5p and 26b-5p. One of the key RBP interactors of MALAT1, FUS, which was used as a bait to pull MALAT1 down, is itself of prime importance in neurodegenerative diseases [8]. Previous literature backs up our experimental evidence that levels of miR-200a-3p [9, 10], miR-26a-5p [11] and miR-26b-5p [12, 13] are all significantly disrupted in AD with important ramifications. All these 3 miRNAs were found to be up regulated in our AD model and AD brain. It was logical to know how such an increase of these 3 affected neuronal cell physiologies indirectly through one of their common targets, EPHA2. In recent times, a growing body of evidence points to the fact that Eph family of RTKs are involved in AD [14] and that they might play protective roles [15]. By transiently over expressing mature miRNA mimics, it was shown that miR-26a and miR-26b strongly repressed EPHA2. This experimental data is also supported by existing literature [16, 17] which shows the interaction of miR-26a and miR-26b with EPHA2 3'UTR by luciferase assays. Following this chain of thought, it was found that EPHA2 is down regulated in our AD cell model, probably as a consequence of the increase of its targeting miRNAs. This down regulation of EPHA2 was also reflected in its downstream protein components – CREB and p38, both of which are reported to be deregulated in AD [18-21]. Backed up by existing literature evidences that 2 key signalling components CREB (pro-survival) and p38 MAPK (stress response) are implicated in AD [18-21] and other Eph family members are involved in AD via

CREB pathway [22-24], I aimed to see whether over expressing EPHA2 could confer protection against $A\beta_{1-42}$ in cells. It was shown that EPHA2 was necessary and sufficient to recover cellular viability to normal values after they had been exposed to toxic $A\beta_{1-42}$. The didactic nature of this elegant network **(Cover cartoon)** was highlighted by showing that knocking down MALAT1 led to a subsequent decrease of EPHA2. Moreover, it was also found that the protein component of the miRNA machinery, Ago2, co-localised strongly with the MALAT1 interactor FUS in distinct nuclear clusters (**Fig 4.7. Panels i and ii**) and conversely, FUS co-localised near perfectly with CREB in the nucleus (**Fig 4.7. Panels iii and iv**) hinting at the fact that the miRNA-lncRNA-Transcription factor machinery possibly interact in a closed loop.

The sponging effect of exosomal MALAT1 on miR-26a/b/200a has been shown recently in colorectal cancers via the PI3K/Akt pathway as the downstream signalling cascade [25]. A similar loop involving MALAT1 and miR-200c-3p has been investigated in pancreatic cancer [26]. Apart from these, a MALAT1-miR-200a-3p-PDCD4 axis has been reported to regulate cardiomyocytes apoptosis [27]. But, to our comprehension, this is the first study to unequivocally implicate MALAT1 in AD, by showing it is deregulated in multiple disease models. I have also tried to establish a functional link between MALAT1 and miR-26a/b/200a in a neurodegenerative disease by delineating the role of EPHA2 in AD – from the perspective of its miRNA regulators, the downstream protein it regulates and how it affects gross cellular viability. Finally, a functional link between the MALAT1-miR-26a/b/200a-EPAH2 governing triad in AD was shown. It would be prudent to assume that the extracellular treated $A\beta_{1-42}$ translocate to the nucleus and possibly regulates the levels of MALAT1, de regulated in AD, in terms of its transcription factors. The same can also

be said of the miRNAs and specifically that an abundance of extracellular Aβ $_{1-42}$ is sufficient to elicit such a strong response in the lncRNA and miRNA populations, both of which are predominantly nuclear. Such instances of Aβ$_{1-42}$ acting as a regulator of gene transcription already exists [28-30]. Apart from this, even the extracellular treatment of Aβ $_{1-42}$ affects the RTK pathway signalling; mainly via the adaptor protein Grb2- as shown by data from our lab as well as others [31, 32].

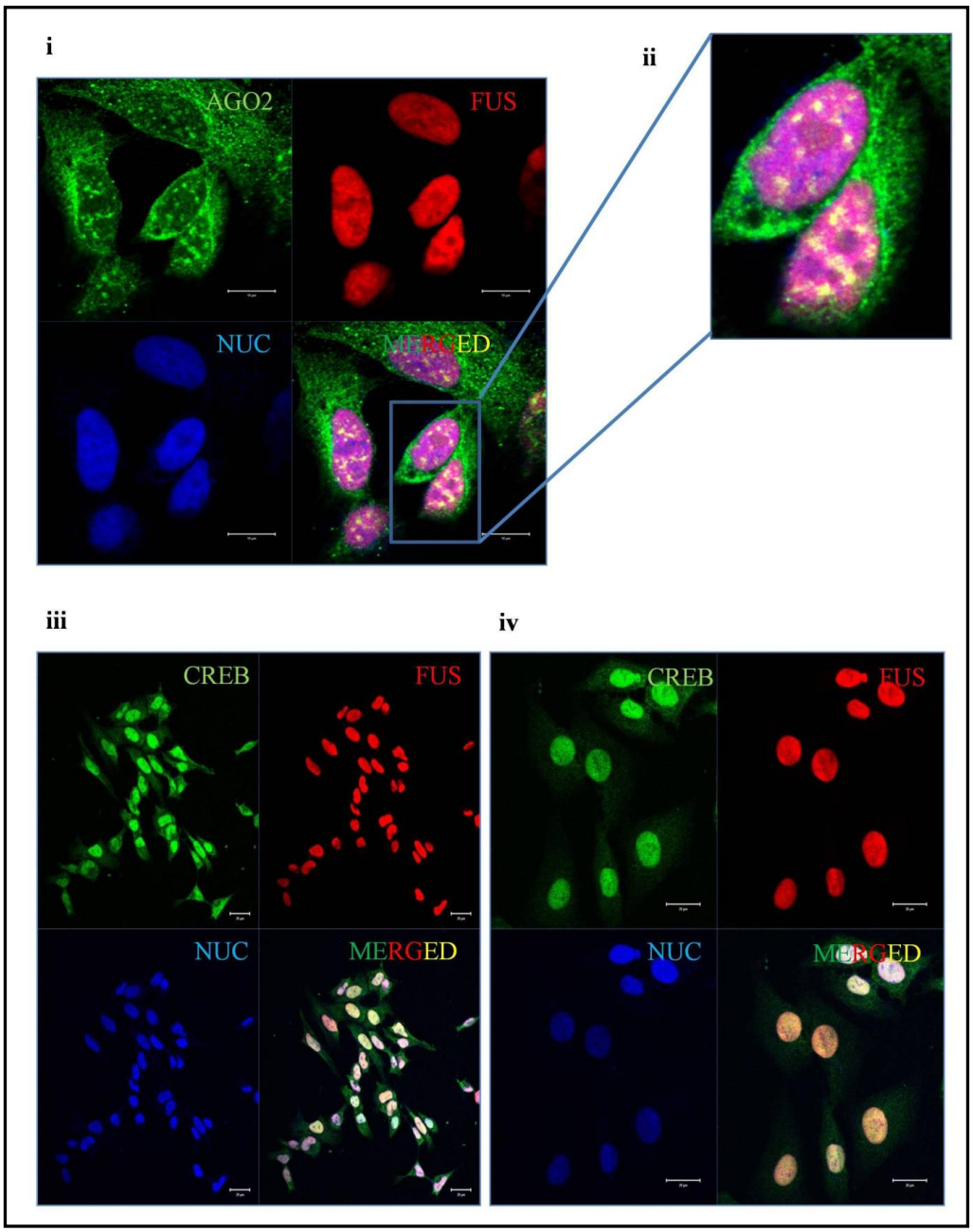

Figure 4.7: Co-localization Analysis - Immunocytochemistry (ICC) assay. AGO2 with FUS in SHSY5Y cells; panel (i) and panel (ii) – inset- showing specific co- localisation of AGO2 and FUS in intra nuclear clusters. Low magnification image (1x) of a cell population – panel (iii) and high magnification image (4x) – panel (iv) - showing co-localisation of CREB and FUS in nucleus in SHSY5Y cells. Scale bars, 20µm; panel (ii) Low magnification (1x) image. Scale bars, 10µm- panel (i); 20 µm – panel (iii) & (iv). For each ICC experiment, images of at least 30 cells (or cell fields) were captured and the experiments were repeated thrice (n = 3).

Summary:

- MALAT1 was deregulated in cell and animal models of AD.
- MALAT1 interacted with and sponged miR-200a-3p, 26a-5p and 26b-5p. These 3 were up regulated in AD.
- These miRNAs repressed RTK EPHA2, which is down regulated in AD.
- Over expression of EPHA2 in presence of Aβ abrogated cellular cytotoxicity through the pro-survival CREB pathway.

4.7. References

[1]. Kim YK, Song J. The Role of Long Noncoding RNAs in Diabetic Alzheimer's Disease. J Clin Med. 2018 Nov 21;7(11). pii: E461. doi: 10.3390/jcm7110461. PubMed PMID: 30469430; PubMed Central PMCID: PMC6262561.

[2]. Bao MH, Szeto V, Yang BB, Zhu SZ, Sun HS, Feng ZP. Long non-coding RNAs in ischemic stroke. Cell Death Dis. 2018 Feb 15;9(3):281. doi: 10.1038/s41419-018-0282-x. Review. PubMed PMID: 29449542; PubMed Central PMCID: PMC5833768.

[3]. Zhao HY, Zhang ST, Cheng X, Li HM, Zhang L, He H, Qin JB, Zhang WY, Sun Y, Jin GH. Long non-coding RNA GAS5 promotes PC12 cells differentiation into Tuj1-positive neuron-like cells and induces cell cycle arrest. Neural Regen Res. 2019 Dec;14(12):2118-2125. doi: 10.4103/1673-5374.262592. PubMed PMID: 31397350; PubMed Central PMCID: PMC6788226.

[4]. Lipovich L, Dachet F, Cai J, Bagla S, Balan K, Jia H, Loeb JA. Activity-dependent human brain coding/noncoding gene regulatory networks. Genetics. 2012 Nov;192(3):1133-48.

[5]. Bernard D, Prasanth KV, Tripathi V, Colasse S, Nakamura T, Xuan Z, Zhang MQ, Sedel F, Jourdren L, Coulpier F, Triller A, Spector DL, Bessis A. A long nuclear-retained non-coding RNA regulates synaptogenesis by modulating gene expression. EMBO J. 2010 Sep 15;29(18):3082-93.

[6]. Zhang QS, Wang ZH, Zhang JL, Duan YL, Li GF, Zheng DL. Beta-asarone protects against MPTP-induced Parkinson's disease via regulating long non-coding RNA MALAT1 and inhibiting α-synuclein protein expression. Biomed Pharmacother. 2016 Oct; 83:153-159.

[7]. Yao J, Wang XQ, Li YJ, Shan K, Yang H, Wang YN, Yao MD, Liu C, Li XM, Shen Y, Liu JY, Cheng H, Yuan J, Zhang YY, Jiang Q, Yan B. Long non-coding RNA MALAT1 regulates retinal neurodegeneration through CREB signaling. EMBO Mol Med. 2016 Sep 1;8(9):1113. doi: 10.15252/emmm.201606749. PubMed PMID: 27587362; PubMed Central PMCID: PMC5009814.

[8]. Deng H, Gao K, Jankovic J. The role of FUS gene variants in neurodegenerative diseases. Nat Rev Neurol. 2014 Jun;10(6):337-48.

[9]. Lau P, Bossers K, Janky R, Salta E, Frigerio CS, Barbash S, Rothman R, Sierksma AS, Thathiah A, Greenberg D, Papadopoulou AS, Achsel T, Ayoubi T, Soreq H, Verhaagen J, Swaab DF, Aerts S, De Strooper B. Alteration of the microRNAs network during the progression of Alzheimer's disease. EMBO Mol Med. 2013 Oct;5(10):1613-34.
[10]. Zhang QS, Liu W, Lu GX. miR-200a-3p promotes b-Amyloid-induced neuronal apoptosis through down-regulation of SIRT1 in Alzheimer's disease. J Biosci. 2017 Sep;42(3):397-404.
[11]. Leidinger P, Backes C, Deutscher S, et al. A blood based 12-miRNA signature of Alzheimer disease patients. *Genome Biol*. 2013;14(7):R78.
[12]. Absalon S, Kochanek DM, Raghavan V, Krichevsky AM. MiR-26b, upregulated in Alzheimer's disease, activates cell cycle entry, tau-phosphorylation, and apoptosis in postmitotic neurons. J Neurosci. 2013 Sep 11;33(37):14645-59.
[13]. Chu T, Shu Y, Qu Y, Gao S, Zhang L. miR-26b inhibits total neurite outgrowth, promotes cells apoptosis and downregulates neprilysin in Alzheimer's disease. Int J Clin Exp Pathol. 2018 Jul 1;11(7):3383-3390.
[14]. Cissé M, Checler F. Eph receptors: new players in Alzheimer's disease pathogenesis. Neurobiol Dis. 2015 Jan;73:137-49.
[15]. Hu R, Wei P, Jin L, Zheng T, Chen WY, Liu XY, Shi XD, Hao JR, Sun N, Gao C. Overexpression of EphB2 in hippocampus rescues impaired NMDA receptors trafficking and cognitive dysfunction in Alzheimer model. Cell Death Dis. 2017 Mar 30;8(3):e2717.
[16]. Good RJ, Hernandez-Lagunas L, Allawzi A, Maltzahn JK, Vohwinkel CU, Upadhyay AK, Kompella UB, Birukov KG, Carpenter TC, Sucharov CC, Nozik-Grayck E. MicroRNA dysregulation in lung injury: the role of the miR-26a/EphA2 axis in regulation of endothelial permeability. Am J Physiol Lung Cell Mol Physiol. 2018 Oct 1;315(4):L584-L594.
[17]. Jin Q, Li XJ, Cao PG. MicroRNA-26b Enhances the Radiosensitivity of Hepatocellular Carcinoma Cells by Targeting EphA2. Tohoku J Exp Med. 2016 Feb;238(2):143-51.
[18]. Pugazhenthi S, Wang M, Pham S, Sze CI, Eckman CB. Downregulation of CREB expression in Alzheimer's brain and in Aβ-treated rat hippocampal neurons. Mol Neurodegener. 2011 Aug 19;6:60.
[19]. Vitolo OV, Sant'Angelo A, Costanzo V, Battaglia F, Arancio O, Shelanski M. Amyloid beta -peptide inhibition of the PKA/CREB pathway and long-term potentiation: reversibility by drugs that enhance cAMP signaling. Proc Natl Acad Sci U S A. 2002 Oct 1;99(20):13217-21.
[20]. Munoz L, Ammit AJ. Targeting p38 MAPK pathway for the treatment of Alzheimer's disease. Neuropharmacology. 2010 Mar;58(3):561-8.
[21]. Sun A, Liu M, Nguyen XV, Bing G. P38 MAP kinase is activated at early stages in Alzheimer's disease brain. Exp Neurol. 2003 Oct;183(2):394-405.
[22]. Cissé M, Halabisky B, Harris J, Devidze N, Dubal DB, Sun B, Orr A, Lotz G, Kim DH, Hamto P, Ho K, Yu GQ, Mucke L. Reversing EphB2 depletion rescues cognitive functions in Alzheimer model. Nature. 2011 Jan 6;469(7328):47-52.
[23]. Miyamoto T, Kim D, Knox JA, Johnson E, Mucke L. Increasing the Receptor Tyrosine Kinase EphB2 Prevents Amyloid-β-induced Depletion of Cell Surface Glutamate Receptors by a Mechanism That Requires the PDZ-binding Motif of EphB2 and Neuronal Activity. J Biol Chem. 2016 Jan 22;291(4):1719-34.
[24]. Yu LN, Sun LH, Wang M, Wang LJ, Wu Y, Yu J, Wang WN, Zhang FJ, Li X, Yan M. Ephrin B-EphB Signaling Induces Hyperalgesia through ERK5/CREB Pathway in Rats. Pain Physician. 2017 May;20(4):E563-E574.
[25]. Xu J, Xiao Y, Liu B, et al. Exosomal MALAT1 sponges miR-26a/26b to promote the invasion and metastasis of colorectal cancer via FUT4 enhanced fucosylation and PI3K/Akt pathway. *J Exp Clin Cancer Res*. 2020;39(1):54.
[26]. Zhuo M, Yuan C, Han T, Cui J, Jiao F, Wang L. A novel feedback loop between high MALAT-1 and low miR-200c-3p promotes cell migration and invasion in pancreatic ductal adenocarcinoma and is predictive of poor prognosis. *BMC Cancer*. 2018;18(1):1032.
[27]. Sun R, Zhang L. Long non-coding RNA MALAT1 regulates cardiomyocytes apoptosis after hypoxia/reperfusion injury via modulating miR-200a-3p/PDCD4 axis. *Biomed Pharmacother*. 2019;111:1036-1045.
[28]. Johnstone EM, Babbey LE, Stephenson D, Paul DC, Santerre RF, Clemens JA,Williams DC, Little SP. Nuclear and cytoplasmic localization of the beta-amyloid peptide (1-43) in transfected 293 cells. Biochem Biophys Res Commun. 1996 Mar27;220(3):710-8.
[29]. Barucker C, Harmeier A, Weiske J, Fauler B, Albring KF, Prokop S, HildebrandP, Lurz R, Heppner FL, Huber O, Multhaup G. Nuclear translocation uncovers the amyloid peptide Aβ42 as a regulator of gene transcription. J Biol Chem. 2014 Jul 18;289(29):20182-91.

[30]. Barucker C, Sommer A, Beckmann G, Eravci M, Harmeier A, Schipke CG, Brockschnieder D, Dyrks T, Althoff V, Fraser PE, Hazrati LN, George-Hyslop PS,Breitner JC, Peters O, Multhaup G. Alzheimer amyloid peptide aβ42 regulates gene expression of transcription and growth factors. J Alzheimers Dis.2015;44(2):613-24.

[31]. Pratt RL, Kinch MS. Activation of the EphA2 tyrosine kinase stimulates the MAP/ERK kinase signaling cascade. *Oncogene*. 2002;21(50):7690-7699.

[32]. Majumder P, Roy K, Bagh S, Mukhopadhyay D. Receptor tyrosine kinases (RTKs) consociate in regulatory clusters in Alzheimer's disease and type 2 diabetes. *Mol Cell Biochem*. 2019;459(1-2):171-182

Chapter 5: Cytoskeletal functions of ROR1 in AD

5.1. ROR1 and key cytoskeletal proteins are deregulated in $A\beta_{1-42}$ treated cell model compromising the cytoskeletal architecture

To begin with, the deregulated levels of ROR1 were looked at, both at the transcript and protein levels in SHSY-5Y cells treated with $A\beta_{1-42}$ and compared with DMSO control (considered as 1). Both mRNA (fold change 0.43 **Figure 5.1 a**) and protein levels (fold change 0.37 **Fig 5.1 b. & c**) showed that treatment with $A\beta_{1-42}$ elicited downregulation of ROR1.

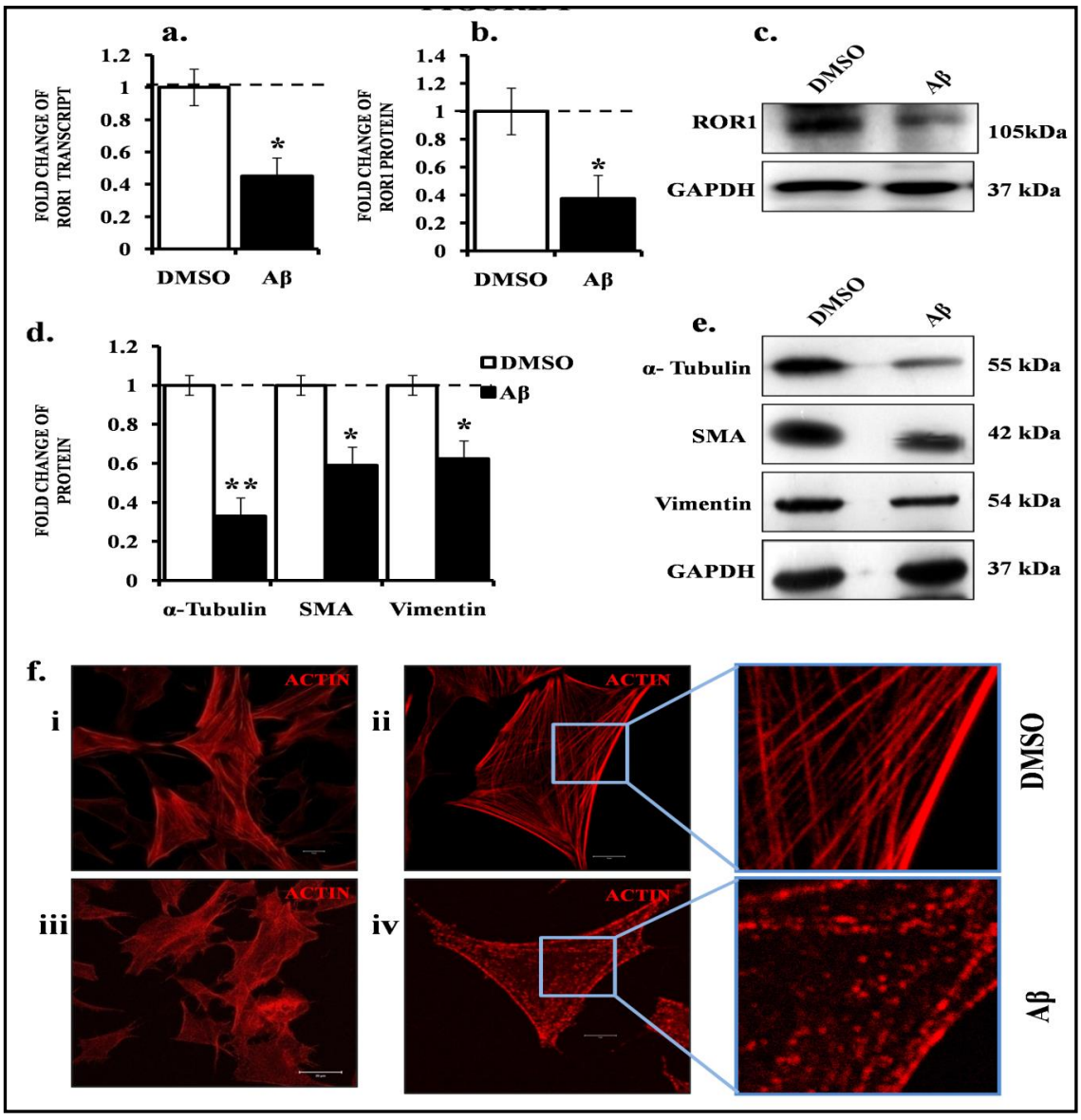

Figure 5.1: Deregulation of ROR1, key signalling proteins and actin cytoskeleton in $A\beta_{1-42}$ treated cell model. (a). Graph depicting three (n = 3) independent biological replicates

quantifying levels of ROR1 by qRT-PCR in SHSY-5Y cells treated with 1µM $A\beta_{1-42}$ or treated with only DMSO. (b). Graph depicting the mean value of optical density of the ROR1 bands, normalized against GAPDH. (c). Western blot (n=3) showing the ROR1 and GAPDH levels in $A\beta_{1-42}$ treated cell model**.** (d). Graph depicting the mean value of optical density of the α-Tubulin, SMA and Vimentin bands, normalized against GAPDH. (e). Western blot (n=3) showing the α-Tubulin, SMA, Vimentin and GAPDH levels in $A\beta_{1-42}$ treated cell model**.** (f). Confocal microscopy images of phalloidin-561 (actin) stained SHSY-5Y cells; DMSO treated (Panel i. 1X zoom), DMSO treated (Panel ii. and inset. 3X zoom), Scale bars, 5µm; $A\beta_{1-42}$ treated (Panel iii. 1X zoom), $A\beta_{1-42}$ treated (Panel iv. and inset. 3X zoom), Scale bars, 5µm; For each confocal experiment, images of at least 30 cells (or cell fields) were captured and the experiments were repeated thrice (n = 3). Error bars indicate ± SD. Significance level between different experimental pairs is shown (NS, not significant; *, $p < 0.05$; **, $p < 0.01$; ***, $p < 0.001$) (for all experiments, unless stated otherwise).

Owing to ROR1's association with cytoskeleton, I wanted to see if our cell model showed deregulation of cytoskeletal representative proteins, namely α- Tubulin (microtubule), Smooth Muscle Actin (SMA) (intermediate filament) and Vimentin (microfilament). On exposure to $A\beta_{1-42}$, the levels of α- Tubulin (fold change 0.33), SMA (fold change 0.59) and Vimentin (fold change 0.62) decreased significantly **(Figure 5.1 d. & e.)**. The same treatment was also sufficient to show visible phenotypic changes in the actin network of cells (assayed by phalloidin staining). In comparison to DMSO control, $A\beta_{1-42}$ exposure led to marked disruption of the mesh like actin assembly in cell clusters **(Figure 5.1 f, panels i & iii)**. Higher magnification images showed in more detail that the fibril like actin mesh (DMSO) (**Figure 5.1 f (ii))** was absent in the $A\beta_{1-42}$ cells (**Figure 5.1 f (iv))**, in which the actin were mostly present in punctate clusters.

5.2. ROR1 over expression abrogates $A\beta_{1-42}$ induced degradation of cytoskeletal components

ROR1 having been down regulated in the study model, the next logical approach would be to see if ROR1 over expression produced significant phenotypic changes. Fluorescent confocal microscopy, 24 hours post transfection with a ROR1-GFP Spark clone in SHSY-5Y cells, showed its sub-cellular distribution and marked alterations in the cellular structure (**Figure5. 2 a., panels i & iii).**

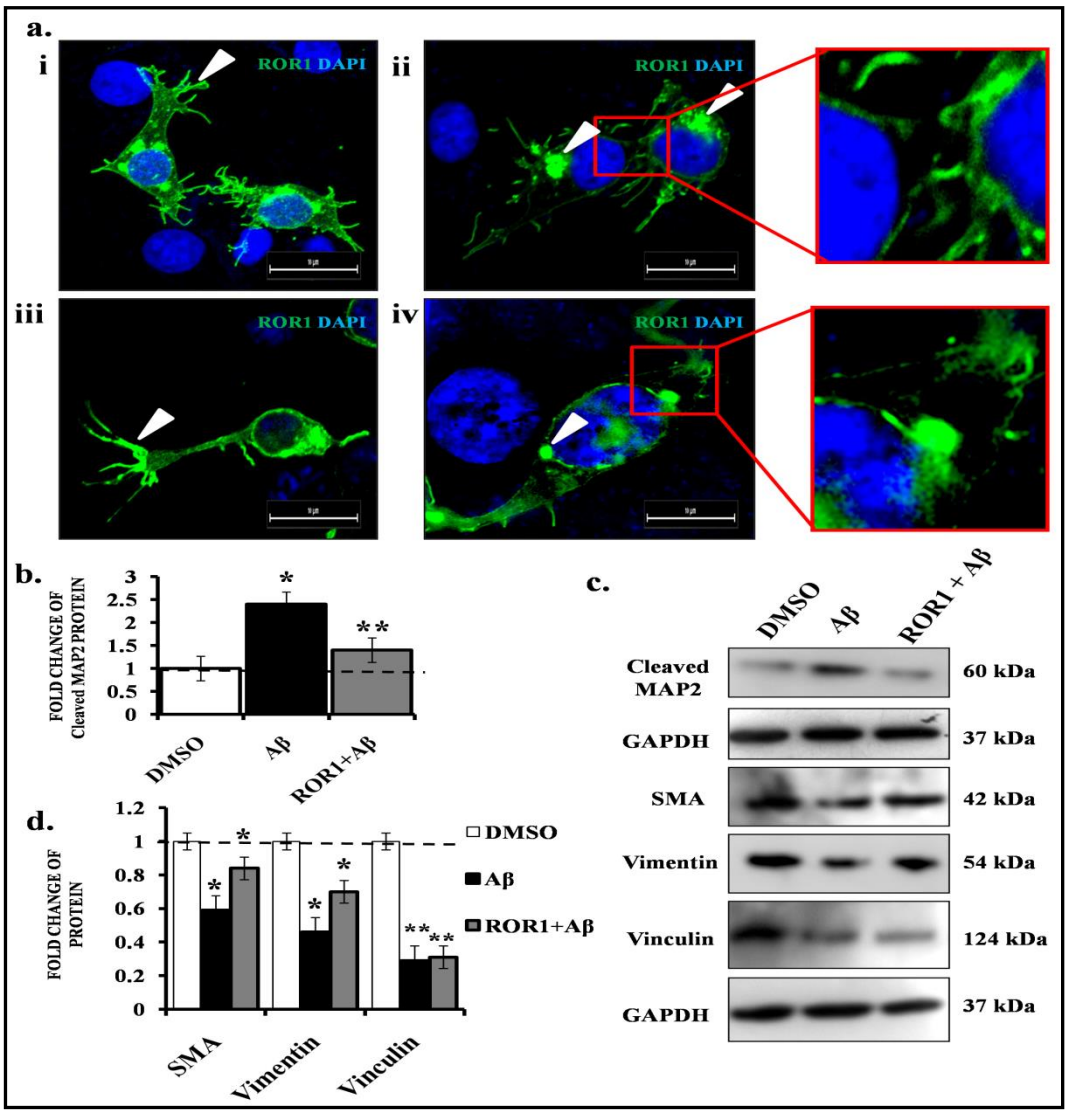

Figure 5.2: Consequences of ROR1 over expression on cytoskeletal components in $A\beta_{1-42}$ treated cells. (a). Confocal microscopy images of SHSY-5Y cells transfected with ROR1-GFPSpark and stained with DAPI – panel i and iii. ROR1 over expression leads to aberrant

terminal neurite outgrowths (white wedge); panel ii and iv. and insets. In dividing cells, ROR1 is localised to the cytokinetic bridge and terminal MTOCs (white wedge), Scale bars, 10μm; For each confocal experiment, images of at least 30 cells (or cell fields) were captured and the experiments were repeated thrice (n = 3). (b). Graph depicting the mean value of optical density of Cleaved MAP2 bands, normalized against GAPDH. (c). Western blot (n=3) showing the Cleaved MAP2, SMA, Vimentin, Vinculin and GAPDH levels in cells treated with DMSO (control), $A\beta_{1-42}$ and ROR1+ $A\beta_{1-42}$. (d). Graph depicting the mean value of optical density of SMA, Vimentin and Vinculin bands, normalized against GAPDH.

A transient over expression of ROR1 led to the generation of multiple neurites in cells (marked with white arrows) limited to the cell terminals. Super-resolution microscopic images showed that in dividing cells, ROR1 was distinctly enriched in the cytokinetic bridge **(Figure 5.2 a. panel ii and inset)** and the terminally located MTOCs **(Figure 5.2 a. panel iv and inset,** marked by white arrows). Following the observation that a transient increase in ROR1 promoted neurite generation, it was further shown that ROR1 over expression prior to $A\beta_{1-42}$ treatment hindered the cleavage of MAP2, indirectly indicating that ROR1 helped preserve the microtubule network **(Figure 5.2 b. and c.)**. Similar changes were also observed in the SMA and Vimentin levels (**Figure 5.2 d. and c.),** but Vinculin did not show any significant recovery.

5.3. Over expressed ROR1 promotes neurite elongation in presence of $A\beta_{1-42}$

Following a similar line of thought, it was next investigated if the aberrant neurite generation due to ROR1 over expression could also occur on treatment of $A\beta_{1-42}$, and if so, then how it would affect the cellular architecture. Indeed, it was found that a transient increase of ROR1 and $A\beta_{1-42}$ led to an increase of neurites **(Figure 5.3 a. panel i & ii and inset).**

However, unlike only ROR1 over expression, here, the neurites were significantly elongated in length, but less in number **(Figure 5.3 b.)**. Another interesting observation was that the elongated neurites were directed towards juxtaposed cells where they made contacts (marked by white arrows) and ROR1 was specifically enriched in the neurite terminals **(Figure 5.3 a. panel ii inset).** In order to better understand how ROR1 itself, or in conjunction with $A\beta_{1\text{-}42,}$ were affecting the cytoskeletal dynamics, a Filamentous: Globular (F: G) actin

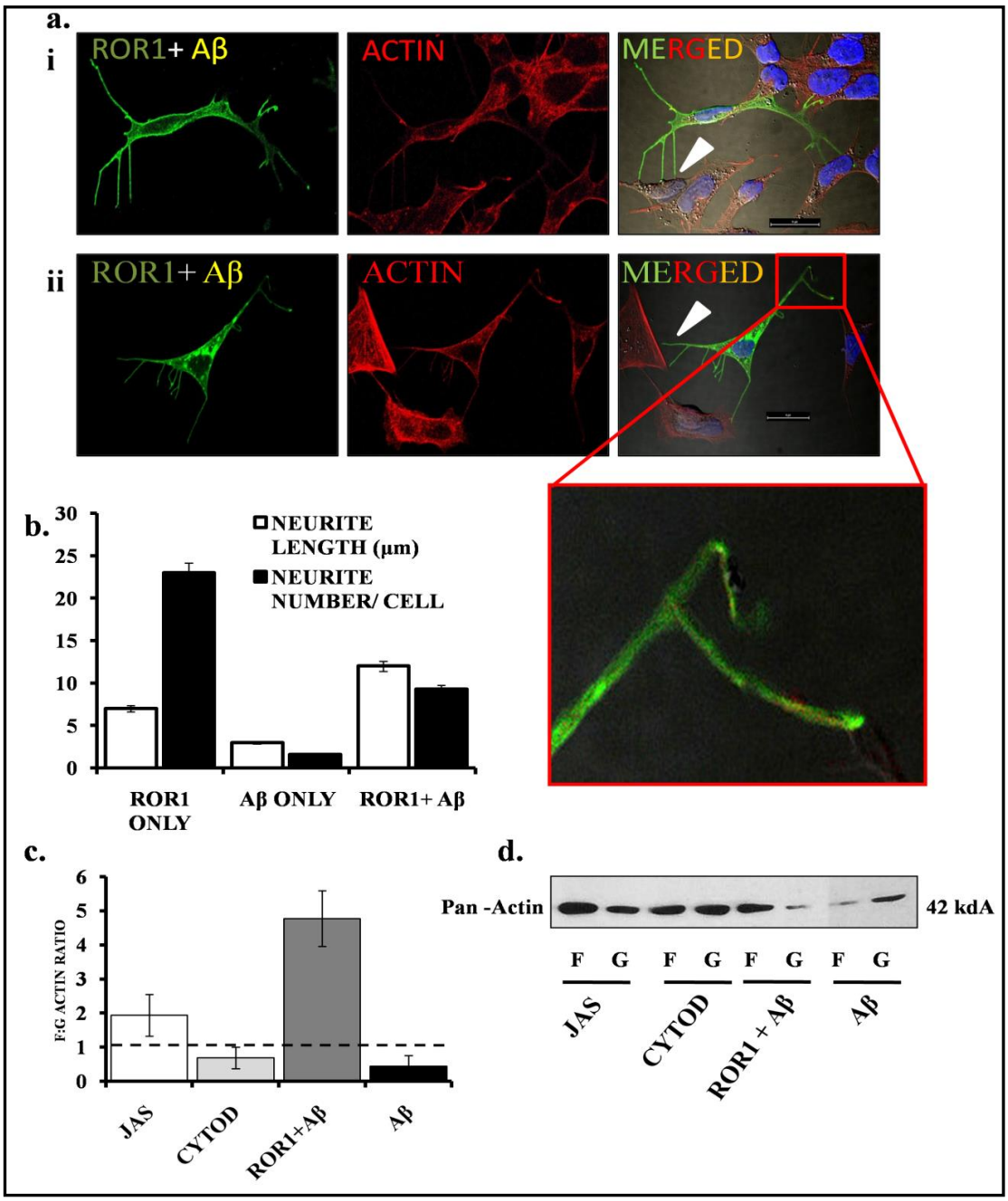

Figure 5.3: Effect of ROR1 over expression on neurite elongation and actin dynamics in $A\beta_{1-42}$ treated cells. (a). Confocal microscopy images of SHSY-5Y cells transfected with ROR1-GFPSpark, treated with $A\beta_{1-42}$ and stained with DAPI – panel i, ii and inset. ROR1 + $A\beta_{1-42}$ leads to fewer but more elongated neurites which makes contact with adjacent cells (white wedge), Scale bars, 10µm; For each confocal experiment, images of at least 30 cells (or cell fields) were captured and the experiments were repeated thrice (n = 3). (b). Graph depicting the mean value of neurite length and neurite numbers in ROR1, $A\beta_{1-42}$ and ROR1 + $A\beta_{1-42}$ cells. (c). Graph depicting the mean value of F: G actin ratio in Jasplakinolide, Cytochalasin-D, ROR1 + $A\beta_{1-42}$ and $A\beta_{1-42}$ treated cells, compared to their respective controls. (d). Western blot (n=3) showing the Pan -actin levels in the F and G fractions of cells treated with Jasplakinolide, Cytochalasin- D, ROR1 + $A\beta_{1-42}$ and $A\beta_{1-42}$.

Assay was performed. On exposure to Jasplakinolide (actin stabiliser) the F: G ratio was >1 (compared to DMSO control) (**Figure 5.3 c. and d.).** Cytochalasin D (actin depolymeriser) had the reverse effect. Treatment with $A\beta_{1-42}$ markedly decreased the ratio, but on prior increase with ROR1 followed by $A\beta_{1-42}$, there was a strong enrichment of filamentous actin (or inhibition of actin depolymerisation) which led to a subsequent increase of the F: G Actin ratio.

5.4. hsa-miR-146a-5p and 34a-5p are up regulated by $A\beta_{1-42}$ and target ROR1 and Vimentin

To gain a mechanistic insight into the trigger of ROR1 deregulation in $A\beta_{1-42}$ treated cells, the regulatory RNA- protein network model was pursued and the miRNA interacting (and preferably repressing) components of ROR1 network were looked for using ENCORI **(**http://starbase.sysu.edu.cn/index.php). The miRNA-mRNA tool was used with the following parameters - predicting program – 5, miRNA-mRNA with Pan-Cancer analysis -2 and stringency of CLIP data -3. With these attributes, ROR1

was predicted to interact with hsa-miR-146a-5p and hsa-miR-34a-5p. The same bioinformatic search predicted that that these two miRNAs also targeted a cytoskeletal protein of our interest – Vimentin. qRT-PCR with primers designed against the human mature miRNA sequences showed that hsa-miR-146a was more abundant compared to hsa-miR-34a, (normalised against control U6snRNA).

Both the miRNAs were strongly and significantly up- regulated in the $A\beta_{1-42}$ treated cell model (**Figure 5.4 a.)** Subsequent assays using AD transgenic mice brain tissues revealed almost the same patterns of up regulation, although here, the fold change of increase of hsa-miR-146a was much greater than hsa-miR-34a **(Figure 5.4 b.).** In order to validate the bioinformatics prediction, both the miRNAs individually were transiently over expressed

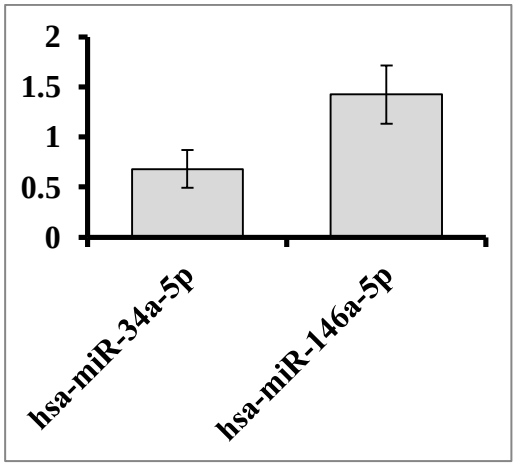

Endogenous expression levels of hsa-miR- 34a-5p and hsa-miR- 146a-5p: Bar graphs representative of three (n=3) independent experiments measuring relative endogenous expression levels of hsa-miR-34a-5p and hsa-miR- 146a-5p in SHSY5Y cells by qRT-PCR.

(using miRNA clones in pMIR vector) and then the transcript levels of ROR1 examined, and indeed both of them targeted and strongly repressed ROR1 levels **(Figure 5.4 c)**, although the effect of hsa-miR-146a-5p was more pronounced. These two ROR1 targeting miRNAs also targeted and repressed Vimentin (**Figure 5.4 d.)**, validating the prediction data. Combining both the results, it was found that hsa-miR-146a-5p was the stronger common repressor of both these proteins. Looking at the effect of these two miRNAs on cytoskeletal proteins, it was posited that they would be involved in neurological processes which are governed by such components.

Hence, a Gene Enrichment analysis was performed with the help of DIANA tools (miRPath module). Intuitively, GSEA revealed that both hsa-miR-146a and hsa-miR-34a were involved in core neurological pathways like Long Term Potentiation, Wnt signalling, Insulin signalling and Mapk signalling pathways (**Figure 5.4 e.)**. However, they were more enriched in the processes like – Regulation of actin cytoskeleton, Neurotrophin signalling and axon guidance, all of which were deregulated in AD. In this analysis too, hsa-miR-146a showed a stronger enrichment compared to hsa-miR-34a (**Figure 5.4 e.)**.

5.5. LncRNA NEAT1 exerts a protective effect by sponging miR146a and miR-34a

Continuing with the ncRNA regulatory networks governing ROR1, another layer of complexity was introduced. The ENCORI database was used to look for the potential lncRNA interactors of hsa-miR-146a-5p and hsa-miR-34a-5p. The miRNA-lncRNA tool was employed which had data from Ago-CLIP seq experiments and predictive data from miRanda, with the search parameters- CLIP data, high stringency (≥3) and Degradome data, the levels of hsa-miR-146a and hsa-miR-34a after NEAT1 knock down were probed for. Compared to a negative control siRNA, treatment with NEAT1 siRNA led to a concomitant increase of both the miRNAs, with hsa-miR-146a showing a higher increase (**Figure 5.5 b**). Conversely, it was also tested if this putative interaction and suppression was bi-directional. A transient over- expression of the mature miRNA clones in cells (**Figure 5.5 c.)** failed to elicit a response in the NEAT1 levels. Combined Immunocytochemistry (ICC) plus RNA –Fluorescence In Situ Hybridisation (RNA FISH) was employed, and RNA Immuno Precipitation (RIP). NEAT1 lncRNA was observed in nuclear locations different from that of the DNA marker, in cell populations (**Figure 5.5 d. panel i)**. A higher magnification

image (**Figure 5.5 d. panel ii)** showed its distinct distribution in defined spots called nuclear paraspeckles. Further, NEAT1 was predicted to interact with an RNA Binding protein (RBP) FUS using the lncRNA-RBP tool from ENCORI**.** Combined ICC of FUS with RNA FISH (**Figure 5.5 d. panel iii),** using NEAT1 specific probes, showed a strong overlap between the two in the cell nucleus.

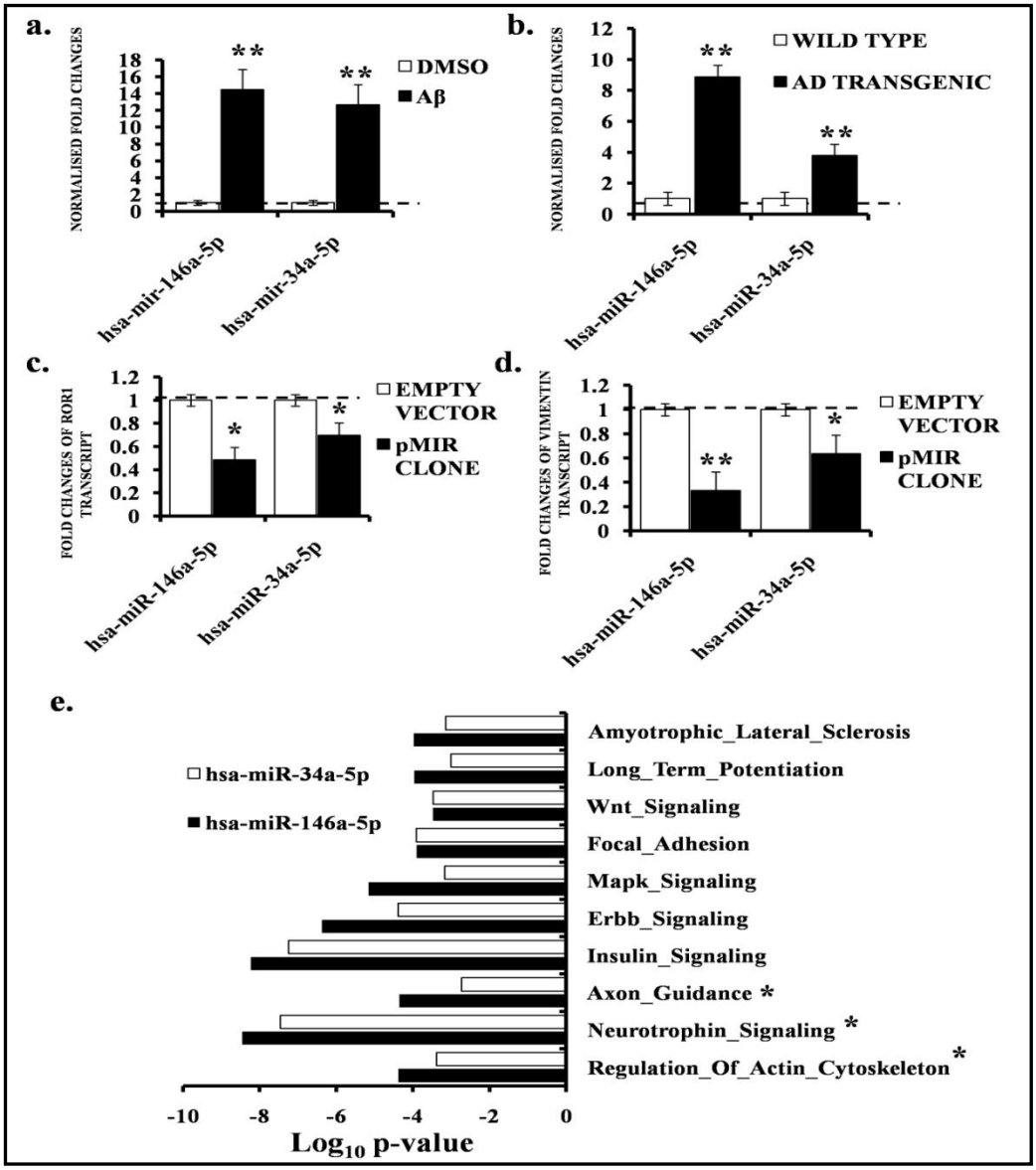

Figure 5.4: Dysregulation of hsa-mir-146a-5p, hsa-mir-34a-5p in $A\beta_{1-42}$ treated cell model and mice AD model. (a). Graph depicting three (n = 3) independent biological replicates quantifying levels of hsa-mir-146a and hsa-mir-34a by qRT-PCR in SHSY-5Y cells treated with 1 µM $A\beta_{1-42}$ or treated with only DMSO. **(**b) Graph depicting three (n = 3) independent

biological replicates quantifying levels of hsa-mir-146a and hsa-mir-34a by qRT-PCR in transgenic AD mice or age matched wild type mice brain tissues. (c). Graph depicting three (n = 3) independent biological replicates quantifying levels of ROR1 by qRT-PCR in SHSY-5Y cells treated with hsa-mir-146a-5p and hsa-mir-34a-5p pMIR clones or corresponding empty vector controls. (d). Graph depicting three (n = 3) independent biological replicates quantifying levels of Vimentin by qRT-PCR in SHSY-5Y cells treated with hsa-mir-146a-5p and hsa-mir-34a-5p pMIR clones or corresponding empty vector controls. Levels of U6snRNA were taken as endogenous control for the miRNAs and levels of GAPDH were taken as endogenous control for the mRNA levels. The levels of individual miRNAs or mRNA were normalized by the corresponding U6snRNA or GAPDH levels. Fold changes were computed by considering the relative levels of lncRNA in corresponding controls to be 1.

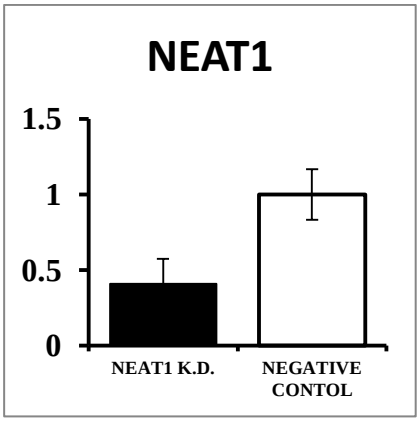

Decrease in expression of NEAT1 after treatment with siRNA: Bar graphs representative of three (n=3) independent experiments measuring expression of NEAT1 by qRT-PCR in SHSY5Y cells transfected with NEAT1 siRNA or corresponding negative control siRNA. U6snRNA was used as endogenous control. Fold change was calculated by considering the normalised levels of NEAT1 in negative control siRNA treated cells to be 1. *Error bars* indicate ± SD. The statistical significance level between experimental pairs is indicated (*,p<0.05; **,p<0.01; ***,p<0.001).

From the theoretical prediction and co-localisation analysis, I next designed a RIP experiment using FUS as the bait. Compared to control IgG, FUS pull down from cell lysates and subsequent assay by qRT-PCR showed a strong enrichment of NEAT1 (**Figure 5.5 e.).** A reanalysis using mature miRNA specific probes from the same FUS pull down RNA also subsequently showed a clear enrichment of the NEAT1 interacting miRNAs - hsa-miR-146a and hsa-miR-34a. In the RIP assay**,** hsa-miR-146a showed near double enrichment compared to hsa-miR-34a, indicating that the former had a stronger interaction with NEAT1. In order to validate that the effect of

NEAT1 knock-down was not just restricted to the miRNA levels, but their target ROR1 as well, transcript levels of ROR1 was looked at after NEAT1 silencing (**Figure 5.5 f.)** and indeed, ROR1 levels went down significantly on transient NEAT1 suppression, thereby confirming the hypothesis that NEAT1, its interacting miRNAs and their target ROR1, essentially constitute a single entity **(Cover cartoon)**.

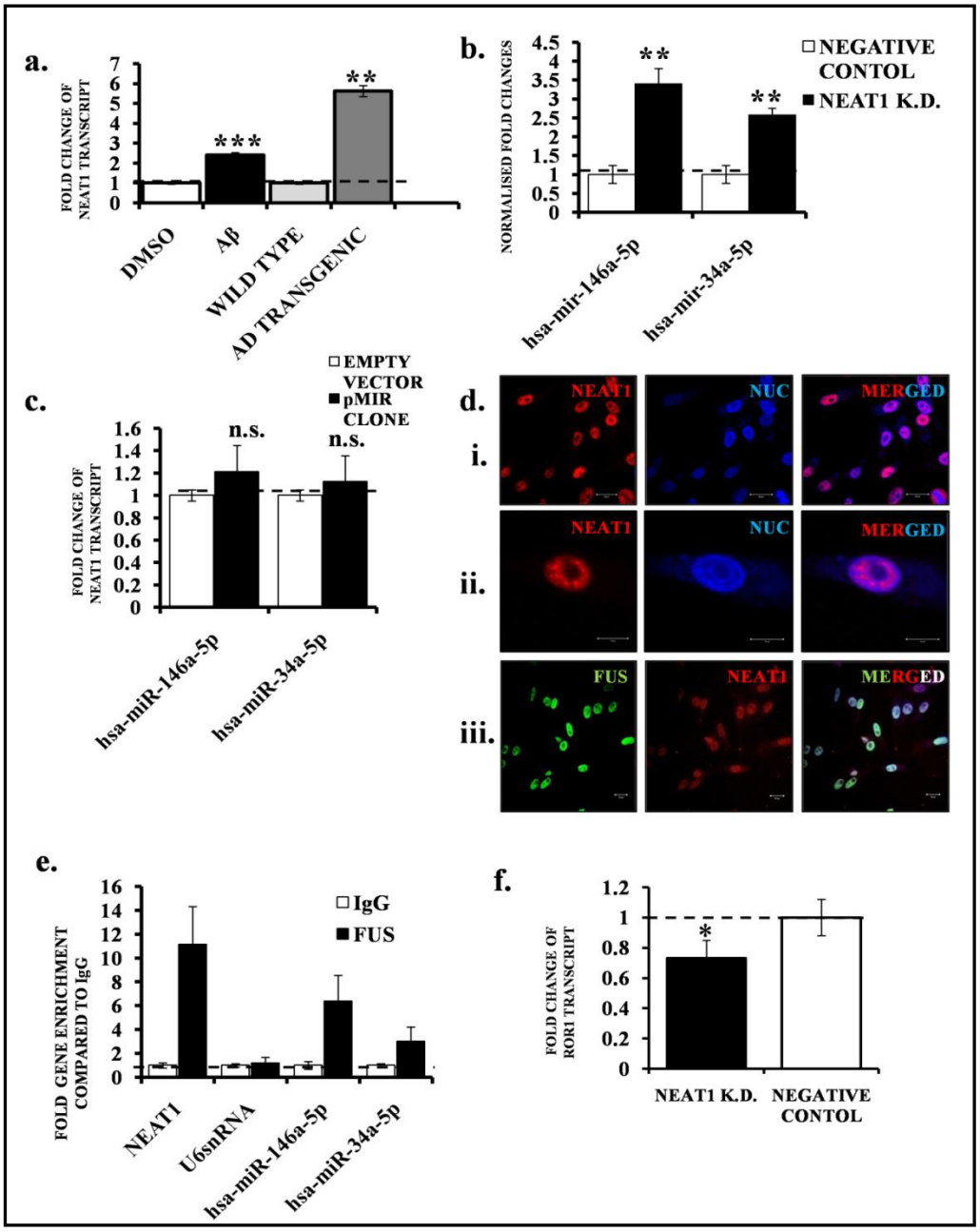

Figure 5.5: Endogenous interaction and regulation of miR146a and miR-34a by NEAT1 in SHSY5Y cells. (a). Graph depicting three (n = 3) independent biological

replicates quantifying levels of NEAT1 by qRT-PCR in SHSY-5Y cells treated with 1 μM $A\beta_{1-42}$ or treated with only DMSO; wild type and AD transgenic mice. (b). Graph depicting three (n = 3) independent biological replicates quantifying levels of miR146a and miR-34a by qRT-PCR in SHSY-5Y cells treated with NEAT1 siRNA or corresponding negative control. (c). Graph depicting three (n = 3) independent biological replicates quantifying levels of NEAT1 by qRT-PCR in SHSY-5Y cells treated with hsa-mir-146a-5p and hsa-mir-34a-5p pMIR clones or corresponding empty vector controls. (d). RNA-FISH assay of NEAT1 in SHSY5Y cells showing its enrichment in the areas of the nucleus distinct from the nuclear stain DRAQ5®; panel (i) Low magnification (1x) image of a cell population. Scale bars, 20μm; panel (ii). High magnification (4x) image of a single nucleus distinct NEAT1 paraspeckles. Scale bars, 5μm; panel (iii). Co localization Analysis - Sequential Immunocytochemistry (ICC) and RNA Fluorescence In Situ Hybridisation (FISH) assay of NEAT1 combined with FUS in SHSY5Y cells - Low magnification (1x) image of a cell population. Scale bars, 20μm. For each FISH or combined ICC-FISH experiment, images of at least 30 cells (or cell fields) were captured and the experiments were repeated thrice (n = 3). (e). Graph depicting three (n = 3) independent biological replicates quantifying enrichment of NEAT1, U6snRNA, hsa-mir-146a-5p and hsa-mir-34a-5p by qRT-PCR in SHSY5Y cells after pull down with FUS antibody or control IgG antibody in RIP Assays. (f). Graph depicting three (n = 3) independent biological replicates quantifying levels of ROR1 by qRT-PCR in SHSY-5Y cells treated with NEAT1 siRNA or corresponding negative control.

5.6. Discussion

In this study, the focus was on ROR1 with the motivation that cytoskeleton disruption in AD due to $A\beta_{1-42}$ is a well-recognised hallmark [1-5] and I could establish the same

through biochemical assays and confocal imaging. Further, in recent times, microtubule associated ROR1 has been implicated in reinforcement of neuronal network [6-9], which was found to be true on ROR1 over expression and subsequent neuritogenesis with the caveat that AD involves significant disruption of the same. Intuitively, it was found that ROR1 levels decrease in our AD model. The same transient over expression of ROR1 in presence of $A\beta_{1-42}$ is found to be necessary and sufficient to hamper cytoskeletal degradation of key proteins, promote neuritogenesis and drastically alter the F: G actin dynamics. In search for the small molecule regulators of ROR1, two miRNAs – miR-146a and miR-34a were identified, which were theoretically predicted to target ROR1. Subsequent validation in our cell model and transgenic mice AD model revealed significant up regulation of both. Using mature miRNA clones, the hypothesis that both miR-146a and miR-34a targeted and repressed ROR1 levels in cells was substantiated, miR-146a being the stronger repressor. Fortuitously, both of these also targeted Vimentin, a cytoskeletal protein of importance in AD. It was surprising that the repression of Vimentin was in fact stronger than ROR1, which leads us to believe that up regulation of these two miRNAs cumulatively affects the cytoskeleton disruption in AD by dual repression of ROR1 and Vimentin. It is not surprising, therefore, to find that miR-146a and miR-34a are parts of core neurobiological pathways implicated in AD, like LTP, axon guidance and regulation of actin cytoskeleton. These novel results are also backed up by literature reports that show miR-146a and miR-34a govern the regulators of actin pathways, namely RhoA and ROCK1 [10-12]. To further understand how these miRNAs were themselves regulated, their interaction with the lncRNA NEAT1 was deciphered, which recently has been shown to be deregulated in a plethora of neurodegenerative scenarios [13-16]. Using the same AD cell and mice model, the up

regulation of NEAT1 was validated. The direct interaction of miR-146a and miR-34a with NEAT1 was characterised with subsequent transient knock down, RIP and combined ICC with RNA- FISH experiments. A direct repercussion of perturbation of the NEAT1 level on ROR1 transcript levels was also shown, completing the proposed RTK-miRNA-lncRNA regulatory loop.

To our cognizance, this is the first consolidated network study to undisputedly connect ROR1 to $A\beta_{1-42}$ treatment in AD, by showing its deregulation both at the transcript and protein levels. In-vivo over expression of ROR1 exerts protective effects on the gross cytoskeletal assembly and neurite formation. A functional link between ROR1 and its targeting miRNAs

is established. Eventually, a regulatory paradigm of ROR1-miRNA 146a/34a – NEAT1 in AD was demonstrated.

Summary:

- $A\beta_{1-42}$ deregulated the expression of RTK ROR1 and relevant cytoskeleton associated components.
- Over expression of ROR1 in presence of Aβ preserved cytoskeletal integrity and promoted neurite formation.
- Cytosolic $A\beta_{1-42}$ affected the mature miRNAs- miR-146a and miR-34a, which in turn repressed ROR1
- Nuclear $A\beta_{1-42}$ differentially regulated NEAT1, which in turn sponged the miRNAs.

5.7. References

[1].Henriques AG, Vieira SI, da Cruz E Silva EF, da Cruz E Silva OA. Abeta promotes Alzheimer's disease-like cytoskeleton abnormalities with consequences to APP processing in neurons. J Neurochem. 2010 May;113(3):761-71. doi: 10.1111/j.1471-4159.2010.06643.x. Epub 2010 Mar 23. PubMed PMID: 20345756.

[2].McMurray CT. Neurodegeneration: diseases of the cytoskeleton? Cell Death Differ. 2000 Oct;7(10):861-5. Review. PubMed PMID: 11279530.

[3].Bamburg JR, Bernstein BW. Actin dynamics and cofilin-actin rods in Alzheimer disease. Cytoskeleton (Hoboken). 2016 Sep;73(9):477-97. doi: 10.1002/cm.21282. Epub 2016 Mar 1. Review. PubMed PMID: 26873625; PubMed Central PMCID: PMC5345344.

[4].Maloney MT, Bamburg JR. Cofilin-mediated neurodegeneration in Alzheimer's disease and other amyloidopathies. Mol Neurobiol. 2007 Feb;35(1):21-44. Review. Erratum in: Mol Neurobiol. 2007 Oct;36(2):201-4. PubMed PMID: 17519504.

[5].Rush T, Martinez-Hernandez J, Dollmeyer M, Frandemiche ML, Borel E, Boisseau S, Jacquier-Sarlin M, Buisson A. Synaptotoxicity in Alzheimer's Disease Involved a Dysregulation of Actin Cytoskeleton Dynamics through Cofilin 1 Phosphorylation. J Neurosci. 2018 Nov 28;38(48):10349-10361. doi: 10.1523/JNEUROSCI.1409-18.2018.
Epub 2018 Oct 19. PubMed PMID: 30341179; PubMed Central PMCID: PMC6596209.

[6].Paganoni S, Ferreira A. Expression and subcellular localization of Ror tyrosine kinase receptors are developmentally regulated in cultured hippocampal neurons. J Neurosci Res. 2003 Aug 15;73(4):429-40. PubMed PMID: 12898527.

[7].Oishi I, Takeuchi S, Hashimoto R, Nagabukuro A, Ueda T, Liu ZJ, Hatta T, Akira S, Matsuda Y, Yamamura H, Otani H, Minami Y. Spatio-temporally regulated expression of receptor tyrosine kinases, mRor1, mRor2, during mouse development: implications in development and function of the nervous system. Genes Cells. 1999 Jan;4(1):41-56. PubMed PMID: 10231392.

[8].Al-Shawi R, Ashton SV, Underwood C, Simons JP. Expression of the Ror1 and Ror2 receptor tyrosine kinase genes during mouse development. Dev Genes Evol. 2001 Apr;211(4):161-71. PubMed PMID: 11455430.

[9]. Paganoni S, Ferreira A. Neurite extension in central neurons: a novel role for the receptor tyrosine kinases Ror1 and Ror2. J Cell Sci. 2005 Jan 15;118(Pt 2):433-46. PubMed PMID: 15654020; PubMed Central PMCID: PMC1351101.

[10].Wang M, Qin L, Tang B. MicroRNAs in Alzheimer's Disease. Front Genet. 2019 Mar 1;10:153. doi: 10.3389/fgene.2019.00153. eCollection 2019. Review. PubMed PMID: 30881384; PubMed Central PMCID: PMC6405631.

[11].Liu Q, Wang W, Yang X, Zhao D, Li F, Wang H. MicroRNA-146a inhibits cell migration and invasion by targeting RhoA in breast cancer. Oncol Rep. 2016 Jul;36(1):189-96. doi: 10.3892/or.2016.4788. Epub 2016 May 6. PubMed PMID: 27175941; PubMed Central PMCID: PMC4899025.

[12].Kim D, Song J, Kim S, Park HM, Chun CH, Sonn J, Jin EJ. MicroRNA-34a modulates cytoskeletal dynamics through regulating RhoA/Rac1 cross-talk in chondroblasts. J Biol Chem. 2012 Apr 6;287(15):12501-9. doi: 10.1074/jbc.M111.264382. Epub 2012 Feb 20. PubMed PMID: 22351754; PubMed Central PMCID: PMC3320999.

[13]. Tollervey, J. R., Curk, T., Rogelj, B., Briese, M., Cereda, M., Kayikci, M., König, J., Hortobágyi, T., Nishimura, A. L., Zupunski, V., Patani, R., Chandran, S., Rot, G., Zupan, B., Shaw, C. E., & Ule, J. (2011). Characterizing the RNA targets and position-dependent splicing regulation by TDP-43. *Nature neuroscience*, *14*(4), 452–458.

[14]. Nishimoto, Y., Nakagawa, S., Hirose, T., Okano, H. J., Takao, M., Shibata, S., Suyama, S., Kuwako, K., Imai, T., Murayama, S., Suzuki, N., & Okano, H. (2013). The long non-coding RNA nuclear-enriched abundant transcript 1_2 induces paraspeckle formation in the motor neuron during the early phase of amyotrophic lateral sclerosis. *Molecular brain*, *6*, 31.

[15]. Chanda, K., Das, S., Chakraborty, J., Bucha, S., Maitra, A., Chatterjee, R., Mukhopadhyay, D., & Bhattacharyya, N. P. (2018). Altered Levels of Long NcRNAs Meg3 and Neat1 in Cell And Animal Models Of Huntington's Disease. *RNA biology*, *15*(10), 1348–1363.

[16]. Yan W, Chen ZY, Chen JQ, Chen HM. LncRNA NEAT1 promotes autophagy in MPTP-induced Parkinson's disease through stabilizing PINK1 protein. *Biochem Biophys Res Commun*. 2018;496(4):1019-1024.

Chapter 6: XIST and X-Chromosome Instability in AD

6.1. Introduction

Neurodegenerative diseases (NDDs) represent the most common form of neuropathologies and are the leading factors for late age disabilities worldwide. In current times, better food habits, better drugs and concise healthcare have drastically elevated the average life expectancy and hence, NDDs constitute the biggest threat. Alzheimer's disease (AD), Huntington's Disease (HD), Parkinson's Disease (PD), Amyotrophic lateral sclerosis (ALS) etc belong to this group and involve major motor and cognitive impairments, collectively affecting nearly half a billion individuals throughout the world, often leading to morbidity. The complex NDDs have multifactorial molecular mechanisms leading to gradual, irreversible loss of specific neuronal sub-populations [1], followed by gross neuronal impairments. The complexity of these NDDs makes therapeutic strategies against them a difficult, if not impossible task.

Adding to this complexity, the X-chromosome Instability phenotype has become an active topic of research in AD. Neuronal cells in AD show a Premature Centromere Separation (PCS) leading to a dysfunctional chromosomal landscape [2]. PCS has been shown to occur specifically on the X-chromosome using FISH experiments. This process, occurring in post mitotic neurons in AD, led researchers to believe that AD involves a faulty and transient cell cycle re-entry of neurons. The more intriguing result was that this PCS X-instability was seen only in women but not in men. Indeed, the fact that AD affects twice as many women as men [3-6] and women affected with AD show skewed X-Chromosome Inactivation (XCI) [7] led us to look into a new set of molecules, the non-coding RNAs (ncRNAs), as a potential link between XCI and AD.

Stretches of sequences in the genome which does not code for any functional transcript are transcribed into ncRNAs that play vital regulatory roles. Abundant and functionally important types of ncRNAs include transfer RNAs (tRNAs) and ribosomal RNAs (rRNAs), microRNAs, siRNAs, piRNAs, snoRNAs, snRNAs, exRNAs, scaRNAs and the long ncRNAs (lncRNAs) such as Xist and HOTAIR. In recent years, long non-coding RNA (lncRNA), a single stranded RNA of more than 200 nucleotides that do not code for proteins, has emerged as regulators of transcription [8-9], cellular homeostasis [10], immune cell development [11] etc., mainly achieved through protein-RNA interaction [12]. In contrast to ancient RNA forms, these lncRNAs came much later in the evolutionary timescale, where they are present in plants, vertebrates and invertebrates, and and about one-third are primate-specific. LncRNAs are believed to be crucial for the development and evolution of the primate brain [13]. Naturally the central nervous system (CNS) harbours a large, diverse population of such lncRNAs that are actively or passively involved in several neurobiological events including neurogenesis, synaptogenesis, neuronal cell fate determination, synaptic signalling cascade, organelle dynamics of neurons and neuronal homeostasis. They maintain features common to protein-coding genes such as promoters, intron–exon boundaries and post-processing features like 5' capping, polyadenylation, alternative splicing and RNA editing [14]; however, in contrast, they are mainly nuclear, less polyadenylated and are very tissue specific. Recent studies show that about 80% of transcription events across the human genome is associated with lncRNAs [15] of which, 27,919 lncRNAs have been identified from various human sources [16].

lncRNAs can arise from the intergenic regions, gene regulatory regions (UTRs, promoters and enhancers) and specific chromosomal regions (telomeres); some

reports even suggest mitochondrial DNA as a source too [17-19]. lncRNAs exert effects on the mRNA and DNA levels by recruiting transcription factors and epigenetic machinery to specific nuclear and genomic sites. They affect the nuclear architecture by concentrating on specific domains close to transcription sites and forming lncRNA-protein complexes [20-23].

The specific abundance of lncRNAs in the neural tissues suggests their strong correlation with the CNS function [24,25]. In the last few years, the implications of several lncRNAs in governing major NDDs have come to light. In AD, the most studied lncRNA is BACE1-AS (BACE1-antisense), an antisense transcript of BACE1 (β-site APP cleaving enzyme 1) which governs the processing of Amyloid Precursor Protein (APP). BACE1-AS is strongly upregulated in AD brains hinting its role in AD pathology [26]. Brain cytoplasmic (BC), specifically BC200 RNA and lncRNA-17A have also been implicated in AD [27,28]. In HD, the lncRNA HttAS_v1, an antisense transcript of Huntingtin protein is found to be down regulated in HD cortex, thereby leading to more Htt transcript and more severity of the disease [29]. Very recently, a nuclear specific lncRNA, NEAT1 (Nuclear Enriched Assembly Transcript) has been found to have a protective role in HD pathogenesis [30]. NaPINK1, a human antisense transcript of PINK1 (PTEN-induced kinase 1) has been found to be a governing molecule affecting PD [31]. Similarly, MALAT1 (Metastasis associated lung adenocarcinoma transcript 1), a neuron enriched lncRNA which governs synapse formation, has been implicated in modulating α-synuclein aggregation in PD [13,32]. Besides these, a large body of literature implicated several lncRNAs in various facets of NDDs and neuronal functions as a whole. Important among these are Evf2 (affects neurogenesis by recruiting transcription factors to important DNA regulatory elements in the Dlx 5/6 locus) [33], Pnky (regulates neurogenesis by interacting with

splicing regulator PTBP1) [34], Miat (affects neurogenesis through Wnt7b pathway) [35], RMST (affects SOX2 mediated firing of neurogenic transcription factors) [36], MEG3 (governs Insulin signalling via FoxO1 mediated gluconeogenesis) [37] and H19 (governs neuroimmune response via HDAC-1) [38].

Originally discovered by Carolyn J. Brown in 1990 [39], XIST (X-inactive specific transcript) is an RNA gene on the X chromosome of the placental mammals that acts as a major effector of the X inactivation process. Recent literature reports and some rudimentary results from our group indicate its strong connection with AD. In this review, I intend to discuss about the emerging roles of this lncRNA with a special focus on Alzheimer's disease. To achieve that, relevant and recent literature on XIST, XCI and NDDs with a focus on AD were retrieved from all possible archives including, but not restricted to Google scholar, Pubmed, Medline and Scopus. Focussed, cross disciplinary reviews and research articles with validated experimental data linking the three are prioritised for this review.

6.2. XIST: A lnc transcript indispensable for X inactivation process

The process of X Inactivation starts with a single locus on the X chromosome, the *Xic*. Silencing of one X chromosome is only triggered in cells which harbours two *Xic*, which shows that both copies are necessary to affect XCI. The XIST gene is located in the *Xic*. The Xist RNA, a large (17 kb in humans) transcript, is exclusive to the inactive chromosome [39]. The Xist RNA coats the inactive X chromosome, which is essential for its inactivation [40]. The X-chromosome inactivation centre [41] (XIC), a molecular complex which actually leads to the silencing of the future inactive X chromosome, includes XIST and two other genes, ***Jpx*** (surrounding the Xist gene and up regulating expression of Xist) and ***Ftx (***[**F**ive prime **t**o **X**ist], a long non-coding RNA surrounding the XIST gene). It upregulates the expression of XIST

and two protein genes (*Tsx* and *Cnbp2*). The ***Jpx*** locus is in immediate 5' proximity to Xist whichproduces an ncRNA that activates Xist in females. Heterozygous deletion mutants of *Jpx* show aberration of XCI initiation. ***Ftx*** is a substantial chromosomal segment 5' to Xist. In mice, ***Ftx*** generates a lncRNA, which is up regulated during XCI. Null mutations of ***Ftx*** generate global changes in *Xic* transcripts, including XIST. The most important RNA regulatory element of Xist is its antisense RNA **Tsix** whose sequence is conserved in humans and mice. **Tsix** is located in *Xic*, downstream of Xist. Both X chromosomes express **Tsix** and it is involved only in the nascent stages of XCI. Unlike Xist, **Tsix** associates with the future active X chromosome by counteracting Xist expression. **Tsix** forms a Xist-Tsix RNA duplex to inhibit the up regulation of Xist, similar to a RNAi mechanism. Another line of evidence suggests that a non-coding transcript called ***RepA*** augments Xist expression by recruiting Polycomb repressive complex 2 (PRC2) and Tsix inhibits this process by competing with PRC2 [42-45].

The complete cDNA sequences of the human genes were analysed to identify conserved sequences. The two genes initiate transcription at approximately the same point and show detectable homology over much of their length, although the human sequence extends significantly further to the 3' than the mouse sequence. Within the gene, homology between human and mouse is interrupted multiple times both by blocks of sequences unique either for human or mouse [14]. A later independent study used sequencing to determine the 714-kb and 233-kb regions of the mouse and bovine X-inactivation centers (Xic), respectively, centered on the *Xist* gene which provided the basis for a fully annotated comparative analysis of the mouse Xic with the 2.3-Mb orthologous region in human and a three-way species comparison of the core central region, including the *Xist* gene [46].

The human Xist RNA gene is located on the X chromosome (Xq13.2 – start – 73,820,651 bp, end – 73,852,723 bp). It includes several tandem repeats, the most 5' of which are evolutionarily conserved. The gene does not contain any significant conserved ORFs and thus does not appear to encode a protein, suggesting that XIST may function as a nuclear structural RNA [8]. The Xist RNA gene is composed of an A region containing 8 repeats separated by U-rich spacers. The A region harbours two long stem-loop structures each of which include four repeats [47]. Using Targeted Structure-Sequencing, a recent paper shows that Xist repeat A region acts as a gene repressor. This repeat A structure comprises of both intra and inter repeats of stems and are mostly conserved across species [48]. Apart from the A repeat, XIST also comprises of the highly repetitive B repeat, which aides in binding hnRNPK and PRC1 protein to XIST bound chromatin [49-51]; the C repeat which governs XIST spreading and localization via the hnRNPU/Saf-A and YY1 proteins [52] and the E repeat, which binds the PTBP1 and TARDBP proteins [53,54]. Very recent literature suggests that XIST RNA harbours several sites for epigenetic modifications, especially methylation [55,56] and this modification works via recruiting the chromatin RNA methylation reader YTHDC1, consequently leading to gene repression [56]. In essence, these protein and RNA interactors of XIST helped us increase our current knowledge about its functions notably. The mouse ortholog is a 15 kb Xist RNA gene localized in the nucleus but does not have the conserved repeats. The locus also consists of a Xist Inactivation Center (XIC), which plays a major role in X inactivation [44, 57].

Apart from its roles in XCI, current literature suggests that XIST is involved in a plethora of pathological conditions. Although typically female specific, XIST expression is found to be non- existent in ovarian, breast and cervical cancer cell lines

[58, 59]. An important finding is the nuclear co-localization of XIST with the tumour suppressor protein BRCA1 and its role in aiding the stability of XCI [60]. Leaving aside cancers that are mostly female specific, XIST expression is also reported in germ line cancer cells [61]. Elevated XIST levels were found in colorectal cancers and here, XIST comprised a network of miR-200b-3p and its target ZEB1 [62]. Similar XIST- miRNA-protein networks are discovered in a glioma angiogenesis study, where the authors report upregulation of XIST and miR-137, but repression of FOXC1 [63]; in cervical cancer, where increased XIST modulates miR-140-5p and ORC1 levels [64] and in non-small cell lung cancers, where elevated XIST governs miR-16 and CDK8 expresssion [65]. It is expected that in future years, such intricate XIST networks would be unearthed in other patho-physiological condition as well.

6.3. Regulatory roles of XIST has now been identified in NDDs

Experimental evidence obtained so far hints at the facts that (i) XIST expression (from bioinformatics and actual sample data) is deregulated in mouse and human cell models of AD as well as in AD brains, (ii) XIST associates with specific miRNA implicated in AD and governs or is governed by the lncRNA/miRNA/protein regulation axis, (iii) XIST is primarily implicated in the Apoptosis pathway in human cell models of AD and (iv) XIST and the X chromosome as a whole could play a definitive role in AD disease dynamics and possible therapeutics.

6.3.1. XIST is identified as a possible gene involved in the early stages of AD using microarray and neural network algorithm

Owing to the higher incidence of AD, several microarray databases exist for specific brain regions of AD patients. Tissue specific data from such a repository (National Certification Board for Alzheimer Care, NCBAC) is used to identify possible genes that are up -or down regulated in AD using neural network algorithms. Five such

libraries are tested and upon comparing normal and defective genes in different cortical layers of the brain, with samples having different disease intensity, a few genes are identified to be common. Among these, XIST shows the highest level of upregulation (fold change of +8.68652) in AD samples compared to controls. By performing a comprehensive analysis of several brain regions, like hippocampus, entorhinal cortex, temporal cortex and frontal cortex, a global picture arises. Deregulated lncRNAs identified by this study could be potentially used as biomarkers for AD [66,67] (**Table 6.2**).

6.3.2. XIST is identified as a major effector of apoptosis in Aβ treated rat hippocampal neurons

In a recent work by Wang et al. [68]), $A\beta_{25-35}$-insulted primary cultured hippocampal neurons were used to study the possible involvement of XIST in the downstream toxicity, oxidative stress, and apoptosis pathways. It was found that $A\beta_{25-35}$ treatment increased XIST RNA levels by ~ 4-fold compared to controls. siRNA mediated transient knockdown of XIST in $A\beta_{25-35}$ treated neurons increased their gross viability. The activity levels of superoxide dismutase (SOD), glutathione peroxidase (GSH-Px) and malonaldehyde (MDA) were restored in these cells upon XIST knock-down as compared to to only $A\beta_{25-35}$ treated controls. Protein levels of apoptotic markers like Bax, Bcl-2, CytC and caspase-3 followed a similar trend. The authors found XIST to interact with and regulate miR- 132. They also showed that miR- 132 alleviated $A\beta_{25-35}$ induced stress and XIST was hindering such a recovery. Although the described protocol is confusing, presumably the authors used primary neuronal culture from 16-18 days embryos in a sex- independent manner. However, no link between functional pathways to XIST was shown and apoptotic protein markers were only used as readouts.

6.3.3. XIST levels were found to be up regulated in mouse tissues and mouse cell models of HD

To gain a slightly different perspective, I checked other conditions which might have close resemblance to AD. A recent report from our laboratory looked at the dysregulated levels of lncRNAs in mouse brain tissues and mouse cell models of HD [69], a monogenic NDD. Using R6/2 transgenic mouse expressing 150 CAG repeats and *STHdh*(*Q111*) mouse striatal cell model expressing 111 CAG repeats Chanda et al. found 12 lncRNAs to be dysregulated, out of which 8 had human homologs. Of these, 3 lncRNAs- Meg3, Neat1 and Xist showed consistent up regulation. Xist showed the highest up regulation in 6-week-old R6/2 mice concordant with 8-week-old R6/2 mice, *STHdh*(*Q111*) cell line as well as a transient cell model of HD (Mouse Neuro2A cell line transfected with mHtt 83Q- DsRed construct). However, neither the mechanism behind up regulation of Xist, nor the molecular implications of it were elaborated.

6.3.4. XIST levels were experimentally found to be consistently and significantly up regulated in human and mouse cell models of AD

Based on the meta-data above, I wanted to see whether the increase in Xist levels observed in several AD models could be repeated in accepted cell models of AD [70] where, the intracellular fragment of Amyloid Precursor Protein or AICD (APP Intra Cellular Domain) had been transfected in human neuroblastoma (SHSY5Y) or mouse neuroblastoma (Neuro2a) followed by extracellular treatment with $A\beta_{1\text{-}42}$. For controls, cell culture, transfection, peptide treatment and RT-PCR experiments, standard published protocols were followed [70]. PCR primers used are listed in

Table 6.1.

Table 6.1: PCR primers used to validate the expression of XIST.

Mouse Xist_RT_F	TTGTGGCTTGCTAATAAT
Mouse Xist_RT_R	AAACCCCATCCTTTATG
Human XIST RT_F	TGACCTTGTTAAGCAAGCG
Human XIST RT_R	ATGGACCACTGTTTGATAGAC
Mouse GAPDH_RT_F	AGCCTCGTCCCGTAGACAAAA
Mouse GAPDH_RT_R	TGGCAACAATCTCCACTTTGC
Human GAPDH_RT_F	TCCCTGCACCACCAACTGTTAG
Human GAPDH_RT_F	GGCATGGCATGTGGTCATGAG

Concordant with literature reports in other models, I found a significant and consistent up regulation of Xist (**Figure 6.1**) in both the human (fold change – 24.67, p <0.004) and mouse (fold change – 4.17, p <0.005) models of AD compared to controls (taken as 1) Due to the presence of AICD and Aβ, the human cell model showed much significant up regulation of Xist, presumably because the AD phenotype would reportedly be very weakly expressed in a mouse model.

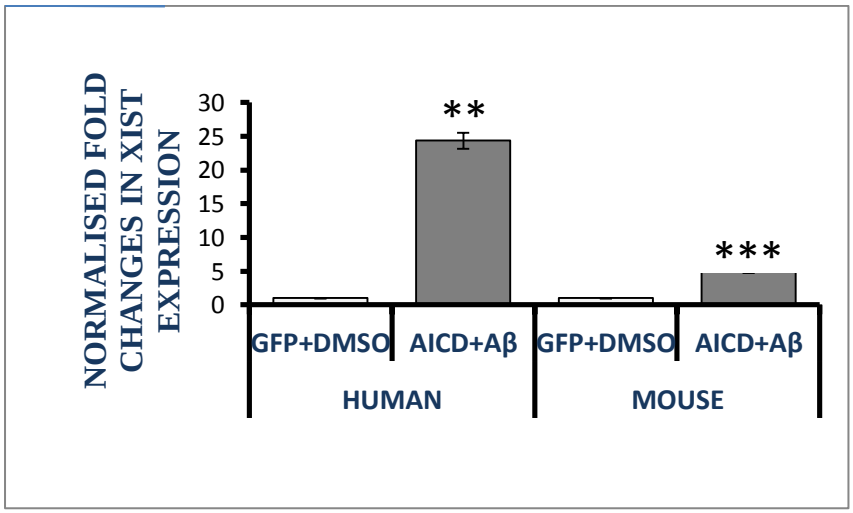

Figure 6.1: Transcript level changes of XIST lncRNA in human and mouse AD cell models. (Error bars – SEM, ** - p value < 0.005, * - p value < 0.0005, n=3)**

The AD model used here was a combination of AICD and Aβ, unlike the mouse model used elsewhere [68], which involved only Aβ treatment. The effect of AICD alone on XIST levels remained to be seen. However, there are ample evidences which show that both AICD and Aβ are in abundance in AD brains where they exert detrimental effects [71-73]. It would only be logical to surmise that such an effect also holds true in XIST regulation in the AD model. The pronounced-up regulation of Xist in SHSY5Y model maybe attributed to the fact that this cell line was female patient derived. Owing to dosage compensation, females exclusively express Xist RNA compared to males [74]. Verifying XIST level in an AD model based on a male derived neuroblastoma cell line like IMR32 would have resolved this. The mouse Neuro2a cell line used here however is male in origin (https://web.expasy.org/cellosaurus/CVCL_0470), which hints at the fact that XIST dysregulation in AD is sex- independent.

From the data obtained here, supported by the cited literature, it is indicative that XIST up regulation is a plausible consequence of AD and abrogating XIST over-activity could be beneficial for cellular health (**Table 6.2**).

Table 6.2: XIST expression in patients and disease models of NDDs.

DISEASE MODEL (REF)	XIST LEVELS (AND HOW MEASURED)	WHERE MEASURED	PROPOSED ROLE	PUTATIVE MECHANISM
AD (66,67)	**UP** (microarray data follwed by neural network analysis)	**HUMAN** : brain regions	DETRIMENTAL	NOT KNOWN
AD (68)	**UP** (qRT-PCR)	**RODENT :** rat cultured hippocampal neurons	DETRIMENTAL	**1.** XIST increase due to $A\beta_{25-35}$. **2.** XIST interaction with miR- 132. **3.** Increased apoptosis due to increased XIST.

HD (69)	**UP** (small rna sequencing followed by qrt-pcr)	**RODENT:** mouse model and mouse cell line	NOT KNOWN	NOT KNOWN
AD (THIS STUDY)	**UP** (qRT-PCR)	**RODENT :** Mouse neuroblastoma cell line Neuro2a **HUMAN** : Human neuroblastoma cell line SHSY5Y	NOT KNOWN	NOT KNOWN

6.4. Discussion and therapeutic association

A cursory look on XIST distribution, regulation and functions in the nervous system (**Table 6.2**) ameliorates the idea that XIST and X chromosomal biology have intertwined pathophysiological significance. The idea is however still emerging and a few lacunae need to be covered for more credibility. Experiments using neuronal and non- neuronal cell lines as well as control tissues from AD mice are required to undisputedly conclude whether and, if so, under which conditions XIST may be neurotoxic or neuroprotective. In order to elucidate the possible outcomes of XIST expression in NDDs, one has to examine: 1) Cell type specific expressions of XIST in neuronal and non-neuronal cell and also to look at gender specific cell lines (e.g, SHSY5Y female derived versus male derived IMR32), so as to show that XIST over expression (or repression) is specifically due to the molecular triggers and not because of the gender; 2) XIST's roles in the normal nervous system at molecular, cellular, tissue and behavioural levels; 3) molecular mechanisms and temporal dynamics of XIST regulation in neuronal populations affected in different NDDs; 4) Whether XIST over expression effects would be independent of the X Chromosome Biology as a whole. That XIST (and X chromosomes) could have a gender specific effect in

NDDs is also substantiated by population studies which show that women are more predisposed to having AD than men [74,75]. A recent review gives us a more comprehensive picture about XCI in AD by bringing to the forefront the processes of epigenetic regulation of the X chromosome and a X linked marker of AD, the PCDH11X gene [76]. Several miRNAs like miR-223 and miR-362 link X chromosome and intellectual disability genes in an intricate network. miR- 374, itself located on the Xic, not only affects the PTEN signalling pathway implicated in AD, but also targets beta-secretase 1. The PCDH11X gene, identified in 2009 is located on the X chromosome and it was found that European origin women homozygous for this locus were more susceptible to AD, compared to women who were heterozygous and male who were hemizygous. This gene could be one of the potential X linked factors that make women and men differentially susceptible to AD. This study further reinforces the skewed women to men ratio in AD. This intricate network of miRNA regulation of XIST and X chromosome is also highlighted in another recent work, where the authors show that XIST levels are elevated in a cell model of AD along with the downregulation of the miRNA -124, which targets BACE-1 [77]. Artificial over expression of miR-124 repressed BACE-1. But artificially silencing XIST restored miR-124 levels and consequently repressed BACE-1 levels. It is expected that in near future, more miRNA targets would come into the forefront which would link AD with X Chromosome.

Besides the bioinformatics analyses that have been included here, a more comprehensive meta-analysis of small RNA sequence data from patients with different NDDs is warranted. A recent article highlighted the fact that XIST could have a causal link in HD pathology via the Polycomb repressive complex 2 (PRC2) machinery, as it is known that PRC2 is recruited to the X-chromosome genomic locus

by XIST, eventually leading to transcriptional silencing [78]. PRC2 in turn is facilitated by Huntingtin protein to govern HD dynamics [79]. The role of XIST in HD, as mentioned before, took into consideration two cell lines, STHdhQ111/HdhQ111 and Neuro2A. While the former does indeed show a female phenotype [80], the latter is male in origin. This leads us to believe that XIST dysregulation occurs primarily due to the disease trigger and is sex independent.

Owing to the fact that XIST and its protein partners are the key components of chromosome silencing machinery (summarised in **Figure 6.2a**), one could think one step further and plan to specifically silence chromosomes in a variety of chromosomal aberrations especially chromosomal trisomy (which have one extra copy of a specific chromosome) like Trisomy 18 (Edwards syndrome), Trisomy 13 (Patau syndrome), Klinefelter syndrome (one or two extra sex chromosome(s)) and Trisomy 21(Down syndrome).

In fact, scientists inserted one copy of XIST in the extra chromosome 21 in Down's syndrome (DS) pluripotent stem cells [81]. It was found that this ectopically inserted XIST and its RNA efficiently coated the extra chromosome 21, induced heterochromatin modifications leading to chromosome-wide silencing. Since the link between DS and AD is apparent, APP gene being located on chromosome 21, they also showed that the total load of APP decreased proportionately post silencing. As a proof-of-concept, this study highlights the enormous potential of XIST regulatory networks to be used as a therapeutic strategy, which is exemplified by the fact that in recent times, XIST interacting protein PRC2, which binds to *RepA* region of XIST, was found to be dysregulated in AD, which affected its associated epigenetic roles [82]. Similarly, PTBP1, which binds to XIST E repeat, was also implicated in AD, where it works via suppressing a CD33 exon linked to AD risk [83]. Finally, the well-

studied transcriptional repressor, TARDBP, which also binds to XIST E repeat, was also found to be a contributor to AD genetics [84].

A word of caution is required though as over expression of XIST has been earmarked as a cellular damage inducing response rather than a beneficial one [63]. In the absence of more conclusive data, the obvious discrepancy between the two studies only strengthens the fact that more in-depth knowledge is required to rule out either of the two possibilities. Indeed, as with all new hypotheses, there are also conflicting reports which show that XIST transcripts are under-expressed in AD [85]. Here the authors used network-based gene co expression analysis from datasets in the ADNI database. However, they have reported the downregulation of 3 XIST gene

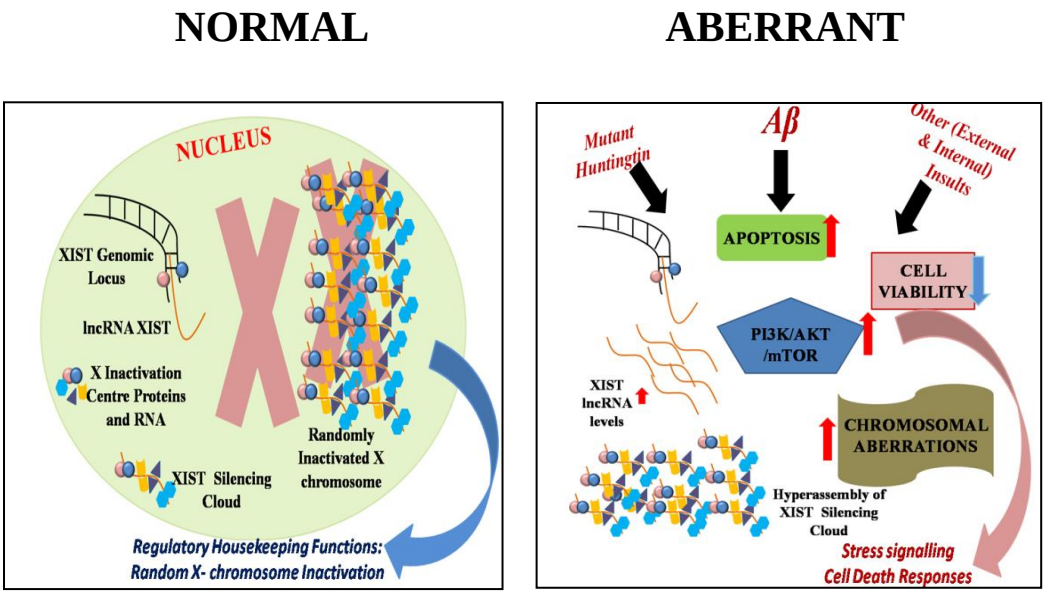

Figure 6.2: XIST IN NDDs: A cartoon representing the working model of XIC and its aberration in NDDs. a. Under basal conditions, levels of XIST in cells are maintained at a normal level in females. Housekeeping functions of the XIST lncRNA are specified to the random inactivation of one X Chromosome in females. b. During pathological changes typical for NDDs, XIST lncRNA levels increase significantly in response to Aβ, mutant Huntingtin protein and other unknown external and internal stimuli. Data suggests so far that this increase is detrimental for cellular health.

transcripts, but have not stated the significance values of the same. Further, a combination of all existing data about XIST in AD supports that the idea of XIST being up regulated in AD is predominant. The use of XIST to silence a specific chromosome in chromosomal aneuploidies obviously has a big caveat – the "off target" effect. Evolutionarily, XIST is programmed to randomly silence one of the X Chromosomes in females; hence, the XIST RNA from one X chromosome silences the adjacent one. It is not known extensively whether this XIST silencing depends on proximity or if there are unique signatures of its silencing substrate. A gross cellular over expression of XIST could potentially lead to random silencing of other chromosomes essential for normal cellular functions. Recent researches probably hint at this same fact **(Figure 6.2b, [68]).** This over expression in NDD scenarios and its downstream result of hyper assembly of the XIST silencing complex could be one reason why there could be chromosomal abnormalities which could in turn trigger the DNA damage response and apoptosis machinery as exemplified by the activation of Bax, Bcl-2 etc.

It would be prudent to find a key balance between the expressions of XIST in physiological and disease scenarios and use such a minimal threshold value to decide if one could use XIST (or its absence) as a therapeutic measure in a plethora of NDDs.

Summary:

- XIST was identified as a probable candidate involved in the early stages of AD using microarray data.
- XIST affected apoptosis in Aβ treated rat hippocampal neurons.
- XIST expression was up regulated in mouse tissues and mouse cell models of HD.
- XIST levels were experimentally found to be significantly up regulated in human and mouse cell models of AD (preliminary data).

References:

[1]. Pringsheim, T., Fiest, K., & Jette, N. (2014). The international incidence and prevalence of neurologic conditions: How common are they? Neurology, 83(18), 1661–1664.doi:10.1212/wnl.0000000000000929 .
[2]Bajić VP, Spremo-Potparević B, Zivković L, Bonda DJ, Siedlak SL, Casadesus G, Lee HG, Smith MA. The X-chromosome instability phenotype in Alzheimer's disease: a clinical sign of accelerating aging? Med Hypotheses. 2009 Dec;73(6):917-20.
[3]Corbo RM, Gambina G, Ruggeri M, Scacchi R. Association of estrogen receptor alpha (ESR1) PvuII and XbaI polymorphisms with sporadic Alzheimer's disease and their effect on apolipoprotein E concentrations. Dement Geriatr Cogn Disord 2006;22:67–72.
[4]Casadesus G, Atwood CS, Zhu X, et al. Evidence for the role of gonadotropin hormones in the development of Alzheimer disease. Cell Mol Life Sci 2005;62:293–298.
[5]Corbo RM, Gambina G, Ulizzi L, Moretto G, Scacchi R. Genetic Variation of CYP19 (Aromatase) Gene Influences Age at Onset of Alzheimer's Disease in Women. Dement Geriatr Cogn Disord 2009;27:513–518.
[6]Casadesus G, Puig ER, Webber KM, et al. Targeting gonadotropins: an alternative option for Alzheimer disease treatment. J Biomed Biotechnol 2006;2006:39508.
[7]Bajic V, Mandusic V, Stefanova E, Bozovic A, Davidovic R, Zivkovic L, Cabarkapa A, Spremo-Potparevic B. Skewed X-chromosome inactivation in women affected by Alzheimer's disease. J Alzheimers Dis. 2015;43(4):1251-9.
[8]. Kopp F, Mendell JT. Functional classification and experimental dissection of long noncoding RNAs. Cell. 2018 Jan 25;172(3):393– 407.
[9]. Böhmdorfer G, Wierzbicki AT. Control of chromatin structure by long noncoding RNA. Trends Cell Biol. 2015;25:623–632.
[10]. Sin O, Ellen AA. Regulation of protein homeostasis in neurodegenerative diseases: the role of coding and ncgenes. Cell Mol Life Sci. 2015;72:4027–4047.
[11]. Elling R, Chan J, Fitzgerald KA. Emerging role of long noncoding RNAs as regulators of innate immune cell development and inflammatory gene expression. Eur J Immunol. 2016;46:504–512.
[12]. Szcześniak MW, Makałowska I. lncRNA-RNA interactions across the human transcriptome. PLoS One. 2016 Mar 1;11:e0150353.
[13]. Barry G. Integrating the roles of long and small non-coding RNA in brain function and disease. Mol Psychiatry. 2014 Apr;19(4):410-6.
[14]. Quinn, J.J. and H.Y. Chang, Unique features of long non-coding RNA biogenesis and function.Nature reviews. Genetics, 2016. 17(1): p. 47-62.
[15].Kapranov P, Cheng J, Dike S, Nix DA, Duttagupta R, Willingham AT, Stadler PF, Hertel J, Hackermüller J, Hofacker IL, Bell I, Cheung E, Drenkow J, Dumais E, Patel S, Helt G, Ganesh M, Ghosh S, Piccolboni A, Sementchenko V, Tammana H, Gingeras TR (June 2007). "RNA maps reveal new RNA classes and a possible function for pervasive transcription". Science. 316 (5830): 1484-8.
[16].Hon CC, Ramilowski JA, Harshbarger J, Bertin N, Rackham OJ, Gough J, Denisenko E, Schmeier S, Poulsen TM, Severin J, Lizio M, Kawaji H, Kasukawa T, Itoh M, Burroughs AM, Noma S, Djebali S, Alam T, Medvedeva YA, Testa AC, Lipovich L, Yip CW, Abugessaisa I, Mendez M, Hasegawa A, Tang D, Lassmann T, Heutink P, Babina M, Wells CA, Kojima S, Nakamura Y, Suzuki H, Daub CO, de Hoon MJ, Arner E, Hayashizaki Y, Carninci P, Forrest AR (March 2017). "An atlas of human long non-coding RNAs with accurate 5' ends". Nature. 543 (7644): 199–204.
[17]. Qureshi, I.A. and M.F. Mehler, Emerging roles of non-coding RNAs in brain evolution, development, plasticity and disease. Nat Rev Neurosci, 2012. 13(8): p. 528-41.
[18]. Ma, L., V.B. Bajic, and Z. Zhang, On the classification of long non-coding RNAs. RNA biology,2013. 10(6): p. 925-33.
[19]. Wu, H., L. Yang, and L.L. Chen, The Diversity of Long Noncoding RNAs and Their Generation. Trends in genetics: TIG, 2017. 33(8): p. 540-552.
[20]. Wang, K.C. and H.Y. Chang, Molecular mechanisms of long noncoding RNAs. Mol Cell, 2011.43(6): p. 904-14.
[21]. Ponting, C.P., P.L. Oliver, and W. Reik, Evolution and functions of long noncoding RNAs. Cell,2009. 136(4): p. 629-41.
[22]. Quinodoz, S. and M. Guttman, Long noncoding RNAs: an emerging link between gene regulation and nuclear organization. Trends Cell Biol, 2014. 24(11): p. 651-63.

[23]. Chen, L.L. and G.G. Carmichael, Decoding the function of nuclear long non-coding RNAs. Current opinion in cell biology, 2010. 22(3): p. 357-64.
[24]. Riva, P., A. Ratti, and M. Venturin, The Long Non-Coding RNAs in Neurodegenerative Diseases: Novel Mechanisms of Pathogenesis. Current Alzheimer research, 2016. 13(11): p.1219-1231.
[25]. Salta, E. and B. De Strooper, Noncoding RNAs in neurodegeneration. Nat Rev Neurosci, 2017.18(10): p. 627-640.
[26]Faghihi M.A., Modarresi F., Khalil A.M., Wood D.E., Sahagan B.G., Morgan T.E., Finch C.E., St Laurent G., 3rd, Kenny P.J., Wahlestedt C. Expression of a noncoding RNA is elevated in Alzheimer's disease and drives rapid feed-forward regulation of beta-secretase. Nat. Med. 2008;14:723–730.
[27]Muddashetty R., Khanam T., Kondrashov A., Bundman M., Iacoangeli A., Kremerskothen J., Duning K., Barnekow A., Hüttenhofer A., Tiedge H. Poly(A)-binding protein is associated with neuronal BC1 and BC200 ribonucleoprotein particles. J. Mol. Biol. 2002;321:433–445.
[28]Massone, S., Vassallo, I., Fiorino, G., Castelnuovo, M., Barbieri, F., Borghi, R., Tabaton, M., Robello, M., Gatta, E., Russo, C., et al. (2011). 17A, a novel non-coding RNA, regulates GABA B alternative splicing and signaling in response to inflammatory stimuli and in Alzheimer disease. Neurobiol. Dis. 41, 308–317.
[29]Chung D.W., Rudnicki D.D., Yu L., Margolis R.L. A natural antisense transcript at the Huntington's disease repeat locus regulates HTT expression. Hum. Mol. Genet. 2011;20:3467–3477
[30]Sunwoo J.S., Lee S.T., Im W., Lee M., Byun J.I., Jung K.H., Park K.I., Jung K.Y., Lee S.K., Chu K. Altered expression of the long noncoding RNA NEAT1 in Huntington's disease. Mol. Neurobiol. 2017;54:1577–1586.
[31]Scheele C., Petrovic N., Faghihi M.A., Lassmann T., Fredriksson K., Rooyackers O., Wahlestedt C., Good L., Timmons J.A. The human PINK1 locus is regulated in vivo by a non-coding natural antisense RNA during modulation of mitochondrial function. BMC Genomics. 2007;8:74
[32]Zhang Q.S., Wang Z.H., Zhang J.L., Duan Y.L., Li G.F., Zheng D.L. Beta-asarone protects against MPTP-induced Parkinson's disease via regulating long non-coding RNA MALAT1 and inhibiting α-synuclein protein expression. Biomed.Pharmacother. 2016;83:153–159.
[33] Ramos AD, Diaz A, Nellore A, Delgado RN, Park KY, Gonzales-Roybal G, Oldham MC, Song JS, Lim DA. Integration of genome-wide approaches identifies lncRNAs of adult neural stem cells and their progeny in vivo. Cell Stem Cell. 2013 May 2;12(5):616-28.
[34] Ramos AD, Andersen RE, Liu SJ, Nowakowski TJ, Hong SJ, Gertz C, Salinas RD, Zarabi H, Kriegstein AR, Lim DA. The long noncoding RNA Pnky regulates neuronal differentiation of embryonic and postnatal neural stem cells. Cell Stem Cell. 2015 Apr 2;16(4):439-447.
[35] Aprea, J.; Prenninger, S.; Dori, M.; Ghosh, T.; Monasor, L.S.; Wessendorf, E.; Zocher, S.; Massalini, S.; Alexopoulou, D.; Lesche, M.; et al. Transcriptome sequencing during mouse brain development identifies long non-coding RNAs functionally involved in neurogenic commitment. EMBO J. 2013, 32, 3145–3160.
[36] Ng SY, Bogu GK, Soh BS, Stanton LW. The long noncoding RNA RMST interacts with SOX2 to regulate neurogenesis. Mol Cell. 2013 Aug 8;51(3):349-59.
[37] Zhu X, Wu YB, Zhou J, Kang DM. Upregulation of lncRNA MEG3 promotes hepatic insulin resistance via increasing FoxO1 expression. Biochem Biophys Res Commun. 2016 Jan 8;469(2):319-25.
[38] Goyal N, Sivadas A, Shamsudheen KV, Jayarajan R, Verma A, Sivasubbu S, Scaria V, Datta M. RNA sequencing of db/db mice liver identifies lncRNA H19 as a key regulator of gluconeogenesis and hepatic glucose output. Sci Rep. 2017 Aug 16;7(1):8312.
[39].Brown CJ, Hendrich BD, Rupert JL, Lafrenière RG, Xing Y, Lawrence J, Willard HF (October 1992). [39]"The human XIST gene: analysis of a 17 kb inactive X-specific RNA that contains conserved repeats and is highly localized within the nucleus". Cell. 71 (3): 527–42. doi:10.1016/0092-8674(92)90520-M. PMID 1423611.
[40].Ng K, Pullirsch D, Leeb M, Wutz A (January 2007). "Xist and the order of silencing"(Review Article). EMBO Reports. 8 (1): 34 9 doi:10.1038/sj.embor.7400871.
[41].Chow JC, Yen Z, Ziesche SM, Brown CJ (2005). "Silencing of the mammalian X chromosome". Annual Review of Genomics and Human Genetics. 6: 69–92.
[42] Chureau C, Chantalat S, Romito A, Galvani A, Duret L, Avner P, Rougeulle C. Ftx is a non-coding RNA which affects Xist expression and chromatin structurewithin the X inactivation center region. Hum Mol Genet. 2011 Feb 15;20(4):705-18.

[43] Tian D, Sun S, Lee JT. The long noncoding RNA, Jpx, is a molecular switch for X chromosome inactivation. Cell. 2010 Oct 29;143(3):390-403.
[44] Lee JT, Davidow LS, Warshawsky D. Tsix, a gene antisense to Xist at the X-inactivation centre. Nat Genet. 1999 Apr;21(4):400-4.
[45] Augui S, Nora EP, Heard E. Regulation of X-chromosome inactivation by the X-inactivation centre. Nat Rev Genet. 2011 Jun;12(6):429-42.
[46]. Chureau C, Prissette M, Bourdet A, Barbe V, Cattolico L, Jones L, Eggen A, Avner P, Duret L (June 2002). "Comparative sequence analysis of the X-inactivation center region in mouse, human, and bovine". Genome Research. 12 (6): 894–908.
[47]. Brockdorff N, Ashworth A, Kay GF, McCabe VM, Norris DP, Cooper PJ, Swift S, Rastan S (1992). "The product of the mouse Xist gene is a 15 kb inactive X-specific transcript containing no conserved ORF and located in the nucleus". Cell. 71 (3): 515–26.
[48] Fang R, Moss WN, Rutenberg-Schoenberg M, Simon MD. Probing Xist RNA Structure in Cells Using Targeted Structure-Seq. PLoS Genet. 2015 Dec 8;11(12):e1005668.
[49].Kawaguchi, R., and Kiryu, H. (2016). Parallel computation of genome-scale RNA secondary structure to detect structural constraints on human genome. BMC Bioinformatics 17, 203.
[50].Chu, C., Zhang, Q. C., da Rocha, S. T., Flynn, R. A., Bharadwaj, M., Calabrese, J.M., et al. (2015). Systematic discovery of Xist RNA binding proteins. Cell 161, 404–416.
[51].da Rocha, S. T., Boeva, V., Escamilla-Del-Arenal, M., Ancelin, K., Granier, C., Matias, N. R., et al. (2014). Jarid2 is implicated in the initial Xist-induced targeting of PRC2 to the inactive X chromosome. Mol. Cell 53, 301–316.
[52]Sarma, K., Levasseur, P., Aristarkhov, A., and Lee, J. T. (2010). Locked nucleic acids (LNAs) reveal sequence requirements and kinetics of Xist RNA localization to the X chromosome. Proc. Natl. Acad. Sci. U.S.A. 107, 22196–22201.
[53]Cirillo, D., Blanco, M., Armaos, A., Buness, A., Avner, P., Guttman, M., et al. (2016). Quantitative predictions of protein interactions with long noncoding RNAs. Nat. Methods 14, 5–6.
[54] McHugh, C. A., Chen, C. K., Chow, A., Surka, C. F., Tran, C., McDonel, P., et al. (2015). The Xist lncRNA interacts directly with SHARP to silence transcription through HDAC3. Nature 521, 232–236
[55].Dominissini, D., Moshitch-Moshkovitz, S., Schwartz, S., Salmon-Divon, M., Ungar, L., Osenberg, S., et al. (2012). Topology of the human and mouse m6A RNA methylomes revealed by m6A-seq. Nature 485, 201–206.
[56].Patil, D. P., Chen, C. K., Pickering, B. F., Chow, A., Jackson, C., Guttman, M., et al. (2016). m(6)A RNA methylation promotes XIST-mediated transcriptional repression. Nature 537, 369–373.
***[57].* Shevchenko AI, Malakhova AA, Elisaphenko EA, et al. Variability of sequence surrounding the Xist gene in rodents suggests taxon-specific regulation of X chromosome inactivation. *PLoS One*. 2011;6(8):e22771.**
[58]Benoit MH, Hudson TJ, Maire G, et al. Global analysis of chromosome X gene expression in primary cultures of normal ovarian surface epithelial cells and epithelial ovarian cancer cell lines. Int J Oncol. 2007; 30:5–17.
[59]Kawakami T, Zhang C, Taniguchi T, et al. Characterization of loss-of-inactive X in Klinefelter syndrome and female-derived cancer cells. Oncogene. 2004; 23:6163–6169.
[60]Ganesan S, Silver DP, Greenberg RA, et al. BRCA1 supports XIST RNA concentration on the inactive X chromosome. Cell. 2002; 111:393–405.
[61]Looijenga LH, Gillis AJ, van Gurp RJ, et al. X inactivation in human testicular tumors. XISTexpression and androgen receptor methylation status. Am J Pathol. 1997; 151:581–590.
[62]Chen DL, Chen LZ, Lu YX, Zhang DS, Zeng ZL, Pan ZZ, Huang P, Wang FH, Li YH, Ju HQ, Xu RH. Long noncoding RNA XIST expedites metastasis and modulates epithelial-mesenchymal transition in colorectal cancer. Cell Death Dis. 2017 Aug 24;8(8):e3011.
[63]Yu H, Xue Y, Wang P, Liu X, Ma J, Zheng J, Li Z, Li Z, Cai H, Liu Y. Knockdown of long non-coding RNA XIST increases blood-tumor barrier permeability and inhibits glioma angiogenesis by targeting miR-137. Oncogenesis. 2017 Mar 13;6(3):e303.
[64].Chen X, Xiong D, Ye L, Wang K, Huang L, Mei S, Wu J, Chen S, Lai X, Zheng L, Wang M. Up-regulated lncRNA XIST contributes to progression of cervical cancer via regulating miR-140-5p and ORC1. Cancer Cell Int. 2019 Feb 28;19:45.
[65]Zhou X, Xu X, Gao C, Cui Y. XIST promote the proliferation and migration of non-small cell lung cancer cells via sponging miR-16 and regulating CDK8 expression. Am J Transl Res. 2019 Sep 15;11(9):6196-6206.

[66]. Barati M, Ebrahim M. A Gene Expression Profile of Alzheimer's Disease Using Microarray Technology, Zahedan J Res Med Sci. 2016 ; 18(8):e7950. doi: 10.17795/zjrms-7950.
[67]. Barati M, Ebrahimi M. Identification of Genes Involved in the Early Stages of Alzheimer Disease Using a Neural Network Algorithm, Gene Cell Tissue. 2016 ; 3(3):e38415. doi: 10.17795/gct-38415.
[68]. Wang X, Wang C, Geng C, Zhao K. LncRNA XIST knockdown attenuates Aβ25-35-induced toxicity, oxidative stress, and apoptosis in primary cultured rat hippocampal neurons by targeting miR-132. Int J Clin Exp Pathol 2018;11(8):3915-3924.
[69]. Chanda, K., Das, S., Chakraborty, J., Bucha, S., Maitra, A., Chatterjee, R., Mukhopadhyay, D., Bhattacharyya, N. P. (2018). Altered Levels of Long NcRNAs Meg3 and Neat1 in Cell and Animal models of Huntington's Disease. RNA Biology.doi:10.1080/15476286.2018.1534524
[70].Majumder, P., Roy, K., Singh, B. K., Jana, N. R., & Mukhopadhyay, D. (2017). Cellular levels of Grb2 and cytoskeleton stability are correlated in a neurodegenerative scenario. Disease Models & Mechanisms, 10(5), 655–669.
[71].Bamburg, J. R. and. Bloom, G. S. (2009). Cytoskeletal pathologies of Alzheimer disease. Cell Motil. Cytoskelet. 66, 635-649.
[72].Liem, R. K. H. and Messing, A. (2009). Dysfunctions of neuronal and glial intermediate filaments in disease. J. Clin. Invest. 119, 1814-1824.
[73].Ghosal, K., Vogt, D. L., Liang, M., Shen, Y., Lamb, B. T. and Pimplikar, S. W.(2009). Alzheimer's disease-like pathological features in transgenic miceexpressing the APP intracellular domain. Proc. Natl. Acad. Sci. USA 106, 18367-18372.
[74]. Brown CJ, Ballabio A, Rupert JL, Lafreniere RG, Grompe M, Tonlorenzi R, Willard HFA gene from the region of the human X inactivation centre is expressed exclusively from the inactive X chromosome.. Nature. 1991 Jan 3;349(6304):38-44.
[75]. Mielke MM, Vemuri P, Rocca WA Clinical epidemiology of Alzheimer's disease: assessing sex and gender differences.Clin Epidemiol. 2014 Jan 8; 6:37-48.
[76] Bajic VP, Essack M, Zivkovic L, et al. The X Files: "The Mystery of X Chromosome Instability in Alzheimer's Disease". *Front Genet*. 2020;10:1368.
[77]Yue D, Guanqun G, Jingxin L, Sen S, Shuang L, Yan S, Minxue Z, Ping Y, ChongL, Zhuobo Z, Yafen W. Silencing of long noncoding RNA XIST attenuated Alzheimer's disease-related BACE1 alteration through miR-124. Cell Biol Int. 2020Feb;44(2):630-636.
[78].Kerschbamer E, Biagioli M. Huntington's Disease as Neurodevelopmental Disorder: Altered Chromatin Regulation, Coding, and Non-Coding RNA Transcription. *Front Neurosci*. 2016;9:509.
[79].Seong IS, Woda JM, Song JJ, Lloret A, Abeyrathne PD, Woo CJ, Gregory G, Lee JM, Wheeler VC, Walz T, Kingston RE, Gusella JF, Conlon RA, MacDonald ME. Huntingtin facilitates polycomb repressive complex 2. Hum Mol Genet. 2010 Feb15;19(4):573-83.
[80].Singer E, Walter C, Weber JJ, et al. Reduced cell size, chromosomal aberration and altered proliferation rates are characteristics and confounding factors in the STHdh cell model of Huntington disease. *Sci Rep*. 2017;7(1):16880
[81].Jiang J, Jing Y, Cost GJ, Chiang JC, Kolpa HJ, Cotton AM, Carone DM, Carone BR, Shivak DA, Guschin DY, Pearl JR, Rebar EJ, Byron M, Gregory PD, Brown CJ, Urnov FD, Hall LL, Lawrence JB. Translating dosage compensation to trisomy 21. Nature. 2013 Aug 15;500(7462):296-300.
[82].Kouznetsova VL, Tchekanov A, Li X, Yan X, Tsigelny IF. Polycomb repressive 2 complex-Molecular mechanisms of function. Protein Sci. 2019 Aug;28(8):1387-1399.
[83].van Bergeijk P, Seneviratne U, Aparicio-Prat E, Stanton R, Hasson SA. SRSF1 and PTBP1 Are trans-Acting Factors That Suppress the Formation of a CD33 Splicing Isoform Linked to Alzheimer's Disease Risk. Mol Cell Biol. 2019 Aug 27;39(18).
[84].Brouwers N, Bettens K, Gijselinck I, Engelborghs S, Pickut BA, Van Miegroet H, Montoya AG, Mattheijssens M, Peeters K, De Deyn PP, Cruts M, Sleegers K, Van Broeckhoven C. Contribution of TARDBP to Alzheimer's disease genetic etiology. J Alzheimers Dis. 2010;21(2):423-30.
[85]. Cohen, D., Pilozzi, A., & Huang, X. (2020). Network Medicine Approach for Analysis of Alzheimer's Disease Gene Expression Data. *International Journal of Molecular Sciences, 21(1), 332.*

Chapter 7: lncRNA Transcriptome in HD

7.1 Introduction

Huntington's disease is a rare, autosomal dominant neurodegenerative disorder caused by expansion of polymorphic CAG repeats at exon1 of the gene *Huntingtin* (*HTT*) [**1]**. The disease is characterized by behavioural and psychiatric abnormalities, dementia, motor defects and choreatic movements due to random muscle contractions [**2]**. Increase in length of glutamine (Q) stretch at N-terminal of HTT due to the expansion of CAG repeats alters the conformation of HTT leading to cytoplasmic and nuclear aggregates. Over the years, alterations of various cellular processes like transcription, excitotoxicity, axonal transport, proteasomal degradation, autophagy, and apoptosis; cellular conditions like oxidative stress, endoplasmic reticulum stress, and mitochondrial dysfunctions have been implicated in HD **[3]**. Altered levels of protein-coding genes in HD, identified in diverse models of HD and different tissues including post-mortem brains of HD patients and enrichment of different biological pathways indicates that altered levels of protein-coding genes could contribute to HD pathogenesis. Altered levels of genes were identified in the early stage before the neurodegeneration starts and is considered to be a hallmark for HD. Modified interactions of transcription factors with wild-type HTT, direct binding of mutant HTT with DNA and epigenetic changes could contribute to the deregulation of genes in HD [**4,5**]. Differential levels of microRNA (miRNA), generally a negative regulator of a protein-coding gene, has also been identified in HD models and post-mortem brains of HD patients and other neurodegenerative diseases [**4-16**]. In cellular models, some of these miRNAs have been shown to modulate neuronal survival [**9**], disease progression by influencing neurogenesis [**10**], cell cycle [**11-13**], mitochondrial dynamics [**14**] and target HTT [**16**]. Age at onset of HD has been correlated with levels of miR10b [**5, 6**]. Thus, miRNA could also contribute to the

altered expression of protein-coding genes and may modulate HD pathogenesis by targeting protein-coding genes including HTT [**7, 16**].

In recent years, long non-coding RNA (lncRNA), defined as single-stranded RNA > 200 nucleotides long without potential for coding proteins, has emerged as the regulator of transcription [**17,18**], cellular homeostasis [**19**], immune cell development [**20**] and other biological processes possibly by interacting with proteins and RNA [**21**]. It is thus possible that altered levels of lncRNAs contribute to the deregulation of genes observed in HD and modulate HD pathogenesis. Altered levels of lncRNA have been observed in neurological diseases [**22,23**]. It has been shown that levels of *2010001M06Rik/ Abhd11os* (designated as ABHD11-AS1 in human) are reduced in the striatum of mouse R6/2 models of HD [**24**]. Exogenous levels of *Abhd11os* protects against the toxic effects of N-terminal mutant HTT in mouse, while the loss of *Abhd11os* enhances the toxicity, although the mechanism is still elusive [**25**]. Re-analysis of gene expression data in HD identifies seven long non-coding RNAs (*TUG1*, *LINC00341*, *RPS20P22*, *NEAT1*, *MEG3*, *DGCR5*, and *LINC00342*), of which only *NEAT1* shows over expression. Putative promoter regions of NEAT1, MEG3, and DGCR5 genes harbor binding sites of REST/NRSF, a transcription repressor [**26**]. Human accelerated region 1 non-coding RNA (*HAR1*) is repressed by REST and is down-regulated in postmortem brains of HD patients [**27**], although the functional consequence of decreased *HAR1* in HD remains unknown. Levels of natural antisense *HTT* (*HTT-AS1),* a lncRNA localized in the nearby upstream region of *HTT*, depends on the CAG repeat numbers in the *HTT* gene and mutated *HTT* reduces levels of *HTT-AS1*. Decreased levels of *HTT-AS1* results in higher levels of *HTT* indicating its possible role in HD pathogenesis [**28**]. Increased levels of NEAT1 have been recently reported in human brains of HD patients and R6/2 mice. Exogenous levels of short

isoforms of NEAT1 protect cells from death induced by H_2O_2 [**28**]. Considering the thousands of lncRNAs coded by human genome and their possible roles in brain development and plasticity [**29, 30**] and many other HD associated processes, it is expected that lncRNAs, might be involved in HD pathogenesis.

The aim of the present study is to identify altered levels of lncRNAs in HD, decipher the roles of lncRNA in the disease and to understand their intricate regulatory mechanism in HD pathogenesis.

7.2. Altered levels of non-coding RNAs in the mouse model of HD

I compared the small RNA sequence data from the cortex of R6/2 mice at ages of 6 weeks (early stage of HD) and 8 weeks and age-matched control mice. Excluding the sequence data that aligned to annotated miRNA in the mouse genome, I focused on the rest of the aligned sequences for other non-coding RNA. It was observed that sequences were aligned against the annotated non-coding regions with sufficient depth. Levels of Xist (X inactive specific transcript), Peg3os and Meg3 (maternally expressed gene 3) were increased and levels of Snora21, Snord53, Snhg12, and Vaultrc5 were decreased significantly in the cortex of 6-week old mice compared to the control (**Figure 7.1**).

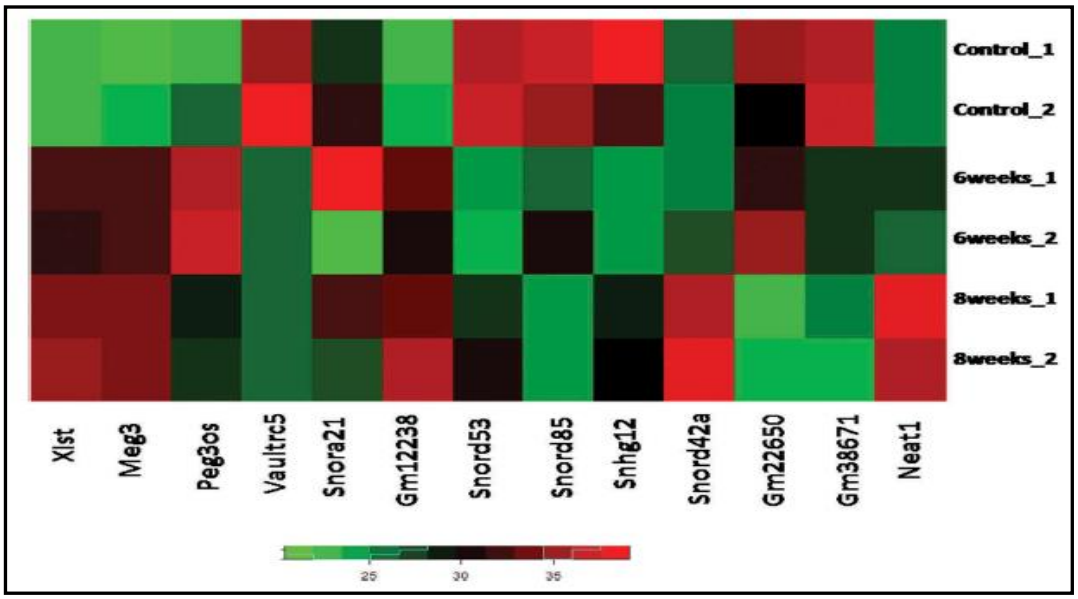

Figure 7.1. Heatmap of statistically significant differentially regulated ncRNAs Xist, Meg3, Peg3os, Vaultrc5, Snora21, Gm12238, Snord53, Snord85, Snhg12, Snord42a, Gm22650, Gm38671and Neat1 in early stage and late-stage Huntington's mouse cortex compared to the control cortex from small RNA sequencing (n=2). Color codes indicate normalized fold changes- Red = up regulation; Green = downregulation.

Levels of Meg3, Xist, and additional genes Snord42a, Gm12238 and Neat1 (Nuclear Paraspeckle Assembly Transcript 1) were significantly increased in the 8-week-old mice compared to control. In the older mice, however, levels of Vaultrc5 and additional genes Gm38671, Gm22650, and Snord85 decreased significantly. Combining the results, I observed that levels of Meg3 and Xist were increased and the level of Vaultrc5 was decreased in both early and late stage of HD, the level of Peg3os was increased and the levels of Snhg12, Snora21, Snord53 were decreased in the early stage of HD. The levels of Neat1, Gm12238, Snord42a (increased), Snord85/Snord103, Gm22650, and Gm38671 (decreased) altered in the late stage of HD **(Figure 7.1).**

To identify the human orthologs of these non-coding RNAs, I searched the NCBI database (https://www.ncbi.nlm.nih.gov/gene/) and found that 8 of the 13 mouse ncRNAs namely Meg3, Xist, Neat1, Snhg12, Snora21 Snord53, Snord85, Snord42a had human orthologs (**Table 7.1**).

Table 7.1: Summary of the levels of non-coding RNAs in different models of HD

Noncoding RNA (Entrez ID)	**Human homolog**	**Levels in**			
		The cortex of R6/2 (6week)	**The cortex of R6/2 (8week)**	**ST*Hdh*^{Q111}/*Hdh*^{Q11}** [1]	**ST*Hdh*^{Q7}/*Hdh*^{Q7} Cells transfected with 83Q**
Brip1os (74038)	No	⬆	-	-	⬆
Meg3 (17263)	Meg3	⬆	-	-	⬆
Xist (213742)	Xist	⬆	-	-	⬆

Neat1	Neat1	-	⬆	⬆	⬆
Snhg3	Snhg3	-	-	-	-
Snhg12 (ID: 10003986)	Snhg12	⬇	-	-	⬆
Snora21 (100302498)	ACA21	⬇	-	-	-
Snord53	snoRNA U53	⬇	⬇		
Snord85/Snord103	Snord85/Snord103	⬇	⬇	-	-
Vaultrc5	No	⬇	⬇	⬇	⬇

7.3. Validation of the results in animal and cell models of HD using real-time PCR

To validate the data obtained in small RNA sequencing the levels of Meg3, Neat1, Xist, Snhg12, Snora21, Snord53, Snord85, Vaultrc5 ncRNAs and those of additional ncRNAs (Snhg3 and Brip1os) whose levels were not altered were checked using real-time PCR and gene-specific PCR primers. Results are shown in **Figure 7.2(i), panels A and B,** revealed that

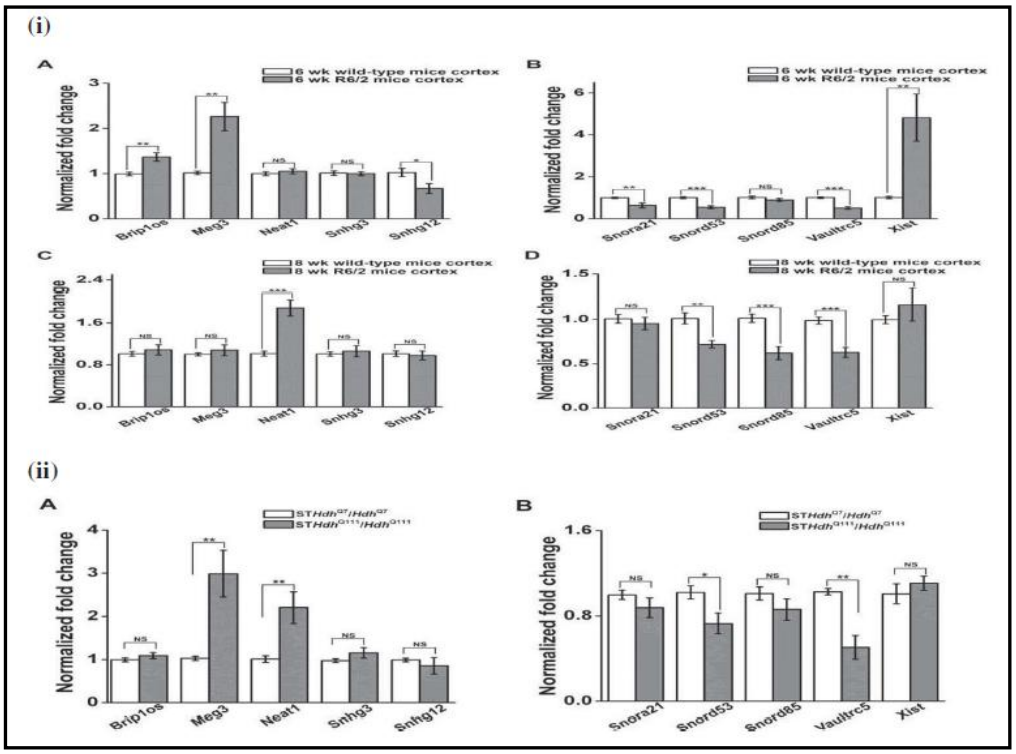

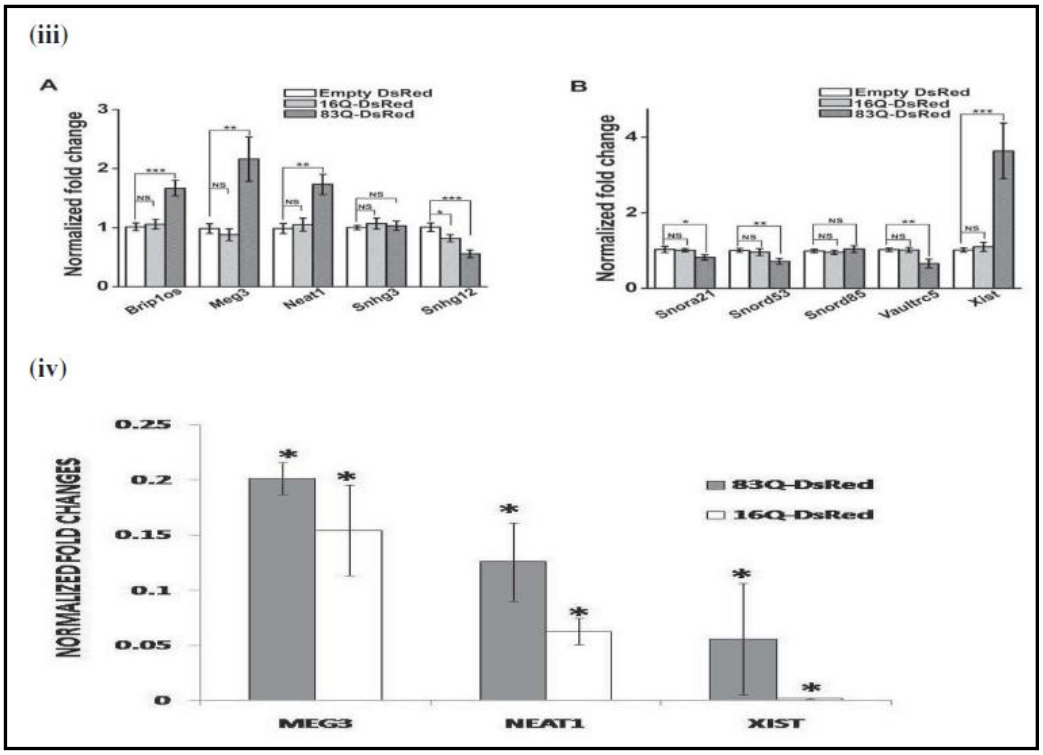

Figure 7.2: Altered levels of non-coding RNAs in HD animal model and in cells expressing N-terminal mutant Huntingtin. **(i).** Bar graphs representative of three (n=3) independent experiments measuring levels of *Brip1os*, *Meg3*, *Neat1*, *Snhg3*and *Snhg12* (panels A and C); *Snora21*, *Snord53*, *Snord85*, *Vaultrc5* and *Xist* (panels B and D) by qRT-PCR in cortex region of 6-weeks old (panels A and B) and 8-weeks old (panel C and D) R6/2 mice and age-matched wild-type mice. **(ii).**Bar graphs representative of three (n=3) independent experiments measuring levels of *Brip1os*, *Meg3*, *Neat1*, *Snhg3*and *Snhg12* (panel A); *Snora21*, *Snord53*, *Snord85*, *Vaultrc5* and *Xist* (panel B) by qRT-PCR in mouse immortalized striatal cells expressing full-length *huntingtin* (*Hdh*) gene with 7 (ST*Hdh*^{Q7}/*Hdh*^{Q7} cells) and 111 (ST*Hdh*^{Q111}/*Hdh*^{Q111}cells) glutamine repeats.**(iii)** Bar graphs representative of three (n=3) independent experiments measuring levels of *Brip1os*, *Meg3*, *Neat1*, *Snhg3*and *Snhg12* (panel A); *Snora21*, *Snord53*, *Snord85*, *Vaultrc5* and *Xist* (panel B) by qRT-PCR in ST*Hdh*^{Q7}/*Hdh*^{Q7} cells transiently expressing empty DsRed vector or *huntingtin* exon 1 having 16 and 83 glutamine repeats cloned in DsRed vector (designated as 16Q-DsRed and 83Q-DsRed respectively). Levels of *β-actin* were taken as endogenous control. The levels of individual non-coding RNAs were normalized by the corresponding *β-*

actin levels. Fold change was calculated by considering the relative levels of non-coding RNA in empty vector (DsRed) transfected cells (control) to be 1.**(iv)** Bar graphs representative of three (n=3) independent experiments measuring levels of *Meg3*, *Neat1*, and *Xist*) by qRT-PCR in Neuro2A cells transiently expressing *huntingtin* exon 1 having 16 and 83 glutamine repeats cloned in DsRed vector (designated as 16Q-DsRed and 83Q-DsRed respectively). Levels of *β-actin* were taken as endogenous control. The levels of individual non-coding RNA were normalized by the corresponding *β-actin* levels. *Error bars* indicate ± SD. The statistical significance level between different experimental pairs is indicated (NS, not significant; *, $p<0.05$; **, $p<0.01$; ***, $p<0.001$).

out of 10 ncRNAs tested, levels of 9 ncRNAs Meg3, Xist, Neat1, Snhg12, Snora21, Snord53, Snord85, and Vaultrc5 and Snhg3 were in concordance with the data obtained by sequencing in 6-week-old mice. Levels of Brip1os increased significantly in this assay for 6-week-old mice, while it was unaltered in the sequencing data. In 8-week-old R6/2 mice, levels of Meg3 were increased in sequencing data, while remaining unaltered in real-time PCR assay. Levels of all other 9 ncRNAs were in concordance with the sequencing data. Results obtained from sequencing data analysis, in general, were conforming to the low throughput PCR based assay. (**Figure 7.2(i), panels C and D**).

7.4. Validation of the differential gene expressions in cell models

I further used different cell models of HD to validate the observations from mouse R6/2 model. STHdh^{Q7}/Hdh^{Q7}cells had been established from wild-type (Q7/7) Hdh knock-in mice which expressed full-length *HTT* with 7 Glu (Q) residues (wild-type HD) endogenously. STHdh^{Q7}/Hdh^{Q7}cells were used for control, while STHdh^{Q111}/Hdh^{Q111} cells, expressing endogenous full-length mutant *HTT* gene with 111Glu (Q) residues, were used as HD cells. This cell model, described earlier [**30**], had been used widely to identify the molecular mechanism of HD pathogenesis. The

results revealed that except for Snhg12 and Xist, levels of all other genes in ST*Hdh*^{Q111}/*Hdh*^{Q111} cells compared to control cells were similar to that observed in the R6/2 mouse model. (**Figure 7.2(ii)).**

ST*Hdh*^{Q7}/*Hdh*^{Q7}cells transfected with N-terminal HTT with 83Q (83Q-DsRed) was also used as an alternative cell model of HD [**31**]. I also used ST*Hdh*^{Q7}/*Hdh*^{Q7}cells expressing wild-type N-terminal HTT with 16Q (16Q- DsRed) coded by exon1 of wild-type *HTT*. Levels of wild-type N-terminal HTT did not alter the levels of the genes tested in comparison with ST*Hdh*^{Q7}/*Hdh*^{Q7}cells except for Snhg12. In 83Q-DsRed expressing cells, levels of Brip1os, Meg3, Xist, and Neat1 were increased and levels of Snord53, Snhg12, Snora21, and Vaultrc5 were decreased (**Figure** 7.**2(iii)**). The decrease in Snord85 level was not significant. Moreover, the levels of *Meg3*, *Neat1*, and *Xist* were also checked (by qRT-PCR) in Neuro2A (mouse neuroblastoma) cells transiently expressing 16Q-DsRed and 83Q-DsRed. Meg3, Neat1, and Xist levels were significantly increased (**Figure** 7.**2(iv)**). In summary, levels of Snord53 and Vaultrc5 were decreased in all the models, levels of Meg3 and Neat1 were increased in 3 models and levels of Brip1os and Xist were increased in 2 models of HD. Summary of all the results is shown in **Table 7.1.**

7.5. Meg3 and Neat1 enhance aggregation of mutant N-terminal HTT in cell models of HD and stabilize Tp53

To determine the role of Meg3 and Neat1 in the formation of aggregates of mutant HTT coded by exon1, I used commercially available siRNAs against Meg3 and Neat1 for transiently knocking down Neat1 and Meg3 in mouse Neuro2a and human SHSY5Y cells. It was observed that both the siRNAs reduced the levels of endogenous Meg3 and Neat1 significantly in both cell lines in comparison to untransfected control.

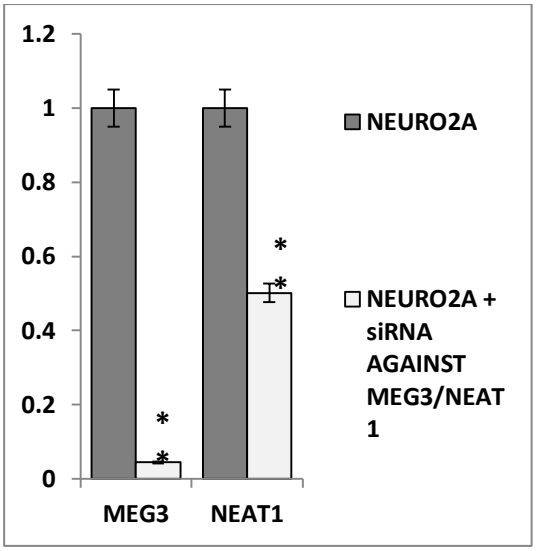

Decrease in expression of lncRNAs Meg3 and Neat1 on transfection of respective siRNAs in Control Neuro2A cells: 1.**(iv)** Bar graphs representative of three (n=3) independent experiments measuring expression of *Meg3* and *Neat1* by qRT-PCR in untransfected Neuro2A cells or Neuro2A cells transiently expressing siRNA against Meg3 or Neat1. Expression of *β-actin* was taken as endogenous control. The expression level of individual non-coding RNA was normalized by the corresponding *β-actin* expression level.

Co-transfection of 83Q-DsRed and siRNA specific for Neat1 or Meg3 resulted in decreased intracellular aggregates of 83Q-DsRed in both the cell lines (**Figure 7.3**).

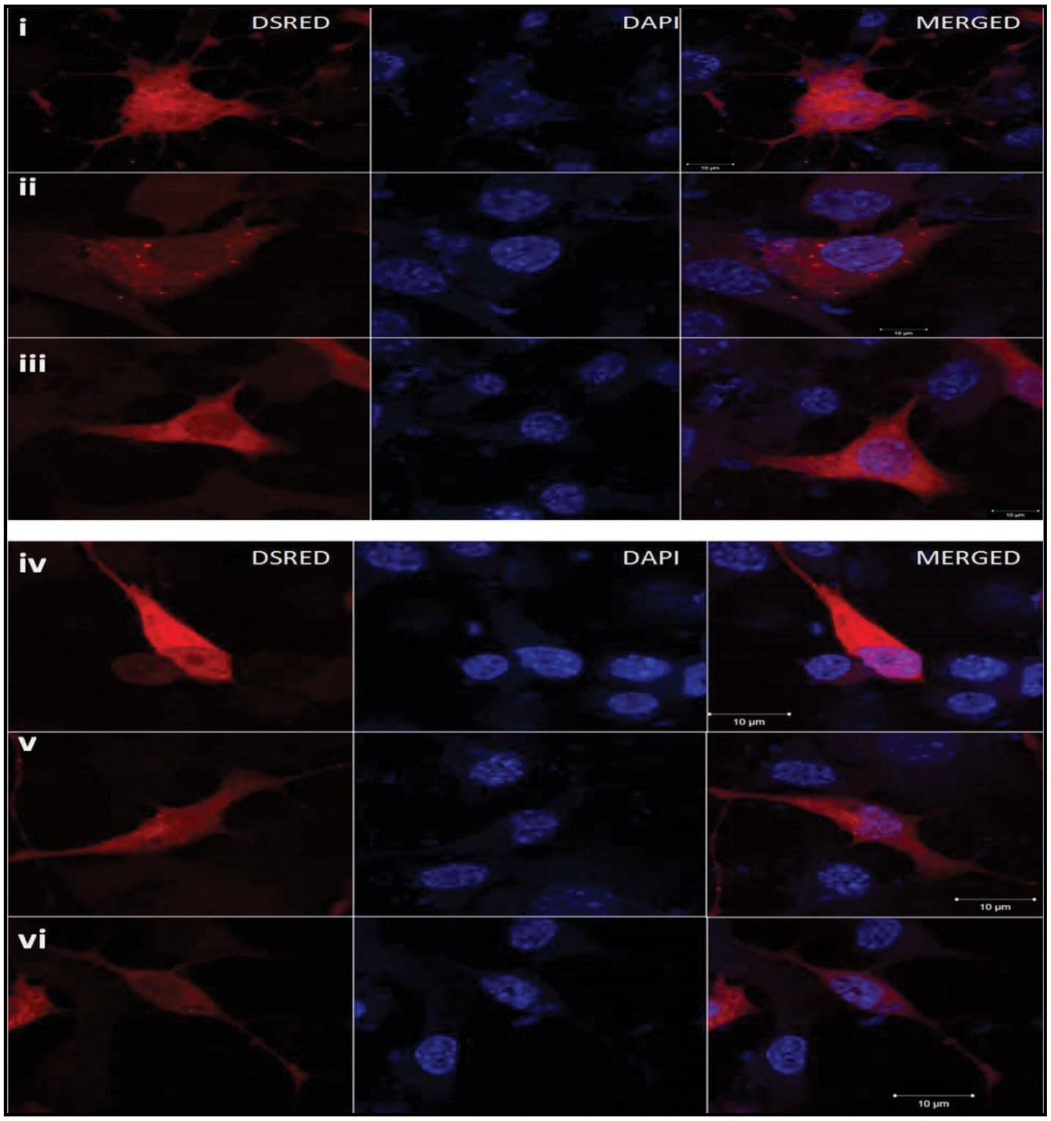

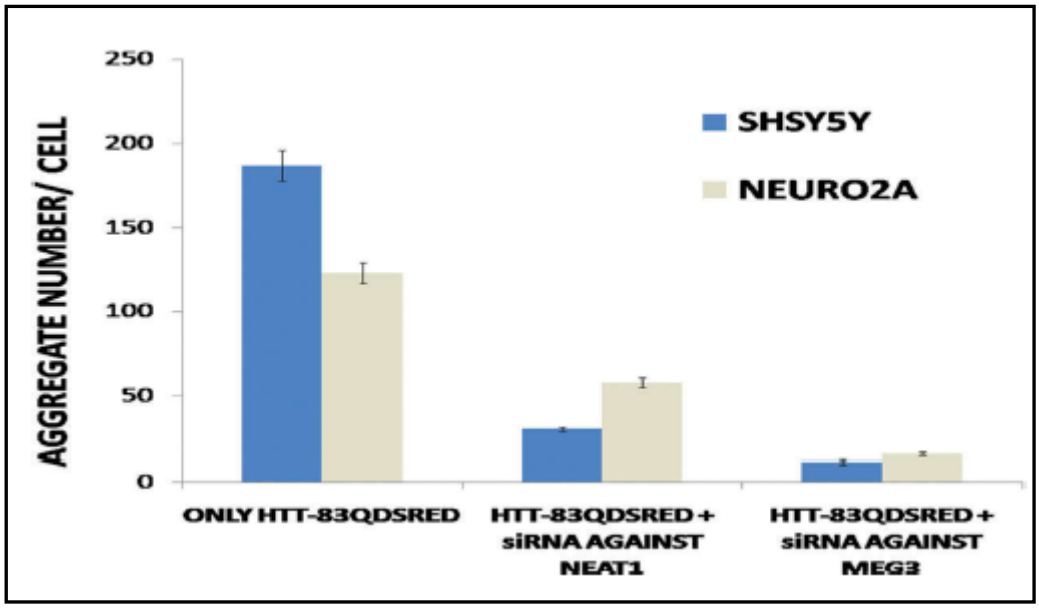

Figure 7.3: Reduction in the numbers of HTT-83Q-DsRed aggregates in Neuro2A and SHSY5Y cells. **(i)** & **(iv)** HTT-83Q-DsRed aggregates in Neuro2A and SHSY5Y cells respectively, **(ii)** & **(v)** HTT-83Q-DsRed aggregates in Neuro2A and SHSY5Y cells respectively co-transfected with siRNA against Neat1 **(iii)** & **(vi)** HTT-83Q-DsRed aggregates in Neuro2A and SHSY5Y cells respectively co-transfected with siRNA against Meg3. All representative images were acquired 24 hours post-transfection**. (vii)** Bar graphs representative of three (n=3) independent experiments, taking 30 cells each time shows the decrease in aggregate numbers per cell in cells transfected with HTT-83Q-DsRed and treated with siRNAs against Meg3 or Neat1 compared to cells transfected with HTT-83Q-DsRed only.

In summary, Meg3 and Neat1 directly or indirectly modulate the formation of aggregates of mutant HTT.

I compared the steady-state levels of TP53 in Neuro2A cells transiently expressing 83Q-DsRed. When 83Q-DsRed was co-transfected with siRNAs against Meg3 or Neat1, the steady-state levels of Tp53 decreased significantly compared to the control (**Figure 7.4)**. It was observed that knocking down both lncRNAs even in the absence of 83Q- DsRed had significant effects on steady-state Tp53 levels. In both

knockdown cases, Tp53 levels decreased. However, the decrease in Tp53 levels in Meg3 knockdown was more pronounced than that in Neat1 knocked down cells in the presence as well as the absence of 83Q-DsRed. Thus, levels of Tp53 could be modified by Meg3 or Neat1 directly or indirectly.

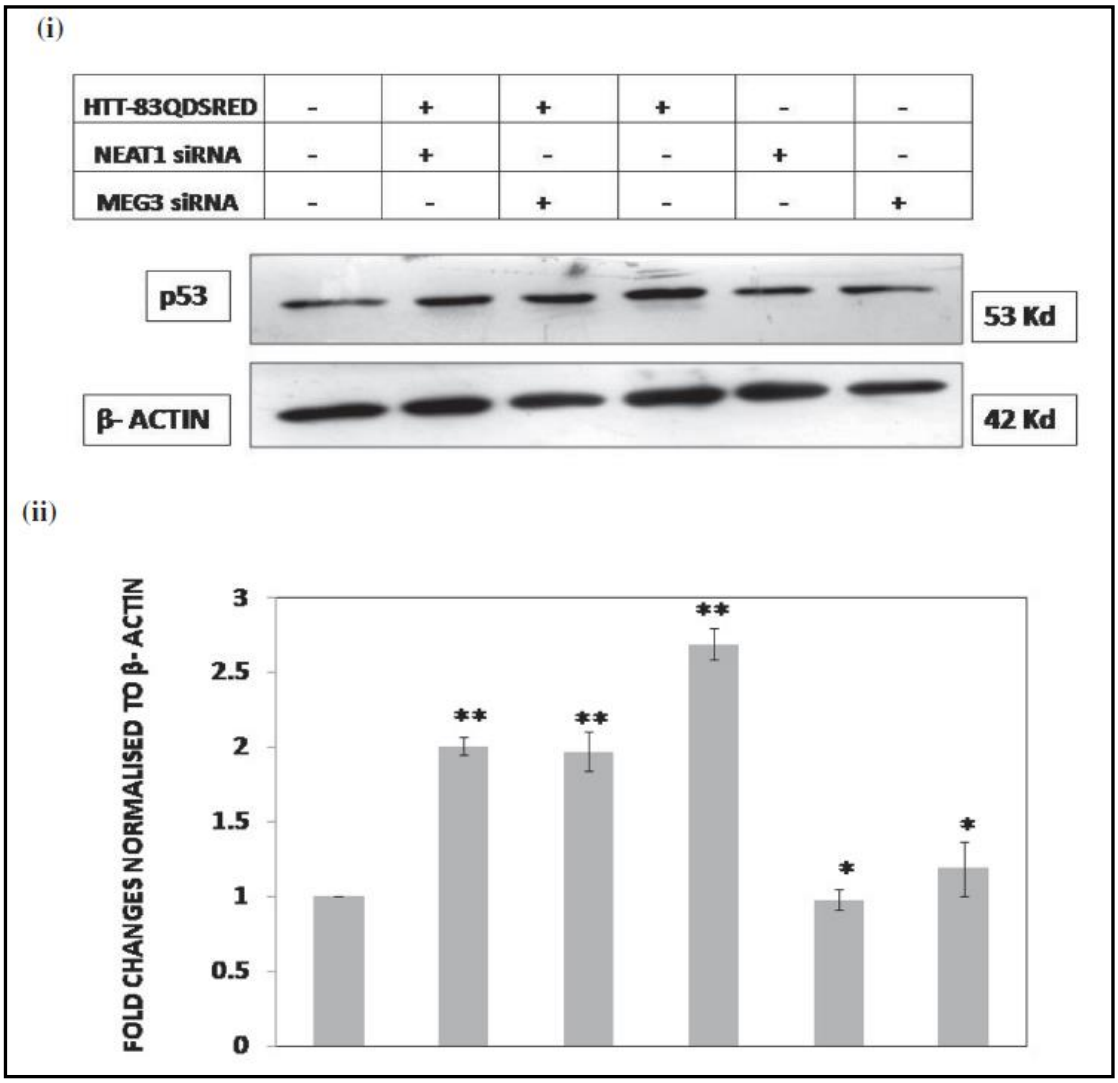

Figure 7.4: **Endogenous p53 protein levels alter after treatment with siRNA against Meg3 or Neat1 in HD cell model. (i)** Representative western blot of three independent experiments (n=3) shows (Left to Right) decrease in endogenous levels of p53 in wild-type (WT) Neuro2A cells, Neuro2A cells co-transfected with HTT-83Q-DsRed and siRNA against Meg3 or Neat1, Neuro2A cells transfected with HTT-83Q-DsRed only and Neuro2A cells transfected only with siRNA against Meg3 or Neat1 without HTT-83Q-DsRed, 24 hours post-transfection.**(ii)** Histogram representing the fold changes of p53 in the different conditions compared to WT cells in **(i)** normalized to *β-actin*. Fold change was calculated by considering the relative levels of p53 in WT cells (control) to be 1.

7.6. Interactions of MEG3, NEAT1, and XIST with protein-coding genes and microRNA

Extending the paradigm that protein-coding genes carry out their functions by interacting with other proteins [**32-33**] for lncRNAs, I attempted to derive functions of lncRNAs from functions of their interacting partners. lncRNAs are known to interact with many proteins, microRNAs (miRNA) and mRNAs [**21**] that are cataloged in the database NPInter [43] based mainly from published high throughput experimental data, as described in materials and methods. To identify the possible functional roles of Meg3, Neat1, and Xist that were increased in HD models, I enlisted the interacting partners of these genes from the NPInter database (**Table 7.2**).

Table 7. 2: Summary of protein and miRNA interactions of non-coding RNAs Meg3, Neat1, and Xist.

Noncoding RNA	Total number of interacting partners in		No of a different category of genes in human	
	Human	Mouse*	Protein	MicroRNA
MEG3	26	9	11	15
NEAT1	2577	264	2265	312
XIST	546	88	21	525

Evidently more data was available for interactions with human genes compared to that known for mouse genes probably due to a smaller number of studies in the mouse. Human MEG3 was found to interact with 11 proteins, while mouse Meg3 was found to interact with 6 proteins; interactions of Tp53 and UPF1 were common, indicating that these interactions were conserved between the species. MEG3 was found to interact with 13 human miRNAs and mouse Meg3 with 3 miRNAs.

7.7. Enrichment of biological processes and pathways with MEG3, NEAT1, and XIST interacting proteins

To identify possible functions of MEG3, NEAT1, and XIST, I carried out an enrichment analysis of their protein interacting partners using GeneCodis3. It was observed that 280 biological processes defined by Gene Ontology were enriched significantly ($p \leq 0.05$) after multiple testing correction. The most significant biological process was the regulation of DNA dependent transcription, (GO: 0006355); enriched with 229 proteins. This result showed that MEG3, NEAT1, and XIST with its protein interacting partners might be involved in regulation of transcription. Other representative biological processes that were significantly enriched are shown in **Figure 7. 5.**

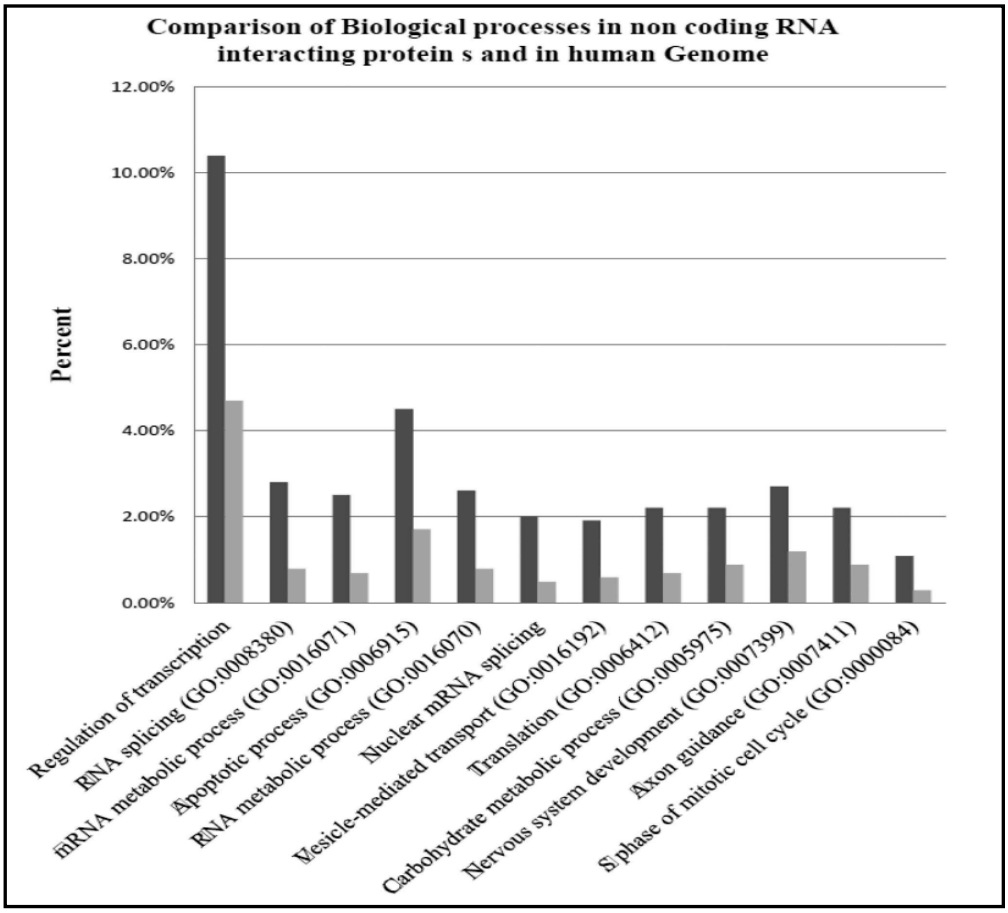

Figure 7.5: Comparison of Biological processes in noncoding RNA interacting proteins (dark black) and in human Genome (light black). GO ID is shown within parenthesis, except for Regulation of transcription (GO: 0006355) and Nuclear mRNA splicing (GO: 0000398).

Further, GeneCodis3 revealed that 101 KEGG pathways and 43 PANTHER were enriched with protein interacting partners of MEG3, NEAT1, and XIST. Among these, Endocytosis, Huntington's disease, and Ubiquitin-mediated proteolysis pathways were the top hits. Others include Regulation of actin cytoskeleton, Insulin signaling, Neurotrophin signaling, MAPK signaling, mRNA surveillance, Spliceosome, Ribosome and Proteasome, all having significant p-value ($p \leq 0.0002$) after multiple test correction. Among pathways described by PANTHER the topmost significantly enriched were Heterotrimeric G-protein signaling pathway, Gi alpha and Gs alpha-mediated pathway, Integrin signaling pathway, PI3 kinase pathway, p53 pathway, Inflammation mediated by chemokine and cytokine signaling pathway, PDGF signaling pathway, Insulin/IGF pathway, protein kinase B signaling cascade and Huntington's disease pathway.

7.8. Huntington's disease pathway (KEGG: 05016 and PANTHER: P00029): probable involvement of MEG3, NEAT1, and XIST in HD pathogenesis

Significant over-representation of protein interacting partners of MEG3, NEAT1 and XIST in Huntington's disease pathways described by both KEGG and PANTHER placed these lncRNAs as new players involved in HD pathogenesis by modulating the HD pathway. Huntington's disease pathway in KEGG had 180 proteins and PANTHER had 126 proteins. 36 proteins were enriched in KEGG HD pathway and 21 proteins were enriched in the PANTHER HD pathway of which 49 were unique. NEAT1 showed interaction with all 49 proteins including TP53, while MEG3 showed interaction with TP53 only.

Relevance for NEAT1 and MEG3 interacting protein partners in HD pathway was further evident from their involvement in transcription deregulation in postmortem brains **[34, 35]** and induced pluripotent stem cells (iPSCs) derived from HD patients

[**36**]. Among the 49 unique genes associated with HD pathway and coding for NEAT1 and MEG3 interacting proteins, no data for altered expression in HD was available for 20 genes; levels of 19 genes were decreased; levels of 6 genes were increased while levels of 4 genes increased in one experiment and decreased in the other **[34-36].** Altered levels of 29 genes that code for NEAT1 and MEG3 interacting proteins and discovered through large-scale microarray or RNA sequencing of HD tissues **(Table 7.3)**, revealed that NEAT1 and MEG3 might be associated with altered HD pathway.

Table 7.3: Expression of genes in HD associated with Huntington's disease pathway **(KEGG: 05016 and PANTHER: P00029)** and coded for protein interacting partners of NEAT1 or MEG3

Increased	Decreased	Opposite trend	Not identified (unknown)
ARPC1B, CREB3, NCOR2, PLCB3, POLR2H TP53 (6)	AP2A1, ARF3, ARPC1A, ARPC5L, ATP5G1, COX6B2, COX6C, CREB3L4, CYC1, DCTN2, DLG4, GAPDHS, GRIK5, GRIN1, GRIN2D, NDUFA3,NDUFB10, NDUFB2, POLR2E (19)	ACTG1, CLTB, DYNLL2 TUBB3 (4)	ATP5E, AKT1, AP2S1, BAX, BBC3, COX7A1, CREB3L3, DNAH2, NDUFA13, NDUFA4L2, NDUFB7, NDUFS6, NDUFS8, NDUFV3, POLR2I, POLR2J , POLR2J2, POLR2J3, SIN3A TUBB1 (20)

7.9. Interacting partners of MEG3, NEAT1, and XIST associated Huntington's disease pathways (KEGG: 05016 and PANTHER: P00029) are also co-expressed

Co-expression, a statistical correlation between the expressions of two genes in similar levels in the same direction (increase or decrease) in diverse conditions in a large number of samples can be used to assign putative functions to poorly annotated genes. Co-expressed genes are likely to be regulated by the same transcription factors/regulators and might have similar functions, possibly through physical interactions of the protein products of the co-expressed genes**.** I used Gene Friends

database (http://genefriends.org/) that catalogs data for co-expression of genes derived from more than 4000 microarray datasets in various experimental conditions for 19080 human genes. Co-expression value defined as the correlation coefficient varies between 1 to 0 (for positive correlation), are also computed for a given query. Content and procedure for obtaining the co-expressed genes are described in material and methods [**71**]. Identification of genes co-expressed with MEG3, NEAT1 or XIST should provide additional functional information about the lncRNAs. I utilized search options for microarray-based results in Gene Friends database. In this analysis I consider only the positively correlated genes; increase in expression of the lncRNA is correlated with an increase in the expression of the co-expressed genes. A summary of the list of co-expressed genes retrieved from this database is shown in **Table 7.4.**

Table 7.4: Summary of co-expressed genes of MEG3, NEAT1, and XIST

Long non-coding genes	**No of genes with Pearson coefficient (Co-expression value) ≥ +0.2**	**No of genes with Pearson coefficient (Co-expression value) ≥ +0.5**
MEG3	17993	5054
NEAT1	14709	126
XIST	14310	2

It was observed that MEG3 co-expressed with more than 5000 genes with co-expression value ≥ + 0.5. MEG3 co-expressed with GRIK5, GRIN1, DLG4, COX7A1, TP53 and other 42 genes known to involve in HD pathway. It is interesting to mention that MEG3 also known to physically interact with TP53 as discussed above. NEAT1 co-expressed in the same direction with many lncRNAs like INE1, LINC00312, HCG4B, LINC00663, LINC00574, LINC00472 and others including

NEAT1 and XIST. Role of other lncRNAs co-expressed with MEG3 remains unknown. Increased expressions of MEG3, NEAT1, and XIST, increased in our experiments indicate that these 3 lncRNAs might be regulated by same transcription factors.

NEAT1 co-expressed with many genes including ARPC1B, TP53, NDUFA4L2, BAX, COX7A1, TUBB1, AKT1, CLTB, ARPC1A, PLCB3, BBC3, CREB3, POLR2E, CYC1, POLR2J, NDUFS6, DLG4, and others associated with HD pathway (**Table 7.5**).

Table 7.5: MEG3, NEAT1 and XIST interacting protein enriched with HD pathway

Gene	Interacting protein (total number)	Co-expressed (total number, the range of Pearson's coefficient)
NEAT1	COX6B2, CREB3L3, SIN3A, NDUFB10, POLR2J2, NDUFV3, POLR2J3, AP2A1, ACTG1, DYNLL2, ARPC1B, TP53, NDUFA4L2, BAX, COX7A1, TUBB1, AKT1, CLTB, ARPC1A, PLCB3, BBC3, CREB3, POLR2E, CYC1, POLR2J, NDUFS6, DLG4, ARPC5L, COX6C, GRIN2D, TUBB3, ARF3, ATP5G1, GAPDHS, ATP5E, NCOR2, AP2S1, POLR2H, GRIK5, NDUFB7, DCTN2, NDUFA13, POLR2I, NDUFB2, DNAH2, GRIN1, NDUFA3, NDUFS8, CREB3L4 (49)	ARPC1B, TP53, NDUFA4L2, BAX, COX7A1, TUBB1, AKT1, CLTB, ARPC1A, PLCB3, BBC3, CREB3, POLR2E, CYC1, POLR2J, NDUFS6, DLG4, ARPC5L, COX6C, GRIN2D, TUBB3, ARF3, ATP5G1, GAPDHS, ATP5E, NCOR2, AP2S1, POLR2H, GRIK5, NDUFB7, DCTN2, NDUFA13, POLR2I, NDUFB2, DNAH2, GRIN1, NDUFA3, NDUFS8, CREB3L4 (39, 0.455-0.24)

MEG3	TP53 (1)	COX7A1, DLG4, NDUFA4L2, GRIK5, GRIN1, GRIN2D, TUBB3, GAPDHS, TUBB1, CLTB, ARF3, NCOR2, BBC3, CREB3, DNAH2, PLCB3, DCTN2, TP53, AKT1, POLR2I, NDUFB7, ARPC1A, ATP5G1, NDUFA3, ARPC5L, COX6C, ARPC1B, NDUFA13, POLR2E, NDUFB2, BAX, AP2S1, CYC1, NDUFS6, NDUFS8, POLR2H, POLR2J, ATP5E, CREB3L3, COX6B2, AP2A1, POLR2J2 (42, 0.577-0.205)
XIST1	None	COX7A1, NDUFA4L2, TP53, GAPDHS, ARPC1B, TUBB1, GRIK5, GRIN2D, DLG4, BBC3, BAX, TUBB3, CREB3, CLTB, ATP5G1, GRIN1, NDUFA3, DNAH2, AKT1, POLR2I, ARPC1A, ARF3, CYC1, COX6C, NDUFA13, PLCB3, POLR2E, NCOR2, NDUFB7, NDUFS6, DCTN2, ARPC5L, AP2S1, POLR2H, POLR2J, NDUFB2, ATP5E, NDUFS8, CREB3L3, COX6B2 (40, 0.385-0.205)

Other than XIST and MEG3, NEAT1 co-expressed with many other lncRNAs. It is to be found our whether these co-expressed lncRNAs might also be involved in HD. Many genes co-expressed with XIST are also associated with HD pathway (**Table 7.5**). This result indicated that MEG3, NEAT1, XIST and these common 37 genes were likely to be regulated by the similar transcription machinery and together might participate in the same biological processes and pathways.

7.10. Transcription regulation of NEAT1, MEG3, and XIST

Levels of lncRNAs are regulated by transcription factors (TFs), similar to that observed in protein-coding genes. Estrogen receptor alpha ERα **[37]** and TP53 **[38]** were reported to bind to the putative promoter of NEAT1 and regulated its levels in

prostate cancer cells and leukemic cells, respectively. In a hypoxic condition, HIF-2α activated the expression NEAT1 and enhanced cell growth **[39]**. YY1 was seen to bind to the putative promoters of XIST and regulated its expression **[40]**. To identify additional transcription factors that could bind within 5 Kb upstream sequences of NEAT1, MEG3, and XIST, I utilized the database http://deepbase.sysu.edu.cn/chipbase/ that cataloged ChiP data **[41]**. It has been observed that three transcription factors namely HEY1, HNF4A, NRSF could bind to the putative promoters of these lncRNAs. It remains to be found out whether such binding activates or represses the expression. Summary of the results is shown in **Table 7.6**.

Table 7.6: Transcription factors that bind within 5 Kb upstream sequences of NEAT1, MEG3, and XIST

Non-Coding RNA	No of TF binds 5Kb Upstream sequence	Representative TF
NEAT1	86	E2F1, E2F4, E2F6, ERalpha, GATA2, HEY1, HNF4A, HSF1, Myc, NFKB, NRSF, p300, p63, p68, TCF7L2, YY1
MEG3	15	AR, CDX2, CTCF, E2F4, ERalpha, FOXH1, GATA6, HEY1, HNF4A, NRSF, p300, SETDB1, SMAD3, SMAD4, ZNF263
XIST	14	c-Myc, CTCF, EWS_ERG, GTF2B, HEY1, HNF4A, NANOG, NFKB, NRSF, Pbx3, POU2F2, Rad21, SP1, TAF1

7.11. Discussion

In the present study, I analysed the small RNA sequencing data in a mouse model of HD, designed originally to identify differential levels of miRNA. Such customized analysis identified differentially expressed ncRNAs other than miRNA that was subsequently validated using low throughput assays in an animal model and two cell models of HD. Knockdown of Meg3 and Neat1 modulated the aggregation of mutant

HTT and decreased the levels of Tp53. Using various databases that catalogue interacting partners and co-expressed genes of Meg3, Neat1, and Xist, I observed that protein interacting partners and co-expressed protein-coding genes of Neat1 were associated with Huntington's disease pathways. Taking these together, I have provided evidence in support of the involvement of Meg3 and Neat1 in HD pathogenesis.

Additional lines of evidence implicating Meg3 and Neat1 in HD pathogenesis include: (i) altered levels of Meg3, Neat1 and Xist altered in R6/2 mice and various cell models of HD, (ii) loss of function of Meg3 and Neat1 modulated aggregate formation of mutated N-terminal HTT coded by exon1 of *HTT* in cell models of HD and concurrent modulation of Tp53 levels (iii) identification of protein interacting partners of NEAT1, MEG3 and XIST enriched with biological processes and pathways are known to be involved in HD, (iv) expressions of more than 50% of NEAT interacting proteins associated with HD pathway that were altered in HD brains and (v) co-expression of NEAT1 interacting protein partners associated with HD pathways with NEAT1.

MEG3 is expressed in many normal human tissues, with the highest observed expression in the pituitary gland followed by different regions of the brain (http://www.gtexportal.org/home/gene/MEG3). Mining the existing microarray data, levels of MEG3 has been reported to be decreased in HD **[25]**, although this has not been validated by low throughput assays. In R6/2 mice, Meg3 was increased in the early stage (6 weeks) and continued to increase up to 8 weeks (late stage). In other cellular models also increased levels of Meg3 could be identified. Differences between the results obtained in this study and those reported earlier **[25]** could be due to the differences in species or techniques used. Increased levels of NEAT1 have been reported earlier by data mining [25] and also in models of HD and postmortem

samples from HD patients **[42]**. I identified similarly increased levels of Neat1 in the late stage of HD (8 weeks) in R6/2 mice and in several cell models of HD. To the best of our knowledge, altered in the levels of Xist in HD has not been reported yet.

Decreased aggregates of mutant N-terminal HTT observed in cells, where endogenous Meg3 or Neat1 was knocked down, could be explained by effects of Meg3 or Neat1 on the levels of Tp53. Meg3 is known to stabilize Tp53 by interacting with it. Increased levels of Tp53 could also be mediated through destabilization of MDM2 by interacting with Meg3 [**37-39**]. Binding of Tp53 at -3485 of TSS of MEG3 (chromosomal position 100775826-100776022) has been identified **[41]** although it remains unknown whether such binding activates the transcription of MEG3.

NEAT1 has two isoforms, the shorter variant NEAT1_1, also known as MENepsilon is 3756 bp long, while the longer variant NEAT1_2, also known as MENbeta is 22743 bp long. Both the isoforms are conserved at the 5'-end and are also observed in mouse. The longer isoform NEAT1_2, which is mostly localized in the nucleus, acts as a scaffold of RNAs and RNA binding proteins to form nuclear bodies known as "paraspeckles". The PCR primers that I used to detect the levels of NEAT1 detected a region from the longer isoform. Our results indicated that the reduction of Neat1 reduced the levels of Tp53 which further indicated that Neat1 might interact with Tp53 and alter its stability. However, NEAT1 has been shown to bind active chromatin sites near Tp53 genes along with other genes **[43]**. Tp53 directly regulates the transcription of Neat1 by binding to the promoter of the gene **[44, 45]**. Levels of Neat1 and Tp53 are thus under the control of a feedback loop. MEG3, NEAT1, and XIST can interact with many miRNAs possibly through sequence complementarity. Interaction of lncRNAs with miRNAs may contribute to functional deregulation of target mRNAs of those miRNAs by reducing their effective levels by acting as a "sponge" or as a competitor for binding with the target mRNAs **[43]**. Due to the

miRNA- lncRNA interactions, the stability of lncRNAs might also be compromised leading to their silencing **[46].** Levels of miR-132, miR-221, miR-222, and miR-9 have been reported to decrease in various models of HD as well as in HD postmortem tissues [**6**]. Levels of miR-125b, miR-146a, miR-150 are reduced in cell and animal models of HD [**6, 40].** NEAT1 interacts with these miRNAs thereby contributing to the HD pathogenesis.

It has been shown earlier that inhibition of proteasomal degradation increased the levels of Neat1, with a concomitant increase in length and size of nuclear paraspeckles. Cytoplasmic and nuclear aggregates with ubiquitinated proteins are also identified in this condition **[47]**. Given that proteasomal degradation is compromised **[48-51]** and levels of Neat1 increased in HD - observed here as well by others **[25, 42],** it is likely that Neat1 may influence the proteasomal degradation in HD. This contention is further supported by our observation that in the KEGG pathway, ubiquitin-mediated proteolysis is enriched significantly with 28 NEAT1 interacting proteins. Among these proteins, levels of 7 genes (BRCA1, HUWE1, SMURF2, UBE2D3, UBE2G2, UBE2S and UBR5) increased and the levels of 9 genes (FZR1, HERC, MGRN1, PML, RHOBTB2, SMURF1, TCEB1, UBE2M, and UBE2Z) decreased in postmortem brains of HD patients **[34, 35]** or induced pluripotent stem cells (iPSCs) derived from HD patients **[36]**. Modulation of proteasomal degradation by miRNAs due to the interaction of NEAT1 with more than 300 miRNAs cannot be ruled out.

Levels of NEAT1 are increased in the temporal cortex and hippocampus of patients with Alzheimer's disease (AD) to negatively regulate *CDK5R1* **[52]**. The role of NEAT1 in modulating neuronal excitability and its association with pathological seizure states has recently been reported **[44, 53]**. It has also been found that ALS

associated TDP-43 and FUS/TLS proteins were enriched in paraspeckles and bound to NEAT1_2 lncRNA directly **[54]**.

Enriched biological process like regulation of gene expression [**4, 5, 55, 56**], RNA splicing, mRNA metabolic processes, RNA metabolic process, nuclear mRNA splicing [**57**], apoptosis [**58, 59],** carbohydrate/ lipid /cholesterol metabolism **[60-62**], nervous system development **[25, 55**] and S phase of mitotic cell cycle [**12,13**] were known to be associated with HD. Such association of known biological processes with HD and enriched with interacting proteins of MEG3, NEAT1 and XIST indicated that increased expression of these lncRNAs in HD models might contribute to HD pathogenesis through their interacting protein partners.

Small nucleolar RNAs (snoRNAs), mostly 60–170 nucleotides long, belong to a class of non-coding RNAs that are involved in the post-transcriptional processing of other ncRNAs like ribosomal RNAs. snoRNAs are mostly localized in the nucleolus and have also been implicated in various processes like microRNA-dependent gene silencing and alternative splicing. Altered levels of snoRNAs have been identified in cancer **[63]**.

In summary, the involvement of lncRNAs in neurodegeneration pathologies is quite evident from our work. This apparently new avenue of research warrants further investigation.

Summary:

- Several lncRNAs were deregulated in cell and mice models of HD from sequencing data.
- MEG3, NEAT1 and XIST showed the most uniform and strong deregulation in validation sets.
- Transient knockdown of MEG3 and NEAT1 decreased mutant Huntingtin aggregates in cell and stabilised Tp53 levels.

7.12. References

1.Huntington's Disease Collaborative Research Group (1993) A novel gene containing a trinucleotide repeat that is expanded and unstable on Huntington's disease chromosomes. *Cell*, 72, 971-983

2.Roos RA (2010) Huntington's disease: a clinical review, Orphanet J Rare Dis. 5, 40

3. Imarisio S, Carmichael J, Korolchuk V, Chen CW, Saiki S, Rose C, Krishna G, Davies JE, TtofiE, Underwood BR, Rubinsztein DC (2008) Huntington's disease: from pathology and genetics to potential therapies, Biochem J. 412, 191-209.

4. Seredenina T, Luthi-Carter R (2012) What have I learned from gene expression profiles in Huntington's disease? Neurobiol Dis. 45, 83-98

5. Ruepp A, Kowarsch A, Schmidl D, Buggenthin F, Brauner B, Dunger I, Fobo G, Frishman G, Montrone C, Theis FJ (2010) PhenomiR: a knowledgebase for microRNA expression in diseases and biological processes, Genome Biol. 11, R6

6. Sinha M, Mukhopadhyay S, Bhattacharyya NP (2012) Mechanism(s) of alteration of micro RNA expression in Huntington's disease and their possible contributions to the observed cellular and molecular dysfunctions in the disease, Neuromolecular Med. 14, 221-243

7. Goodall EF, Heath PR, Bandmann O, Kirby J, Shaw PJ (2013) Neuronal dark matter: the emerging role of microRNAs in neurodegeneration, Front Cell Neurosci.7, 178.

8. Qiu L, Tan EK, Zeng L (2015) microRNAs and Neurodegenerative Diseases, Adv Exp Med Biol. 888, 85-105

9. Hernandez-Rapp J, Rainone S, Hébert SS (2016) MicroRNAs underlying memory deficits in neurodegenerative disorders, Prog Neuropsychopharmacol Biol Psychiatry. Apr 23. pii: S0278-5846(16)30057-4. doi: 10.1016/j.pnpbp.2016.04.011. [Epub ahead of print]

10. Liu T, Im W, Mook-Jung I, Kim M (2015) microRNA-124 slows down the progression of Huntington's disease by promoting neurogenesis in the striatum, Neural Regen Res. 10, 786-791

11.Das E, Jana NR, Bhattacharyya NP (2015) Delayed Cell Cycle Progression in STHdh(Q111)/Hdh(Q111) Cells, a Cell Model for Huntington's Disease Mediated by microRNA-19a, microRNA-146a and microRNA-432, Microrna. 4, 86-100

12. Das E, Jana NR, Bhattacharyya NP (2013) MicroRNA-124 targets CCNA2 and regulates cell cycle in STHdh(Q111)/Hdh(Q111) cells, Biochem Biophys Res Commun, 437, 217-224

13.Das S, Bhattacharyya NP (2015) Heat Shock Factor 1-Regulated miRNAs Can Target Huntingtin and Suppress Aggregates of Mutant Huntingtin, Microrna,4, 185-93

14. Bucha S, Mukhopadhyay D, Bhattacharyya NP (2015) Regulation of mitochondrial morphology and cell cycle by microRNA-214 targeting Mitofusin2, BiochemBiophys Res Commun., 465, 797-802

15. Hoss AG, Labadorf A, Latourelle JC, Kartha VK, Hadzi TC, Gusella JF, MacDonald ME, Chen JF, Akbarian S, Weng Z, Vonsattel JP, Myers RH (2015) miR-10b-5p expression in Huntington's disease brain relates to age of onset and the extent of striatal involvement, BMC Med Genomics. 8,10.

16.Sinha M, Ghose J, Bhattacharyya NP (2011) Micro RNA -214,-150,-146a and-125b target Huntingtin gene, RNA Biol. 8, 1005-1021

17. Kopp F, Mendell JT. Functional Classification and Experimental Dissection of Long Noncoding RNAs. Cell. 2018 Jan 25;172(3):393-407

18. Böhmdorfer G, Wierzbicki AT (2015) Control of Chromatin Structure by Long Noncoding RNA, Trends Cell Biol. 25, 623-632

19. Olga Sin and Ellen AA (2015) Regulation of protein homeostasis in neurodegenerative diseases: the role of coding and non-coding genes, Cell Mol Life Sci. 72, 4027-4047

20. Elling R, Chan J, Fitzgerald KA (2016) Emerging role of long noncoding RNAs as regulators of innate immune cell development and inflammatory gene expression, Eur J Immunol., 46, 504-512

21 . Szcześniak MW, Makałowska I. lncRNA-RNA Interactions across the Human transcriptome, PLoS One, 2016 Mar 1; 11:e0150353

22. Lekka E, Hall J. Noncoding RNAs in disease. FEBS Lett. 2018 Jul 4. doi: 10.1002/1873-3468.13182. [Epub ahead of print]

23.Wan P, Su W, Zhuo Y (2016) The Role of Long Noncoding RNAs in Neurodegenerative Diseases, Mol Neurobiol. 2016 Feb 24 [Epub ahead of print]

22.Kerschbamer E, Biagioli M (2016) Huntington's Disease as Neurodevelopmental Disorder: Altered Chromatin Regulation, Coding, and Non-Coding RNA Transcription, Front Neurosci., 509

24.Brochier C, Gaillard MC, Diguet E, Caudy N, Dossat C, Ségurens B, Wincker P, Roze E, Caboche J, Hantraye P, Brouillet E, Elalouf JM, de Chaldée M (2008) Quantitative gene expression profiling of mouse brain regions reveals differential transcripts conserved in human and affected in disease models, Physiol Genomics. 33, 170-179
25.Francelle L, Galvan L, Gaillard MC, Petit F, Bernay B, Guillermier M, Bonvento G, Dufour N, Elalouf JM, Hantraye P, Déglon N, de Chaldée M, Brouillet E (2015) Striatal long noncoding RNA Abhd11os is neuroprotective against an N-terminal fragment of mutant huntingtin in vivo, Neurobiol Aging, 36, 1601.e7-16
25. Johnson R (2012) Long non-coding RNAs in Huntington's disease neurodegeneration, Neurobiol Dis. 46, 245-254 (Review)
26. Johnson R, Richter N, Jauch R, Gaughwin PM, Zuccato C, Cattaneo E, Stanton LW (2010) The Human Accelerated Region 1 noncoding RNA is repressed by REST in Huntington's disease, Physiol Genomics, 41, 269-274
27.Chung DW, Rudnicki DD, Yu L, Margolis RL (2011) A natural antisense transcript at the Huntington's disease repeat locus regulates HTT expression, Hum Mol Genet., 20, 3467-3477
28.Qureshi IA, and Mehler, MF (2012) Emerging roles of non-coding RNAs in brain evolution, development, plasticity and disease Nat. Rev. Neurosci., 13, 528–541.
29.Sauvageau M, Goff LA, Lodato S, Bonev B, Groff AF, Gerhardinger C, Sanchez-Gomez DB, Hacisuleyman E, Li E, Spence M, Liapis SC, Mallard W, Morse M, Swerdel MR, D'Ecclessis MF, Moore JC, Lai V, Gong G, Yancopoulos GD, Frendewey D, Kellis M, Hart RP, Valenzuela DM, Arlotta P, Rinn JL (2013) Multiple knockout mouse models reveal lincRNAs are required for life and brain development, Elife, 2, e01749.
30.Trettel F, Rigamonti D, Hilditch-Maguire P, Wheeler VC, Sharp AH, Persichetti F, Cattaneo E, MacDonald ME. Dominant phenotypes produced by the HD mutation in STHdh(Q111) striatal cells. Hum Mol Genet 2000; 9:2799-2809; PMID:11092756; http://dx.doi.org/10.1093/hmg/9.19.2799
31.Majumder P, Raychaudhuri S, Chattopadhyay B, Bhattacharyya NP (2007) Increased caspase-2, calpain activations and decreased mitochondrial complex II activity in cells expressing exogenous huntingtin exon 1 containing CAG repeat in the pathogenic range, Cell MolNeurobiol. 27, 1127-1145
32. Stuart JM, Segal E, Koller D, Kim SK (2003) A gene-coexpression network for global discovery of conserved genetic modules, Science, 302, 249-255
33.Ayroles JF, Carbone MA, Stone EA, Jordan KW, Lyman RF, Magwire MM, Rollmann SM, Duncan LH, Lawrence F, Anholt RR, Mackay TF (2009) Systems genetics of complex traits in Drosophila melanogaster, Nat Genet., 41, 299-307
34. Hodges A, Strand AD, Aragaki AK, Kuhn A, Sengstag T, Hughes G, Elliston LA, Hartog C, Goldstein DR, Thu D, Hollingsworth ZR, Collin F, Synek B, Holmans PA, Young AB, Wexler NS, Delorenzi M, Kooperberg C, Augood SJ, Faull RL, Olson JM, Jones L, Luthi-Carter R.Regional and cellular gene expression of changes in human Huntington's disease brain, Hum Mol Genet. 2006 Mar 15;15(6):965-77.
35. Labadorf A, Hoss AG, Lagomarsino V, Latourelle JC, Hadzi TC, Bregu J, MacDonald ME, Gusella JF, Chen JF, Akbarian S, Weng Z, Myers RHRNA Sequence Analysis of Human Huntington's Disease Brain Reveals an Extensive Increase in Inflammatory and Developmental Gene Expression, PLoS One. 2015 Dec 4;10(12):e0143563.
36.Ring KL, An MC, Zhang N, O'Brien RN, Ramos EM, Gao F, Atwood R, Bailus BJ, Melov S, Mooney SD, Coppola G, Ellerby LM.Genomic Analysis Reveals Disruption of Striatal Neuronal Development and Therapeutic Targets in Human Huntington's Disease Neural Stem Cells.Stem Cell Reports. 2015 Dec 8;5(6):1023-1038.
37. Chakravarty D, Sboner A, Nair SS, Giannopoulou E, Li R, Hennig S, Mosquera JM, Pauwels J, Park K, Kossai M, MacDonald TY, Fontugne J, Erho N, Vergara IA, Ghadessi M, Davicioni E, Jenkins RB, Palanisamy N, Chen Z, Nakagawa S, Hirose T, Bander NH, Beltran H, Fox AH, Elemento O1, Rubin MA (2014)The oestrogen receptor alpha-regulated lncRNA NEAT1 is a critical modulator of prostate cancer, Nat Commun. 5, 5383
38. Blume CJ, Hotz-Wagenblatt A, Hüllein J, Sellner L, Jethwa A, Stolz T, Slabicki M, Lee K, Sharathchandra A, Benner A, Dietrich S, Oakes CC, Dreger P, teRaa D, Kater AP, Jauch A, Merkel O, Oren M, Hielscher T, Zenz T (2015)p53-dependent non-coding RNA networks in chronic lymphocytic leukemia, Leukemia, 29, 2015-2023
39. Choudhry H, Albukhari A, Morotti M, Haider S, Moralli D, Smythies J, Schödel J, Green CM, Camps C, Buffa F, Ratcliffe P, Ragoussis J, Harris AL, Mole DR (2015)Tumor hypoxia

induces nuclear paraspeckle formation through HIF-2α dependent transcriptional activation of NEAT1 leading to cancer cell survival, Oncogene, 34, 4482-4490
40. Makhlouf M, Ouimette JF, Oldfield A, Navarro P, Neuillet D, Rougeulle C (2014) A prominent and conserved role for YY1 in Xist transcriptional activation, Nat Commun., 5, 4878
41. Yang JH, Li JH, Jiang S, Zhou H and Qu LH (2013) ChIPBase: A database for decoding the transcriptional regulation of long non-coding RNA and microRNA genes from ChIP-Seq data, Nucleic Acids Res. 41, D177-D187
42. Sunwoo JS, Lee ST, Im W, Lee M, Byun JI, Jung KH, Park KI, Jung KY, Lee SK, Chu K, Kim M, Altered Expression of the Long Noncoding RNA NEAT1 in Huntington's Disease.Mol Neurobiol. 2017 Mar;54(2):1577-1586.
43. West JA, Davis CP, Sunwoo H, Simon MD, Sadreyev RI, Wang PI, Tolstorukov MY, Kingston RE. The long noncoding RNAs NEAT1 and MALAT1 bind active chromatin sites. Mol Cell. 2014 Sep 4;55(5):791-802. doi: 10.1016/j.molcel.2014.07.012. Epub 2014 Aug 21.
44. Barry, G. *et al.* The long non-coding RNA NEAT1 is responsive to neuronal activity and is associated with hyperexcitability states. Sci Rep. 2017 Jan 5;7:40127. doi: 10.1038/srep40127
45.Idogawa M, Ohashi T, Sasaki Y, Nakase H, Tokino T, Long non-coding RNA NEAT1 is a transcriptional target of p53 and modulates p53-induced transactivation and tumor-suppressor function, Int J Cancer. 2017 Jun 15;140(12):2785-2791. doi: 10.1002/ijc.30689. Epub 2017 Mar 27.
46. Yoon JH, Abdelmohsen K, Gorospe M (2014) Functional interactions among microRNAs and long noncoding RNAs, Semin Cell Dev Biol., 34, 9-14
47. Hirose T, Virnicchi G, Tanigawa A, Naganuma T, Li R, Kimura H, Yokoi T, Nakagawa S, Bénard M, Fox AH, Pierron G. NEAT1 long noncoding RNA regulates transcription via protein sequestration within subnuclear bodies.Mol Biol Cell. 2014 Jan;25(1):169-83.
48. Wade BE, Wang CE, Yan S, Bhat K, Huang B, Li S, Li XJ (2014) Ubiquitin-activating enzyme activity contributes to the differential accumulation of mutant huntingtin in the brain and peripheral tissues, J Neurosci. 34, 8411-8422
49. Hyrskyluoto A, Bruelle C, Lundh SH, Do HT, Kivinen J, Rappou E, Reijonen S, Waltimo T, Petersén A, Lindholm D, Korhonen L (2014) Ubiquitin-specific protease-14 reduces cellular aggregates and protects against mutant huntingtin-induced cell degeneration: involvement of the proteasome and ER stress-activated kinase IRE1α, Hum Mol Genet. 2014 Nov 15;23(22):5928-39
50. Bhat KP, Yan S, Wang CE, Li S, Li XJ (2014) Differential ubiquitination and degradation of huntingtin fragments modulated by ubiquitin-protein ligase E3A , Proc Natl Acad Sci U S A. 111, 5706-5711.
51. Li X, Wang CE, Huang S, Xu X, Li XJ, Li H, Li S (2010) Inhibiting the ubiquitin-proteasome system leads to preferential accumulation of toxic N-terminal mutant huntingtin fragments, Hum Mol Genet. 19, 2445-2455
52.Spreafico M, Grillo B, Rusconi F, Battaglioli E, Venturin M. Multiple Layers of CDK5R1 Regulation in Alzheimer's Disease Implicate Long Non-Coding RNAs.Int J Mol Sci. 2018 Jul 11;19(7). pii: E2022.
53. Barry, G. Integrating the roles of long and small non-coding RNA in brain function and disease. Mol Psychiatry. 19, 410–416 (2014).
54. Nishimoto, Y. et al. The long non-coding RNA nuclear-enriched abundant transcript 1_2 induces paraspeckle formation in the motor neuron during the early phase of amyotrophic lateral sclerosis. Mol Brain. 6, 31 (2013).
55. Walsh MJ, Cooper-Knock J, Dodd JE, Stopford MJ, Mihaylov SR, Kirby J, Shaw PJ, Hautbergue GM (2015) Invited review: decoding the pathophysiological mechanisms that underlie RNA dysregulation in neurodegenerative disorders: a review of the current state of the art, Neuropathol Appl Neurobiol., 41, 109-134
56. Neueder A, Bates GP (2014) A common gene expression signature in Huntington's disease patient brain regions, BMC Med Genomics, 7, 60
57. Labadorf AT, Myers RH (2015) Evidence of Extensive Alternative Splicing in Post Mortem Human Brain HTT Transcription by mRNA Sequencing, PLoS One., 10, e0141298
58. Ekshyyan O, Aw TY (2004) Apoptosis: a key in neurodegenerative disorders, Curr Neurovasc Res., 1, 355-371
59. Ghavami S, Shojaei S, Yeganeh B, Ande SR, Jangamreddy JR, Mehrpour M, Christoffersson J, Chaabane W, Moghadam AR, Kashani HH, Hashemi M, Owji AA, Łos MJ (2014) Autophagy and apoptosis dysfunction in neurodegenerative disorders, Prog Neurobiol., 112, 24-49.

60. Nambron R, Silajdžić E, Kalliolia E, Ottolenghi C, Hindmarsh P, Hill NR, Costelloe SJ, Martin NG, Positano V, Watt HC, Frost C, Björkqvist M, Warner TT (2016) A Metabolic Study of Huntington's Disease, PLoS One. 11, e0146480
61. Hottman DA, Chernick D, Cheng S, Wang Z, Li L (2014) HDL and cognition in neurodegenerative disorders, Neurobiol Dis.72, 22-36
62. Block RC, Dorsey ER, Beck CA, Brenna JT, Shoulson I (2010) Altered cholesterol and fatty acid metabolism in Huntington's disease, J Clin Lipidol. 4, 17-23
63. Jorjani H, et al. An updated human snoRNAome. Nucleic Acids Res. 2016;44:5068–5082. doi: 10.1093/nar/gkw386.

Thesis Keywords

Name of the Student: KAUSHIK CHANDA

Name of the CI/OCC: SAHA INSTITUTE OF NUCLEAR PHYSICS

Enrolment No.: LIFE05201504005

Thesis Title: UNDERSTANDING THE ROLES PLAYED BY RECEPTOR TYROSINE KINASES AND NON-CODING RNAs IN NEURODEGENERATION.

Discipline: Life Sciences **Sub-Area of Discipline: Molecular Neurobiology**

Date of viva voce: 22.04.2021.

KEYWORDS:

Alzheimer's disease, Huntington disease, AICD**,** Amyloid Beta, Receptor Tyrosine Kinase, ROR1, Cytoskeleton**,** miRNA expression, long non-coding RNA, MALAT1, NEAT1, MEG3, X Chromosome Instability, Xist.

THESIS HIGHLIGHTS

Name of the Student: KAUSHIK CHANDA.

Name of the CI/OCC: SAHA INSTITUTE OF NUCLEAR PHYSICS.

Enrolment No.: LIFE05201504005.

Thesis Title: UNDERSTANDING THE ROLES PLAYED BY RECEPTOR TYROSINE KINASES AND NON-CODING RNAs IN NEURODEGENERATION.

Discipline: Life Sciences. **Sub-Area of Discipline: Molecular Neurobiology.**

Date of viva voce: 22.04.2021.

Altered expressions of protein-coding genes and microRNAs have been implicated in the pathogenesis of Alzheimer's disease (AD) by the causative agents Aβ and AICD. The involvement of RTKs and other long non-coding RNAs (lncRNA) is being realized recently.

Using small RNA sequencing from an AD cell model, we observed perturbations in the levels of several miRNAs and lncRNAs. An Aβ treated cell model showed deregulation of two key RTKs- EPAH2 and ROR1. Effect of Aβ and AICD, individually and in combination, were validated with top regulated miRNA hits. Several of these miRNAs were found to target these RTKs. An additional layer of complexity revealed that two strongly deregulated lncRNAs MALAT1 and NEAT1 governed the aforesaid miRNA-RTK network. This network is functionally relevant in AD research as the miRNA- MALAT1-EPHA2 axis governs memory formation and/or impairment via the CREB pathway while the miRNA-NEAT1-ROR1 axis governs cytoskeletal degradation and rearrangement. Using a similar high throughput sequencing approach, we could identify two key lncRNAs – MEG3 and NEAT1 which regulated Tp53 expression and the phenotypic changes observed in cell and animal models of Huntington's disease (HD). Understanding the total cellular non-coding transcriptome (the network of miRNA-lncRNA-RTK-Transcription Factor in the context of Neurodegenerative diseases (NDDs) is likely to open up new putative targets for the disease intervention.

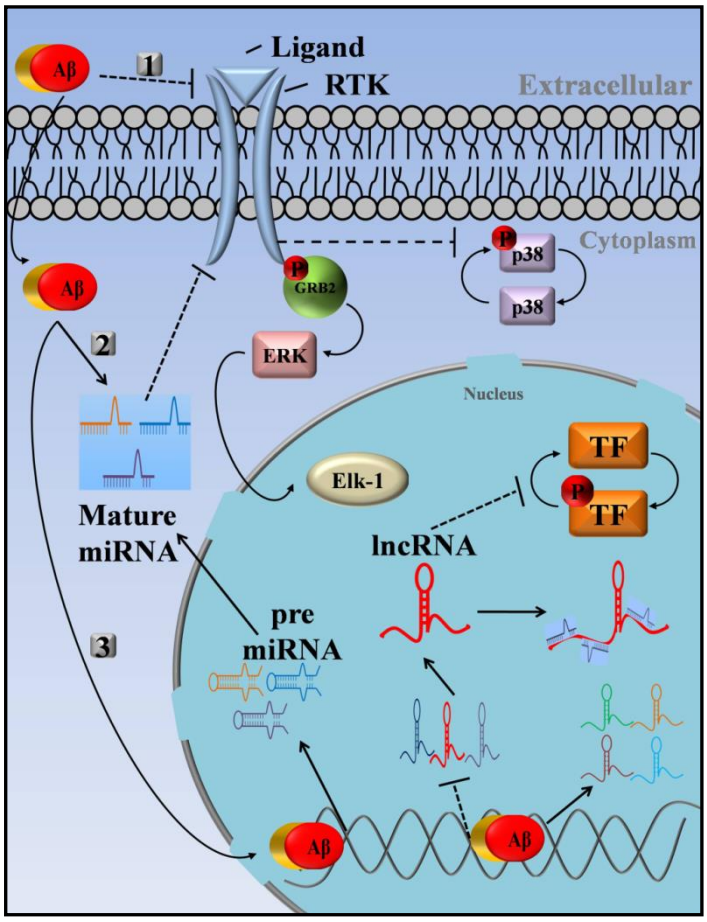

Fig: **Schematic representation of molecular events in cell models of AD.** Extracellular treatment of $A\beta_{1-42}$ has multiple effects on cells- 1.Extracellular $A\beta_{1-42}$ seems to inhibit the basal levels of RTKs and their downstream effectors, notably CREB and p38. 2. Cytosolic $A\beta_{1-42}$ affects the mature miRNA pool, which targets and inhibits the RTKs. 3. Nuclear translocated $A\beta_{1-42}$ differentially activates miRNAs and a subset of lncRNAs, but represses another subset of lncRNAs. Out of the repressed lncRNAs, several sponge the miRNAs and affect the TFs.